Incorporation of Gallium into Zeolites: Syntheses, Properties and Catalytic Application

Rolf Fricke,* Hendrik Kosslick, Günter Lischke,† and Manfred Richter

Institute of Applied Chemistry, Richard-Willstätter-Str. 12, D-12489 Berlin, Germany and Technische Fachhochschule Wildau, Bahnhofstrasse, D-15745 Wildau, Germany

Received May 18, 1999

Contents

* Corresponding author.
† Technische Fachhochschule Wildau.

10.1021/cr9411637 CCC: $35.00
Published on Web 05/24/2000

I. Introduction

Zeolites are members of the tectosilicate family of minerals.[1,2] Zeolite frameworks consist of 4-fold-connected TO_4 tetrahedra (T = Si, Al) forming three-dimensional networks. The corner linkage of tetrahedra is accomplished through T−O−T bridges. Therefore, each oxygen atom is shared between two neighboring tetrahedra and the binding capability is at its maximum. Thus, ideal zeolite crystals should have terminal silanol groups only on their external surface.[3]

In contrast to other tectosilicates, the linkage of tetrahedra (Figure 1) within zeolites leads to open network structures. The tetrahedra (primary building units) form rings of various sizes which are linked to form complex units (secondary building units).[4] These secondary building units may be assembled in many ways to give a large number of different zeolite structure types. The network of interconnected tetrahedra constitutes the zeolite framework (Figure 2). The zeolite lattice comprises the (charged) framework, and cations at distinct sites needed to balance charge as well as guest molecules if present.

Zeolite crystals contain pore or channel systems of molecular dimensions with fixed geometry and size (Table 1). The pores are composed of oxygen rings. The number of oxygen atoms involved within these rings determine their assignment O*n*R, thus O10R stands for a connection of 10 oxygen atoms. Oxygen atoms with radii of ca. 1.36 Å surround the smaller central atoms of the tetrahedra nearly completely. Consequently, the interior surface of zeolites is nearly entirely composed of oxygen atoms (Figure 3). Nonframework cations and molecules within the pore system coordinate to framework oxygen atoms. Further interactions between these cations and sorbed molecules occur. Water, if present, can coordinate to these cations and interact with other sorbed molecules.

According to the pore size, zeolites are classified into small-pore (pore size ≤ 5 Å, O8R), medium-pore (pore size 5−6 Å, O10R), and large-pore (pore size 7−8 Å, O12R) types. Typical representatives of the different types are zeolite A, ZSM-5, and the faujasites (X and Y), respectively.

Any tetrahedral Si^{4+} is surrounded by four O^{2-} ions. The resulting SiO_2 lattice is neutral because each O^{2-} ion is shared by two tetrahedra. The isomorphous substitution of Si^{4+} by Al^{3+} or Ga^{3+} causes a negative excess charge of the framework. This framework anionic charge is compensated by loosely fixed cations located in the channels. In contrast to the semipolar character of bonds within the zeolite framework, the interaction between cations and the framework is of substantially ionic character. Unlike framework atoms, the interstitial cations can be exchanged by other cations from aqueous solutions. If cations are exchanged by pro-

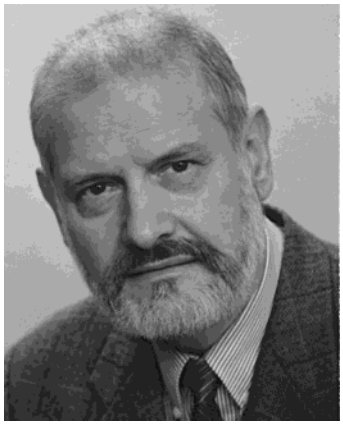

Rolf Fricke obtained his scientific education at the Technical University Dresden and the Humboldt University of Berlin where he graduated in 1971 after performing a spectroscopic study on Tellur. In the same year he started ESR spectroscopic work on vanadium-exchanged zeolites at the Catalysis Department of the Central Institute of Physical Chemistry. In 1978 he received his Ph.D. degree after doing an ESR study on silica-supported vanadium catalysts. In the following years he extended his research on supported and nonsupported heteropoly acid catalysts. In 1986 he returned to zeolites and established a group that was engaged in the synthesis, characterization, and catalytic application of new aluminophosphate molecular sieves. In 1994 he joined the newly founded Institute of Applied Chemistry Berlin-Adlershof where he, up to now, leads the environmental catalysis group. Together with his co-workers he has carried out basic work on the characterization of the new type gallophosphate cloverite and its first application as a catalyst and the use of MCM-41 as host material for chiral salen complexes. Current projects deal with the NO_x abatement of stationary and nonstationary exhaust sources and the development and application of mesoporous materials in catalysis.

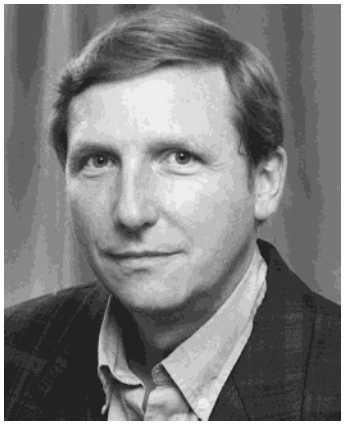

Hendrik Kosslick studied chemistry at the Humboldt University of Berlin and graduated after studying photoorganic chemistry. He received his Ph.D. degree from the Academy of Sciences of the G.D.R. in 1984, studying the application of infrared spectroscopy for structural characterization of zeolites. After a four-year stay in research management, he returned to the Catalysis Department of the Central Institute of Physical Chemistry in 1988. In 1994 he joined the zeolite catalysis research group at the Institute of Applied Chemistry. His current research interests are the synthesis, modification, characterization, and catalysis with microporous and mesoporous molecular sieves.

Günter Lischke was born in Freiberg, Germany. He graduated from the Institute of Chemical Engineering of Leipzig University in 1959, studying the phenomena of cool flames and explosions at low temperatures in stationary hydrocarbon/oxygen mixtures. Subsequently, he worked on the mechanism and kinetics of the slow combustion of *n*-heptane and isooctane in the gas phase investigating the distribution of individual compounds within reaction products. After receiving his doctor's (rer. nat.) degree in 1967, he continued scientific work at the Central Institute of Physical Chemistry of the Berlin Academy of Sciences on the fields of heterogeneous catalysis, studying oxidative dehydrogenation and selective oxidation of hydrocarbons in the gas phase. Later on, investigations were extended to catalytic reactions (e.g., conversion of methanol to hydrocarbons) over acidic molecular sieves of aluminosilicate (mordenite, ZSM-5) and aluminophosphate (cubic and hexagonal faujasite) types. Studies on the catalytic conversion of acetone over isomorphously substituted zeolite-like materials (MCM-41 and MCM-48) were continued at the Technische Fachhochschule Wildau, near Berlin.

Manfred Richter graduated from the Ernst-Moritz-Arndt-University Greifswald in 1971 with a diploma work on the kinetics of reaction networks. He received his Ph.D. degree from the Institute of Physical Chemistry in Berlin in 1976, studying the fields of heterogeneous catalysis applying transient-response methods for mechanistic studies of alcohol oxidation over vanadium and chromium oxo species anchored to high surface area silica. During the 1980s, his research interests focused on the development and catalytic utilization of zeolite-based materials for acid-catalyzed reactions, including isomerization of butenes and alkylaromatics, etherification of alcohols by isobutene to ethers and other compounds. Shape-selective effects of small pore aluminophosphate structure $AlPO_4$-17 were successfully exploited for the separation of *n*-butene stereoisomers. In 1994 he joined the newly founded Institute of Applied Chemistry in Berlin and started research projects on environmental catalysis. Current projects tackle problems of NO_x removal from exhaust gas streams on zeolite-based multifunctional solid catalysts.

tons, the zeolite acquires considerable Brønsted acidic properties and can be viewed as a solid acid.

Altogether, the structural diversity of zeolites discussed above is responsible for a wide range of interesting zeolite properties such as ion-exchange capacity, specific adsorption behavior, catalytic activity due to acidity, shape selectivity caused by size and polarity of molecules, high thermal stability and resistance against solvents, and wide flexibility for adjustments by isomorphous substitution of framework constituents.

The phenomenon of isomorphous substitution is well-known in the field of mineralogy.[5,6] By isomorphous substitution, framework atoms of crystalline compounds are replaced by atoms of other elements without changing the type of the crystal structure.[7] It could be shown that most elements are able to undergo substitution, at least to a very low degree. Even chromium, which prefers octahedral coordination, may substitute silicon in tetrahedral framework positions to a certain extent.[8,9] Extremely low degrees of substitution (0.2 atom %) can give rise to a remarkable change of properties.

Isomorphous substitution and replacement of exchangeable cations are important ways to modify zeolite properties for practical applications and have achieved considerable interest in the field of zeolite chemistry.[1,4,6] The thermodynamics of isomorphous substitution have been considered by Barrer.[10]

Ione and Vostrikova[11] summarized the main factors governing the isomorphous substitution as follows. (1) The tendency of substitution depends on the ratio of radii of the atoms involved. With an increasing difference of the radii Δr of atoms A and B, the substitution becomes energetically less favored. Substitution will occur if $\Delta r/r \leq 0.15$, with r denoting the radius of the atoms to be replaced in the framework by atoms of another element. (2) A larger atom A replaces a smaller atom B more easily if the replacement leads to a decrease of the coordination number of atom A and vice versa. (3) The substitution is influenced by the electronegativity ratio and the ionization potentials of exchanging atoms. (4) During isomorphous replacement of A by B with maintenance of the local environment (coordination number), a minimum free energy is being achieved with $\Delta r/r = 0.025-0.03$. (5) Isomorphous substitution is facilitated as long as replacement of A by B does not change long-range electrostatic interactions. (6) Substitution may also occur when the charges of exchanged atoms differ by 1, 2, or 3 units. (7) Exchanging atoms should not react with each other.

Pauling[13] formulated the main criteria for the occurrence of isomorphous substitution, which are primarily derived from crystal chemistry and geometric considerations. The basic idea is that frameworks of crystals, i.e., silicates including zeolites, consist of packages of negatively charged oxygen anions (O^{2-}). Therefore, tetrahedral and octahedral vacancies are formed. The size of these vacancies depends on the size of the anions. According to Pauling, cations prefer tetrahedral coordination if $\rho = r_{Me}/r_{O^{2-}} = 0.214-0.4$ and octahedral sites if $\rho = 0.4-0.6$. Ions larger than 0.55 Å, therefore, prefer octahedral coordination in oxygen lattices. A list of representative atoms and corresponding ρ values is given in Table 2.

According to Pauling's rule of gradients, Ga is located close to the frontier between tetrahedral and

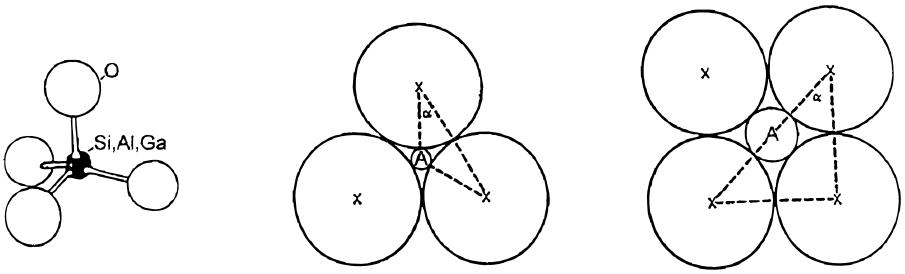

Figure 1. Representation of $(Si,Al,Ga)O_4$ zeolite tetrahedra (primary building units) showing the limited size of the tetrahedral in comparison with the octahedral gap. (Reprinted with permission from ref 175. Copyright 1985 The Chemical Society of Japan.)

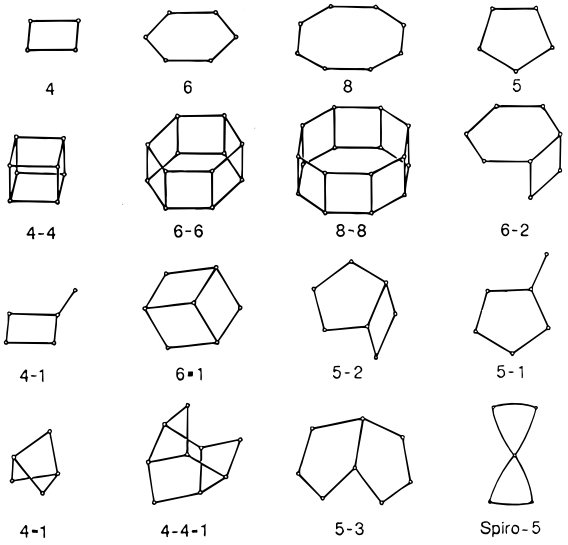

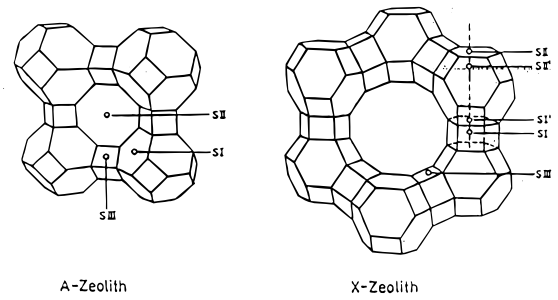

Figure 2. Topology of secondary building units of zeolites obtained by linkage of tetrahedra through corners and their shortcut designations. Framework of the LTA and FAU structure type with indicated nonframework cation positions.

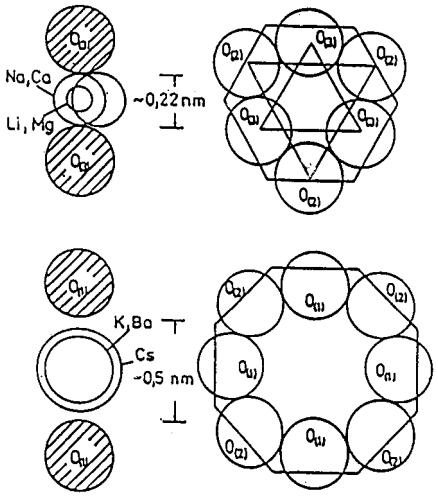

Figure 3. Oxygen rings of zeolites. Radii of cations in comparison to the free diameter of O6R and O8R. Balls represent oxygen atoms. Full lines connect the centers of tetrahedra (T-atoms).

octahedral coordination. Taking into account that gallium in alkaline solutions prefers the formation of tetrahedrally coordinated galliate anions,[16] it is also conceivable that this element has a good chance to substitute silicon in tetrahedral framework positions.

It is worth mentioning that all rules cited above are not strict laws. Additionally, the free space available in oxygen polyhedra is partly dependent on the crystal structure. For instance, in the case of aluminophosphates or gallophosphates with large AlO_4, GaO_4 and small PO_4 tetrahedra,[17,18] 4-fold coordinated Me^{3+} sites may also be accessible to larger atoms[19−21] like Co^{2+} and Mg^{2+}. The ability of the framework to change its fine structure (bond angles and distances) by rotation of the tetrahedra, by tilting, or by inversion is important in order to relax the strain resulting from the substituting atom.[22]

The motivation for replacing aluminum in aluminosilicate zeolite structures by other elements arose from the need to adjust their properties to intended applications. The aim of substitution is the complete integration of the modifying element into the framework while preserving the structure type. Often a certain percentage of the modifier remains on positions outside the framework (nonframework Me species). Depending on the synthesis conditions, a certain part of the element can be deposited in the form of clusters or cluster oxides in the porous network or on the external surface of the zeolite crystals. A postsynthesis modification by ion exchange (and partially by impregnation) replaces cations predominantly on cation positions (lattice sites).

Zeolitic materials are vastly applied as ion exchangers, selective adsorbents, catalysts, and catalyst supports. Industrial applications of zeolites are discussed in several reviews.[23−25] Zeolites as catalyst components are no longer confined to production of bulk chemicals and to the petroleum refining industry (cracking, hydrocracking, dewaxing, isomerization, alkylation, disproportionation). The breakthrough of gallium-bearing zeolites was found in the

Table 1. Main Characteristics of Zeolite Structures

zeolite	IZA code[a]	pore size[b]	pore opening	Al rich	medium	Si rich	SBU[c]		FD[d]	PD[e]
MCM-41	M41S[f]	mes			(×)	×	4, 5, 6[g]			1
MCM-48	M41S	mes			(×)	×	4, 5, 6[g]			3
cloverite	CLO	l	O20R				4	4−4	11.1	3
VPI-5	VFI	l	O18R				6		14.2	
AlPO-5	AFI	l	O12R				4, 6		17.5	
EMC-2	EMT	l	O12R		×		4, 6	6−6	12.9	3
faujasite	FAU	l	O12R	×			4, 6	6−6	12.7	3
offretite	OFF	l	O12R		×		6		15.5	2
gmelinite	GME	m−l	O12R		×		4, 6, 8	6−6	14.6	
ginde L	LTL	l	O12R		×		6		16.4	1
mazzite	MAZ	l	O12R	×			4	5−1	16.1	1
ZSM-18	MEI	l	O12R		×	×	3	6−1	14.3	
mordenite	MOR	m−l	O12R		×			5−1	17.2	2
beta	BEA	m−l	O12R			×	4	5−3	15.0	3
ZSM-12	MTW	m−l	O12R			×	4	5−1	19.4	1
ZSM-11	MEL	m	O10R			×		5−1	17.7	3
ZSM-5	MFI	m	O10R			×		5−1	17.9	3
ZSM-22	TON	m	O10R			×	6	5−1	19.7	1
ZSM-23	MTT	m	O10R			×		5−1	20.0	
cancrinite	CAN	m	O12R	×			6		16.7	
EU-1	EUO	m	O10R			×	4	5−1	18.2	
ferrierite	FER	m	O10R		×			5−1	17.7	3
erionite	ERI	s	O8R		×		6, 4		15.6	3
Li-A(BW)	ABW	s	O8R	×			4, 6,8		19.0	
A	LTA	s	O8R	×			4, 6	4−4	12.9	3
natrolite	NAT	s	O8R		×			4−1	17.8	
sodalite	SOD	v-sl	O6R	×	(×)		4, 6		17.2	3

[a] IZA code based on IUPAC rules. [b] mes = mesoporous, l = large, m−l = medium to large, m = medium, s = small, v−s = very small. [c] SBU = secondary building units. [d] FD = framework density as T-atoms per 1000 Å^3. [e] PD = dimensionality of the pore system. [f] Proposed name of the family of mesoporous materials, no IZA code. [g] Possible oxygen rings occurring in the walls of MCM-41, derived from framework modeling.

Table 2. Electronegativities, Radii, and Radii Ratios of Substituted Atoms after Allred, Pauling, Shannon

	electronegativity		radius/Å	distance/Å	radius ratio
element	Allred[12]	Pauling[13]	r_{Me}^{z+} [14]	r_{Me-O}[a]	$Q = r_{Me}/r_{O^{2-}}$
Si^{4+}	1.74	1.90	0.26	1.62	0.20
B^{3+}	2.01	2.04	0.11	1.47	0.08
Al^{3+}	1.47	1.61	0.39	1.75	0.29
Ga^{3+}	1.82	1.81	0.47	1.83	0.35
Fe^{3+}	1.64	1.83	0.47[15]	1.83[12d]	0.35
In^{3+}	1.49	1.78	0.62	1.98	0.46

[a] For $r_{O^{2-}}$ = 1.36 Å.

aromatization of lower alkanes (Cyclar process) where the activity is ascribed predominantly to nonframework gallium species. A further field of catalytic application is the isomerization of alkylaromatics.

Catalytic processes for fine chemical productions and oxidation reactions are amenable to the employment of tuned and novel zeolites.[26−28]

Another prospective area of zeolite application can be seen in environmental catalysis,[29,30] where hazardous substances in exhaust streams are effectively converted in less noxious or harmless substances by the catalytic action of modified zeolites. The reduction of NO and NO_2 in exhaust gas streams of mobile and stationary engines is processed in excess air under addition of methane by gallium-based zeolites in a selective way.[31−33]

A. Scope of the Review

The present review considers the synthesis, characterization, and catalytic application of gallium-containing microporous and mesoporous materials focusing on the isomorphous substitution of gallium into zeolite frameworks. Usually, incorporation of gallium into the solid material is achieved during the crystallization process, mostly performed in the presence of a suitable templating agent. Basic principles of the applied procedures, which are of fundamental importance for the synthesis of any aluminosilicate zeolite, are outlined by an introductory chapter. Experimental ways of postsynthesis incorporation of gallium into framework positions of zeolites are considered in section III. Physicochemical methods to characterize the nature and the properties of gallium incorporated into the framework as well as cations or nonframework species are described in section IV.

Section V summarizes the knowledge of the role of lattice defects and the hydrothermal stability of gallium in framework positions. The classification of Ga-substituted zeolite structures according to their Si/Ga ratio is given in a separate section. A special emphasis is placed on the catalytic properties of gallium-containing porous solid materials including gallophosphates and gallium-substituted mesoporous silica.

B. Terminology

Frequently, linguistic usage does not clearly distinguish between *zeolites* and *molecular sieves*. Molecular sieves is a generic term comprising crystalline microporous solid materials of various compositions. The designation emphasizes one of the favorite properties of these materials, viz. to act as a sieve of molecular dimensions. The term *zeolite* refers to crystalline microporous aluminosilicates built of SiO_4 and AlO_4 tetrahedra. In a strict sense, alumino- and

gallophosphate structures consisting of AlO_4 or GaO_4 and PO_4 tetahedra are not zeolites.

For microporous crystalline materials of zeolite-analogous structures with $Me^{II}O_4$ and SiO_4 tetrahedra arranged according to the framework topology of zeolites, designations such as metal silicate, metallosilicate, or metal-modified zeolite are used synonymously.

The most widely studied metallosilicate systems are gallosilicates, ferrisilicates, borosilicates, and titanium silicates. Even among this family of metallosilicates, no unique terminology exists. Instead of gallosilicate, the term galliosilicates is found. The term ferri- for iron-substituted silicalite obviously states that iron is incorporated in the valence state of 3+.

In the case of synthetic materials, one has to differentiate between the as-synthesized products which contain the occluded organic template and the calcined products obtained after burning off the templates. Prior to catalytic or adsorptive application, the template has to be removed, otherwise the pore system would be blocked.

Each unique framework topology (i.e., four-connected net) is designated by a structure-type code consisting of three capital Roman letters, only. These mnemonic codes are generally derived from the names of the type materials and do not depend on composition and distribution of the tetrahedrally coordinated atoms (Si, Al, P, Ga, Ge, B, Be, etc.), cell dimensions, or symmetry. The assignment of structure-type codes follows the IZA Structure Commission. To date, 126 structure-type codes have been introduced. Ninety-eight of these codes appear in the fourth edition of the *Atlas of Zeolite Structure Types*.[34] This is accessible on-line under the address http://www.iza-sc.ethz.ch/IZA-sc/AtlasHome.html.

In this review, materials which were synthesized without any aluminum source in the synthesis gel (aside from traces of impurity aluminum which is often contained in other ingredients) will be designated as gallosilicates. Following the zeolite literature where the ions at exchange positions are often indicated by simply adding the chemical symbol of the metal to the zeolite acronyms, we indicate a framework-substituted element by combining the symbol (e.g., gallium) enclosed into brackets with the name of the given zeolite or the structure-type code. Thus, [Ga]-ZSM-5 symbolizes a gallosilicate of MFI structure where aluminum is completely replaced by gallium in framework positions. If, additionally, aluminum is present besides gallium, both symbols are given in brackets, e.g., [Ga,Al]-ZSM-5. The term Ga-ZSM-5 will be chosen for any gallium-modified aluminosilicate ZSM-5 with gallium cations introduced by ion-exchange procedures. Samples synthesized by impregnation or mechanical mixing are designated as Ga/ZSM-5. Abbreviations used for samples prepared by other procedures will be explained as they appear.

Generally, the term *lattice* is distinguished from the term *framework*. *Lattice* is understood to comprise cations both within the *framework* and at defined *interstitial exchange positions* located in the oxygen rings, windows, and cavities.

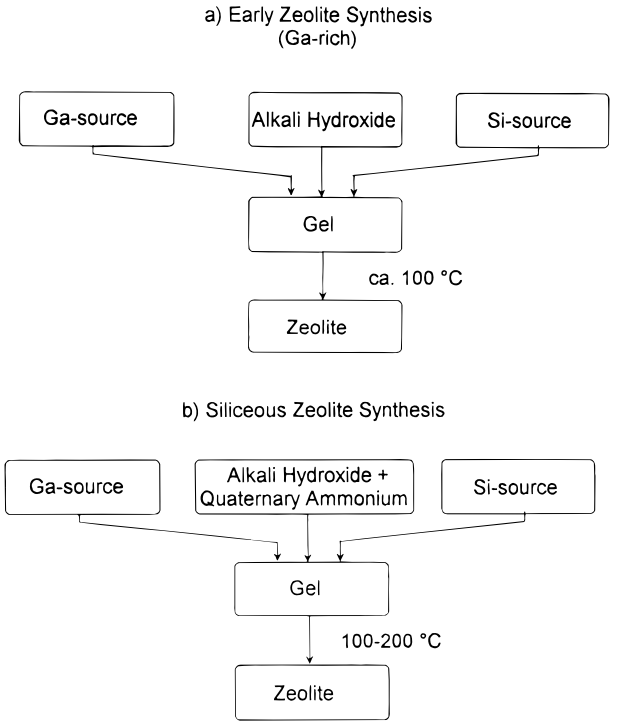

Figure 4. Schematic representation of synthesis methods for (a) Ga-rich zeolites (adapted from "early" Al-rich syntheses) and (b) siliceous Ga-substituted zeolites.

Within this review, the above nomenclature will be obeyed as long as the necessary information has been provided by the authors of the cited paper.

II. Synthesis of Zeolites

A. General Aspects

The fundamental procedures for the synthesis of zeolites are fairly similar irrespective of composition and structure. Generally, synthesis comprises the key steps schematically illustrated for Me^{3+}-rich ("early") and novel silicon-rich zeolites in Figure 4.[35]

In any case, zeolite synthesis gels contain the silicon source, an alkaline base, one or more Me^{3+} compounds (mostly salts), and organic templates (alkylamines or other organic compounds) as structure-directing agents. The gel, which contains highly condensed anions, is usually aged for a certain time below the crystallization temperature. Frequently, this *aging period* is crucial for obtaining a desired product at appropriate rates and with high yield. Moreover, aging may influence the structural type of the synthesized zeolite.[36] To avoid postsynthesis changes of the synthesis product (e.g., by redissolution processes[37]), the reaction is stopped after completion by quenching the autoclave in cold water or in an ice bath. In the as-synthesized zeolite, the negative framework charge is balanced by interstitial alkaline, alkaline earth, and/or alkylammonium ions. The removal of alkaline bases by thorough washing is essential, because residual alkaline bases decrease the thermal stability of the crystal structure or promote a structural collapse of the synthesized zeolite in the final calcination step. Calcination, usually carried out at 550 °C in air for ca. 2 h, is

necessary to remove organic template molecules by thermal decomposition[38,39] and by burning off. SiO_2, a possible coproduct, can be removed from the as-synthesized solid by careful treatment with a NaOH solution at elevated temperatures.[40] The success of synthesis is ascertained by determining the Si/Me^{3+} ratio of the bulk phase by ICP, EDX, etc., or the Si/Me^{3+} ratio of the surface by XPS.

The concentration and kind of cation of the alkaline base influence the structure type of the synthesized molecular sieve. Hydroxides (usually NaOH, sometimes LiOH, KOH, CsOH, and alkaline earth hydroxides) are necessary for the formation of tetrahedral metalate ions $Me(OH)_4^-$ which condense to silicate species incorporating tetrahedrally oxygen-coordinated metal ions such as Al, Ga, Fe, or Co and others. Due to their mineralizing properties, hydroxides cause depolymerization of polycondensed silicate species and hydrolysis of silicon−organic compounds such as tetraethyl orthosilicate.[44] Besides their mineralizing role, alkaline cations play a directing role in the formation of silicate species and can additionally affect zeolite formation by ordering water clusters via their structure-making (Na^+, Li^+) or structure-breaking (K^+, Rb^+, Cs^+ and NH_4^+) properties.[10,44−46] Various ion-exchange processes are applied to transform the template-free zeolite into the standard alkaline (usually Na form)[41−43] or hydrogen form. The latter is obtained after exchanging the interstitial alkaline cations by ammonium ions and their thermal decomposition.

Usually, synthesis gels are aqueous solutions. Water acts as solvent and as a guest molecule. Host−guest interactions stabilize the porous structure of the formed zeolites.

The silicon source, the structure-building component of the zeolites, is mostly a silica−sol, water−glass, silica gel, or SiO_2 of high surface area (>200 m^2/g). In some cases, hydrolyzable silicon−organic compounds, like tetraethyl orthosilicate, are used.

The conditions of chemical and thermal treatment have an important impact on the physicochemical and catalytic properties of the synthesized zeolite.[40]

Me^{3+} ions, which give rise to ion-exchange capacities and to acid sites, act as structure modifiers. Their presence in the gel increases its ionic strength, resulting in the immediate appearance of solid gel units with a network of colloidal particles.[47] To prepare Ga-containing zeolites, the use of reactive $Ga(OH)_4^-$ complex salts is recommended. This way, disturbing influences by additional anions, present in the case of the metal salts, are avoided. Nevertheless, gallium nitrate or sulfate as well as $Ga(CH_3)_3$ have been applied.

B. Role of Templates

Organic template molecules exert a structure-directing influence. Typically, primary, secondary, tertiary, and quarternary amines, alcohols, and crown ethers are used. Obtained zeolite structures are stabilized by the included organic compounds. They increase crystallinity and influence the Si/Me framework ratios. In certain cases, crystallization of a zeolite type fails without the use of a template.

Unlike many T−O−T angles, the Si−O−Si angle within silicate-like compounds is highly flexible.[48,49] Therefore, a great variety of structures with differently sized oxygen rings and their mutual connections is attainable.[50] Silicon-rich framework structures often contain large fractions of oxygen-5-rings, the formation of which is less favored in Me^{3+}-rich zeolites with low-angle Me-O−Si bridges. The angle of Si−O−Si bridges is close to 145°. It exhibits only a low energetic barrier to variations between 135° and 165°. Larger and smaller bridge angles would cause a sharp increase in the energy and are less favored. A study of naturally occurring silicates shows that compounds containing oxygen-4-rings and oxygen-6-rings are abundant, whereas oxygen-5-ring and oxygen-3-ring silicates are rare.[51] The Si−O−Si angles in all these configurations are close to the angle of energy minimization (Figure 5).

By variation of the nature of the organic template, the broad spectrum of silicon-rich zeolites[52,53] with large intertetrahedral angles or other framework structures containing energetically unfavorable T−O−T bridges becomes accessible. Thus, new alumino-[54] and gallophosphate[55] molecular sieve structures could be synthesized.

The template in the synthesis gel can act in different ways:[56] (a) as space-filling species, (b) as a structure-directing agent, or (c) by directly coining the symmetry of the zeolite cage.

Since the surface of silicon-rich zeolites is mainly hydrophobic, the organic will migrate from the hydrophilic aqueous reaction mixture into these regions. With increasing chain length of alkyl groups, the template becomes increasingly hydrophobic. Template molecules thermodynamically stabilize the zeolite structure due to host−guest interaction. This action is similar to that found with intercalation compounds.[8] Additionally, alkylammonium ions can counterbalance negative framework charges such as those of defect SiO^- groups, which may be formed at strained Si−O−Si bridges. There, geometric constraints of the framework require the formation of energetically unfavorable Si−O distances and angles. The interaction of the template with precursors in the gel or in parts of the framework may stabilize and promote the formation of either energetically less favored oxygen-ring structures or of internal not fully interconnected SiO^- defect groups.

Lobo et al.[50] studied the transfer of different alkylammonium ions from an aqueous solution to a chloroform phase as a function of the C/N^+ ratio (Figure 6). The percentage of transfer is a measure for the hydrophobic character of the templates. The authors found that in the range $11 < C/N^+ < 15$, alkylammonium ions show an intermediate position between hydrophilic and hydrophobic behavior. Interestingly, these ions work well as templates and make the crystallization of a great variety of new high-silica molecular sieves possible.[57−59]

Attempts to use templates for the synthesis of chiral molecular sieve structures have failed until now. Adsorbed or incorporated prochiral or chiral molecules show an unexpected high mobility[36,47] despite their location at specific sites in the zeolite

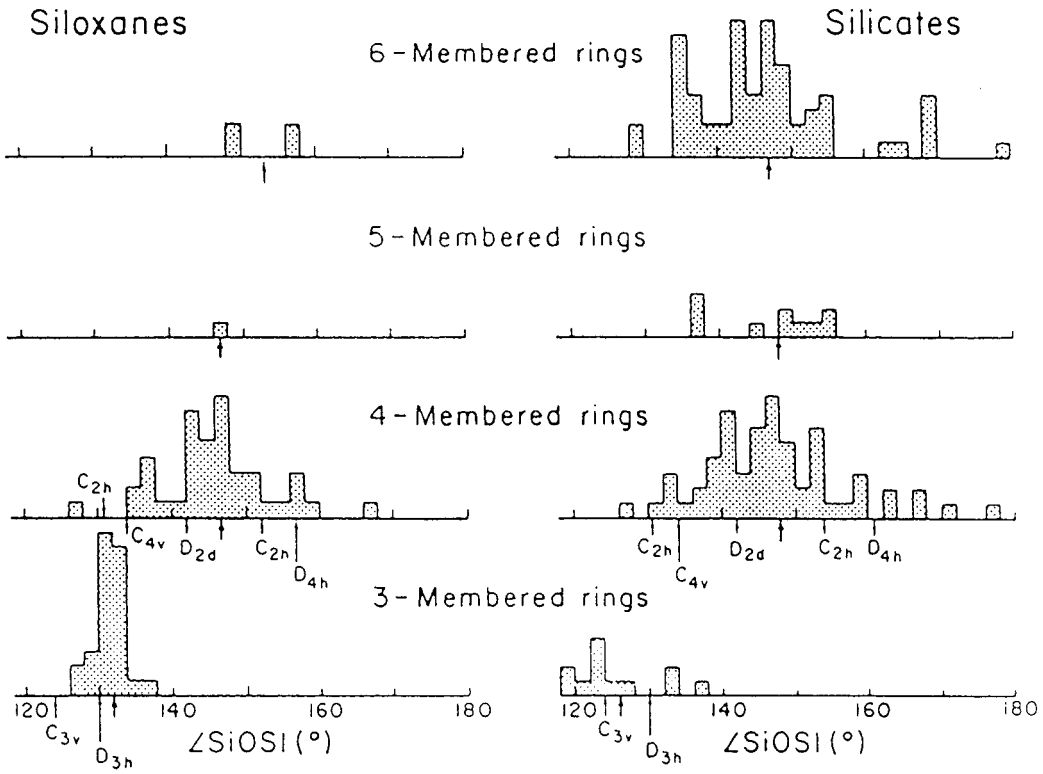

Figure 5. Si−O−Si angle frequency distributions for Si-containing tetrahedral rings observed for silicates and siloxanes. The bold arrows indicate the mean values, and the other arrows with Schoenflies notation mark the Si−O−Si angles calculated for the ab initio optimized geometries for cyclotrisiloxane and cyclotetrasiloxane. (Reprinted with permission from ref 51. Copyright 1981 Mineralogical Society of America.)

cavity.[60,61] Such high mobility is detrimental to the actual templating function.

From these considerations, the importance of the templates for the synthesis of new high-silica zeolites and of other framework structures containing energetically unfavorable T−O−T bridges such as aluminophosphate and gallophosphate molecular sieves is understandable. However, a detailed understanding of the role of the template during synthesis is not yet achieved.

C. Mechanism and Kinetics of the Crystallization Process

One important step that occurs during crystallization is the (partial) dissolution or depolymerization of the silica.[62] Different chainlike, cyclic, double-ring, and other oligomeric silicate species are formed.[36,45−47,62,63] In the range of alkalinity $9 < pH < 12$, where synthesis of zeolites usually proceeds, silica chemistry is characterized by simultaneous polymerization−depolymerization processes. The coordination number of silicon in these anionic silicate species is four. Due to the hydrolytic action of hydroxides OH^-, these species are negatively charged:

$$[Si_xO_y(OH)_z] + OH^- \rightarrow [Si_xO_y(OH)_{z-1}O]^- + H_2O \quad (1)$$

The presence of high-valent cations such as Ga^{3+} leads to a decrease in the solubility of silicate anions due to coagulation and condensation.[11,64] Primarily, a heteropolymerization reaction of the type catalyzed by hydroxyl ions occurs:

$$\begin{array}{l} \text{-Me—OH} \\ \quad | \\ \text{O} + \text{Si}_n\text{O}_m(\text{OH})_4 \\ \quad | \\ \text{-Me—OH} \end{array} \rightarrow \begin{array}{l} \text{-Me—O} \\ \quad | \quad \backslash \\ \text{O} \quad \text{Si}_n\text{O}_m(\text{OH})_2 + 2\,\text{H}_2\text{O} \\ \quad | \quad / \\ \text{-Me—O} \end{array} \quad (2)$$

It is still a matter of debate whether crystallization proceeds in the liquid or solid phase and what the properties and the function of the precursor gel are like.[56,65,66] There is some indication that formation and transformation of the precursor gel play an important role in the crystallization of MFI-type zeolites.[67,68] However, a direct liquid-phase crystallization has been reported also.[69] Three possible mechanisms of zeolite formation from these gels have been hypothetically established: (1) Solid-phase transformation of the precipitated solid gel without contribution of the surrounding sol−gel phase;[70] (2) Rearrangement processes including surface diffusion mechanism of reactive species within the gels;[71] (3) Crystallization of the zeolite from the liquid phase (probably from special silicate anions which represent subunits by themselves or are easily rearranged into different subunits) where the cations play an important role.[72,73]

Precursor aggregates, appearing during nucleation and subsequent rearrangement in the course of crystal growth of silicalite-1 in the liquid phase, were

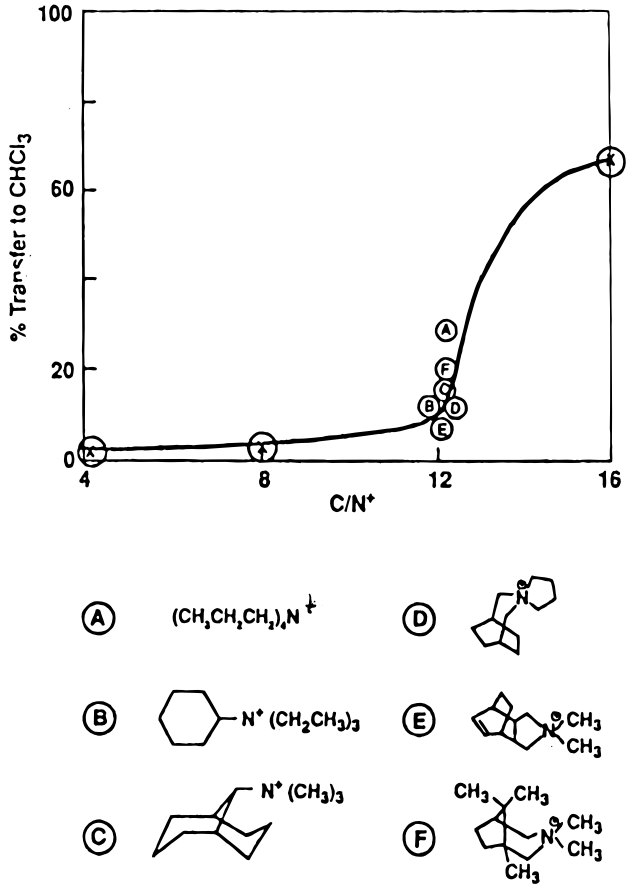

Figure 6. Partition of quarternary organic ammonium ions between water and chloroform depending on the carbon number of the hydrophobic rest (expressed as C/N^+ ratio). $C/N^+ = 4$ tetramethylammonium, $C/N^+ = 8$ tetraethylammonium, $C/N^+ = 16$ tetrabutylammonium. (Reprinted with permission from ref 50. Copyright 1995 Kluwer Academic Publishers.)

studied in situ by low- and wide-angle X-ray diffraction (SAXS and WAXS).[65] Crystallization starts with the formation of large aggregates with rough (fractal) surfaces and is completed forming crystals with energetically favorable smooth external surfaces proved by light scattering experiments.[74] Hence, crystallization has to be understood as a continuous process with overlapping areas of nucleation and crystallization.[75−79] This kind of mechanism explains why the rate of formation of nuclei passes through a maximum.

The process in the liquid phase is not really homogeneous but involves complex transformation and reorganization steps (Figure 7). SAXS and WAXS experiments show that both, "homogeneous" and "heterogeneous" crystallization are involved. They are connected with the presence of an intermediate gel phase. In heterogeneous systems, the precipitated solid gel must be dissolved before zeolite crystallization starts.[65]

Kinetics of the crystallization process are often represented by S-shaped curves.[80] Although carefully studied, the derived values of apparent energies of nucleation and crystallization should be considered with caution. Zeolite crystallization experiments are quite commonly analyzed by means of a "crystallization curve" which represents the evolution of zeolite

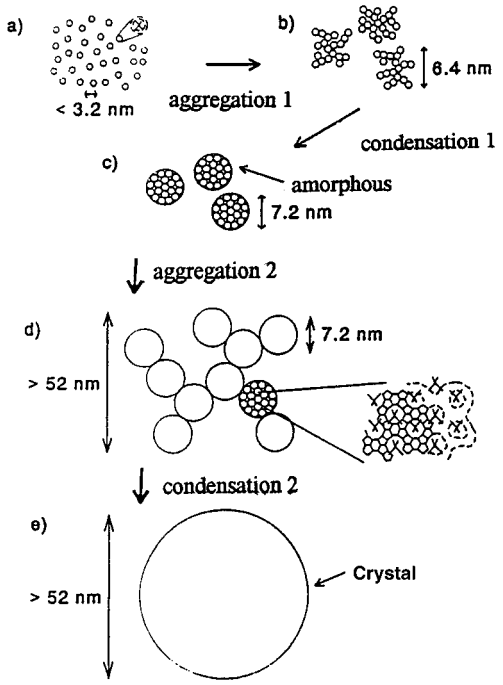

Figure 7. Possible steps of zeolite formation in the gel: (a) silicalite-1/TPA cluster in solution, (b) primary aggregates (fractural dimension) of silicalite-1/TPA clusters (6.4 nm), (c) condensation of primary aggregates, (d) aggregation of condensed particles into secondary particles of fractural dimension followed by crystallization, (e) condensation of secondary aggregates and crystal growth. (Reprinted with permission from ref 65. Copyright 1995 VCH Verlagsgesellschaft mbH.)

mass in the batch in the course of time. This curve involves the determination of the induction time and of the slope of the crystallization curve to quantify nucleation and crystallization rates.

D. Other Synthesis Techniques

1. Rapid Crystallization

This method comprises special experimental measures during zeolite synthesis, which have proved to reduce the crystallization time considerably, simultaneously guaranteeing a uniform crystal size. The most pronounced effect is observed when the precipitated gel is ball-milled and hydrothermal synthesis is performed by a temperature-programmed procedure. A structural series of ZSM-5 zeolites has been synthesized following features of preparation.[81,82] (i) The crystallization process is performed nonisothermally, i.e., the temperature is raised from 160 to 310 °C at a constant heating rate of 0.16 deg/min under constant stirring of the autoclave at 60 rpm. (ii) After centrifugal separation of the gel mixture from the mother liquor, the gel is mechanically ground in a mortar and then returned to the mother liquor. The nonisothermal procedure for crystallization is maintained. (iii) Addition and combination of solutions are modified in order to minimize local differences in composition and to maintain constant pH values and temperatures during the precipitation.

The combined application of all variants, which is also applied for the synthesis of metallosilicates, is actually understood by the term "rapid crystallization

method". Additionally, metal-preloaded seed materials (supported metal salts on α and γ alumina) may be used in the process.

2. Synthesis from Nonalkaline Media

To prevent the presence of Na or any other alkali ion, the NH_4 forms of high-silica MFI zeolites with heteroatom-containing frameworks (boron, aluminum, and gallium) have been synthesized directly from an alkali-free system in the presence of fluoride ions by Dwyer et al.[83]

Using this method, a fairly high degree of substitution by heteroatoms can also be achieved in the gallium−silica system. The composition of products can be controlled by modifying the fluoride concentration and the pH value of the reaction mixtures. Fluoride ions are able to increase the solubility of the raw material sources[84] and keep the crystallization environment at pH < 7. This way, the TPA^+/NH_4^+ form of ZSM-5 was obtained directly in large crystals and metal-containing zeolites can be prepared conveniently.[85]

Axon and Klinowski[86] demonstrated by ^{29}Si MAS NMR and nitrogen adsorption isotherms that MFI zeolites synthesized by the "fluoride" method are virtually free from structural defects. Such defects (e.g., internal silanol groups) are usually present in crystals prepared by conventional synthesis methods and can be removed by a longer hydrothermal treatment only, as reported for ZSM-5 by Dessau et al.[87] Fluoride anions may turn out to be a multifunctional tool for the synthesis of microporous gallophosphate solids as will be shown later.

3. Template-Free Synthesis Routes

A template-free synthesis of zeolite ZSM-5[88−91] and of Ga−silicates with MFI structure has been reported. Depending on the surface area of the silica source, the dense silica phase of the synthesized gallosilicate may amount up to 50%. Its fraction, however, could be reduced by decreasing the surface area of the silica source[91] drastically from 380 to 22 m^2. The highest [Ga]-MFI contents (70%) were achieved with molar ratios of $SiO_2/Ga_2O_3 = 119-140$. Formation of dense silica could be suppressed by using an X-ray amorphous seeding gel (i.e., a gallosilicate gel which was aged for several days at a temperature between 20 and 90 °C). Synthesis was performed by the addition of NaOH, amorphous silica, $GaCl_3$ solution, and water to the seeding gel. Hydrothermal treatment yields pure Ga-MFI crystals with almost homogeneous Ga distribution (electron microprobe analysis) with Ga completely in framework positions, as follows from the balance between Brønsted acidic sites estimated by ^1H MAS NMR and the chemically determined total concentration.

4. Microwave-Supported Synthesis

Recently, microwave heating has been applied increasingly to synthesize zeolites. By heating at a frequency of 2.45 GHz, hindered rotations of the water molecules are promoted[92] and the energy of microwave radiation is converted into heat by internal friction. A selective heating of areas containing water is achieved. Due to "internal" warming up, the heating rate is considerably increased and heat gradients occurring in the period of temperature rise are diminished. This way, a rapid temperature increase of the synthesis gel is obtained and synthesis times are reduced substantially. Zeolites A and X, hydroxy sodalite, and TMA sodalite were prepared in very short times. Effects on isomorphous substitution and on the Si/Me framework ratio (Zeolite Y) have also been reported. Metal-substituted aluminophosphate molecular sieves could be synthesized in 1 min instead of hours. Microwave synthesis of gallosilicate zeolites has not been reported so far. However, the gallophosphate large-pore molecular sieve cloverite has been synthesized advantageously by this technique.

The benefits of microwave heating are as follows: (i) An increased condensation rate according to

$$Si-OH\cdots HO\text{-}Me \rightarrow Si-O-Me + H_2O \qquad (3)$$

owing to a faster transport of released water (volume heating). (ii) Availability of diversified modifications of synthesis conditions by varying the time and regime of microwave radiation (continuous and pulsed radiation, temperature regime, controlled and reproducible energy input). (iii) Fast supersaturation by the rapid dissolution of precipitated gels due to volumetric heating.

Application of microwave heating is limited by the penetration depth of ca. 2.5 cm in the aqueous solution.

III. Gallosilicates and Gallium-Modified Zeolites

A. Gallium Framework Substitution via Hydrothermal Crystallization

1. Principles

Trivalent gallium incorporated into the framework is the origin of the negative charge of the lattice which gives rise to Brønsted acidic Si−OH−Ga bridging hydroxyl groups and hence to ion-exchange properties. In Ga-rich zeolites, the GaO_4 tetrahedra may act as a framework builder by themselves.

The knowledge about chemical processes occurring during the synthesis of gallosilicate zeolites is still incomplete. By analogy with results from studies of aluminosilicate solutions, it can be assumed that the gallosilicate formation with respect to kinetics and structure type is influenced by the existence of various (gallo)silicate species in the gel.[93,94] The distribution among them depends strongly on the pH value of the solution, the composition of the gel, and the nature of the hydroxide. The latter reflects the influence of cations and organics (templates) on the structuring. A thorough understanding of the chemistry between silicate and gallate anions in dilute solutions might be a first step toward the understanding of the zeolitization of gallosilicates as a whole.

With regard to its chemical behavior, gallium displays a strong similarity to aluminum[16,79] exhibiting, however, a higher basicity. Gallium is mainly

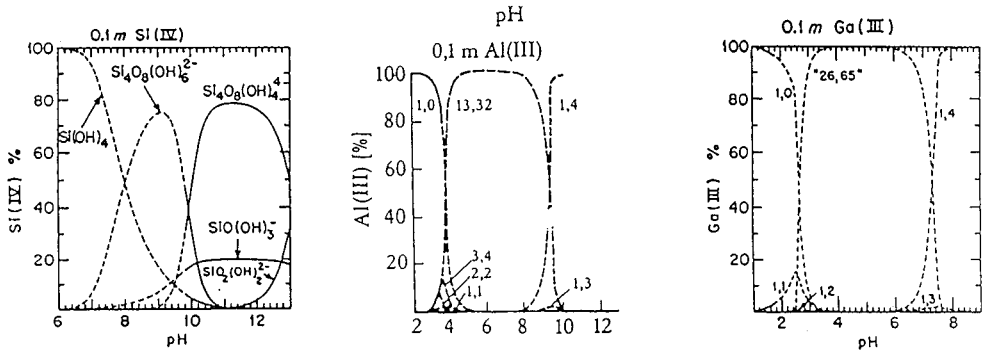

Figure 8. Distribution of Si species in a 0.1 M Si(IV) solution and of $Me_x(OH)_y^{(3x-y)+}$ (Me = Al, Ga) species in a 0.1 M Al(III) and 0.1 M Ga(III) solution, respectively, at 25 °C depending on the pH value. "13,32" and "26,65" indicate hypothetical polymeric species which fit the data. (Reprinted with permission from ref 16. Copyright 1986 Robert E. Krieger Publishing Company.)

present as $Ga(OH)_4^-$ ions in the alkaline solutions of synthesis gels. Like aluminum, gallium may also form more complex heterocations such as GaO(OH), $Ga(OH)_2^+$, etc. in alkaline solutions (Figure 8). It is apparent that higher condensed species may precipitate or form more complex gallosilicate ions. Some of them are not involved into zeolite formation. This is found, in particular, for high-silica zeolites of the ZSM type.

NMR studies on aluminum-containing zeolites revealed that tetrahedrally coordinated silicon ions may be connected to 1−4 aluminum atoms via oxygen bridges (second coordination sphere) forming three-dimensional 4-fold-connected $SiO_{4/2}$ frameworks.[95] This was recently confirmed also for gallosilicate frameworks, where $Si(OGa)^n$ groups with $n = 1-4$ were found.[96−101] Each gallium is connected (via oxygen bridges) to silicon atoms in the second coordination sphere. In accordance with the Loewenstein avoidance rule,[100] Ga−O−Ga framework linkages have not be detected so far. Computation has shown that the formation of Si−O−Me bridges is energetically favored over the formation of Si−O−Si bridges.[101] The sum of the bond energies of two Al−O−Si groups is lower than that of one Al−O−Al and one Si−O−Si group. This is reflected in the precipitation behavior of metal hydrosilicates during the dissolution of complex silicates.[102] As long as silicon is available, Si−O−Ga bridges will be formed. The number n in $Si(OGa)_n$ depends on the gallium content of the synthesis gel, i.e., increasing gallium content is expected to give lower Si/Ga ratios in the zeolites. Whether Ga or Al is distributed statistically in the zeolite framework is not clear. The intensity ratios of Si NMR signals belonging to the different $Si(OMe)_n$ groups ($n = 1-4$) can be simulated assuming both a statistical and an ordered arrangement of Ga atoms.[103−106] It is supposed that the conditions of the hydrothermal crystallization and/or of the following postsynthesis treatment may have an essential influence on the distribution of the different kinds of atoms within the framework.

Depolymerization of silica as well as $Ga(OH)_4^-$ formation consume OH^- ions causing a drop of the pH value of the gel. On the other hand, preceding condensation, crystal growth and Ga incorporation release OH^- ions. All these processes may occur simultaneously. Generally, the gallosilicate species are less soluble than pure silicate species and precipitate easily.[102]

Basic solutions favor the formation of gallate ions $Ga(OH)_4^-$ which are essential for a successful incorporation of gallium. Gallosilicate solutions obtained by dissolving fumed silica in aqueous TPAOH or TMAOH followed by addition of gallium nitrate solution were investigated by means of ^{29}Si and ^{71}Ga NMR spectroscopy at room temperature to clarify the ratio of silicate and gallosilicate species and their nature.[107] The Si/Ga ratios of the gels varied from 5 to ∞. Si/TPA_2O ratios (TPA_2O = tetrapropylammonium oxide) were held between 0.05 and 2. Under these conditions, no solid gel precipitates. Immediately after the addition of small amounts of gallium to the silicate solution, new peaks appear in the NMR spectra that can be attributed to gallosilicate anions. This finding supports and explains IR results which conclusively prove the formation of Ga−O−Si gallosiloxane groups in the amorphous hydrogel during the nucleation period[108] already. With gallium, only anions with Si(1Ga) groups are observed. Aluminum, in contrast, is incorporated forming a broad variety of anions, among them Si(1Al) and Si(2Al) groups. Thus, higher contents of the trivalent cation are gained. Consequently, attainable maximum Ga contents of silicon-rich gallosilicate zeolites should be lower than Al contents of comparable aluminosilicate structures. Nevertheless, Ga-rich zeolites do exist.

In gallosilicate solutions,[107] mainly three-membered rings (S3R), branched S3R, and double three-membered rings (D3R) are detectable (Figure 9). The latter are extremely stable and become dominant at temperatures commonly applied for zeolite synthesis. In contrast to the corresponding aluminosilicate solutions, linear dimers and trimers could not be observed.[94] The ^{29}Si NMR and ^{71}Ga NMR signals broaden after addition of Ga or Si compounds to the solutions. The ^{71}Ga signal of monomeric gallate $Ga(OH)_4^-$ anions in aqueous alkaline solution appears at 222 ppm. The upfield shift of the ^{71}Ga resonance to 215 ppm after silicon addition is tentatively assigned to the formation of Ga connected to 0 or 1 siloxane bond. The broad signal at <180 ppm is attributed to Ga connected with 2 or 3(4) siloxane bonds. Signal broadening is assumed to be caused by a rapid exchange of gallium and silicon atoms between gallosilicate species and solution. Remarkably,

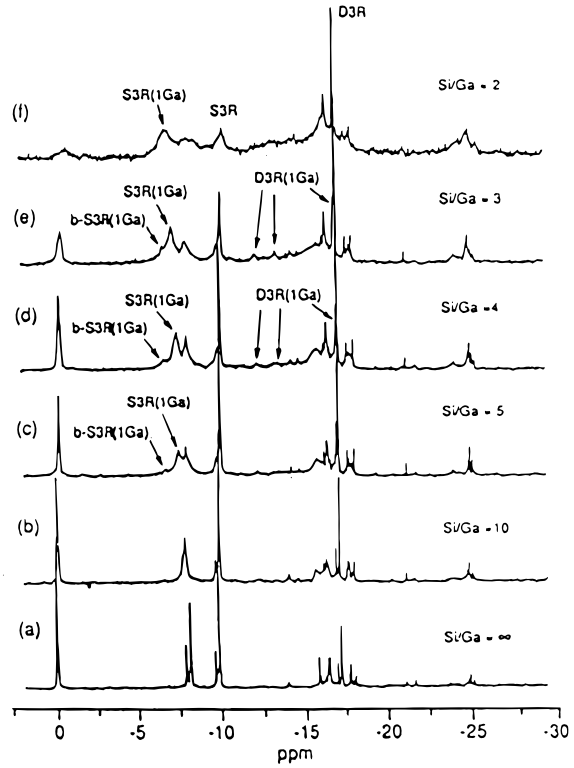

Figure 9. ^{29}Si NMR spectra of tetrapropylammonium (TPA) gallosilicate solutions prepared by mixing fumed silica dissolved in 40 wt % aqueous TPAOH and aqueous $Ga(NO_3)_3$; $[SiO_2]/[(TPA)_2O]$ molar ratio = 1: (a) Si/Ga molar ratio = ∞, (b) Si/Ga = 10, (c) Si/Ga = 5, (d) Si/Ga = 4, (e) Si/Ga = 3, (f) Si/Ga = 2. Ga incorporates into single three rings (S3R), branched S3R (b-S3R), and double three-ring (D3R) anions. Spectra recorded at 0 °C. (Reprinted with permission from ref 107. Copyright 1992 American Chemical Society.)

this exchange would be faster than in aluminosilicate solutions. This conclusion, however, must be considered with caution because field inhomogenities, ion pairing, and other factors may contribute to line broadening.[109] The observed broadening (and shift of the ^{71}Ga signal) is closely related to the silicon content and the basicity of the gallosilicate gels (Figure 10). Broadening increases with growing silicon and decreasing TPAOH contents, indicating that both are related to the connectivity of gallosilicate species. Higher silicon contents favor the formation of gallosilicate anions at the expense of monomeric gallate anions. Lower basicity enhances the condensation of low condensed silicates. Thus, line broadening might be an effect of the distortion of the Si−O−Si or Si−O−T bridges in the gallosilicate species. Generally, variations in bond lengths and angles are known to cause ^{29}Si line shifts and broadening. The Si−O−Ga angle (≈120°) is rather low.

In contrast to aluminosilicate solutions, the formation of higher oligomers of gallosilicates such as D4R (1Ga) is not observed. This might be explained by the long Ga−O bond length of $r_{Ga-O} \approx 1.9$ Å in comparison with the Al−O and Si−O bond lengths of $r_{Al-O} \approx 1.77$ Å and $r_{Si-O} \approx 1.62$ Å. The resulting strain makes the D4R (1Ga) anion rather unstable.[110]

Results can be explained by a simple set of reactions. First, SiO_2 dissolves in the alkaline solution

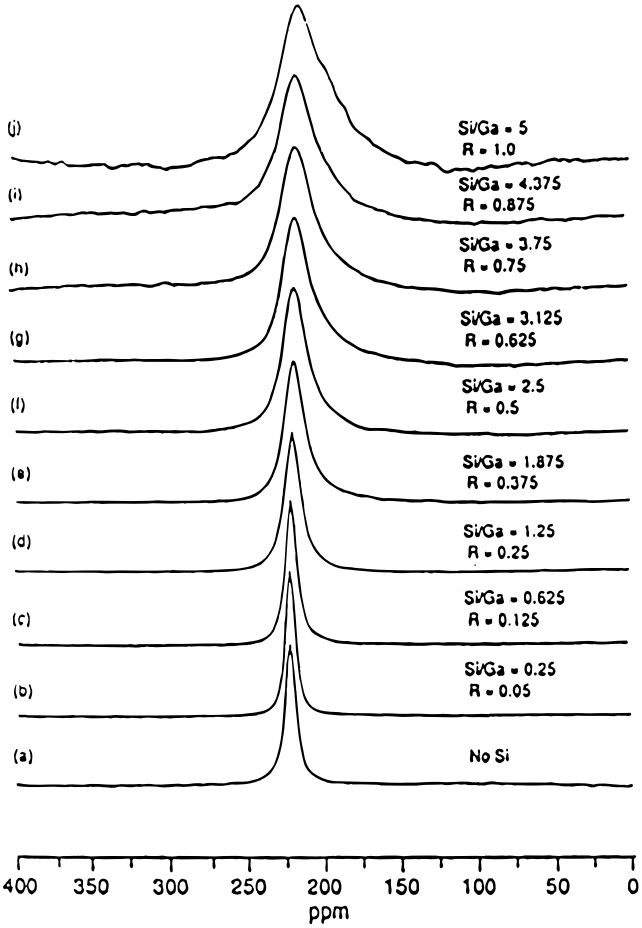

Figure 10. ^{71}Ga NMR spectra of tetrapropylammonium (TPA) gallosilicate solutions taken at 22 °C: 0. 4 mol % Ga, 2 mol % $(TPA)_2O$, (a) no Si, (b) $R = 0.05$, Si/Ga molar ratio = 0.25, (c) $R = 0.125$, Si/Ga = 0.625, (d) $R = 0.25$, Si/Ga = 1.25, (e) $R = 0.375$, Si/Ga = 1.875, (f) $R = 0.5$, Si/Ga = 2.5, (g) $R = 0.625$, Si/Ga 3.125, (h) $R = 0.75$, Si/Ga = 3.75, (i) $R = 0.875$, Si/Ga = 4.375, (j) $R = 1.0$, Si/Ga = 5. ^{71}Ga spectral frequencies are referenced to a 1 M aqueous $Ga(NO_3)_3$ solution. $R = [SiO_2]/[(TPA)_2O]$. (Reprinted with permission from ref 107. Copyright 1992 American Chemical Society.)

yielding monomeric silicate anions (S_1^{x-}) according to

$$SiO_2 + xOH^- + (2 - x)H_2O \leftrightarrow [SiO_x(OH)_{4-x}]^{x-},\ x = 2 \quad (4)$$

These monomers polymerize via condensation of silanol groups

$$\equiv Si-OH + HO-Si\equiv \rightarrow \equiv Si-O-Si\equiv + H_2O \quad (5)$$

and yield oligomeric species S_n^{x-}. Subsequently, gallate anions (Ga_1^-) react with these silicate species

$$Ga_1^- + mS_n^{x-} \rightarrow (Ga_1(S_n)_m)^{(x+1)-} \quad (6)$$

releasing hydroxide groups. Thus, the influence of pH, gel composition, and temperature on the distribution of silicate and gallosilicate species is explained.

Rapid formation of gallosilicate species within silicon-rich synthesis gels is also evidenced by EXAFS and XANES studies. In the aqueous as well as in the solid gel phase, gallium is found in tetrahedral coordination only. The EXAFS spectra are very similar to those of crystalline zeolites, indicating that their gallosilicate networks in the respective states are comparable. Only small deviations in the XANES fingerprints indicate some differences in the local environment of gallium in the different states.[111] Ga EXAFS spectra of silicon-rich gallosilicate gels are quite different from those of pure gallate solutions and of solid Ga_2O_3, indicating the absence of gallate or oxidic species in the gel. Ga−O−Ga bridges are absent in the dissolved state already, i.e., the neighbors of gallium are silicon atoms only. Gallium atoms are isolated and highly dispersed even at the very beginning of the hydrothermal reaction.[112]

In contrast, gallium-rich (low-silicon) gel mixtures with Si/Ga ratios lower than 2, e.g., gels used for gallofaujasite synthesis, also contain free gallate anions as well as gallosilicate species with 1−2 siloxane linkages.[107] Then, the formation of gallo-rich zeolite structures is enabled. Gallosilicate faujasites exhibit the same Si/Me^{3+} framework ratios as the corresponding aluminosilicates. No D4R is found in the liquid gallosilicate gels, not even after addition of TMA/DMSO, which is known to support D4R formation. This finding agrees with conclusions drawn by Lechert and Kocirik.[113] From their kinetic (model) studies of faujasite-type zeolites, they concluded that crystal growth in low-silicon (Al-rich) zeolites proceeds by a stepwise deposition of monomeric low-condensed species rather than of secondary subunits (aggregates) on the crystal faces.

In summary, silicate and gallate anions of the gel react very rapidly. The reactions are similar to those appearing in aluminosilicate solutions and follow the same patterns if the silica, metal, or base contents are changed. Remarkable differences, surely due to structural constraints (size of gallium, Ga−O distance, and Si−O−Ga bond angle), however, become apparent: (a) a tendency to form strained anions of S3R-type (restricted gallate-silicate reaction), (b) a lower degree of gallium incorporation, and (c) the absence of larger silicate oligomers with gallium. In addition, alumino- and gallosilicate solutions may differ in the distribution of different types of species. It has to be concluded that the synthesis of gallosilicate zeolites is more sensitive to gel composition and preparation conditions.

2. The Temporal Course of Crystallization

Studies on the temporal course of the crystallization process leading to gallium-substituted zeolites are relatively rare. The majority of available studies[37,108,114−116] deal with MFI-type zeolites (Figure 11). A detailed knowledge on the crystallization steps is essential for the optimization of synthesis parameters (like time, temperature, and composition), for the replacement of expensive gel ingredients, and for the control of the synthesis procedure. With respect to isomorphous substitution, it is of interest to investigate whether the substitution of aluminum or

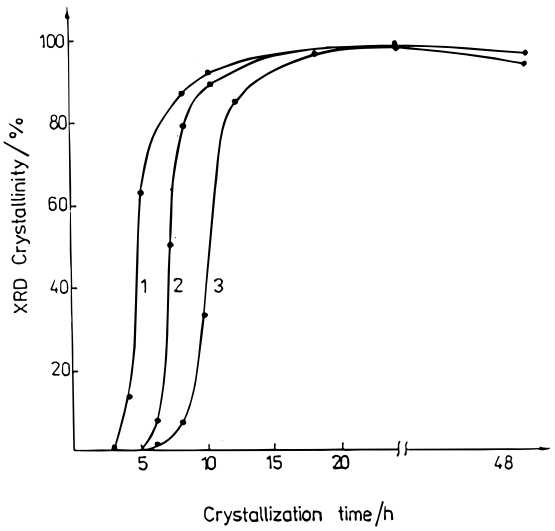

Figure 11. Influence of the Si/Ga ratio in the synthesis gel on the temporal course of crystallization of [Ga]-ZSM-5: (1) Si/Ga = 100, (2) Si/Ga = 25, (3) Si/Ga = 50. (Reprinted with permission from ref 108. Copyright 1992 Akademie Verlag GmbH.)

silicon by the larger gallium atoms leads to any changes in the crystallization process. A "disruptive nature" of isomorphous substitution was proposed from comparative studies on MFI-type zeolites with and without Al substitution ([Al]-ZSM-5 and silicalite-1, respectively).[43] Crystallization studies[5] have shown that the presence of aluminum hinders the growth of MFI-type structures. A negative impact might be indicated by increased values of the activation energies of nucleation and crystallization.

Difficulties and uncertainties in comparing crystallization results reported in the literature arise mostly from varying experimental parameters (i.e., different chemicals and synthesis conditions) and from the nonconformity of the criteria applied to evaluate the obtained data. Apparently, [Ga]-ZSM-5 zeolites of identical chemical composition (often expressed in terms of the Si/Ga ratios) can differ in the actual degree of isomorphous substitution. The extent of isomorphous substitution of high-silica zeolites is not easily determined.

Awate et al.[114] investigated the course of crystallization of gallosilicates with MFI structure from sodium gallosilicate gels using triethyl-*n*-butylammonium bromide (Si/Ga = 20, 42, 200, ∞; T = 160, 180, and 200 °C). The products were characterized by XRD, mid-IR, TG-DTA, as well as ^{29}Si and ^{71}Ga NMR in order to follow gallium incorporation into the framework. Isomorphous substitution by gallium is evidenced by the increase of the unit cell volume from 5280 to 5400 Å. The Si/Ga ratio of the product was close to that in the gel. Crystallization kinetics were analyzed by the Avarami−Erofeev equation[117] $\ln[1/(1-\alpha)] = kt^m$, with α and t being the fractional conversion into zeolite and the synthesis time, respectively. k and m are constants. k, which is related to the velocity of crystallization, increases and m decreases with rising temperature. Temperature mainly affects the rate of nucleation due to the increased dissolution of silicate/gallosilicate species and to the consequently enhanced supersaturation

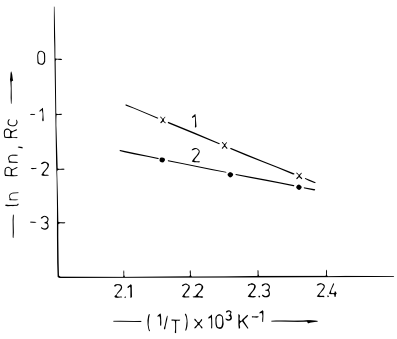

Figure 12. Arrhenius plots for (1) nucleation and (2) crystallization of [Ga]-ZSM-5 (Si/Ga = 50). Apparent activation energies for nucleation and crystallization amount to 42.5 and 20.4 kJ/mol, respectively. (Reprinted with permission from ref 108. Copyright 1992 Akademie Verlag GmbH.)

Table 3. Activation Energies of Crystallization (E_c) and Nucleation (E_n) of Al-, Ga-, and Fe-Substituted Zeolite ZSM-5[115]

	E_c (kJ/mol)	E_n (kJ/mol)
[Al]-ZSM-5	78.6	118.0
[Ga]-ZSM-5	94.3	155.7
[Fe]-ZSM-5	92.5	145.0

of the synthesis gel. This is in agreement with general expectations of the temperature dependence of the nucleation and the crystallization process (Figure 12).[108]

Values of the activation energies of nucleation E_n = 155.7 kJ/mol and of crystallization E_c = 94.3 kJ/mol are obtained from the Arrhenius plots of $\ln(1/\theta)$, $\ln(K)$ vs $1/T$. θ represents the induction period and K is the point of the crystallization curve, when 50% of crystallization is completed. Derived energies (Table 3) are substantially higher than those of [Al]-ZSM-5 and [Fe]-ZSM-5 crystallized under similar conditions.[115]

Increasing radii of the substituting atoms give rise to growing activation energies, indicating that crystallization is rendered more difficult in the order Al > Fe > Ga. It is considered that the nucleation rate depends on the nature of the metal cations and on their ability to condense with silicate species. This finding may evidence the "disruptive" nature of metal incorporation into the silicate framework. After 5 h of crystallization, Si/Ga = 39 is reached. A further increase of crystallization time (to ca. 28 h) results in a slight increase of the gallium content in the solid only (Si/Ga ratio = 37). The Ga/Na ratio in the solid changes distinctly after the onset of crystal growth, indicating a progressive incorporation of the template during the formation of the gallosilicates. Triethylbutylammonium (TEBA) ions compete with sodium ions for the compensation of the negative framework charge created by the incorporated Ga. This suggests that the same liquid-phase transportation mechanism may be operative during formation of [Ga]-ZSM-5 crystals as has been reported for [Al]-ZSM-5.[118]

An increase of the relative nucleation time of MFI-type zeolites after addition of different heteroatoms (Me^{3+}) was also reported.[116] Crystallization was carried out in the temperature range from 150 to 200 °C using hexamethylendiamine as template. Typically, the Si/Me gel ratios varied from 10 to 35. Besides gallium, B, Al, In, Fe, Ge, Sn, Ti, Zr, V, Cr, Mo, W, and Mn were included for comparison. The authors considered the influence of the different elements on the rates of the steps gel dissolution, nucleation, and the crystal growth rate using a kinetic model of crystallization.

In this system, nucleation rate decreases in the order B > Al > Ga > Fe. The rate of crystal growth is related to the extent of gel dissolution. According to the liquid-phase transportation mechanism of the formation of zeolites, the dissolution of the solid gel phase is important for the growth of zeolite crystals. In contrast, the nucleation depends mainly on the nature of the metal species involved in the nucleation reaction. Metal species may also influence the polymeric state of silicates. This reaction is described by the condensation of the general type

$$\text{Me}-\text{OH} + \text{HO}-\text{Si}\equiv \rightarrow \equiv\text{Me-O}-\text{Si}\equiv + \text{H}_2\text{O} \quad (7)$$

A relatively fast crystallization of [Ga]-ZSM-5 has been reported by Gianetto et al.[119] They compared the rates of crystallization for [Al]-ZSM-5 and [Ga]-ZSM-5 (Si/Al and Si/Ga ratios amounting to 58 and 60, respectively) at 170 °C from sodium aluminosilicate/gallosilicate gels containing tetrapropylammonium bromide. The pH value of nearly 9 adjusted by the addition of sulfuric acid guaranteed optimal condensation of Al, Ga, and Si oligomers and enhanced nucleation and growth of zeolite crystals. [Ga]-ZSM-5 crystallized more rapidly than [Al]-ZSM-5 and exhibited a higher XRD crystallinity. Incorporation of both elements into tetrahedral framework positions is proven by the shift of IR framework vibration bands to lower wavenumbers. The antisymmetric vibration band is shifted from 1112 (silicalite-1) to 1100 cm^{-1} for [Al]-ZSM-5 and to ca. 1090 cm^{-1} for [Ga]-ZSM-5 (Figure 13). Tetrahedral coordination of Ga is also revealed by ^{71}Ga MAS NMR spectroscopy. The differences in the crystallization are discussed in terms of a slightly different solution chemistry of aluminate and gallate ions. Free gallate ions are assumed to be more stable than aluminate ions.[120] Aluminate ions also tend to form dimeric, trimeric, and polymeric species in solutions, whereas gallate ions are more stable in the monomeric state. Differences in behavior are explained by the polarizing effect of d^{10} electrons of Ga^{3+} which is supposed to enhance the tendency toward tetrahedral coordination of Ga, although the size of Ga is larger than that of aluminum.[121] Recent studies on the chemistry of pure aluminate solutions, however, have shown that aluminate forms polymeric anions in concentrated solutions only.

Formation of more stable Al−TPA complexes has also been discussed to explain the different crystallization behavior.[122] Such complexes should only react slowly with silicate species. In contrast, gallium forms very stable and reactive monomeric gallate anions under basic conditions.[123] Other studies suggest the partial oligomerization of Ga^{3+} ions[16] forming a $[GaO_4Ga_{12}(OH)_{24}(H_2O)_{12}]^{7+}$ polyoxo cation upon hydrolysis in alkaline solutions.[124] So far, NMR

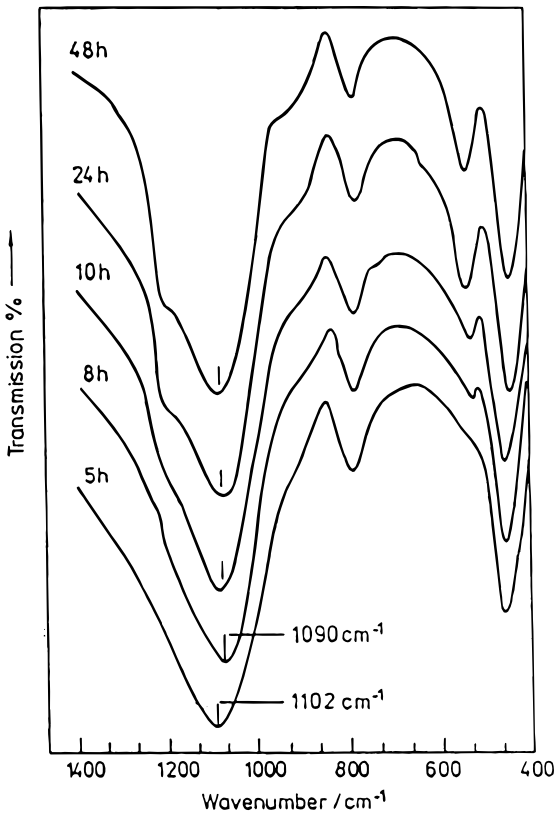

Figure 13. IR lattice vibration spectra of [Ga]-ZSM-5 at various synthesis times. (Reprinted with permission from ref 108. Copyright 1992 Akademie Verlag GmbH.)

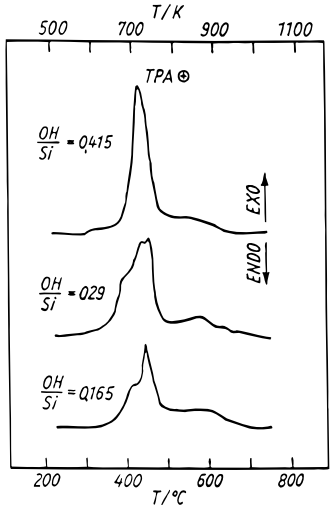

Figure 14. DTA curves of as-synthesized [Ga]-ZSM-5 crystallized from gels with different alkalinity. (Reprinted with permission from ref 125. Copyright 1991 Akademie Verlag GmbH.)

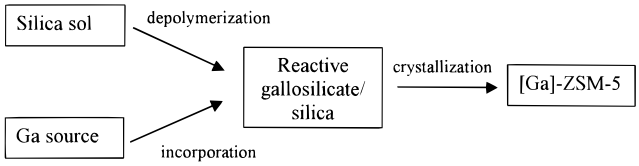

Figure 15. Scheme of [Ga]-ZSM-5 crystallization. (Reprinted with permission from ref 125. Copyright 1991 Akademie Verlag GmbH.)

investigations of TPA−aluminosilicate solutions, however, do not support this idea.[94] Unfortunately, results cannot be compared directly because compositions and temperatures of solutions studied by NMR were substantially different from those used for zeolite synthesis. To optimize synthesis conditions in the presence of tetrapropylammonium bromide as a template, Kosslick et al.[125,126] studied the influence of the Si/Ga ratio, alkalinity of the starting gel, and synthesis temperature on crystallinity, synthesis yield, and Ga distribution in Ga-ZSM-5. A strong influence of the OH^- concentration on the synthesis efficiency is found and discussed in terms of an increased depolymerization of the precipitated gel yielding low condensed "reactive" silica species. Hydroxide concentrations that are too high as well as temperatures >170 °C lead to an opposite effect. Monomeric silicic acid is formed, which is not suitable for zeolite crystallization. Additionally, the hydroxide concentration affects the nature of the reaction product with respect to the distribution of gallium in the ZSM-5 framework. The DTA peak of template decomposition (Figure 14), which is clearly related to the Si/Ga framework ratio, often has to be split into several maxima indicating a heterogeneous distribution of Ga atoms in the crystals or a simultaneous occurrence of crystals with different Si/Ga framework ratios within one synthesis product.[125] It was concluded that the rates of depolymerization and condensation of silica species and the rate of Ga incorporation into silicate species should be of the same order of magnitude at optimum crystallization conditions (Figure 15).

In summary, many factors have to be taken into account and single results should be considered with caution if the influence of gallium framework substitution on the course of crystallization of zeolites is to be described generally.

3. Stability of Gallium in Tetrahedral Framework Positions

Usually calcination is the last step in zeolite synthesis, after the organic template of the as-synthesized product has been decomposed thermally and NH_4^+ ions introduced by the ion exchange have been destroyed, provided that the H^+ form of the zeolite is the desired product. Removal of the template and deammoniation, however, may lead to undesired degalliation. This is demonstrated by Choudhary et al.[127] for a series of [Ga]-ZSM-5 samples. Calcination causes degalliation, the extent of which depends on the Si/Ga ratio of the samples. Two calcination procedures in static air were applied, one at 550 °C for 15 h to remove the occluded organic template from the synthesized material and a second one at 600 °C for 4 h to transform the gallosilicates into their H^+ forms after ion exchange with a NH_4NO_3 solution. Si/Ga ratios of the as-synthesized form and of the final H^+ form were determined by chemical analysis. The degalliation was as high as 35.2% at a Si/Ga ratio of 31.3 in the as-synthesized product but amounted to 2.7% only at a Si/Ga ratio of 123.3. On the latter sample, the ratio of nonframework Ga to framework Ga is 1 order of magnitude lower (Table 4).

Table 4. Degalliation of [Ga]-ZSM-5 Gallosilicates Due to Calcination (600 °C, 4 h)[127]

Si/Ga ratio[a]	31.3	48.9	65.1	123.3
degalliation (%)	35.2	18.2	7.2	2.7
NF-Ga/F-Ga[b]	0.4	0.22	0.08	0.03

[a] As-synthesized. [b] Ratio of nonframework (NF) to framework (F) gallium in the H-form.

It is obvious that the appreciable high degree of degalliation depends on the Si/Ga ratio of the as-synthesized material: At higher Si/Ga ratios, degalliation is less severe. As the amount of water released by the as-synthesized material during hydrothermal treatment up to 550 °C is high, calcination under static conditions proceeds in a moist atmosphere, which—as is known from the so-called steaming of zeolites—favors the removal of the trivalent elements from the framework.

As shown in Table 5, the hydrothermal treatment (48 mol of steam) of [Ga]-ZSM-5 samples at temperatures above 400 °C decreases the crystallinity, degalliates the framework, and diminishes the concentration of strong acid sites. Steaming was carried out by passing a $H_2O_{(g)}/N_2$ mixture with H_2O concentrations of 13−80 mol % and a GHSV of about 5000 h^{-1} over the zeolite in a quartz reactor for 4 h at 673−1073 K. The loss of crystallinity is less severe at lower steam contents. The steam content has less effect on the crystallinity than the temperature. It is reported that the presence of 18, 48, or 80 mol % H_2O has only minor effects on the crystallinity of [Ga]-ZSM-5 samples during steaming at 600 °C.[127]

Degalliation caused by hydrothermal treatments has been confirmed by other authors.[128,129] The hydrothermal treatment of a [Ga]-ZSM-5 sample (Si/Ga = 45) at 923 K causes a more severe degalliation than "dry" calcination. ^{71}Ga MAS NMR spectra show (Figure 16) that removal of framework gallium leads to the appearance of adequate amounts of octahedrally coordinated nonframework gallium. Degalliation continues over a period of steam treatment up to 24 h.

After water vapor equilibration of the samples at room temperature, no signal at $\delta = 0$ ppm of octahedrally coordinated gallium could be observed. Only after equilibration with acetyl acetonate (acac), which is known to improve the detection of octahedrally coordinated species for aluminosilicate zeolites in certain cases,[130] the signal at 0 ppm became visible.

An IR vibration band at 1461 cm^{-1} appears after adsorption of pyridine over hydrothermally treated [Ga]-ZSM-5 gallosilicates. This band is assigned to Lewis acid sites[131] located on nonframework gallium species. Khodakov et al.[132] observed the release of gallium from the framework of gallosilicates with MFI structure during catalyst regeneration. The authors could distinguish between two kinds of nonframework gallium species. Only one of them was partly located on the external crystal surface and found to be catalytically active for 125 h in the aromatization of propane performed under autogenous pressure at 428 K.

In summary, the hydrothermal stability of the gallosilicate MFI structure is lower than that of the aluminosilicate. Although experimental evidence is still missing, this conclusion can be assumed to be valid for other types of zeolitic gallosilicates too.

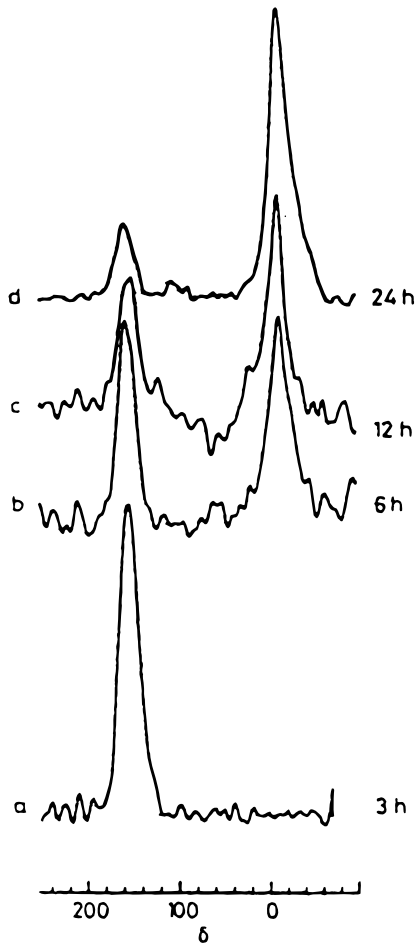

Figure 16. ^{71}Ga MAS NMR spectra of NH_4[Ga]-ZSM-5 (Si/Ga = 45) after postsynthesis steaming at 650 °C for various times (recorded after impregnation of samples with acetylacetone at room temperature). (Reprinted with permission from ref 128. Copyright 1989 The Royal Society of Chemistry.)

Table 5. Comparison of [Ga]-MFI and [Al]-MFI Zeolites Hydrothermally Treated (HTT) with 48 mol % of Steam at Different Temperatures[127]

	crystallinity (%)		Si/(Ga or Al) framework		strong acidity (mmol/g)[a]	
HTT-temp (°C)	[Ga]-MFI	[Al]-MFI	[Ga]-MFI	[Al]-MFI	[Ga]-MFI	[Al]-MFI
400	97	100	44	37	0.24	0.26
600	83	99	64	51	0.09	0.20
800	62	92	224	66	0.04	0.14

[a] Determined in terms of pyridine chemisorbed at 400 °C.

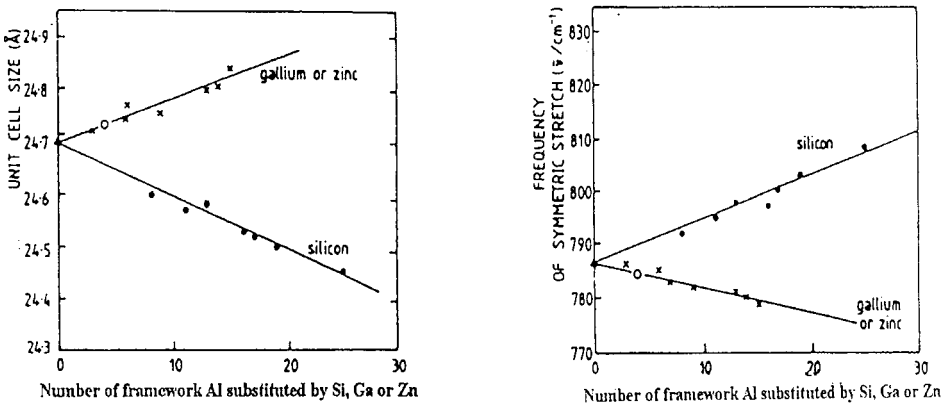

Figure 17. Change of the unit cell size (left) and of the symmetric T−O−T framework vibration frequency (right) of zeolite Y with Ga substituted by postsynthesis galliation. (Reprinted with permission from ref 139. Copyright 1991 Elsevier Science.)

B. Gallium Framework Substitution by Postsynthesis Treatments

1. Galliation

The *postsynthesis* replacement of tetrahedrally coordinated framework constituents by heteroatoms is a suitable method to introduce heteroatoms into tetrahedrally coordinated framework positions in cases if direct synthesis of the material fails or synthesis is difficult to achieve.

Postsynthetic galliation is usually attained by zeolite treatment with alkaline gallate solutions. The siliceous end members of zeolite structures such as silicalite-1 (structure type MFI) or silicalite-2 (structure type MEL) exclusively offer Si^{4+} for substitution. Thomas and Liu[133] could show that silicalite-2 undergoes facile substitution of framework Si^{4+} by Ga^{3+} when exposed to aqueous solutions of $NaGaO_2$.[134] A typical preparation procedure of galliated silicalite-2 is described as follows: 1 g of silicalite-2 previously calcined at 550 °C (to remove residual organic molecules inside its channels) is added to 30 mL of a solution of $NaGaO_2$ (0.0278 mol/L of Ga_2O_3 and 0.1 mol/L of NaOH) under constant stirring for 10 min. The mixture is placed in a plastic bottle, sealed, and kept in an oven at ca. 100 °C for 24 h. The product is filtered, washed with distilled water, and dried at 100 °C.

Galliation of H-ZSM-5 (Si/Al ratio = 639), Na−ZSM-5 (Si/Al ratio = 685), and Na−ZSM-11 (Si/Al ratio = 1066) was reported by Endoh et al.[135] The zeolites were treated with an aqueous solution of Ga_2O_3/NaOH at 100 °C for 24 h. It turned out that H-ZSM-5 and Na-ZSM-11 were not galliated at all whereas Na-ZSM-5 was galliated though to a low extent only, as shown by IR framework spectra. Due to the high Si/Al ratios, the samples can practically be viewed as silicalite structures with aluminum being present in traces only.

Galliation seems to depend on the degree of crystallinity because the mechanism of gallium incorporation is believed to require crystal defects. Differences in the degree of galliation reported in the literature can be caused by the defect site concentration of the zeolite. A correlation is found between the degree of isomorphous substitution and the reactivity of the material for the isotopic exchange of oxygen. About six framework oxygen atoms have to be activated for the insertion of one Ga atom, which suggests that Ga occupies a corner of the four-membered oxygen ring.

Galliation of zeolite beta (Si/Al = 10) was performed in the liquid phase.[136] It was found that gallium species are inserted into vacancies created by thermal treatment of the zeolite or by alkaline leaching. Preferentially, galliation starts at the external surface of the zeolite crystals and then migrates into their interior. Aluminum and gallium species present in the liquid phase behave similarly during the process. In the case of aluminosilicates, gallium can substitute either for Si^{4+} or Al^{3+}. A complete substitution of all framework Al^{3+} through these secondary synthesis, however, has not been achieved. Thus, the transformation of aluminum-containing zeolite structures into the pure gallium analogues is hardly attainable by postsynthesis methods.

Isomorphous substitution of Al^{3+} by Ga^{3+} in the framework of wide pore zeolites Y, ZSM-20, USY, and beta is described by Karma et al.[137] through reaction with aqueous gallium fluoride solutions. Characterization by XRD, solid-state NMR, FTIR, SIMS, and sorption studies demonstrates that gallium can be incorporated into the framework, except in the case of USY where gallium substituted only nonframework aluminum. Results from the catalytic gas-phase conversion of *n*-hexane showed that reaction rates increased with increased amounts of framework gallium.

Another example is given by Dwyer et al.[138,139] Ammonium-exchanged zeolite Y (Si/Al = 2.5) was dried at 170−180 °C and treated with a solution of gallium nitrate and ammonium fluoride for 3−4 h. Subsequently, the products were filtered off and heated to 80−85 °C for 2 h with ammonium sulfate solution (1.5 mol/L) using a ratio of solid to solution of 1:10. This treatment was repeated to remove the fluoride. The degree of framework substitution of Al^{3+} by Ga^{3+} was controlled by varying the concentration of gallium fluoride used. The incorporation of Ga^{3+} into framework tetrahedral sites was confirmed by XRD, FTIR, and solid-state NMR.

Figure 17 shows how the unit cell parameters of (cubic) faujasite change depending on the degree of

Al^{3+} replacement by Ga^{3+}. For comparison, results on the substitution of Al^{3+} by Si^{4+} achieved by an analogous treatment with SiF_4 are included. The latter procedure enhanced the Si/Al framework ratio. Therefore, it can be viewed as a dealumination process because the overall aluminum concentration diminishes. As observed for other zeolites, the unit cell size decreases and the frequency of the symmetric IR framework T−O stretching band shifts to higher values with dealumination. The increase of the unit cell size in the case of Al^{3+} substitution by Ga^{3+} can be attributed to the larger size of Ga^{3+} (in comparison to Si^{4+} and Al^{3+}) and reflects the increase of the T−O bond length leading to a reduced vibration frequency.

As mentioned before, the incorporation of heteroatoms into zeolitic frameworks by postsynthesis treatment probably occurs at framework vacancies or defect sites. The complex mechanism of galliation by postsynthesis treatment in alkaline solution, however, is not yet fully understood. The insertion of gallium into the framework is influenced by the amount of alkaline solution used. If small amounts of the zeolite are contacted with large volumes of solution, a dissolution of the zeolite proceeds as known for silica and silicates. For silica, an equilibrium between the solid (s) SiO_2 and the monosilicic acid in the liquid phase (l) exists:

$$[SiO_2]_{n(s)} \leftrightarrow Si(OH)_{4(l)} \quad (8)$$

The solubility of quartz amounts to about 10−70 ppm at 25 °C.[78] Dissolved zeolite species (at equilibrium concentrations) might react with $Ga(OH)_4^-$. Formed gallosilicates can react with zeolite crystals or grow into new crystals. This way, gallium is "reincorporated". In alkaline solution, galliation may proceed via a dissolution−condensation mechanism (recrystallization) simultaneously with a direct attachment of $Ga(OH)_4^-$ to framework defect sites.

Besides galliation in the liquid phase, an adequate gas-phase procedure is feasible. Bayense et al.[140] used trimethylgallium as modifying agent, which decomposes over dealuminated H-ZSM-5 and H−Y zeolites in hydrogen or nitrogen atmosphere. In the presence of hydrogen, decomposition of trimethylgallium occurs at lower temperatures (approximately 400 °C) than in the presence of nitrogen. Methane was the main decomposition product. In the presence of surface silanol groups, gallosilane structures may be formed:

$$Si{-}OH + Ga(CH_3)_3 \rightarrow Si{-}O{-}Ga(CH_3)_2 + CH_4 \quad (9)$$

An equivalent reaction is considered to occur between trimethylgallium and Brønsted acid sites:

$$Si{-}(OH){-}Al + Ga(CH_3)_3 \rightarrow Si{-}(O{-}Ga(CH_3)_2){-}Al + CH_4 \quad (10)$$

Dealumination of zeolites prior to trimethylgallium treatment was performed either by washing with HCl solution or by a two-step procedure comprising a treatment with $SiCl_4$ vapor for 2 h at 450 °C followed by an acid treatment as described before. It is assumed that defect sites (silanol nests) are created this way due to the removal of framework aluminum. These sites can accept gallium during the galliation procedure under renewed stabilization of the framework. Trimethylgallium treatment of the dealuminated zeolites was carried out by saturating a helium stream with the modifying agent at 0 °C and passing this stream over the zeolite bed in a microreactor. Gallium loading of the samples was controlled by varying the time of the trimethylgallium treatment.

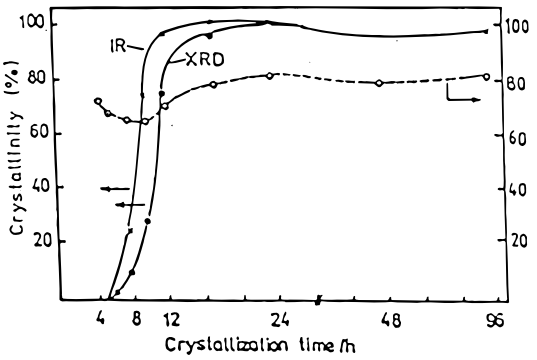

Figure 18. Genesis of [Ga]-ZSM-5 according to XRD and IR analysis (left) and percentage of solid material in the gel (right). (Reprinted with permission from ref 141. Copyright 1991 Elsevier Science.)

Dealumination of the parent H-ZSM-5 and NaHY zeolites enhanced the original Si/Al ratios from 20 and 2.15 to more than 200 and 6.2, respectively. The authors considered the existence of silanol nests as a necessary prerequisite for the subsequent incorporation of gallium according to the following equation:[140]

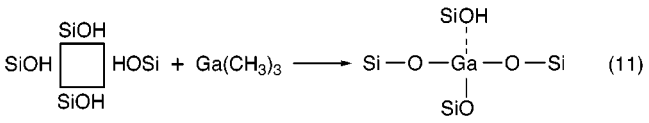

(11)

Side reactions of trimethylgallium with isolated silanol groups or Brønsted acid sites result in the formation of (attached) nonframework gallium species. The incorporation of gallium into the framework could be verified by IR lattice vibration spectra and by ^{71}Ga MAS NMR spectroscopy.

2. Recrystallization

The temporal course of crystallization of MFI (ZSM-5)-type zeolites was studied by various authors.[108,114,141] It was shown by Kosslick et al.[141] that a prolongation of the synthesis time initiates a recrystallization process of the gallosilicate accompanied by further incorporation of gallium into framework positions (Figures 18 and 19). The process is supposed to proceed via partial dissolution of smaller crystallites in favor of the growth of larger ones. Gallium incorporation into the zeolite structure during growth introduces framework disorder. In the progress of crystallization, this framework disorder is successively reduced due to Ostwald redissolution (aging).[37] The critical size of the crystals to initiate dissolution or growth depends on the supersaturation of the synthesis gel and, in general, increases with

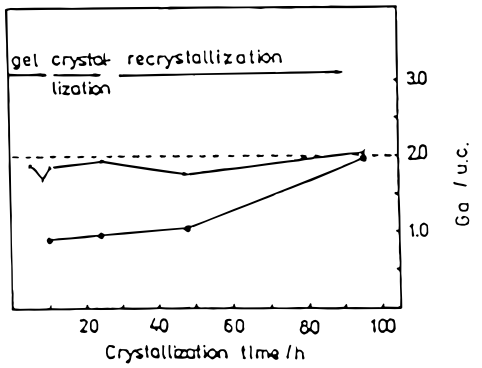

Figure 19. Influence of the crystallization time on the total Ga content (×) according to chemical analysis and on the Ga framework content (●) estimated from TPDA. Ga content is expressed as atoms per unit cell. (- - -) Ga content of the starting gel. (Reprinted with permission from ref 141. Copyright 1991 Elsevier Science.)

decreasing supersaturation, e.g., at longer crystallization times (Figure 20). The driving force is the minimization of the free energy of the crystals with growing crystal size.[142] Hysteresis is observed[37] in the adsorption isotherms of *n*-hexane for gallosilicate ZSM-5 with Si/Ga ratios higher than 25. This deviation from the isotherm type I points to the existence of mesopores and hence implies changes of the zeolitic morphology.

C. Modification of Zeolites by Gallium on Nonframework Positions

1. Impregnation

Joly et al.[143] applied wet or incipient wetness impregnation of MFI (ZSM-5) samples of various Si/Al ratios using a Ga nitrate solution as the gallium source. Wet impregnation means dosing of solution in excess. Incipient wetness impregnation uses amounts of solution which can be completely absorbed by the pore volume of the zeolite.

It was observed that the pH value of the solution during impregnation influences the gallium dispersion. Nevertheless, the gallium phase being introduced by wet or incipient wetness impregnation is found to be closely restricted to the outer surface of the zeolite crystals as thin platelets with average sizes in the range of 5−400 μm. Incipient wetness impregnation resulted in smaller platelets of the gallium phase. Only small amounts of gallium are found inside the zeolite crystals.

2. Ion Exchange

The ability of hydrated Ga^{3+} cations to penetrate into the pore system of medium-pore zeolites such as ZSM-5 is questionable. According to various authors, gallium cations are too large to gain access to the exchangeable protons of Brønsted sites inside the zeolite pores. Yakerson et al.[144] prepared Ga-modified H-ZSM-5 zeolites by ion exchange and additional impregnation with the mother solution. Large aggregates of Ga_2O_3 were mostly located on the outer crystal surfaces (SEM). Instead, it was shown that gallium cations can be transferred to ion-exchange positions of a zeolite by a solid-state ion exchange. The basic experimental procedure for solid-

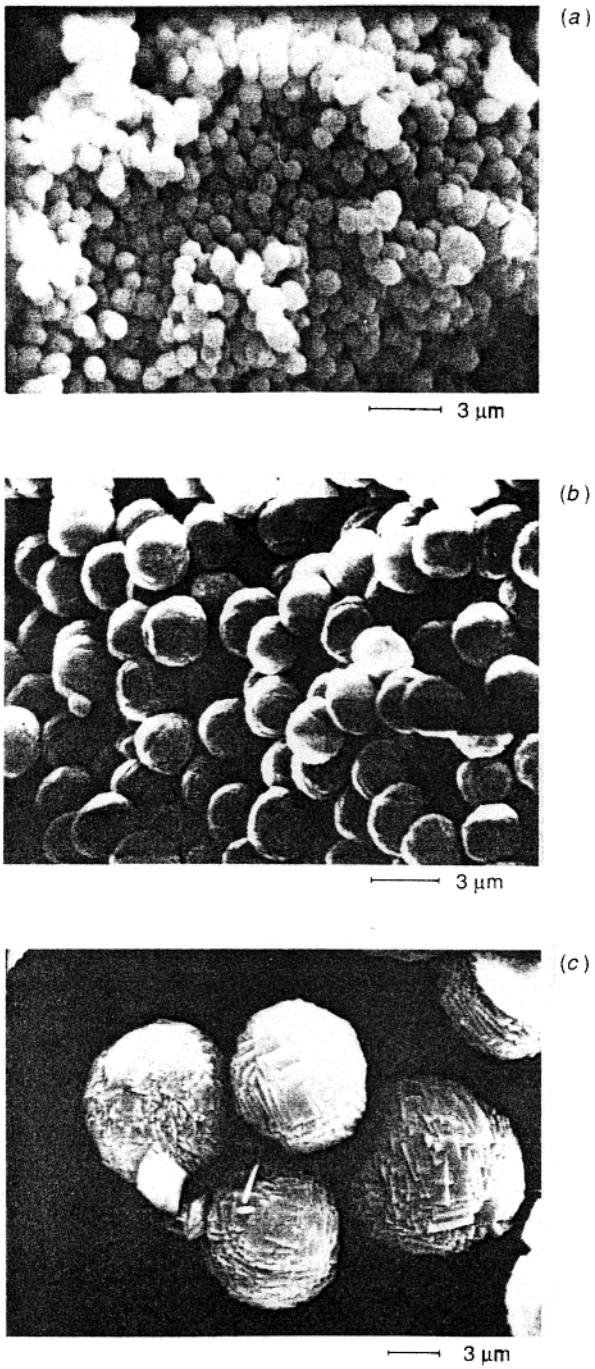

Figure 20. Crystal growth of [Ga]-ZSM-5 (Si/Ga = 50) during the Ostwald redissolution process. SEM pictures after synthesis times of (a) 10, (b) 24, and (c) 48 h. (Reprinted with permission from ref 37. Copyright 1993 The Royal Society of Chemistry.)

state ion exchange of zeolites is rather simple and has been repeatedly reviewed by Karge.[145,146] An intimate mixture of the zeolite powder and the modifying compound, e.g., halides or oxides of the element to be exchanged, is heated under vacuum or in a stream of inert gas to remove volatile products such as HCl, H_2O, and NH_3. The ion exchange can be carried out under completely water-free conditions. The mixture of the powders can be performed by grinding in a mortar, ball-milling, or suspension in an inert solvent (e.g., *n*-heptane) followed by evaporation. The latter preparation route was applied by Carli et al.[147] in order to introduce Ga into H-ZSM-

Table 6. EDAX Microanalysis of Selected Modified ZSM-5 Zeolite Particles Loaded with 5 wt % of Gallium after Reductive Solid-State Ion Exchange (RSSIE)[149]

	composition (wt %)				
	before reduction		after reductive treatment		
	particle no. 1	particle no. 2	particle no. 3	particle no. 4	particle no. 5
Al_2O_3	4.238	4.010	4.571	4.838	4.542
SiO_2	95.762	95.990	90.944	90.042	90.944
Ga_2O_3	0.000	0.000	4.485	3.12	3.598

5. Dried Ga_2O_3 (15 wt %) and H-ZSM-5 (85 wt %) were dispersed in distilled *n*-hexane, stirred under ultrasonic wave submission, and dried after evaporation of the solvent.

Reductive solid-state ion-exchange (RSSIE) procedure follows the same route described above but includes a final reductive treatment in a flow of hydrogen.[148]

Processes occurring in a mixed Ga_2O_3/H-ZSM-5 sample after treatment with flowing hydrogen were studied thoroughly by Kanazirev et al.[149] The reduction was performed in a microbalance with 80 kPa of hydrogen in argon following a temperature-programmed mode (heating rate 10 deg/min) up to 800 °C under normal pressure. Hydrogen consumption starts at ca. 450 °C. TEM coupled with EDAX microanalysis as well as with XPS was applied to characterize the mechanical mixture of gallium oxide and zeolite H-ZSM-5 before and after reductive treatment. The results give rise to the view that separate gallium oxide microcrystals detected by TEM before reduction had almost completely disappeared after reduction. Results of EDAX analysis are rationalized assuming that the gallium species are transferred into the zeolite. Neither foreign gallium phases at zeolite crystallites nor gallium enrichment on the zeolite particle surface were observed (Table 6).

Hydrogen reduction causes a spreading of gallium over the zeolite surface. This is concluded from the increase of the intensity of the Ga(3d) peak of XPS spectra by a factor of about 10 following reduction. Removal of 15−20 monolayers of the sample surface by Ar^+ sputtering changes the Ga(3d) peak intensity only marginally, thus confirming a transfer of gallium into the zeolite interior. A lowering of the oxidation state is concluded from the shift of the Ga(3d) peak to lower binding energies after reduction (Figure 21).

Reductive solid-state ion exchange (with H_2) extends the scope of the classic solid-state ion exchange. The state of oxidation of the exchanged gallium is reduced from 3+ to 1+. This way, negative charges of the framework can be balanced by cations of a usually higher valence in a 1:1 ratio. Thus, a higher metal density can be achieved:

$$Ga_2O_3 + 2H_2 \rightarrow Ga_2O + 2H_2O \quad (12)$$

$$Ga_2O + 2H^+Z^- \rightarrow 2Ga^+Z^- + H_2O \quad (13)$$

$$Ga_2O_3 + 3H_2 \rightarrow 2Ga + 3H_2O \quad (14)$$

Z^- symbolizing zeolite framework sites. This method can also be applied to incorporate In by using In_2O_3.

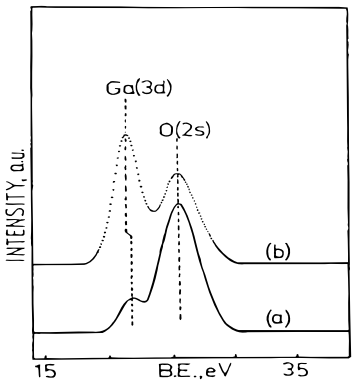

Figure 21. XPS spectra of ZSM-5 modified with gallium by reductive solid-state ion exchange: (a) before and (b) after reduction in flowing H_2 (80 kPa of H_2 in a total flow of 50 mL/min). (Reprinted with permission from ref 149. Copyright 1991 Elsevier Science.)

According to the thermodynamic $\Delta G°$ values for the reduction of Me_2O_3 to Me_2O, the reductive depletion of the In_2O_3 phase is facilitated since the change of the standard free energy of the reduction of the indium oxide is less positive. Other zeolite types can be modified as well (Y, mordenite, offretite).[150] Currently, RSSIE was also applied to prepare In- and Ga-modified SAPO materials (SAPO-5, SAPO-34, SAPO-37).[151]

3. Chemical Vapor Deposition (CVD)

The dried and calcined zeolite is mixed with $GaCl_3$ in a glovebox, and the mixture is subsequently heated temperature-programmed up to 773 K in a stepwise manner at low heating rates. The reaction of $GaCl_3$ with H_2O and protons results in the formation of the gallyl ion GaO^+ as the primary species

$$GaCl_3 + H_2O + H^+ \rightarrow GaO^+ + 3HCl\uparrow \quad (15)$$

Under severe reduction conditions, the gallyl ion is reduced to Ga^+. This way, Kwak and Sachtler[152] prepared H-ZSM-5 (Si/Al = 20.5) zeolites loaded with various amounts of gallium. TPR shows the formation of GaO^+ ions and Ga_2O_3 particles. The authors concluded that the CVD technique acts as a true ion exchange replacing protons by GaO^+ ions. Brønsted acidity is markedly lowered by introducing Ga via CVD. A quantitative evaluation discussed by the authors does not seem to be justified on the basis of the presented NH_3 TPD profiles, which consist of at least three strongly overlapping peaks.

In a preceding work, the same process was shown to operate with a Na,H-ZSM-5 sample (Si/Al = 16, Na content 0.60%).[153] The authors succeeded in distinguishing between isolated Ga^{3+}, GaO^+, and

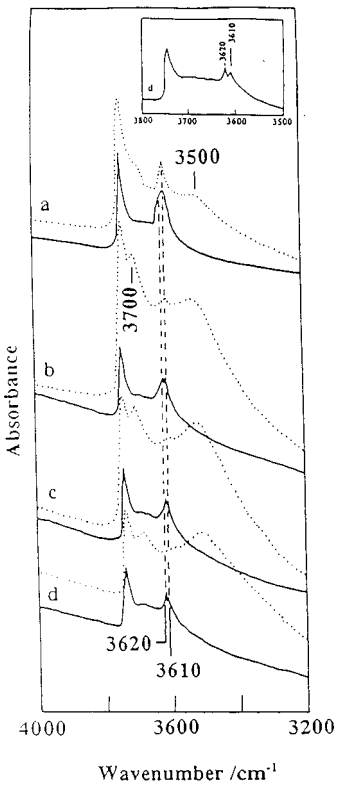

Figure 22. IR spectra (OH region) of (Al,Ga) mordenite with various Si/Al ratios (—) prepared by atom planting of dealuminated [Al]-mordenite (· · ·) with $GaCl_3$ vapor at 600 °C: (a) Si/Al = 171, (b) Si/Al = 151, (c) Si/Al = 195, (d) Si/Al = 220. Inset shows spectrum d with two resolved Brønsted OH vibration bands. (Reprinted with permission from ref 154. Copyright 1997 Elsevier Science.)

Ga_2O_3 species by using CO-TPR techniques combined with reoxidation experiments. A distribution of 0:7:3 was estimated for a sample containing 1.32 wt % of gallium.

Recently, the acidity of partially dealuminated mordenite was modified by isomorphous substitution of trivalent (Ga) atoms in framework sites using the atom planting method.[48,154] After treatment with $GaCl_3$ vapor at 600 °C, the IR band owing to acidic bridging Si−OH−Ga groups at 3620 cm^{-1} appears in the OH vibration spectrum (Figure 22). In the ^{71}Ga MAS NMR spectrum, the characteristic peak of tetrahedrally coordinated Ga is found at 159 ppm.

IV. Physicochemical Characterization

A great variety of characterization techniques is applicable for ascertaining the substitution of elements into the zeolite framework. Most frequently, infrared spectroscopy, nuclear magnetic resonance spectroscopy, thermoanalytical methods, and temperature-programmed characterization techniques as well as the determination of ion-exchange capacities have been applied. X-ray diffraction gives indirect evidence according to detectable modifications of unit cell volumes.

The chemical composition is routinely determined by optical emission spectroscopy with ion-coupled plasma (OES−ICP). The method utilizes an inductively coupled argon plasma for atomization and excitation of the dissolved probe material. The plasma, generated through a high-frequency field with temperatures of about 8000 K, emits a spectrum of the characteristic lines of the elements present. For quantitative determination, a calibration based on standards is necessary. Naturally, OES−ICP cannot differentiate between framework and nonframework species. Additional methods, briefly outlined below, have to be applied for discrimination.

A. Gallium in Framework Positions

1. X-ray Diffraction

XRD allows one to identify crystalline material by its diffraction pattern. Substitution of framework constituents leads to a modification of bond lengths and angles and hence to an alteration of the unit cell volume. Its size, however, depends on the concentration of the element to be replaced in the framework and also on the degree of substitution achieved. The change in the unit cell volume of a silica polymorph upon isomorphous substitution of Si by various elements was already discussed on the basis of Pauling's minimum radii concept.

XRD analysis, however, fails in determining bond length variations and coordination numbers if the concentration of the substituting element in the parent framework is low. Further complications of the structural analysis arise if substituting atoms are distributed over crystallographically different tetrahedral T sites. With zeolites of ordered distribution of Si and Ga over available T sites, like with the ABW structure type, coordination as well as bond lengths and angles around the Ga framework atoms can be determined precisely by XRD.

The structures of Ga-substituted zeolites and related materials are presented in section V.

2. Infrared Spectroscopy

Characteristically, IR vibration bands in both the hydroxyl region (wavenumbers beyond 3000 cm^{-1}) and the framework region (wavenumbers below 1500 cm^{-1}) are sensitive to the composition of the framework. Hence, the intensity of the vibrations as well as the wavenumbers are a practical tool for checking the incorporation of gallium in framework positions. Table 7 summarizes results of IR investigations performed on gallosilicate structures.

Hydroxyl Vibrations. In this spectral range, absorption bands of stretching vibrations of the terminal silanol groups of acid-bridging Ga−O(H)−Si groups and of the OH groups located at nonframework gallium species appear. The stretching vibration of terminal silanol groups is found at 3740 cm^{-1}. Stretching vibrations of bridged hydroxyls related to tetrahedrally coordinated framework gallium occur at ca. 3615 to 3625 cm^{-1} for any of the gallosilicate structures. If the crystal structure of the framework is perturbed and some of the silicon atoms are coordinatively unsaturated, internal silanol groups are found at defect sites. An IR band at 3550 cm^{-1} is assigned to the vibration of these internal silanol groups. Stretching vibration bands of P−OH groups of gallophosphate molecular sieves[167] appear at 3650−3700 cm^{-1}.

Table 7. Infrared Characterization Data of Gallium Analogs for Known Zeolite Structures[a]

zeolite data	hydroxyl region	framework vibrations	ref
[Ga]-ZSM-5	3740 Si−OH, 3660 nonframework Ga species, 3615−3620 Ga−OH−Si, 3300 Ga−OH−Si, perturbed by additional H bridging to neighbored O	1220 (sh), 1090 ν_{as} (Ga−O−Si), 930 (sh) δ (SiOH), internal location 800 ν_s (Ga−O−Si), 550 D5R (double five-ring vibration), 450 δ ($GaO_{4/2}$)	108, 132, 155, 156
[Ga]-ZSM-5 (Si/Ga = 17.5−67.6)		1230, 1100, 1030 (Si−O−Ga), 990, 950, 780, 550, 450	165
[Ga]-Y $Na_{59}Ga_{59}Si_{133}O_{384}$		987 ν_{as} (Ga−O−Si)	157
[Ga]-L $K_{10.4}Ga_{10.4}Si_{25.6}O_{72}$		1009 ν_{as} (Ga−O−Si)	
[Ga]-Beta (Si/Ga = 12.5) $Na_{0.074}Ga_{0.074}Si_{0.926}O_2$		1057 ν_{as} (Ga−O−Si)	
[Ga]-Beta (Si/Ga = 24)	3737 terminal SiOH groups, 3625 bridged hydroxyls		166
[Ga]-X (TMA^+/Na^+ form)		660, 611 ν_s (Ga−O−Si)	154
[Ga]-Y		768 ν_s (Si−O−Si), 660, 611 ν_s (Ga−O−Si)	
[Ga]-sodalite		768 ν_s (Si−O−Si), 611 ν_s (Ga−O−Si)	
Ga−silicalite-2 (prepared by galliation)	3742 (Si−OH), 3622 (Ga−OH−Si)	1215, 1080 ν_{as} (Ga−O−Si), 790 ν_s Ga−O−Si), 550 D5R (double five-ring vibration), 450 δ ($GaO_{4/2}$)	159
[Ga]-mordenite (Si/Ga = 21)		1230, 1082, 1069 ν_{as} (Ga−O−Si), 779, 721, 668, 571, 550, 457	160
[Ga]-mordenite (Si/Ga = 9.5)	3740 (Si−OH), 3616 (Ga−OH−Si)	1230 (w), 1065 (ms), 811 (vw), 786 (vw), 722 (w), 650 (m), 618 (vw), 452 (ms), 373 (vw)	161
[Ga]-NU 23, as-synthesized		1215, 1065, 800, 790, 740, 580, 540, 445	162
[Ga]-Omega (Si/Ga = 3.4−3.7)		1139 (sh), 1025 (vs), 815 (m), 770 (sh), 730 (mw), 615 (vw), 450 (ms)	163
[Ga]-ZSM-22 $K_{0.34}Ga_{0.34}Si_{23.66}O_{48}$ (anhydrous)		1212 (m), 1080 (s), 806 (w), 782 (w), 640 (w), 549 (m), 483 (m), 462 (s)	164

[a] s strong, ms medium strong, mw medium weak, w weak, vw very weak, sh shoulder ν_s symmetric stretching vibration, ν_{as} asymmetric stretching vibration, δ bending .

Khodakov et al.[132] assigned a band at 3300 cm^{-1} of [Ga]-ZSM-5 to vibrations of the Ga−OH−Si unit perturbed through additional H bridging to neighboring oxygens. Vibration bands of hydroxyls located at nonframework gallium species of [Ga]-ZSM-5 are found at 3670 cm^{-1}. For structures with nonequivalent tetrahedral sites, vibrations of the bridged hydroxyls appear at different frequencies depending on the kind of tetrahedral sites involved.

The occurrence of Si−OH−Ga stretching vibrations prove that gallium is incorporated into zeolite framework positions. If aluminum is additionally present, its contribution to the signal is difficult to estimate although the wavenumber of the stretching vibration of the Si−OH−Al unit is somewhat lower (ca. 10−20 cm^{-1}) than that of Si−OH−Ga.

Framework Vibrations. Framework vibration bands are observed in the spectral range between 1250 and 400 cm^{-1}. Besides symmetric and antisymmetric stretching modes as well as bending modes of TO_4 tetrahedra, structure-sensitive vibration bands, so-called double-ring vibration bands, are observed. Assignments are as indicated in Table 8.

The positions of bands shift with changing composition depending on the kind and the content of the framework atoms. Increasing framework Al content leads to a low-frequency shift of framework vibrations (Figure 23).[170]

For [Al]-ZSM-5, a systematic shift of the asymmetric T−O−T stretching vibration is known to be dependent on the Al content in framework positions.[171] The asymmetric T−O−T vibration occurs at 1090 cm^{-1} if the aluminum framework concentration is high (5 Al per unit cell) and is shifted to 1104 cm^{-1} at low aluminum contents (0.6 Al per unit cell). Si−O−Si framework vibrations in pure silicalite-1 are reported to occur at ca. 1105 cm^{-1}. The wavenumber of the antisymmetric T−O−T mode decreases in the order silicalite-1 > [Al]-ZSM-5 > [Ga]-ZSM-5. With increasing gallium contents, T−O−T vibration bands of [Ga]-ZSM-5 shift to lower frequency (Figure 24).[114,172]

Table 8. Range of IR Framework Vibration Modes in Zeolites and Their Assignments (According to Flanigen (1976) and Jacobs (1981))[168,169]

range of wavenumbers (cm^{-1})	assignment
1250−980	asymmetric T−O−T stretching
870−630	symmetric T−O−T stretching
550−620	structure-sensitive double five-ring vibration
ca. 450	T−O bending mode

The shift of the T−O−T framework vibration frequency to lower wavenumbers after isomorphous substitution of Si by larger atoms is due to the change in the reduced mass of the Si−O−T harmonic oscillator and the lengthening of the T−O bond by large T atoms (Figures 25 and 26).[173,174]

Band intensities and positions of framework vibrations are influenced by the crystallinity of the sample. Two examples will be given. Tuna et al.[108] monitored framework IR spectra for a gallosilicate [Ga]-ZSM-5

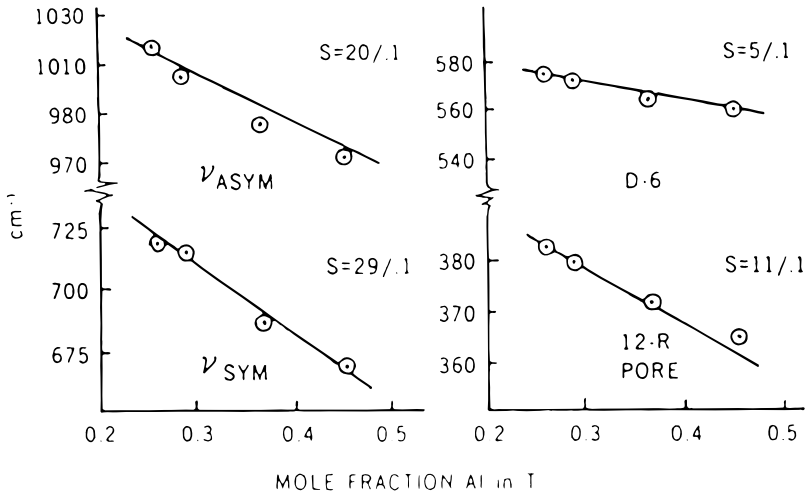

Figure 23. Frequencies of lattice vibration bands of faujasite-type zeolites X and Y vs atom fraction of Al in the framework. ν_{sym} and ν_{asym} = symmetric and anti-symmetric Si−O−Al vibration bands, D-6 = D6R mode, 12-R pore = O12R pore opening mode, S = slope ($\Delta\nu$ per 0.1 Al mole fraction change).

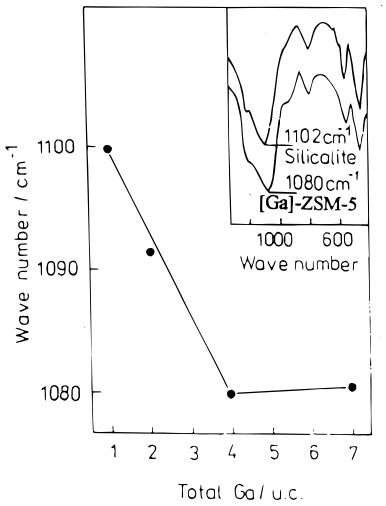

Figure 24. Dependence of the IR wavenumber of the asymmetric T−O−T stretching vibration band on the total gallium content per unit cell of [Ga]-ZSM-5 (H form). (Reprinted with permission from ref 172. Copyright 1993 Elsevier Science.)

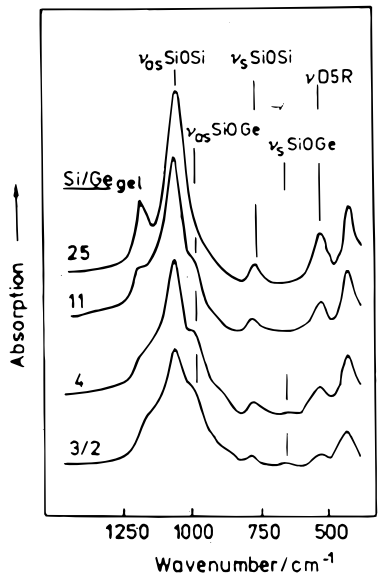

Figure 25. IR lattice vibration spectra of [Ge]-ZSM-5 zeolites with various degrees of substitution.[173] (Reprinted with permission from ref 173. Copyright 1993 American Chemical Society.)

(Si/Ga = 50) at various stages of the crystallization process (Figure 27). At the beginning of the crystallization process (5 h), the vibration band of the double five-membered ring (D5R) at 550−620 cm^{-1} is absent in the spectrum of the synthesis gel. After 8 h of crystallization time, a weak absorption arises at 550 cm^{-1}, which becomes more pronounced after 10 h of crystallization, indicating the onset of the zeolite crystal growth. Then the initially asymmetric very broad T−O−T vibration band at 1102 cm^{-1} has become narrower. An additional shoulder emerges at 1220 cm^{-1}. Further prolongation of the crystallization time leads to an increase of the D5R vibration intensity. The broad shoulder at 930 cm^{-1} appearing at crystallization times exceeding 24 h is ascribed to lattice defects represented by internal silanol groups.

With [Ga]-omega, Mirajkar et al.[163] found a very broad band at 1060 cm^{-1} due to the asymmetric Si−O−Ga stretching vibration characteristic of poorly crystallized samples. With improving crystallinity, this band narrows and is shifted to lower frequency (1030 cm^{-1}). The shoulder at 1105 cm^{-1} is shifted to 1130 cm^{-1} and gains intensity with progressing crystallinity. Absorption at 852 cm^{-1} observed on the amorphous sample is not present on the crystalline sample. Upon crystallization of zeolite [Ga]-omega, all framework vibration bands are shifted to lower wavenumbers.

It is clearly indicated that one single framework IR spectrum alone cannot, by far, provide full proof for a successful gallium incorporation. Spectra of the hydroxyl region are more reliable, at least for pure gallosilicates. In both cases, the spectra, however, do not provide quantitative values of gallium concentration. If recording is performed in the normal transmission mode using self-supporting disks, the intensity of the resulting IR vibrations can be normalized upon the mass of the disks. Then a more or less quantitative comparison of results received with different

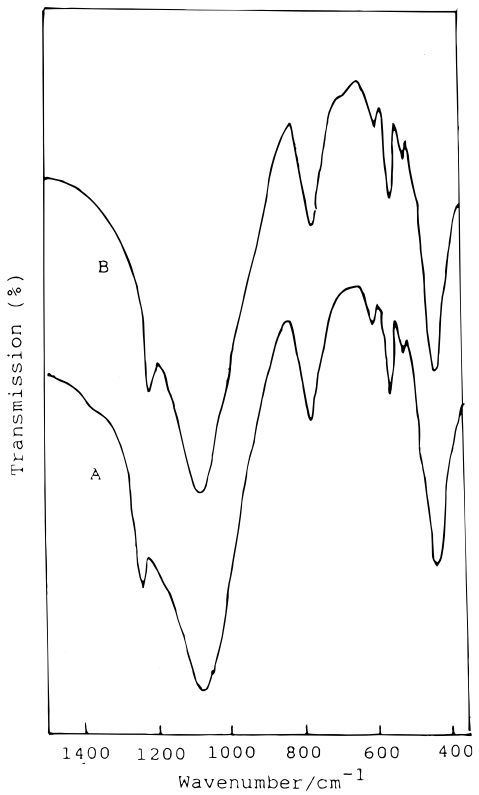

Figure 26. IR lattice vibration spectra of (A) [Fe]-ZSM-12 and (B) [Ga]-ZSM-12.[174]

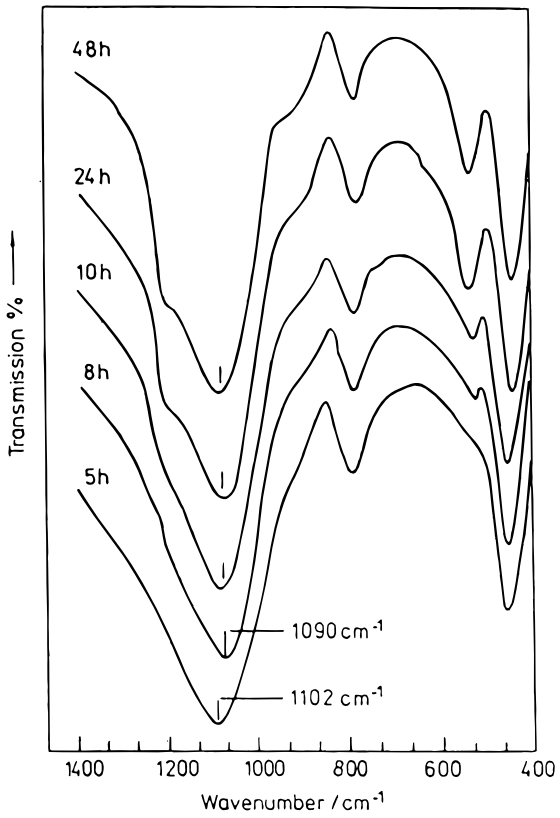

Figure 27. IR lattice vibration spectra monitoring the appearance of zeolite [Ga]-ZSM-5 at various times of crystallization. (Reprinted with permission from ref 108. Copyright 1992 Akademie Verlag GmbH.)

samples is allowed. The FTIR mode of operation, however, is not amenable to this quantification.

3. NMR Spectroscopy

Because of their inherent advantages, solid-state NMR spectra have a great potential for the characterization of zeolites. Information on the whole volume of the solid allows a quantitative determination of element concentrations. Additionally, the spectra inform on short-range ordering. By modification of the operation mode, the method even allows one to investigate transport processes. One of the few shortcomings is the relatively low sensitivity and the problems which arise in the presence of paramagnetic nuclei. The resolution is lower than in the case of liquid-phase spectra. More recent techniques, however, have allowed considerable improvements (MAS, CRAMPS, DOR, DAS).

^{29}Si MAS NMR Spectroscopy. The chemical shift, δ, of a ^{29}Si nucleus in a zeolite depends primarily on the number of T atoms in the first neighboring shell and on the T−O−T angles (T = tetrahedral species, Si, Al, Ga, Fe, Ge, etc.) of the bridging oxygen atoms that coordinate the ^{29}Si nucleus. For example, the ^{29}Si MAS NMR spectrum of an aluminosilicate zeolite with only one crystallographically unique type of silicon site generally exhibits up to five lines corresponding to the five possibilities for the linkage of one SiO_4 tetrahedron to n TO_4 tetrahedra (n = 1−4) through oxygen bridges. The evaluation of the percentage of each Si(nT) configuration is based upon the ratios of corresponding line intensities. For faujasites, a discrete set of five Si−nT peaks arises. Thus, the recorded ^{29}Si MAS NMR spectrum is a superposition of spectra resulting from silicon nuclei with different environments. As even for a single T site the Si(nT) peaks for adjacent values of n overlap to a certain degree, these spectra are difficult to deconvolute. Determination of framework compositions from superimposed spectra was achieved for zeolite omega and zeolite offretite which both have two structurally different T sites.[175] The characterization of H-ZSM-5 by high-resolution ^{29}Si MAS NMR spectroscopy led Fyfe et al.[176] to the suggestion that the observed spectrum contains contributions from crystallographically nonequivalent sites. The T-site configuration of a further aluminosilicate, zeolite ZSM-12, where three resonance lines at −109.2, −111.5, and −112.9 ppm are observed, is discussed on the basis of ^{29}Si MAS NMR data by Trewella et al.[177] The line at δ = −112.9 ppm is assigned to T atoms in four-membered rings.

The ^{29}Si MAS NMR spectra of [Ga]-ZSM-5-type zeolites[37] show main signals at $\delta = -105 \pm 0.8$ and $\delta = -112.8 \pm 0.8$ ppm, which are assigned to Si(1Ga) and to Si(0Ga) groups, respectively (Figure 28). Typically, a shoulder in the range of −115 to −117 ppm exists, which can be assigned to extraordinarily stable nonequivalent Si(OT) sites located in the pentasil structure. Another explanation for the high-field shoulder could be that substitution causes a decrease in the T−O−T angles at the site of replacement which has to be balanced by an increase of neighboring T−O−T angles (high-field shift of ^{29}Si MAS NMR signal). The Si(1Ga) peak is overlapped by the signal of (mainly internal) silanol groups appearing at ca. −103 ppm. Therefore, the estimation

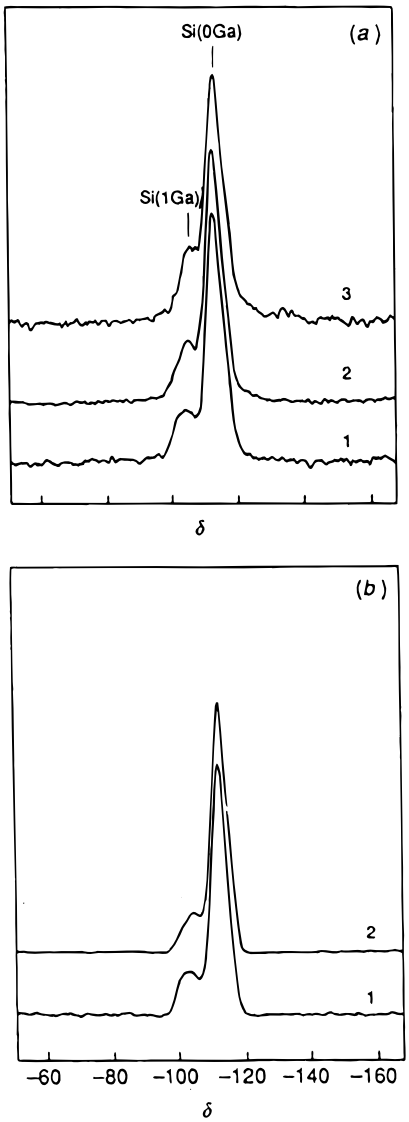

Figure 28. (a) ^{29}Si MAS NMR spectra of as-synthesized [Ga]-ZSM-5 with various Ga contents: (1) SiGa = 100; (2) Si/Ga = 50; (3) Si/Ga = 25. (b) ^{1}H−^{29}Si CP/MAS NMR spectra of as-synthesized [Ga]-ZSM-5: (1) Si/Ga = 100; (2) Si/Ga = 50. (Reprinted with permission from ref 37. Copyright 1993 The Royal Society of Chemistry.)

of Si/Ga ratios from ^{29}Si MAS NMR signal intensity ratios is rendered difficult. The contribution of Si(1Ga) and SiOH groups to the signal at −105 ppm was estimated by using independent values of the concentration of Brønsted acid sites derived from results of TPD of ammonia. This value corresponds to the number of Si(1Ga) groups.

With gallosilicate [Ga]-ZSM-12, signals at ca. −112 and −104 ppm are observed in the ^{29}Si MAS NMR spectrum which are assigned to Si(OGa) and Si(1Ga) units, respectively. The following formula was applied to calculate lattice Si/Ga values from the signal intensities (I) of the fitted NMR spectra.[178,179]

$$(\mathrm{Si/Ga})_{\mathrm{lattice}} = \sum_{n=0}^{4} I_{\mathrm{Si}(n\mathrm{Ga})} \Big/ \sum_{n=0}^{4} 0.25 n I_{\mathrm{Si}(n\mathrm{Ga})} \quad (16)$$

Ga MAS NMR Spectroscopy. Ga MAS NMR spectroscopy is the preferred tool for the characterization of solids containing gallium. Both ^{69}Ga and ^{71}Ga nuclei can be used. ^{69}Ga MAS NMR spectroscopy was used by Ione et al.[180] to characterize zeolitic gallosilicates. Timken et al.[181] applied both ^{69}Ga and ^{71}Ga MAS NMR but stressed the necessity to use high magnetic field strengths in order to minimize the average second-order line broadening. Moreover, high MAS frequencies are necessary to reduce the chemical shift anisotropy effects on the line width and to avoid an overlap between the central peaks and the spinning sidebands. Investigation on [Ga]-ZSM-5 silicates by Bayense et al.[128] showed that water equilibration of the samples is indispensable to obtain ^{71}Ga MAS NMR signals of the gallium within the framework. Detection of octahedrally coordinated nonframework gallium is even more difficult. In a further work, Bayense et al.[129] obtained ^{71}Ga MAS NMR spectra from [Ga]-ZSM-5 samples applying a pulse width of 2 ms with a field strength of 48 kHz. For quantification, the areas of the NMR lines were compared with those of the lines from a known amount of hexahydrated Ga^{3+} ions in a gallium nitrate solution. Lines are sharp for the gallium in the reference solution (line width ca. 800 Hz) but are broad for gallium in the solid matrix (line width ca. 3300 Hz). It was estimated that the loss of signal intensity with solid gallium is 14.6% compared to gallium in solution. Spinning sidebands can virtually be eliminated by operation at higher spinning frequencies (12 and 14 kHz).

For an uncalcined gallosilicate [Ga]-ZSM-5 containing 3.37 gallium atoms per unit cell (Si/Ga = 28) in the as-synthesized form (i.e., with the tetrapropylammonium template inside the pores), one ^{71}Ga NMR line located at +155 ppm with a line width of about 4.8 kHz was received. This line also observed with other gallosilicate structures is usually assigned to tetrahedrally coordinated framework gallium.[128,181]

Quantification of the ^{71}Ga NMR responses, obtained for the H^+ form of the zeolite, revealed that about (70 ± 2)% of the total gallium content was found. Only the signals of tetrahedrally coordinated gallium were observed in a reproducible manner. The lack of the gallium NMR response of octahedrally coordinated gallium is ascribed to large electric field gradients over a part of the gallium nuclei. Thus, the signal intensity depends on the nature of the counterion in the zeolite. On the other side, the broad resonance at ca. 10 ppm can be due to 6-fold-coordinated nonframework gallium.[179]

A quantitative determination of gallium in zeolites by ^{71}Ga MAS NMR is also reported by Diaz et al.[182] The authors emphasized that the linear correlation between the normalized ^{71}Ga signal intensity of the MAS NMR line and the gallium content is valid only for small flip angles and low field strengths.

Gabelica et al.[123] reported a quantitative evaluation of framework gallium in as-synthesized and in modified gallo- and galloalumino MFI zeolites. With various as-synthesized [Ga]-MFI zeolites, the authors found a correlation between the Ga concentration and the corresponding normalized ^{71}Ga NMR line intensities (Figure 29).

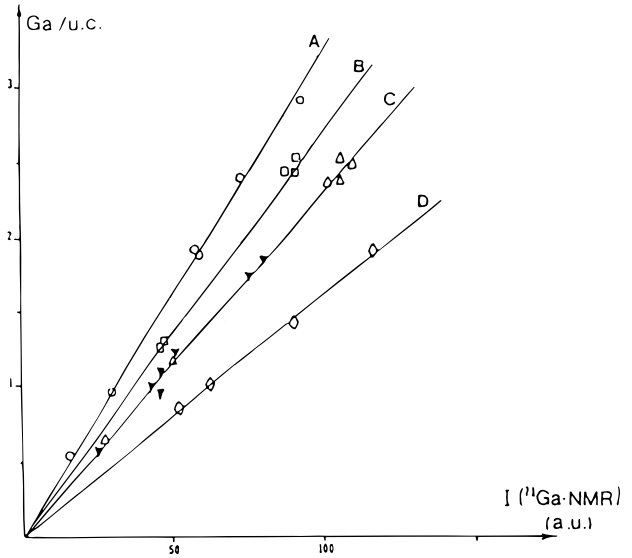

Figure 29. Correlation between the Ga contents (molecules per unit cell) in various as-synthesized [Ga]-ZSM-5 zeolites, as determined by chemical analysis, and the intensities of the corresponding normalized ^{71}Ga NMR line. Correlations A, B, and C are given for gallosilicates synthesized in the presence of F^- ions (○), Na^+ ions (□), and TPA^+ ions (△) and for gallo-aluminosilicates (▼). Correlation D is derived for calcined, NH_4^+-exchanged and water-equilibrated samples (○) as described in Table 14, column 6. (Reprinted with permission from ref 123. Copyright 1992 Van Nostrand Reinhold.)

Linear correlations reveal different slopes depending on the synthesis conditions. The kind of cation (Na^+, TPA^+) or the presence of F^- in the as-synthesized samples seems to exert an influence on the magnetic environment of Ga^{3+} framework ions. Proper linear correlations are only observed for samples with high crystallinity. Otherwise, the determined Ga concentrations do not fit any correlation.

^{129}Xe NMR Spectroscopy. The ^{129}Xe NMR spectrum of xenon adsorbed on zeolite structures contains information on the framework configuration.[183−186] Application to H[Ga]-MFI zeolites is reported by Bradley and Howe.[179] The method is based on the facile polarizability of the xenon atom. Collisions between xenon atoms and zeolite channel walls but also between two or more xenon atoms with each other perturb the xenon orbitals and induce variations in the nuclear shielding of the xenon atoms. This is reflected by changes in the ^{129}Xe NMR chemical shifts. The experimental shift δ with respect to the reference signal is represented by the equation

$$\delta = \delta_{\mathrm{Xe-Xe}\,\rho\mathrm{Xe}} + (\delta_{\mathrm{Xe-Z}} + \delta_{\mathrm{E}}) \qquad (17)$$

where the shift $\delta_{\mathrm{Xe-Z}}$ originates from collisions between Xe atoms and the zeolite framework. The term $\delta_{\mathrm{Xe-Xe}\,\rho\mathrm{Xe}}$ accounts for Xe−Xe collisions and is a function of the Xe density (ρ_{Xe}) as well as of the pore size; δ_{E} refers to the effects of the electric field within the zeolite interior including ionic effects such as interactions between Xe and counterions. Equation 17 implies a linear relation between the observed chemical shift and the xenon density. By extrapolating the straight line to zero xenon density ($\rho_{\mathrm{Xe}} = 0$), numerical values of the intercept ($\delta_{\mathrm{Xe-Z}} + \delta_{\mathrm{E}}$) can be determined, which contain information on the interaction between xenon and the zeolite walls. It could be shown[187] that for aluminosilicate MFI zeolites the chemical shift extrapolated to zero xenon loading is proportional to the concentration of aluminum in the lattice and hence to the concentration of acid sites.

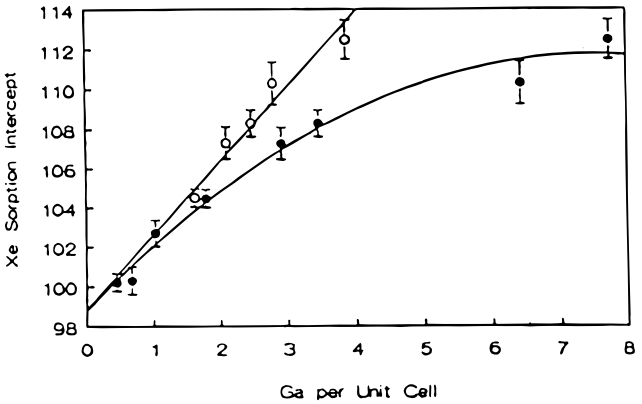

Figure 30. ^{129}Xe spectroscopy of [Ga]-ZSM-5 zeolites: Plot of the extrapolated chemical shift δ_{Xe} ($c_{\mathrm{Xe}} = 0$) over the number of Ga ions per unit cell in: (○) framework positions, (●) nonframework "bulk" positions. Error bars represent double standard deviations. (Reprinted with permission from ref 179. Copyright 1995 Elsevier Science.)

Bradley and Howe[179] investigated a series of [Ga]-ZSM-5 samples with Si/Ga ratios ranging from 11.4 to 210.2 by NMR techniques including ^{129}Xe NMR. The framework gallium content was determined from profile analysis of the ^{29}Si MAS NMR spectra. The relation between the ^{129}Xe chemical shift and the xenon density (expressed as number of Xe atoms added per gram of zeolite), however, was found to be nonlinear. Specifically at higher Ga contents, a curvature toward lower shifts is visible. This indicates that xenon atoms encounter surrounding effects which are not covered by the terms of eq 17. One effect not accounted for is that xenon migrates several micrometers during the acquisition time of the NMR spectrum. This motion averages surrounding effects. A discrimination between the quantities of admitted xenon to the sample and of xenon actually adsorbed on the sample could not eliminate the curvature. Nevertheless, for samples with Si/Ga > 14, observed curves are fairly linear over the abscissa in the range of 2×10^{20} to 7×10^{20} atoms of Xe added to 1 g of zeolite. Values for the chemical shift have been determined by extrapolation and plotted versus the framework and nonframework gallium concentration gained by chemical analysis and calculated from ^{29}Si MAS NMR spectra (Figure 30).

It is well understood that the characterization of framework compositions by ^{129}Xe NMR requires additional information on the concentration and distribution of the substituting atoms in the framework.

4. EXAFS and XANES

X-ray absorption spectroscopy with its two domains XANES (X-ray near-edge spectroscopy) and EXAFS (extended X-ray absorption fine structure spectroscopy) is used to investigate the local environment of

substituting elements.[112,188−192] Coordination numbers as well as bond distances to neighboring atoms can be derived.

Evaluation of the Fourier transforms of Ga K-edge EXAFS spectra of gallosilicates showed that, in accordance with Loewenstein's rule, Ga−O−Ga linkages do not exist in gallosilicates.[112] Peaks at 0.31 and 0.35 nm are assigned to Ga−O−Si distances.

Ga and Fe (or Sr) (Si/Ga = 100, Si/Fe = 100) were simultaneously introduced into the framework of silicalite-1 by adding Ga nitrate and Fe(III) nitrate (or Sr chloride) to the synthesis gel. It was found that Fe and Ga independently substitute framework silicon. The local structure around Sr was the same as that in Sr^{2+}-exchanged gallosilicate.[112] The close similarity of the EXAFS profiles of amorphous and crystalline phases obtained during crystallization of [Ga]-ZSM-5 prove that the local structure around Ga is formed in a very early stage of the hydrothermal crystallization process without formation of Ga oxide or hydroxide. The relative intensity of the peak at 0.35 nm increases and that at 0.31 nm decreases slightly with crystallization time. Parallel XRD studies have shown (change in XRD intensity at a spacing d(501) of the silicates) that silicate crystallizes during a short time interval if crystallization time exceeds 2 h. It can be concluded that the EXAFS peak at 0.31 nm can be assigned to the Ga−O−Si distance in an amorphous gallosilicate, whereas the peak at 0.35 nm stems from the Ga−O−Si distance in the crystalline MFI gallosilicate structure. The regularity of the local structure around Ga in the pentasil framework increased with crystallization time.

In a recent EXAFS and XANES study of MFI gallosilicates with various Si/Ga ratios (Figure 31), the conclusion was drawn that a precise determination of the first-shell coordination of gallium atoms on framework T positions is possible.[192] At low Si/Ga ratios, a substantial part of the gallium remains outside the framework after completion of the synthesis. These nonframework gallium species occur in both tetrahedral and octahedral coordination. Therefore, the detection of tetrahedrally coordinated gallium is not unambiguous proof for its incorporation into the framework. EXAFS cannot differentiate tetrahedral Ga in the gel, in the MFI framework, or localized in the nonframework species. The authors recommend a combined use of appropriate techniques.

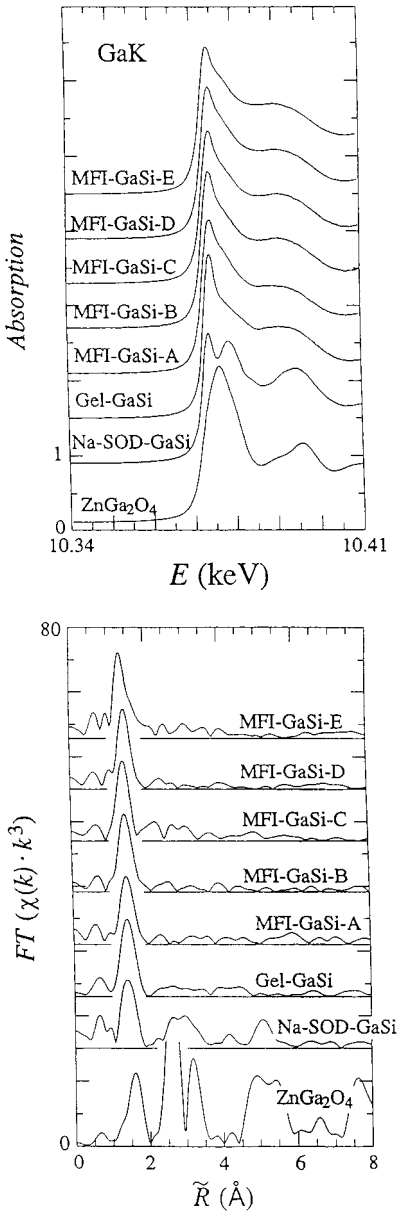

Figure 31. XANES spectra (top) and Fourier transforms of k^3-weighted EXAFS data (bottom) recorded at the GaK edge of [Ga]-ZSM-5 (MFI−GaSi) obtained after different crystallization times. Starting synthesis gels: [Ga]-ZSM-5 (Si/Ga_{gel} = 50) after 0, 5, 24, 48 h of crystallization for Gel-GaSi, MFI−GaSi-A, MFI−GaSi-B, and MFI−GaSi-C, respectively; [Ga]-ZSM-5 (Si/Ga_{gel} = 40, 72 h) for MFI−GaSi-D, and [Ga]-ZSM-5 (Si/Ga_{gel} = 19, 72 h) for MFI−GaSi-E. Reference samples: [Ga]-sodalite with tetrahedrally coordinated Ga; $ZnGa_2O_4$ with octahedrally coordinated Ga. (Reprinted with permission from ref 192. Copyright 1995 Elsevier Science.)

5. Adsorption and Desorption of Bases

Adsorption of bases serves as a routine method for the characterization of the acidity of zeolites and will be discussed in section IV.C in detail.

Generally, the detection of Brønsted acid sites in a gallosilicate structure is an indication that gallium has entered tetrahedral framework positions. The brief discussion in the this section only takes into account papers that are directed primarily to the quantitative determination of gallium-related sites.

The adsorption of ammonia, 2-propanol, and 2-propanamine over H[Ga]-ZSM-5 has been examined through temperature-programmed desorption and thermogravimetric analysis.[193] For each of the adsorbates, a clearly defined adsorption complex with a stoichiometry of one molecule per Ga could be identified. One example is given in Figure 32 for 2-propanamine as a probe molecule. The low-temperature peak (m/e = 44) of unreacted 2-propanamine indicates the existence of weak acid sites. The amount of weakly adsorbed amine is in excess of one molecule per gallium atom (cf. Figure 32, top). At higher temperatures, 2-propanamine decomposes to propene and ammonia. The sum of desorbed products corresponds to a coverage of one molecule of 2-propanamine/Ga. The results encourage the utilization

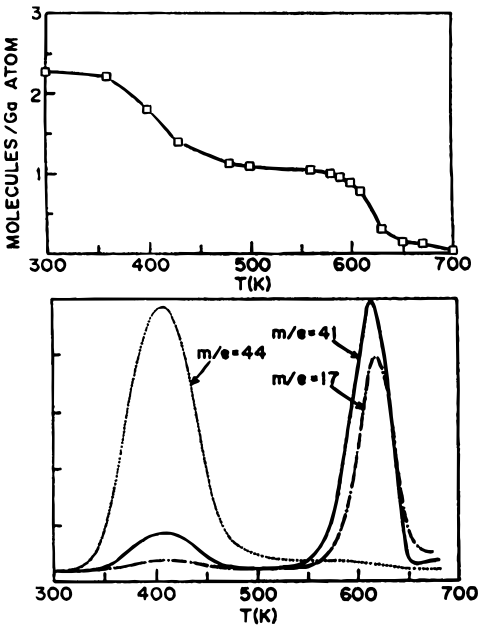

Figure 32. TPD-TG curves of 2-propanamine from zeolite H[Ga]-ZSM-5. The top curve shows the coverage in terms of molecules per Ga obtained from thermogravimetry. The bottom curves show results of mass spectrometric analysis indicating desorption of unreacted 2-propanamine (m/e = 44) at low temperatures and decomposition products water (m/e = 18) along with propene (m/e = 41) at higher temperatures. (Reprinted with permission from ref 193. Copyright 1989 Elsevier Science.)

of probe molecules other than ammonia for the determination of Ga in framework positions of gallosilicates. It has to account for the fact that a chemical or OES−ICP analysis comprises framework and nonframework gallium. Si/Ga framework ratios calculated on the basis of these data will only be correct if all of the gallium is inserted into the framework.

B. Gallium in Nonframework Positions

Nonframework gallium species occur in various forms and can be located at different positions within the solid material. Excess gallium not incorporated into the framework during synthesis will remain either as a separate phase or as gallium located inside the pore system. Calcination of the gallosilicate at about 770 K, to destroy the template by oxidation, converts the residual gallium salts into the oxides. These oxides are not necessarily crystalline but may retain an amorphous state. Inside these materials, gallium can be either tetrahedrally or octahedrally coordinated. When aluminosilicate structures are modified by gallium through postsynthesis procedures such as ion exchange, nonframework gallium ions can also occupy cation positions substituting other metal cations, ammonium ions, or protons. Theoretically, one trivalent gallium ion can compensate for three negative univalent framework charges. An exchange degree of 100% would therefore already be reached at one-third of the gallium concentration offered (in comparison to the total concentration of acid sites). However, this would require a close geometric neighborhood of three acid sites. This is improbable, because the Loewenstein rule forbids such a configuration. Owing to hydrolysis, partial hydroxylation, or oligomerization of gallium cations (e.g., $Ga(H_2O)_6^{3+}$, $[Ga(H_2O)_{6-n}(OH)_n]^{(3-n)+}$, or $[Ga_2(OH)_2(H_2O)_6]^{4+}$) in solution, the effective charge at the gallium is lowered and a nonstoichiometric ion exchange is possible. Exchanged Ga species can be partially bound to the framework oxygen atoms in the vicinity of crystal defects. Processes accompanying a subsequent calcination are not fully understood because calcination is normally performed in atmospheric air and a reduction of Ga^{3+} to Ga^+ is, therefore, not easy to explain.

1. Chemical Analysis

Determination of gallium contents by chemical analysis cannot differentiate between different gallium species. Monque et al.[194] reported an analytical method for the quantitative determination of framework and nonframework gallium in zeolitic materials using flame atomic absorption spectroscopy (AAS). Whereas after dissolution of the sample in HF, AAS analysis provides the total concentration of gallium, a controlled extraction by HCl followed by filtration to remove the undissolved material allows one to determine the nonframework Ga content separately. The amount of framework Ga was derived from the difference of both values. Price et al.[195] estimated the percentage of nonframework Ga and the Si/Ga framework ratios for a series of [Ga]-ZSM-5 samples in this manner. The amount of Ga extracted by HCl was insignificant (<2%) for a sample prepared from a gel with a molar SiO_2/Ga_2O_3 ratio of 63.6 but achieved 30% or 16% for samples with molar ratios of 43.5 or 29.5, respectively. Framework Si/Ga ratios estimated on the basis of the dissolution/extraction method, however, did not agree with the Si/Ga ratios derived from the unit cell sizes (XRD). The reliability of the extraction method needs further corroboration.

2. X-ray Diffraction

For H[Al]-ZSM-5 modified by ball-milling with β-Ga_2O_3 for 3 h (Ga percentage 0.5 wt %), Dooely et al.[196] observed X-ray reflections at 31.7° and 35.2° indicating the presence of small β-Ga_2O_3 crystallites with a size of >30 nm.

The identification of crystalline nonframework gallium species inside the gallosilicate crystals, however, is not reported by XRD.

3. Temperature-Programmed Reduction (TPR)

Framework gallium in an isolated tetrahedral environment[197] cannot be reduced at moderate temperatures. The observed reducibility of gallium-modified zeolites therefore indicates the presence of nonframework gallium species. As nonframework gallium species are the actual active components in the Cylcar-type catalyst (see section VI) and their reducibility is crucial for the catalytic performance, ample work is published on the state of gallium-modified zeolites possessing nonframework gallium species exclusively. Kwak et al.[152] modified H-ZSM-5 (Si/Al = 20.5) with various amounts of Ga obtained by vapor deposition of $GaCl_3$ in a glovebox, followed by temperature-programmed calcination up to 773

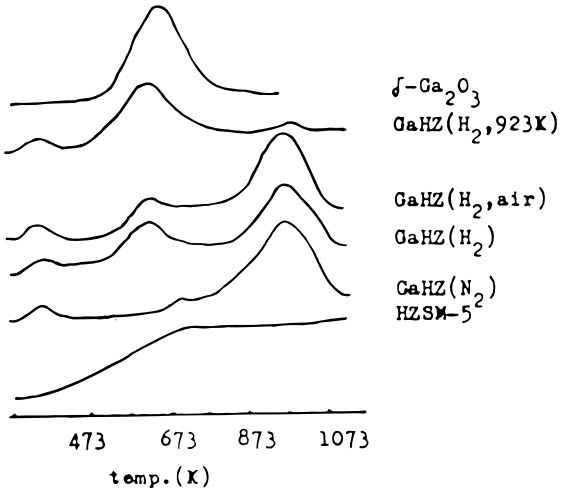

Figure 33. H_2-TPR profiles (10 vol % H_2 in N_2, $\beta = 13.6$ K/min) of H-ZSM-5, δ-Ga_2O_3, and Ga_2O_3/H-ZSM-5 (GaHZ) samples after pretreatment at various conditions of temperature and gas atmosphere. If not otherwise indicated, samples were treated at 773 K for 2 h. GaHZ (H_2, air) was subjected to consecutive pretreatment in H_2 and in air (773 K, 2 h). (Reprinted with permission from ref 198. Copyright 1994 Elsevier Science.)

K. Ga loading amounted to 0.77, 1.36, 2.95, 2.97, 3.70, or 3.76 wt %. TPR profiles are of a diverse nature but are dominated by two major peaks: one peak near 723 K (denoted as α-peak) was assigned to the reduction of highly dispersed Ga_2O_3 and the second peak near 903 K (denoted as β-peak) to the reduction of GaO^+ ions.

Except for the sample with the highest Ga loading, the α-peak is shifted to lower temperatures and the position of the β-peak to higher temperatures with increasing Ga contents. The peak area ratio A_β to A_{total} increases with Ga loading, suggesting that GaO^+ ions are favored at high loading.

Jia et al.[198] performed TPR with H_2 (10 vol % in N_2) at a heating rate of 13.6 K/min (Figure 33).

Catalysts were prepared by mechanical mixing of δ-Ga_2O_3 (received through oxidation of metallic gallium) with H-ZSM-5 or Na−ZSM-5 and calcination at 773 K for 6 h. H-ZSM-5 shows no distinct hydrogen consumption. The pure gallium oxide exhibits one reduction peak centered at 663 K. Gallium-modified samples reveal peaks at 633 and 923 K ascribed to hydrogen adsorption at various (yet unknown) Ga sites (compare Petit et al.[199]). This assignment, however, is not in line with results reported by other authors. From reduction experiments[193] obtained in a microbalance for ion-exchanged materials as well as for mechanically mixed Ga_2O_3/H-ZSM-5, it was concluded that substantial reduction of gallium proceeds at 893 K.

Joly et al.[200] found that the percentage of reduction of Ga ion-exchanged H-ZSM-5 aromatization catalysts (Ga content ca. 3 wt %) during TPR linearly depends on the framework Al content (Figure 34). Brønsted acid sites are assumed to act as "docking" points for highly dispersed Ga_2O species. Ga_2O_3 dispersed over alumina cannot be reduced at all even at high temperatures. For comparison, an Al-free [Ga]-ZSM-5 sample (Al/(Al + Si) = 0) steamed at 873 K is included in the series.

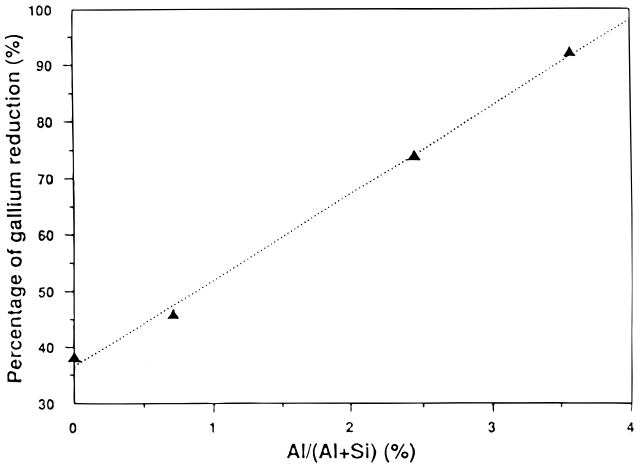

Figure 34. Percentage of reducible Ga species in Ga−H-ZSM-5, according to H_2-TPR results, vs Al mole fraction (×100) of the zeolite. Introduction of Ga (ca. 3 wt %) by reductive solid-state ion exchange from Ga_2O_3/H-ZSM-5 mechanical mixtures. Al/(Al + Si) = 0 indicates an Al-free [Ga]-ZSM-5 sample. (Reprinted with permission from ref 200. Copyright 1992 Butterworth-Heinemann.)

Combined adsorption of bases and TPR with H_2 revealed that gallium ions generated by the reduction of nonframework Ga_2O_3 occupy cation positions in the zeolite channels possibly according to the equation

$$Ga_2O_3 + 2H^+Z^- + 2H_2 \rightarrow 2Ga^+Z^- + 3H_2O \quad (18)$$

where Z^- symbolizes the anionic zeolite framework.[195]

The equation reflects the process of solid-state ion exchange described earlier in this review (see section III.C). It should, however, be mentioned that other reduction processes consuming H_2 are also reasonable, e.g.

$$Ga(OH)^{2+} + 2Z^- + H_2 \rightarrow Ga^+Z^- + H^+Z^- + H_2O \quad (19)$$

Hydroxo cations fixed to the zeolite framework are reduced, and Brønsted acid sites are restored.

4. XPS Spectroscopy

Carli and Bianchi[201] studied mechanical mixtures of Ga_2O_3 and metallic gallium by XPS. A photoelectron signal corresponding to a 3d binding energy of 19.0 eV is assigned to Ga(I). It is, however, difficult to determine the oxidation state of Ga in Ga_2O_3/H-ZSM-5 catalysts activated in a He/H_2 stream up to 848 K on the basis of XPS binding energies. Material inhomogenities or experimental artifacts significantly affect the accuracy of results.

A typical spectrum of unreduced Ga_2O_3/H-ZSM-5 exhibits an overlapping of Ga(3d), corresponding to Ga^+, and O(2s) photoelectron peaks (Figure 35, top). After reduction with H_2 (in situ, pressure 5×10^{-7} Pa) at 473 K, the deconvoluted Ga(3d) peak of the reduced samples consists of two components (Figure 35, middle). Higher reduction temperature (773 K) leads to a decrease of the peak intensity of the Ga-(3d) signal (Figure 35, bottom). The assignment of the XPS peaks to different oxidation states is based on reference measurements with high-purity Ga_2O_3,

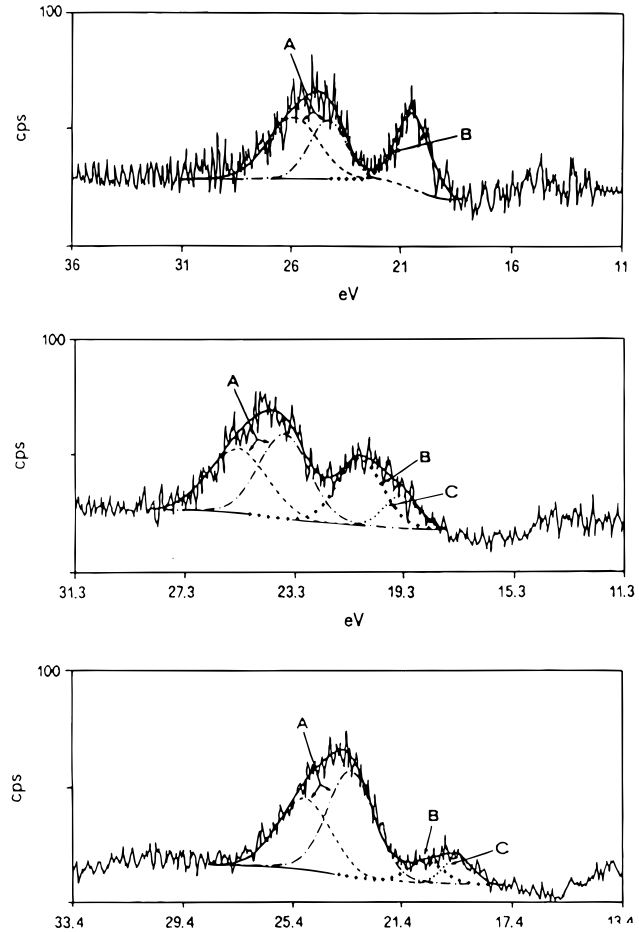

Figure 35. XPS spectra of as-prepared Ga_2O_3/H-ZSM-5 (top) and Ga_2O_3/H-ZSM-5 reduced at 473 K (middle) and at 773 K (bottom) by H_2: (A) O(2s) signals, (B) Ga(3d) signal of high binding energy (HBE) component, and (C) Ga(3d) signal of low binding energy (LBE) component. (Reprinted with permission from ref 147. Copyright 1993 Elsevier Science.)

Ga_2O, and metallic gallium. On the basis of these results, Ga^+ could be unambiguously identified.

XPS spectra of the Ga(3d) and O(2s) region for Ga/H-ZSM-5 treated either in air at 823 K or in hydrogen at 873 K and for a PtGa/H-ZSM-5 treated in hydrogen at 873 K were presented by Shpiro et al.[202] The samples were prepared by treatment of ZSM-5 (Si/Al = 460) with Ga_2O_3 dissolved in NaOH. All samples were calcined in air at 623 K for 3 h.

The Ga(3d) spin−orbital doublet is recorded as a single peak since the difference between the $3d_{3/2}$ and $3d_{5/2}$ levels is very small.

The fraction of Ga in a reduced state is much higher for Pt,Ga/ZSM-5 (ca. 70%) than for Ga/ZSM-5 (30%). Thus, the suggestion is confirmed that Pt has a promoting effect on the reduction of gallium species.

C. Acidity

1. Brønsted and Lewis Acid Sites

Several methods are applicable for the characterization of the acidity of solids (Figure 36). In any case, it has to be specified whether the concentration (an extensive factor) or the strength (an intensive factor) is meant. Results of various methods give information on both the concentration and strength of sites.

Experimentally, the physicochemical properties of the solid per se are amenable to acidity studies but more detailed information is accessible if probe molecules are brought into contact with the surface sites and the mode of interaction is studied. Nevertheless, the information derived is more or less of a qualitative nature.

The way to generate Brønsted acid sites is based either on the thermal decomposition of the ammonium form of as-synthesized zeolites or on the direct ion exchange of Na^+ (usually) by H^+ (with mineral or organic acids). Brønsted acid sites are convertible into Lewis acid sites by dehydroxylation at elevated temperatures.

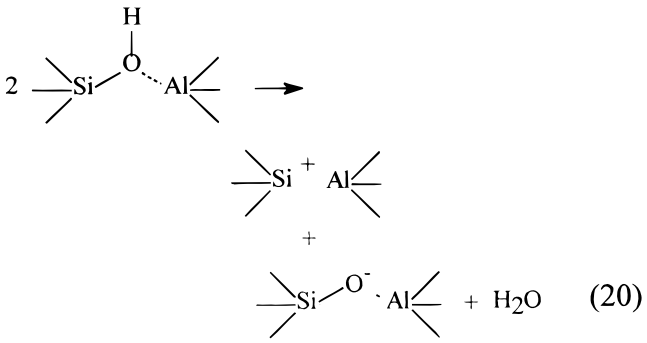

(20)

The acid strength of Brønsted sites depends on both the chemical composition and spatial distribution of the atoms surrounding the site. This 'localized' approach underlies Sandersons' electronegativity concept based on the assumption that the acid strength of an OH group vibrating in a zeolite pore depends on the chemical composition of the environment. The average electronegativity of a compound, say $P_pQ_qR_r$, is viewed as the geometric mean of the free atom electronegativities of all atoms present. The intermediate electronegativity is given by

$$S = (S_{P_p} S_{Q_q} S_{R_r})^{1/p+q+r} \qquad (21)$$

with S_P, S_Q, and S_R denoting the free atom electronegativities of atoms P, Q, and R, respectively.

It is expected that a relation between the average electronegativity S and the acid strength of structural OH groups does exist at least for a homologous series of ZSM-5 zeolites with different substituting elements. Results of this type of calculation[203] are shown in Figure 37.

Estimated S values for the most frequently used trivalent elements incorporated in MFI structures are in the order Ga > B > Al > Fe and do not correctly reflect the order of decreasing acid strength of protonic sites related to gallo-, boro-, alumino-, and ferrisilicates known from IR spectroscopy and TPDA. Later, Dompas et al.[157] reconsidered S values for various zeolite structure types (FAU, LTL, BEA, MOR, MEL, MFI, TON, and MTW) either in their Al forms or as gallosilicate analogues on the basis of the wavenumbers of framework modes. For Al zeolites, the authors derived a linear correlation for the frequency of the T−O asymmetric stretching vibra-

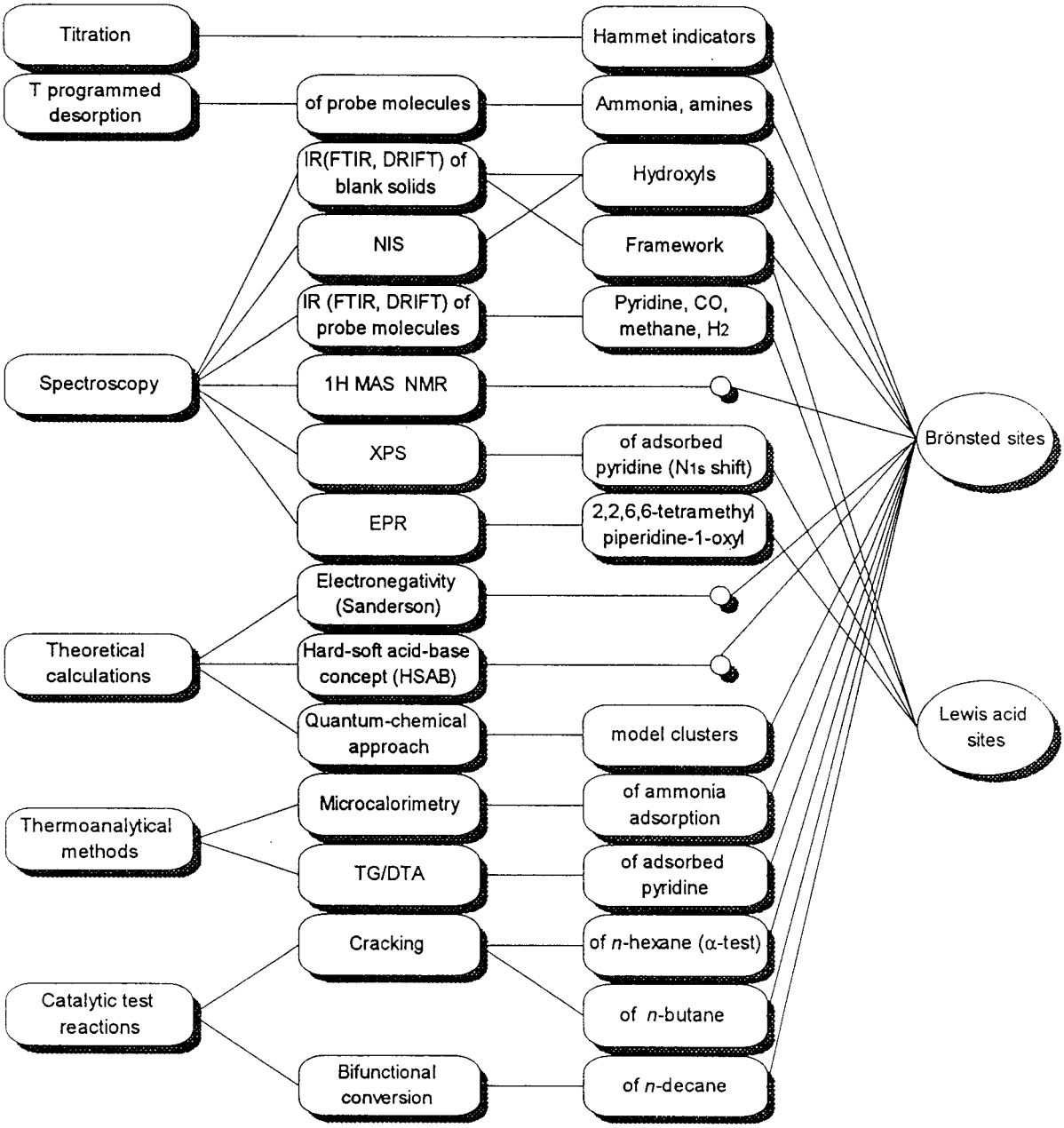

Figure 36. Theoretical studies and experimental methods to characterize the acidity of zeolites.

tion of internal tetrahedra as a function of the average electronegativity (Figure 38).

Applying this correlation and recorded IR frequencies for Ga-containing zeolites, the electronegativity value of Ga was numerically calculated for various Ga contents. This way, an average electronegativity value of 1.59 for Ga was found which is in fact lower than that for Al (1.714), thus implying a higher acid strength of Brønsted protons for Al-substituted zeolites. This is in accordance with experimental findings. The acidity of zeolite MFI structures containing boron, however, remains highly overestimated.

2. Characterization of Brønsted Acidity in Gallosilicates

a. Theoretical Calculations and Molecular Modeling. Quantum chemical calculations have contributed to the understanding of energetic and geometric site configuration. For theoretical calculations, a suitable cluster model has to be selected. Bonds extending into the framework must be terminated, usually by hydrogen atoms or hydroxyl groups. Depending on the cluster size, these arbitrary finite boundaries and the lack of long-range electrostatic interaction may affect the accuracy of the calculations. Most theoretical studies have been based on ab initio molecular orbital theory. The computational demands of ab initio methods rapidly increase with the size of the selected cluster, especially if electron correlation is included. Density functional theory (DFT) is viewed as a viable alternative to ab initio methods because results of comparable accuracy are obtained at considerably lower computing costs. Small cluster models, e.g., $H_3Si(OH)TH_3$ (T = Al, Ga, Fe), assuming C_s geometry were found to give an adequate description of the local properties of bridging hydroxyl groups in zeolites.[204] On the basis of these models, the decrease of Brønsted acidity in the order T = Al, Ga, Fe, which is in agreement with

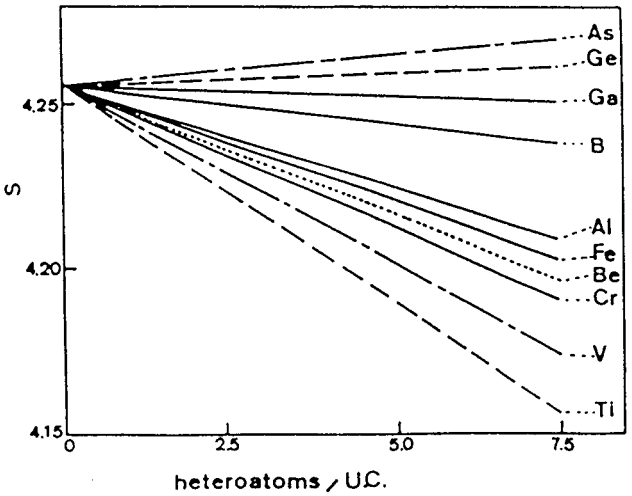

Figure 37. Changes of the Sanderson electronegativity, S, of different isomorphously substituted MFI-type structures (zeolite ZSM-5) depending on the number of heteroatoms per unit cell.[203]

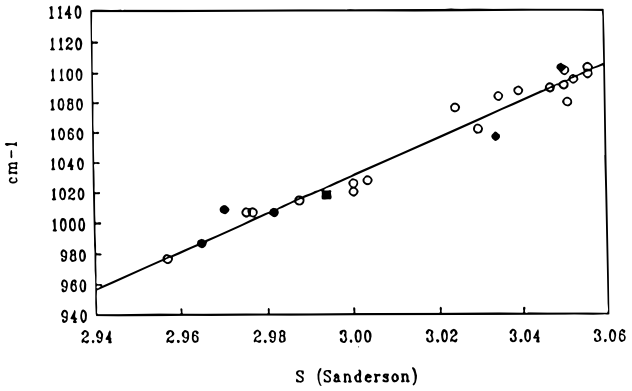

Figure 38. Correlation between the wavenumber of the antisymmetric T−O−T framework vibration and the average Sanderson electronegativity of [Al]-zeolites (○), [Al,-Ga]-zeolites (●), and [Ga]-zeolites (■) of different Si/Al,Ga ratios. (Reprinted with permission from ref 157. Copyright 1991 Academic Press.)

experimental and theoretical results, could be predicted. Stave and Nicolas[205] showed how the increase of the size of the zeolite model affects the results of calculation. The energy and the geometry of clusters of the form $(X)_3Si-OH-T(X)_3$, with X = OH, $OSiH_3$, or $POSi(OH)_3$ and T = Si, Al, B, Ga, or Fe, were calculated by means of the DFT approach. Internal coordinates converge quickly with increasing model size, while deprotonation energies do not converge within the range of models tested. The correct prediction of the acidity trend for the substituted [Al]-ZSM-5, [Ga]-ZSM-5, [Fe]-ZSM-5, and [B]-ZSM-5 in decreasing order required the largest model and extensive geometry relaxation. In other cases, even very small cluster models allow a description of overall lattice properties.

The strongly acidic proton in zeolites (aluminosilicates) is bound to the bridging oxygen atom connecting Si- and Al-containing tetrahedra. The lower valence of the Al atom enhances the proton−oxygen interaction in comparison with the Si−O−Si system. Coordinative bonding to Al^{3+} weakens the OH bond (compared with the free silanol group). The $Al-(O)_3$ framework unit can be considered as a Lewis acid promoting the acidity of the proton of the adjacent silanol group: $SiOH\cdots Al-(O)_3$.

The zeolite lattice is not strictly rigid. It is highly flexible upon substitution of framework atoms, upon cation exchange, adsorption, and proton transfer (e.g., through interaction of the acid site with a basic adsorbate). Compensation of the structural stress of the framework introduced by substitution of T atoms (e.g., Si by Al or by other metals) preferentially occurs by a local deformation of the Si−O−T bridges, i.e., by a rearrangement of the oxygen atoms directly coordinated to T. This maximizes the ionicity of the bridging hydroxyl group. Van Santen et al.[206] concluded that if the topology of the zeolitic network requires adaptation of bond lengths and T−O−T angles, the tetrahedra are deformed. In a flexible lattice the interaction of acidic protons with a basic adsorbate results in a local adjustment of the geometry. Experimentally, this can be observed by the shift of vibrational frequencies of the zeolite framework modes.

The stability of $Si-O^{(-)}-Al,Ga$ bridges is affected by the nature of the charge-compensating cation. Higher stability is observed for more electropositive countercations.

Fundamental differences in acidity between a bridged hydroxyl group and a free or terminal hydroxyl group can be predicted.

Properties of interest from the point of view of acidity are (1) the charge on the proton (q_H), (2) the ionicity of the OH bond ($|q_O q_H|$), (3) the equilibrium OH bond distance (r_{OH}), (4) the calculated force constant (f_{OH}), and (5) the calculated vibrational stretching frequency (ν_{OH}).

Ab initio quantum mechanical calculations of bridging hydroxyl groups are reported by several groups.[207−212] Zahradnik et al.[209] chose the model clusters I−III as prototypes of metallosilicate structural units with isomorphous substitution of the heteroatom M (M = Al, Ga, In, B). Model II represents the hydrate complex:

$$\underset{\text{I}}{H_3Si\,MH_3} \quad \underset{\text{II}}{H_3Si\,MH_3} \quad \underset{\text{III}}{H_3Si\,MH_3} \qquad (22)$$

The molecular geometry of all the structural units was completely optimized. Replacement of Al by Ga confirms the experimental observation that the Brønsted acid sites of Ga-substituted zeolites have a lower acid strength than those of the parent aluminosilicate structures.

Calculations by different authors in a temporal distance of several years show a good reproducibility of relevant parameters of the bridging hydroxyl groups (Table 9). Stretching vibration frequencies of the OH group resulting from the calculations are in a less good accordance with values derived from IR spectroscopic data (Table 10).

The quantity which is commonly acknowledged as a measure of the acid strength in the Brønsted sense is the energy necessary to remove the proton from the bridging hydroxyl group. This deprotonation energy is defined as the difference between the energies of the neutral and the deprotonated aggregates. Deprotonation energy appears to be rather

Table 9. Comparison of Relevant Parameters of Bridging OH Groups from *ab Initio* Quantum Chemical Calculations Based on Dimeric Model Clusters[209]

parameter[a]	T = Al	T = Ga
q_H	0.4755	0.4735
	0.4727	0.4710
r_{OH}	0.967(3)	0.965(3)
	0.967	0.965
$\|q_O q_H\|$	0.4449	0.4391
	0.4415	0.4357

[a] q_H = charge on the proton of the bridging hydroxyls (a.u.), $|q_O q_H|$ = ionicity of the OH bond (au), r_{OH} = equilibrium OH bond distance (Å).

Table 10. Comparison of ν_{OH} Stretching Vibration Frequencies from ab Initio Quantum Mechanical Calculations with Experimental Data from MFI Metallosilicates[209]

	ν_{OH} (cm^{-1})	
method	T = Al	T = Ga
ab initio, theoretical	3931	3940
IR, experimental	3610	3615

Table 11. Deprotonation Energies of $(OH)_3T_1OHT_2(OH)_3$ Complex for T_1 = Al, B, and Ga; T_2 = Si and Ge[213] [a]

	SiAl[b]	SiB[b]	SiGa	GeAl	GeB	GeGa
$r(O-T_1)$	173	146	180	173	146	180
$r(O-T_2)$	163	163	163	169	169	169
$<(T_1OT_2)$	131.5	134.6	134.8	134.8	135	135
$\Delta^{(1)}$	1320.9	1379.4	1304.2	1316.7	1379.4	1300
$\Delta^{(2)}$	1337.6	1400.3				
$\Delta^{(3)}$	1220.6	1224.7		844.4	1228.9	

[a] Distances (r) in pm, $<(T_1OT_2)$ in degrees, and deprotonation energies $\Delta^{(i)}$ in kJ/mol. Superscript (i) is read (1) pseudopotential method, (2) ab initio, and (3) semiempirical method MNDO. The geometry adopted for the pseudopotential calculation (two perfect tetrahedra) was also used in cases 2 and 3. [b] Ab initio calculations at the 6-31G level.

a local property not strictly correlated to the size and to the form of the representative cluster. The efforts spent by theoreticians involve the question of how substitution of Si or Al by other elements would modify the energy and hence the strength of the acidic bridging hydroxyl group. Kassab et al.[213] considered two distinct tetrahedra bound through a hydroxyl group $(OH)_3T_1OHT_2(OH)_3$. They determined deprotonation energies for T_1T_2 pairs BSi, GaSi, AlGe, BGe, and GaGe by the pseudopotential method and by ab initio calculations (Table 11).

It turned out that the acid strength is primarily controlled by the electron-deficient atom (B, Al, Ga) and nearly unaffected by substitution of the tetravalent atoms (Si, Ge). Substitution of Al by B corresponds to a net decrease of the acidic strength, whereas Ga introduction leads to a small inverse effect so that the acidic scale would be in the order B ≪ Al < Ga. This finding is not in line with the commonly accepted view that substitution of aluminum by gallium would lower the acid strength of Brønsted sites. Deviations are considered to be caused by differences of applied methods: full ab initio (for SiAl and SiB) and pseudopotential (for SiGa).

Quantum chemical cluster calculations for a series of gallium-free zeolite structures (LTA, MEL, MFI, OFF, MOR, FAU, and LTL) yielded partial charges of the bridging oxygen of Brønsted sites which correlate with experimental acidities determined by the catalytic activity of the 2-propanol decomposition or estimated from the position of the peak maxima in the desorptograms of NH_3-TPD.[214]

Often discrepancies between calculated deprotonation energies do not reflect real differences of acidity but should rather be ascribed to the methodology or to the cluster unit chosen for calculation. The prediction of acidities for different frameworks or crystallographic positions based on experimentally observed (and hence unavoidably averaged) structures is apparently less reliable.[215]

Inui et al.[216] described NH_3 adsorption on acidic sites of various metallosilicate MFI and BEA structures (Me = Al, Ga, Fe, Zn) by computer simulation based on a Monte Carlo approach comprising the following steps: (i) placing an ammonia molecule at a random position in the framework domain of the metallosilicate, (ii) removal of a random ammonia molecule, (iii) translation, or (iv) rotation of a randomly placed ammonia. The decision of acceptance or rejection of a new configuration is based upon the energy change.

Simulations aiming at the estimation of the potentials of adsorption sites and the amount of adsorbed NH_3 were carried out for structural configurations with four silicon atoms of the T12 site (MFI) being replaced by Al, Ga, or Fe. Potential energies of NH_3 molecules in the metallosilicate were calculated by using the DREIDING II force field.[217] Adsorption was simulated for 300 K and 100 kPa. The calculated amounts of adsorbed NH_3 decreased in the order Al > Ga ≫ Fe for both MFI- and BEA-type metallosilicates. The MFI structure adsorbs more NH_3 than the BEA structure (calculated). This is ascribed to a much more localized and concentrated distribution of adsorption sites in the MFI structure as compared with the BEA structure. One example from a graphic visualization of the results is shown in Figure 39. Results of the simulation consistently corresponded to the experimentally observed NH_3 desorption profiles.

b. Experimental Evidence. The IR vibration band of Brønsted sites (bridged hydroxyl groups) occurs at 3610 cm^{-1} in nonmodified H-ZSM-5. Characteristically, the stretching vibration frequency is shifted to higher values if Al is substituted by Ga, Fe, or B.

On the basis of the observed frequency shifts, the strength of Brønsted acid sites is sorted in the order B(OH)Si ≪ Fe(OH)Si < Ga(OH)Si ≪ Al(OH)Si. As observed with the MFI structure ZSM-5, Ga analogues of other zeolite structures show a shift of the stretching IR vibration of Brønsted acid sites to higher values as compared with pure aluminosilicate structures. This indicates that Ga(OH)Si sites are more covalent than Al(OH)Si sites and, therefore, are of lower acid strength.

It should be noted that the acidity is influenced by the thermal treatment of the samples. Beyer et al.[218]

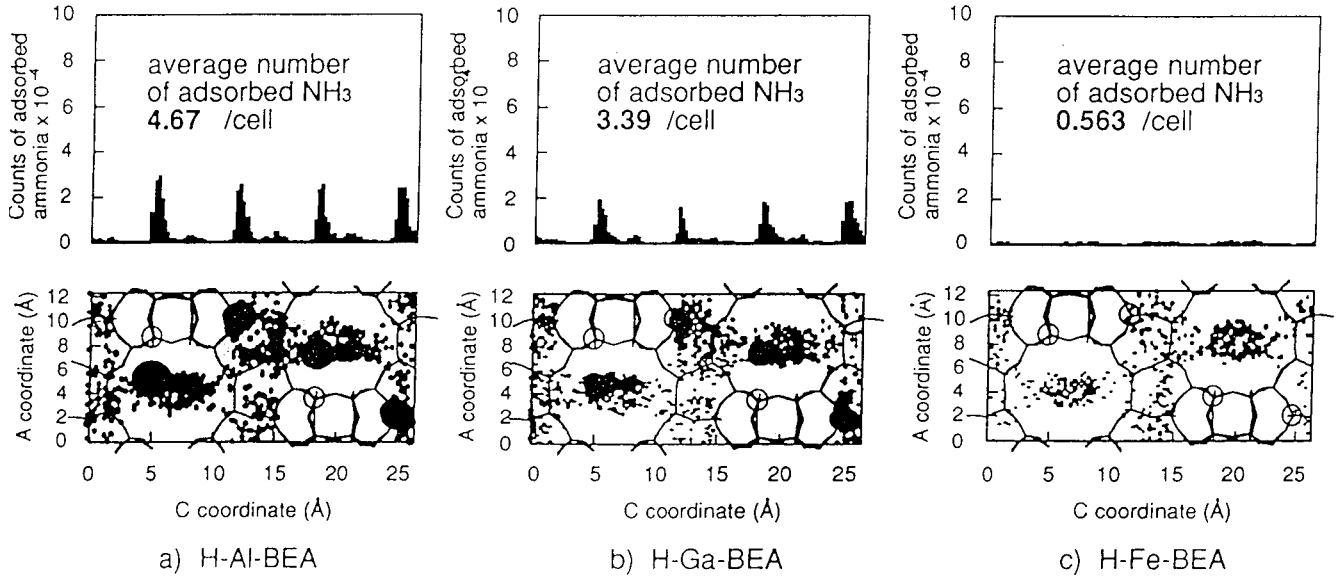

Figure 39. Monte Carlo simulation. Distribution of ammonia adsorbed at BEA-type metallosilicates[216] after 100 000 cycles of random placement of ammonia molecules: (●) positions and counts of adsorbed ammonia; (○) T-sites substituted by metal ions. (Reprinted with permission from ref 216. Copyright 1995 Elsevier Science.)

could show that as-synthesized forms of ZSM-5 and their gallium analogues have practically identical acid properties whereas the calcined template-free form of the gallosilicate was less acidic than the ZSM-5 zeolite.

In analogy to IR spectroscopy, correlating the frequency of bridging OH vibration bands to their acid strength, a similar relation exists between the ^{1}H MAS NMR chemical shift δ_H and the acid strength. δ_H values increase with growing strength of acidity. Magic angle spinning (MAS) of sealed powder samples allows the estimation of chemical shifts with an accuracy of $\delta_H = \pm 0.5$ ppm or better and resolves signals of OH groups with different acid strengths or even of nonacidic OH groups. The total concentration of protons can simply be determined from the area of the proton magnetic resonance line after appropriate calibration. The estimation of the number of structural (bridging) OH groups requires the determination of the total amount of all existing OH groups with subsequent subtraction of the contributions of any other kinds of OH groups.

For a series of H−Y zeolites, Shertukde et al.[219] showed that the integrated peak areas of ^{1}H MAS NMR signals of organic cations correlate with the content of framework aluminum.

Whereas studies on the acid site characterization are available for numerous aluminosilicates, less has been done, so far, concerning group III analogues. On the basis of ^{1}H MAS NMR studies of [Ga]-ZSM-5 (Si/Ga = 15), Challoner et al.[220] made a balance of Ga in framework positions and the amount of cations necessary to compensate for the negative charges of the framework. Ninety percent of the charge is counterbalanced by the protonated template, diethanolamine, and the remainder by Na^+. Calcination at 773 K for 12 h to decompose the template resulted in a partial H-form Na,H[Ga]-ZSM-5. NH_3 desorption profiles, however, indicated a nearly complete absence of strong Brønsted acid sites. The product of calcination has to be considered a "hydrated" form.

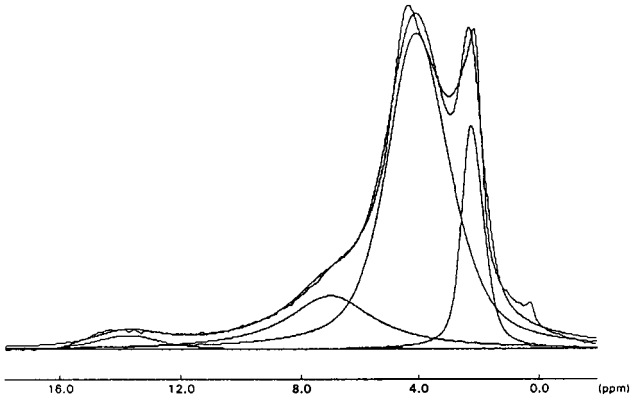

Figure 40. Originally recorded and the deconvoluted ^{1}H MAS NMR spectrum of dehydrated H[Ga]-ZSM-5 (Si/Ga = 50).[174]

The ^{1}H MAS NMR spectrum obtained was compared with further spectra recorded after partial dehydration at 448 K and full dehydration apparently reached after treatment at 673 K for 6 h in a vacuum (10^{-3} Torr).

Two peaks observed for the "hydrated" sample at 4.8 and 2.1 ppm were assigned to the exchange of water between hydrated Brønsted acid sites and Na^+ ions or to the interaction between isolated water molecules and surface silanol groups, respectively. The partially dehydrated form yielded three poorly resolved peaks. The additional peak at 1.7 ppm is attributed to bare surface silanol moieties. The spectrum of the dehydrated gallosilicate exhibits a poor resolution and is dominated by the SiOH signal at 1.7 ppm.

^{1}H MAS NMR spectra of dehydrated H[Ga]-ZSM-5 (Si/Ga = 50) show four signals arising at 2.12, 3.93, 6.95 (shoulder), and 13.67 ppm (Figure 40). They are assigned to silanol groups, acidic bridging Si−OH−Ga groups, (probably) hydrogen-bound acid Si−OH−Ga groups, and a species of still unknown origin, respectively. Owing to the lower acidity of Ga con-

taining zeolites, a shift of the signal of acidic protons is observed after substitution of Al by Ga.

Altogether, the reported ^{1}H MAS NMR spectra and the desorption of ammonia seem to prove that the Ga incorporation in framework positions is negligible.

c. Characterization of Brønsted and Lewis Acidity by Probe Molecules. Temperature-programmed desorption of ammonia (TPDA) is a widespread method to determine sequences in acid strength and concentration of acid sites, provided that desorption peaks are resolved or a mathematical deconvolution of the desorption profile is feasible.

A typical run comprises (i) the loading of ammonia up to saturation at a low but fixed temperature (room temperature or around 373 K), (ii) the isothermal desorption in a flow of inert carrier gas in order to remove ammonia from dead volumes and physically adsorbed ammonia, and (iii) the programmed raise of temperature where ammonia is desorbed according to the strength of interaction with surface sites. Interaction of ammonia with Brønsted acid sites converts the ammonia molecule into a NH_4^+ ion fixed to the Brønsted site. The energy to release free ammonia (reflected by its temperature of desorption) is correspondingly high. Peak positions over the temperature axis in the recorded desorption profiles are indicative of the acidic strength of the sites. The peak areas contain information on the concentration of sites.

Mostly weak and strong acid sites can be distinguished because typically TPDA profiles with two peaks are received. Inui et al.[221] presented TPDA profiles of modified MFI structures obtained from thermogravimetric studies after adsorption of ammonia at 353 K and subsequent desorption at a heating rate of 20 K min^{-1}. Comparison included [Al]-ZSM-5 and [Ga]-ZSM-5 with various Si/Me ratios. Amounts of weakly and strongly adsorbed ammonia were estimated from low-temperature and high-temperature peak areas of the desorption profiles, respectively. A similar quasi-linear relationship between the concentrations of strong and weak acid sites could be established for [Al]-ZSM-5 and [Ga]-ZSM-5 samples (Figure 41).

A correlation of peak maximum temperatures for NH_3 desorption from Brønsted acid sites with IR stretching frequencies of bridged hydroxyls is proposed by Chu et al.[155] and Berndt et al.[222] (Figure 42). Despite the different experimental conditions and a temporal gap of nearly 10 years, the comparability of data is fairly good. Including the results of Mirjosev et al.,[223] it becomes evident that peak maxima from TPDA profiles for the same zeolite may differ by 50 K or more. Experimental differences are without any doubt due to the fact that the dynamic TPDA methods are unsufficiently standardized. Qualitatively an increase of the strength of Brønsted sites shifts the stretching vibration of the hydroxyl group to lower frequencies; the maxima of desorption of ammonia from these acid sites, however, shift to higher temperatures.

Amines are suitable for characterization too. Larger in size than ammonia, they have a limited accessibility to the sites located in micropores. Desorption of

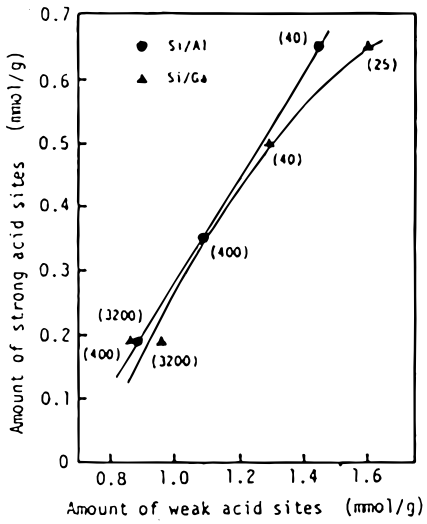

Figure 41. Relation between the amount of weak and strong acid sites for [Al]-ZSM-5 and [Ga]-ZSM-5. Si/Al and Si/Ga ratios are given in parentheses. (Reprinted with permission from ref 221. Copyright 1984 DECHEMA.)

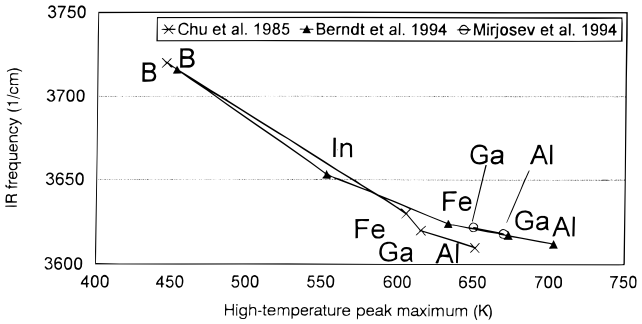

Figure 42. Correlation between the wavenumber of OH stretching vibration bands of acidic bridging OH groups and the maximum temperatures of the NH_3 peak desorbed from Brønsted acid sites of substituted ZSM-5 zeolites. (Adapted from refs 155, 222, and 223.)

larger amines is usually accompanied by their decomposition. Due to its molecular size, quinoline can be used as probe molecule when acid sites of the external surface of zeolites are to be characterized exclusively.[224] Protonation of quinoline at Brønsted acid sites leads to the appearance of IR vibration bands at 1644 and 1412 cm^{-1}. Pyridine can interact with both Brønsted and Lewis acid sites. A differentiation is readily possible by IR spectroscopy. Pyridine adsorbed at Brønsted sites of H-ZSM-5 forms PyH^+ ions with characteristic vibration bands at 1488, 1550, and 1635 cm^{-1}, but if coordinatively bound to Lewis sites, bands at 1446, 1488, and 1600 cm^{-1} appear (Figure 43). For discrimination, the most intense bands, at ca. 1550 cm^{-1} for Bronsted acid sites and at ca. 1450 cm^{-1} for Lewis acid sites, are usually invoked. It should be noted, however, that peak intensities depend on the degree of coverage. Pyridine with weak basic properties is adsorbed first at strong acid sites. Thus, at low coverage, the intensity of bands belonging to pyridine bound to Lewis acid sites is weak.

Anunziata et al.[225] studied the acidity of Ga (and Zn) ion-exchanged Ga-ZSM-11 and Zn-ZSM-5 by adsorption of pyridine. The intensities of vibration bands of pyridine fixed to Brønsted or Lewis sites at

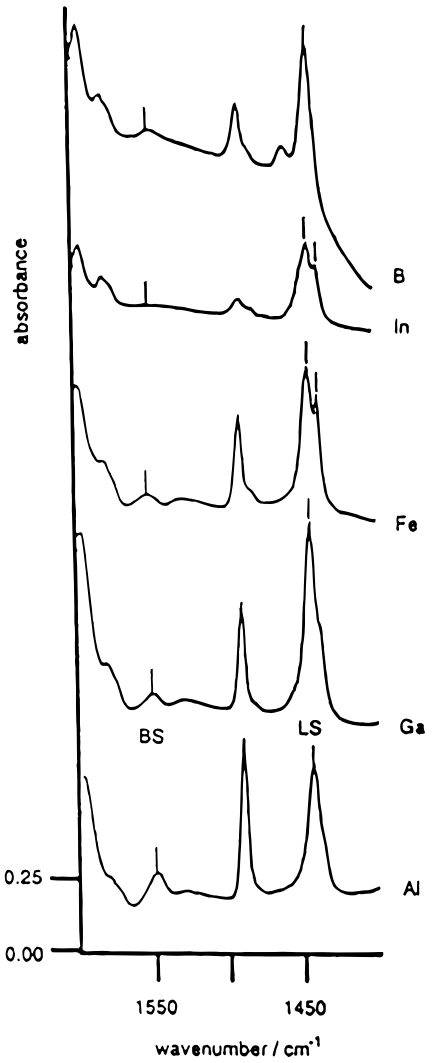

Figure 43. FTIR spectra of pyridine adsorbed at B-, Al-, Ga-, Fe-, and In-substituted ZSM-5:[222] BS = Brønsted acid sites, LS = Lewis acid sites. (Reprinted with permission from ref 222. Copyright 1994 Elsevier Science.)

1545 cm^{-1} and 1450−1460 cm^{-1}, respectively, were determined after outgassing temperatures of 523, 623, and 673 K in a vacuum (10^{-5} Torr). The distribution of sites with regard to their strength was estimated by a stepwise enhancement of outgassing temperatures while recording the residual intensity of the remaining characteristic IR bands. The absorption band disappearing at the lowest temperature was assigned to pyridine fixed to weak (Brønsted or Lewis) sites. The band disappearing at 623 K was attributed to pyridine fixed to sites with medium acid strength, and the vibration band disappearing after outgassing at 673 K was assigned to pyridine fixed to strong acid sites. Results for Ga-ZSM-11 were referred to those received for H-ZSM-11 (Table 12).

Brønsted acidity of the parent H-ZSM-11 (intensity ratios near unity) has not been modified by the Ga ion exchange. This is taken as proof that the large hydrated Ga^{3+} ion had no access to the pores. With Ga-exchanged sample, Lewis acid sites are created obviously due to gallium phases outside the zeolite crystals or at their external surface.

For gallosilicates, two IR bands at 1443 and 1438 cm^{-1} are observed after pyridine adsorption, if pyridine is fixed to Lewis acid sites of [Ga]-ZSM-5 (Si/Ga = 50, gel composition).[222]

Table 12. Modification of Acid Sites of H-ZSM-11 by Ga Ion Exchange According to IR Spectroscopy Using Pyridine as Probe Molecule[225]

	intensity ratio HZSM-11/HGa−ZSM-11[a]	
outgassing temperature (K)[b]	Brønsted sites (1545−1550 cm^{-1})	Lewis sites (1450−1460 cm^{-1})
523	1.3	0.33
623	1.0	0.25
673	0.9	0.26

[a] Si/Al ratio of H-ZSM-11 = 17.25. Exchange with Ga nitrate solution, 0.05 M, 353 K, 4−30 h. Si/Ga ratio of HGa-ZSM-11 = 76.5. [b] Pyridine adsorption at room temperature in vacuo (10^{-5}) Torr. Outgassing at $p = 10^{-5}$ Torr.

Depending on the temperature of the preliminary treatment, concentrations of Lewis and Brønsted acid sites of H-ZSM-5, Ga-ZSM-5, and Zn−ZSM-5 can vary in a wide range.[226] The ratio of Lewis-to-Brønsted acid sites of H-ZSM-5 increases after impregnation with Ga or Zn (1−5 wt % Ga and Zn).

The same behavior is reported for other zeolite structure types. Camblor et al.[166] compared intensities of IR bands at 1545 and 1450 cm^{-1} of [Al,Ga]-beta structures with various Ga/(Ga + Al) ratios (between 0 and 1, corresponding to the pure aluminosilicate or to the pure gallium analogue of zeolite beta, respectively) after pyridine adsorption. With increasing Ga/(Ga + Al) ratio, the concentration of Brønsted sites decreases. Simultaneously, the concentration of Lewis sites increases indicating the existence of Ga on framework positions. Ga in framework positions has a lower thermal stability than Al. The same conclusion was drawn by Chandwadkar et al.[161] They found that the relative concentrations of Brønsted and Lewis acid sites were higher for [Ga]-mordenite (Si/Ga = 38) than for [Al]-mordenite.

Hydrogen adsorption at 77 K on MFI gallosilicates leads to IR vibrations at 4125 and 4065 cm^{-1}. The high-frequency band at 4125 cm^{-1} is attributed to the interaction of H_2 with bridged or terminal OH groups. The signal at 4065 cm^{-1} is attributed to H_2 complexes with electron-acceptor sites of nonframework gallium.[132] This assignment is based on earlier experiences showing that a band at nearly the same frequency is observed when hydrogen interacts with nonframework aluminum species of ZSM-5 zeolites. Adsorption of methane over [Ga]-ZSM-5 yields one form of strongly polarized CH_4 molecules leading to an IR band at 2860 cm^{-1} which is suggested to be indicative of Lewis acid sites (of nonframework species).

A recent FTIR spectroscopic study of the interaction of methane with alumina[227] at low temperatures revealed four distinct IR bands. The authors propose that they are assigned to the interaction of methane with both surface hydroxyls and coordinatively unsaturated oxygen anions. It is obvious that the interpretation of IR spectra from adsorbed methane leaves some space for ambiguity.

CO interacts at low temperatures (77 K) with bridging hydroxyls giving rise to IR bands at 3618

and 3622 cm^{-1} for [Al]-ZSM-5 (Si/Al ratio = 23.8) and [Ga]-ZSM-5 (Si/Ga ratio = 29.5), respectively.[223] Depending on the CO pressure, additional new bands are observed in the region of carbonyl stretching vibrations (2000−2200 cm^{-1}). Within the hydroxyl region, a broad band of H-bound species arises at 3340 cm^{-1} together with a shoulder at approximately 3440 cm^{-1}. This modification of the spectrum is attributed to the formation of 1:1 H-bound complexes between CO and Si(OH)Ga framework hydroxyls. Frequency shifts of the OH stretching mode to lower frequencies are a measure of the H-bond donor strength of the OH groups and hence of their acidic strength, which is lowered with the [Ga]-MFI structure in comparison with [Al]-MFI.

On the basis of CO adsorption at low temperatures at H-ZSM-5 (Si/Al = 190) modified by various elements through ion exchange, Romannikov et al.[228] determined the concentration of Lewis acid sites according to the equation

$$C\ (\mu\text{mol/g}) = (A_0\rho) - \int lg(T_0/T)d\nu \qquad (23)$$

where A_0 is a coefficient of integral absorption in cm/μmol, ρ is the surface density of a pellet (g/cm^2), and T_0 and T are the transmissions for an individual IR frequency through the pellet before and after CO adsorption in percent, respectively. The strength of Lewis sites was characterized by the heat of CO adsorption according to the equation

$$Q_{CO}\ (\text{kJ/mol}) = 10.5 + 0.5(\nu_{CO} - 2143) \qquad (24)$$

It was found that the concentration of Brønsted acid sites is diminished by ion exchange with polyvalent cations. Simultaneously, Lewis acid sites of different strengths are formed which are characterized by differing ranges of Q, roughly classified into weak ($Q_{CO} \leq 39$ kJ/mol), medium ($Q_{CO} = 45-46.5$ kJ/mol), and strong ($Q_{CO} = 51.5-54.0$ kJ/mol) sites.

Qualitatively XPS can also discern Brønsted and Lewis acid sites if suitable probe molecules are used. A method proposed by Defosse and Canesson[229] in 1976 is based on the relative intensities of the N_{1s} XPS peak components following pyridine adsorption. The N_{1s} binding energy of pyridine adsorbed at Lewis acid sites was found to be ca. 2 eV lower than for pyridine fixed to Brønsted sites. Parallel IR studies supported the proposed assignments. Borade et al.[230] applied the method for acidity characterization of ZSM-5,[231] beta and ZSM-20,[232] Y zeolites,[233] and isomorphously substituted MFI structures including [Fe]- and [B]-ZSM-5.[233] Substitution of Fe in the zeolite framework leads to a slight decrease of the binding energy of the N_{1s} Lewis component. In the case of framework substitution by boron, a decrease of the binding energy of all three N_{1s} components is observed. For the parent ZSM-5, the first peak at 398.7 eV is assigned to the N_{1s} level of pyridine adsorbed at Lewis sites while the second and third (at 400.0 and 401.8 eV, respectively) are assigned to N_{1s} levels of pyridine adsorbed at the relatively weak and the strong Brønsted acid sites, respectively.[231] Ratios of the atomic concentration in the outer surface layers of the samples were estimated from the ratios of the corresponding XPS peak area using the relation

$$\left(\frac{M}{Al}\right)_s = \frac{A_M}{A_{Al}}\frac{\sigma_{Al}}{\sigma_M}\frac{\gamma_{Al}}{\gamma_M}\left(\frac{E_{K_M}}{E_{K_{Al}}}\right)^{1/2} \qquad (25)$$

where M stands for silicon or nitrogen and A, σ, λ, and E_K are the normalized XPS peak area, the cross section of the photoelectron emission, the escape depth, and the photoelectron kinetic energy, respectively.[231] The method has not been applied to Ga systems so far. Guimon et al.[234] characterized the surface and subsurface acidity of faujasite-type zeolites in relation to their composition by combined XPS and TPDA studies. It is suggested that at dehydroxylated surfaces a dissociative adsorption of NH_3 is possible as shown by eq 26.

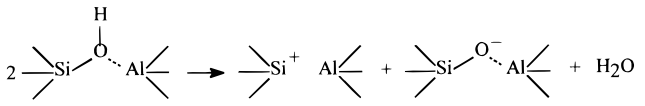

(26)

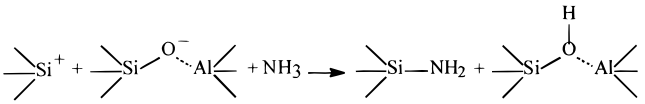

Adsorption and thermal analyses of propane amines (1-propane amine, 2-propane amine) have been utilized for acid characterization of [Ga]-MFI zeolites.[235,236] With H^+-containing materials, NH_3 and propene are simultaneously desorbed above 350 °C. Ga- and In-containing materials release NH_3 below 350 °C and propene and other products above 350 °C. A stable residue remains at temperatures higher than 550 °C. It is suggested that Ga cations interact as Lewis acid sites with propane amine.

For H-ZSM-5, it could be shown[237,238] that amines adsorbed in excess of one molecule per Al are removed unreacted from the sample at ca. 250 °C whereas the remaining molecules, obeying a 1 to 1 coverage, decompose to alkene and ammonia in a relatively narrow temperature range. Secondary amines disproportionate to tertiary and primary amines

$$2R_2NH \rightarrow R_3N + RNH_2 \qquad (27)$$

and subsequently decompose to alkenes and ammonia

$$RCH_2CH_2NH_2 \rightarrow RCH{=}CH_2 + NH_3 \qquad (28)$$

One advantage of applying bulky amines might be the greater versatility concerning the sizes of probe molecules. By choosing amines of appropriate sizes, it is principally possible to discriminate between acid sites located at the external or the internal zeolite surface. A disadvantage is the possible disguise of the desorption/decomposition by secondary reactions.[239]

Calorimetric studies allow one to characterize the acidity of zeolites (acidic strength and number of sites) by determining the values of the heats of

adsorption of a basic compound depending on the degree of loading. Often calorimetric results reveal a greater heterogeneity of acid strength (and hence of acid site configurations) than is amenable by TPDA under flow conditions.

Combined TG−DSC was used by Auroux et al.[240] for the characterization of the acidity of H-ZSM-5, H-Y, and H-ferrierite zeolites elucidating a great heterogeneity of acid strengths. Heats of adsorption of ammonia in the range 140−160 kJ mol^{-1} characterize strong acid sites. The values are in excellent agreement with results recorded under static conditions using a heat-flow microcalorimeter.

By calorimetric studies of the adsorption of ammonia at ZSM-5 samples with exactly the same Ga and Al framework content (Si/Ga = Si/Al = 30), Giannetto et al.[241] showed that [Al]-ZSM-5 has stronger acid sites (maximum heat of adsorption Q_{max} = 135 kJ/mol). The concentration of acid sites is inversely related to the Si/Ga ratio. A slight difference was observed for the strength of acid sites of [Ga]-MFI samples. At Si/Ga = 180, all acid sites were strong (Q > 80 kJ/mol), but at Si/Ga = 50 and 30, only 80% of the sites revealed this high heat of adsorption.

EPR spectra of 2,2,6,6-tetramethylpiperidine-1-oxyl (TEMPO) adsorbed at [Ga]-ZSM-5 indicate the existence of TEMPO complexes fixed to low-coordinated gallium.[132] Owing to its large size, this probe molecule can be coordinated exclusively to sites at the external surface of medium pore zeolite structures. It is suggested that TEMPO molecules are adsorbed at nonframework Ga species of the outer zeolite surface with Lewis acidic character.

d. Characterization of Brønsted Acidity by Catalytic Test Reactions. Classification of zeolite materials in terms of acidity is also possible by catalytic reactions which require Brønsted acid sites. At least three test reactions are well established: cracking of *n*-butane, *n*-hexane, and *n*-decane. The cracking of *n*-hexane was utilized from Mobil laboratories as a standard routine to characterize zeolite acidity and is known as the α-test. For this reaction, relative activity is linearly correlated to the strength and concentration of Brønsted acid sites, at least for zeolite ZSM-5. A similar trend was found for the *m*-xylene conversion over H[Ga]-ZSM-5 obtained after different crystallization times up to 24 h, the borderline value of Ga insertion into the framework (Figure 44).[242]

In principle, other reactions are suited equally well provided that the molecular size of the reactant(s) is small enough to avoid diffusional limitations of the activity. Bifunctional conversion of *n*-decane following modification of the zeolite with noble metals aims at the elucidation of structural features of the zeolite besides its acid characteristics.[243]

The interaction of olefins with the surface-bridged hydroxyls of zeolites is suggested to characterize the bifunctional nature of acid active sites. The Brønsted acid moiety protonates the adsorbed molecule, while interaction with the neighboring basic oxygen converts the initial transition state into more stable covalent intermediates. Considering the possible varying geometry between Brønsted surface sites and neighboring basic sites, Viruela−Martin[244] stressed that Brønsted acid sites should always be considered in conjunction with the neighboring basic sites, i.e., with the negatively charged oxygen atoms bound to the aluminum atoms.

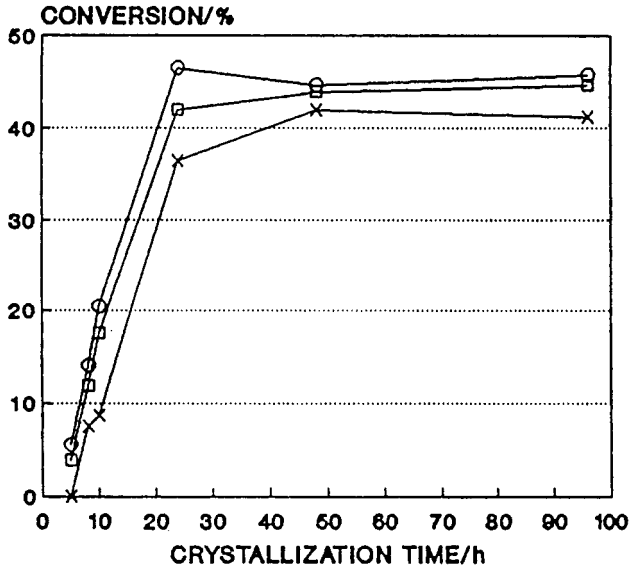

Figure 44. Conversion of *m*-xylene over [Ga]-ZSM-5 at 623 K (×), 673 K (□), and 723 K (○) vs crystallization time. Reaction conditions: sample weight 1 g, flow rate 10 L/h (1 vol % aromatics). (Reprinted with permission from ref 242. Copyright 1992 Wiley-VCH.)

A general quantitative correlation between acidic properties deduced from IR measurements and the results of activity tests for acid-catalyzed reaction is still missing. This is mainly due to the fact that IR characterization obviously does not precisely reflect the dynamic processes taking place during catalytic reactions.

V. Gallium-Substituted Zeolite Structures

A. General Aspects

Generally gallosilicate zeolites are found to have unit cell volumes larger than those of the analogous aluminosilicates.[245] There are exceptions reflecting that unit cell constants not only depend on the mean T−O bond lengths of the TO_4 tetrahedron, but also on the T−O−T angles between adjacent tetrahedra.[246] The term gallosilicate implies complete absence of aluminum during synthesis. This, however, does not necessarily mean that aluminum is not present in detectable quantities in the synthesized crystalline materials. Owing to aluminosilicate seed crystals used to facilitate crystallization, 1−3% aluminum is present in certain cases.[247] Seeds from gallosilicates were ineffective. In other cases, the silicon source utilized for preparation of the synthesis gel contained some aluminum impurities. Although it is claimed that the aluminum in low concentrations does not influence structural features of the crystals, discussion of catalytic results should bear this in mind.

Newsam and Vaughan[97] could already show in 1986 that the internal pore volume (as determined

Table 13. Gallosilicate Analogs of Known Zeolite Structures and Templates Used for Their Synthesis[a]

zeolite type	IZA code	template	ref
Li-A(BW)	ABW		97,246,248,306
analcite, pollucite	ANA		249,250
beta	BEA	tetraethylammonium hydroxide	136,[b]157,166 251,252,353
cancrinite	CAN		110
EU-1	EUO	dimethyldibenzylamine ($DBDM^+$), hexamethonium cations ($HM\text{-}Br^2$)	378
erionite	ERI		253,254
Y, CsY, USY, X, ZSM-20	FAU		97,137,[b]140,[c]157,162,245,255−260,322
Nu-23	FER	cetyltrimethylammonium bromide	162,260
ZSM-35		4-aminocyclohexanol	
L	LTL	no templating agent necessary	97,110,157,245,246,257,261−264, 316−318
mazzite, omega	MAZ	tetramethylammonium bromide, tetra methylammonium hydroxide	97,163,249,257, 265,266
ZSM-11	MEL	tetrabutylammonium bromide	134,[b]159,[b]267, 268
ZSM-5	MFI	tetrapropylammonium bromide (TPABr), triethyl-*n*-butylammonium bromide (TEBABr)	140,[c]157,175, 209,242,257,269,270, 114,141,155,164,188,271−275,358
mordenite	MOR	tetraethylammonium bromide (TEABr)	160,161,270,276
		1,8-diamino-*p*-menthane	332
ZSM-39	MTN	tetraethylammonium hydroxide	5, 277
ZSM-23	MTT		278
ZSM-12	MTW	methyl triethylammonium bromide (MTEABr), triethylmethylammonium bromide (TEMABr)	174,358,365,279
MCM-22	MWW		304
natrolite	NAT	benzyl trimethylammonium hydroxide (BTMAOH)	181,249,250,280
offretite	OFF		97−99,175,257
ECR-10	RHO	none (Cs^+ ions required)	281,332
sodalite	SOD	no templating agent necessary	97,110,175,308,310,321,322,257,282
thomsonite	THO		283,284
theta-1, zsm-22	TON	1-ethylpyridinium bromide	164,285,286
		Mesoporous Materials	
[Si,Ga]-MCM-41		hexadecyltrimethylammonium bromide	398,402,403
[Si,Ga]-MCM-48		hexadecyltrimethylammonium bromide	400
		Pillared Clays (pilc)	
deidellite (synthetic), montmorillonite			287, 288
		Gallophosphates	
$GaPO_4$-34	tricl. CHA	1-methylimidazole, pyridine	289,423
$GaPO_4$ (cubic)		dipropylamine	431
$GaPO_4$ (orthorhombic)		diethylamine	
cloverite		piperidine, quinuclidine, methylquinuclidine, 3-azabicyclo[3,2,2]nonane	423,430,289−291,355,429
ULM-1, ULM-2		diazabicyclo[2,2,2]octane	423
ULM-3		linear amines ($NH_2\text{-}(CH_2)_{3-5}\text{-}NH_2$)	292
ULM-16 ($Ga_4(PO_4)_4F_2$)		cyclohexylamine	293

[a] Ga-zeolites disclosed in patents through 1990−1995 with still unknown crystallographic structures are not included, e.g., SSZ-26,[294] NU-86,[295] SSZ-31,[296] ECR-1,[297] −35,[298] −47,[299] −37,[300] MCM-49,[301] SUZ-9,[302] SSZ-35,[303] GZS-11.[305] [b] Through secondary synthesis (galliation). [c] Postsynthesis introduction of Ga by treatment with trimethylgallium.

by *n*-hexane and water adsorption capacity) of alumino- and gallosilicates does not scale directly with the unit cell volume. In principle, the gallium analogues of the investigated framework structure types ABW, FAU, LTL, MAZ, OFF, and SOD have larger unit cell volumes but their adsorption capacities are lower. This is attributed to at least two factors. First, gallium insertion into the framework does not simply modify the scale but influences the relative orientation of adjacent tetrahedra. These adjustments are framework-specific and might lead to a net increase or decrease of the pore volumes, despite larger unit cell volumes. Second, adsorption may also cover capacities of amorphous impurities, and hence, the sample purity has to be checked profoundly before conclusions are drawn. Sample pretreatment is another factor which may alter the framework composition via dealumination or degalliation. Resulting nonframework species may hinder the accessibility of the pore system. Gallosilicate analogues of known aluminosilicate structures are briefly described in this section. Templates necessary for their synthesis are listed in Table 13.

The relevant gallosilicate structures are treated according to their Si/Ga ratios. The gallium content determines structural properties (and vice versa) because the ideal Si/Ga ratio = 1 is only compatible with the ABW framework. By analogy with the classification of aluminosilicate framework structures, Si/Ga ratios <3 will be considered as low, Si/Ga ratios between 3 and 10 as medium, and Si/Ga ratios >10 are as high. In general, the Si/Ga ratios refer to samples where the gallium supply is high enough to allow maximum incorporation into the framework of the corresponding structure. Postsynthesis treatment that aims at a modification of the

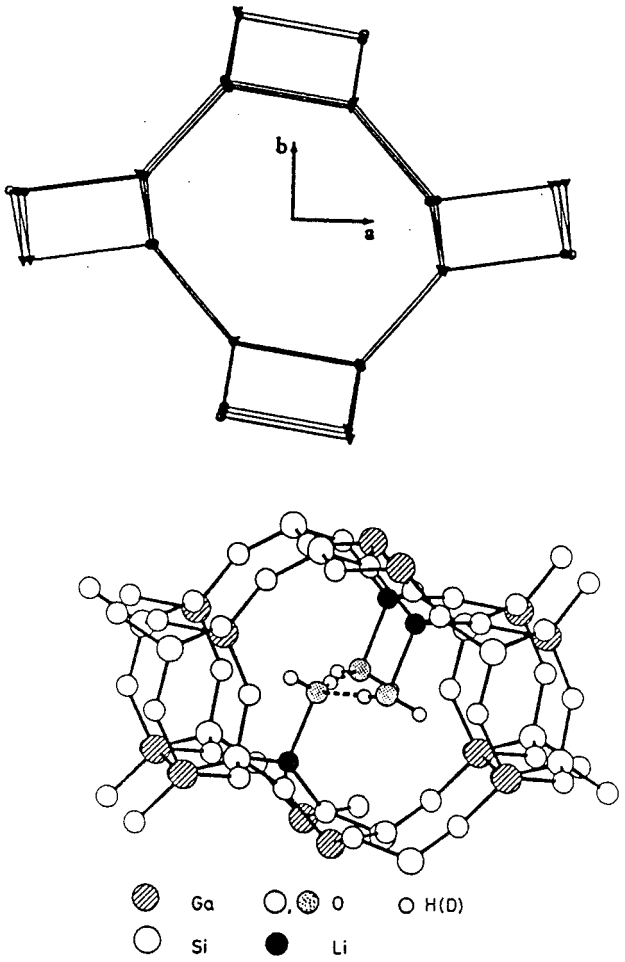

Figure 45. Structure of zeolite Li-A (ABW) framework: (top) eight-membered ring channel viewed along *c*-axis,[307] (bottom) positions of hydrated Li ions in the main channel and of Ga and Si framework atoms.[247] (Reprinted with permission from refs 307 and 247. Copyright 1974 R. Oldenbourg Verlag München and 1986 The Royal Society of Chemistry.)

initial gallium content is not relevant for the classification. Catalytic application of the gallosilicates is presented in section VI.

Besides some examples of porous gallophosphates, Table 13 includes microporous gallosilicates and those mesoporous silicates, the gallium-substituted analogues of which are already available.

B. Zeolites with Low Si/Ga Ratios

1. [Ga]-A(BW)

Synthesis and characterization of gallo- and aluminogallosilicates with a zeolite ABW framework, $LiGa_xAl_{1-x}SiO_4 \cdot H_2O$ with $x = 0$, 0.5, and 1.0, were reported by Newsam in 1988.[306] The ABW framework consists of four-, six-, and eight-membered rings[307] (Figure 45). The latter define the channel system that runs parallel to the crystallographic *c* direction of the orthorhombic unit cell. Pore openings of the channel system are 3.8 × 3.4 Å in size.[34] Synthesis of Li-A(BW) through mere substitution of sodium hydroxide by lithium hydroxide is not successful, because the aluminum source is less soluble in LiOH than in NaOH. Therefore, Newsam applied a modified preparation of the synthesis gel involving evaporation to dryness of the initial slurry and intermediate drying of the residue at 120 °C for ca. 2 h. Then the solid was again slurried by addition of water and afterward subjected to the hydrothermal synthesis procedure at, typically, 180 °C for 4−6 days. Yields of 88−92% of Li-A(BW) have been obtained. From characterization data it followed that the unit cell volume of the ABW framework slightly increased on substitution of gallium for aluminum ([Al]-A(BW) 418.8 Å^3, [Ga]-A(BW) 430.2 Å^3). This was expected on the basis of bond length considerations.

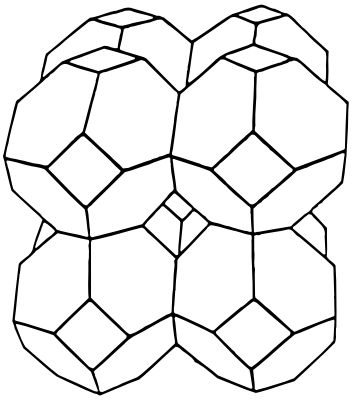

Figure 46. Framework structure of zeolite sodalite (SOD).

In the gallosilicate structure and in its parent aluminosilicate analogue, a complete ordering of the cations is observed and Loewenstein rule is obeyed. Each of the single nonframework Li cations in a tetrahedral position is coordinated by three framework oxygen atoms and one oxygen of a single, adsorbed water molecule (in the hydrated form). Newsam[306] concluded that the affinity toward water is related to a charge-compensating of accessible nonframework cations rather than to the anionic framework charge. The complete structure of the hydrated gallosilicate zeolite with the ABW framework has already been determined by powder neutron diffraction.[245]

2. [Ga]-Sodalite

Suzuki et al.[308] could show that hydrothermal treatment of the system $Na_2O-Ga_2O_3-SiO_2-H_2O$ at 100 °C for 6−7 days under autogenous pressure resulted in a sodium gallosilicate with sodalite structure and molar Ga_2O_3:Na_2O:SiO_2:H_2O ratios from 1:4.25:2.23:52.0 to 1:4.25:4.46:69.4. The Al-sodalite structure consists of a cuboctahedron cage composed of ordered SiO_4 and AlO_4 tetrahedra.[309] The pore apertures are built by six-membered rings only (Figure 46). Compared with hydroxysodalite, a contraction of the unit cell volume upon replacement of Al by Ga is observed. The authors ascribed this contraction to differences in the state of hydroxyl groups as inferred from IR spectroscopic studies. A contraction of the unit cell despite the greater ion radius of Ga^{3+} (in comparison with Al^{3+}) is unusual. Without exception, any other gallium analogue shows an expansion of the unit cell.

McCusker et al.[310] checked the apparent anomalies of the gallosilicate sodalite structure. XRD investiga-

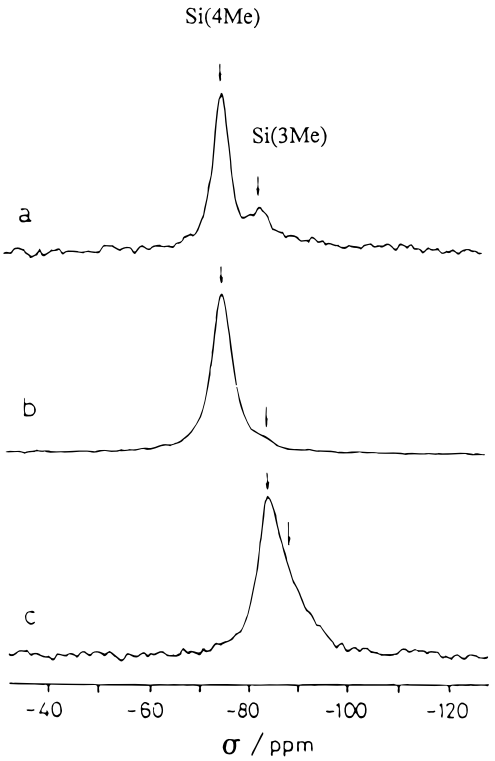

Figure 47. High-resolution ^{29}Si MAS NMR of Ga-containing sodalite (SOD)[175] (a) Si/Ga = 1.05 and (b) Si/Ga = 1.005 and (c) of Al-containing sodalite (Si/Al = 1.10). Arrows indicate Si(3Me) and Si(4Me) units with Me = Al,Ga. (Reprinted with permission from ref 175. Copyright 1985 The Chemical Society of Japan.)

tions showed that the Si/Ga ratio of the gallosilicate sodalite is undoubtedly close to 1. The space group, the Ga−O and Si−O bond lengths, and the Si−O−Ga bond angle are all consistent with an alternating arrangement of Si and Ga. Contraction of the unit cell in the Ga-sodalite framework, however, was confirmed, although Ga−O bond lengths are slightly longer than the Al−O ones. This is explained by the different bond angles found in both samples. A typical Si−O−Ga angle is 135° instead of 145° for Si−O−Al. The Na^+ ions were found to be exclusively octahedrally coordinated, but the sodalite cage contained more Na^+ ions than would be needed for a charge balance. It was suggested that some Na^+ ions are neutralized by OH^- ions. No evidence for bridging hydroxyl groups was found in this sodium form. On the basis of their results, McCusker et al.[310] suggest the following composition of the gallosilicate material: $Na_{6.7}[Ga_{5.9}Si_{6.1}O_{24}]\cdot 9.8(H_2O,OH)$.

High-resolution ^{29}Si MAS NMR spectra of gallium−hydroxosodalite containing different amounts of gallium were evaluated by Hayashi et al.[175] and compared with aluminum hydroxosodalite (Figure 47). The spectrum of the aluminosilicate (Figure 47c) shows one asymmetric line overlapped by Si(4Al) and Si(3Al) signals. In the gallosilicate (Figure 47a,b), the spectra are composed of two lines with $\delta = -75$ and −83 ppm assigned to Si(4Ga) and Si(3Ga) configurations, respectively. Relative intensities of the lines (Sample A, Si/Ga ratio = 1.05 according to NMR) led to the estimation that 81% is contributed by Si(4Ga) and 19% by Si(3Ga) units. The spectrum presented in Figure 47b represents a gallosilicate with Si/Ga ratio of 1.005, with 98% of framework gallium involved in Si(4Ga) units and only 2% in Si(3Ga) units. Si(*n*Ga) lines of gallosilicate sodalites are generally shifted to lower fields than the Si(*n*Al) lines of the corresponding aluminosilicate sodalites.

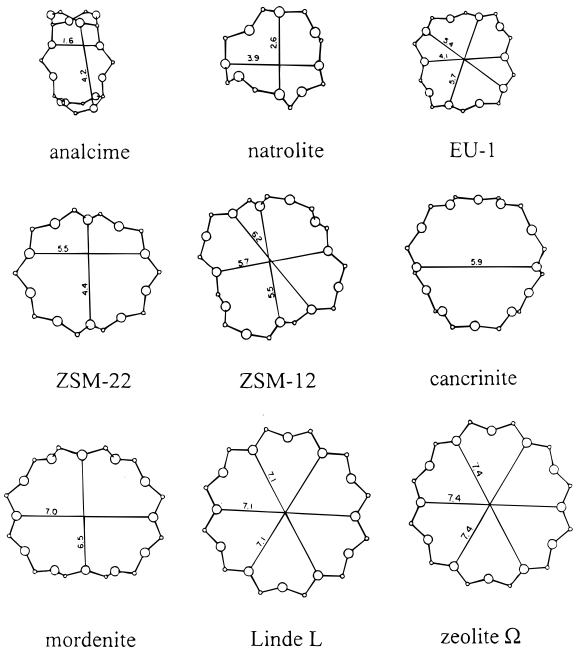

Figure 48. Shapes and sizes of oxygen-ring openings (in Å) of different zeolites. (Reprinted with permission from ref 34. Copyright 1996 Elsevier Science.)

3. [Ga]-Omega

Zeolite omega (ZSM-4) is a synthetic counterpart to the mineral mazzite (Figure 48). The aluminosilicate framework consists of columns of gmelinite cages bridged by oxygen atoms to give a 12-membered cylindrical main channel system along the crystallographic *c* axis.[311−313] Aluminosilicate omega and the [Ga]-omega were synthesized by Mirajkar et al.[163] and Yu et al.[314] from appropriate gel compositions with tetramethylammonium hydroxide (TMAOH) as a template. Syntheses performed under autogenous pressure required 5−20 days at a temperature of 110−140 °C. The [Ga]-omega samples contained 0.09% of Al_2O_3 (not detectable by ^{27}Al MAS NMR), caused by aluminum impurities of the gel components. The SiO_2/Ga_2O_3 ratios lied within the range of 6.87−7.42. The IR lattice vibration bands for [Ga]-omega are shifted to lower wavenumbers as compared with [Al]-omega. The morphology of [Ga]-omega is slightly different from that of [Al]-omega, the crystals of which are spherically shaped (3 μm). [Ga]-omega crystals are cylindrically shaped (3.5−8.0 μm). Both structure modifications are stable up to temperatures of 1000 °C.

4. [Ga]-Natrolite

The name natrolite for a natural fibrous zeolite has been known since 1803. Pore apertures are formed by eight-membered rings with irregular forms creating 0.26 × 0.39 nm pores (Figure 48).[34] Ocelli[315] reported the synthesis of [Ga]-natrolite crystals from

the $Ga_2O_3-SiO_2-Na_2O-K_2O$ template system at 125 °C. A solution of 40 wt % benzyl trimethylammonium hydroxide (BTMAOH) in methanol was used as a template. The authors received (after 7 days at 175 °C under stirring) [Ga]-natrolite crystals consisting of anisotropic columns of 10−20 μm length with an almost square cross section. Crystals are often twinned, and intergrowths were observed. Incorporation of gallium instead of aluminum leads to (i) an increase of the crystal orthorhombic unit cell dimension by ca. 1%, (ii) a shift of the asymmetric Ga−O stretching vibration to lower wavenumbers, and (iii) a ^{29}Si MAS NMR spectrum closely resembling that of the Al analogue.

A Si/Ga ratio of 1.5 is derived in good agreement with chemical analysis. An application of this material has not yet been reported. Owing to its small pore dimensions, it, however, should be suited for gas separation processes

5. [Ga]-Cancrinite

The framework of cancrinite (Figure 48) contains deformed 12-membered ring channels with reduced pore openings of 5.9 Å.[34] Its ideal composition is indicated in the *Atlas* of zeolite structure types to be $Na_6[Al_6Si_6O_{24}]\cdot CaCO_3\cdot 2H_2O$.

Newsam and Jorgenson[110] synthesized the Ga-analogue of the cancrinite structure by addition of NO_3^- anions to gel compositions usually giving gallosilicate sodalites. A solid product containing 85% of [Ga]-cancrinite (Si/Ga = 1.022) was obtained after a synthesis time of 66 h at 180 °C. At shorter synthesis times (20 h), the synthesis product was composed of 40% [Ga]-sodalite, 55% [Ga]-cancrinite, and 5% of an unidentified alien phase.

6. [Ga]-L

Zeolite L contains circle-like- shaped oxygen 12-ring apertures of 7.1 Å diameter (Figure 48). The LTL framework topology and the distribution of cationic sites were described by Barrer and Villigier.[311] Cancrinite cages (ϵ-cages) and double-six rings are alternatively linked along the *c*-axis, constituting a chain. Six of such rings are cross-linked to form flat 12-membered rings that generate a large pore channel system parallel to the *c*-axis. The typical unit cell composition of zeolite L is $(K,Na)_9Al_9Si_{27}O_{72}\cdot nH_2O$ with Si/Al ratios varying between 2.6 and 3.5. The structure shows two nonequivalent T sites. Newsam et al.[306] tried to resolve the partitioning of aluminum or gallium between the two nonequivalent T positions by performing a full profile analysis of ^{29}Si MAS NMR spectra of [Al]-L and [Ga]-L. The close similarity between the mean geometry for the two T sites occupied either by Al or Ga allowed one to simulate the experimental spectra by assuming that only one single set of Si−*n*T (n = 0−4) peaks is present.

For application, the zeolite has to be used in its dehydrated form. Newsam[97,246] studied the effect of dehydration (achieved through a vacuum treatment) of [Al]-L and [Ga]-L with identical Si/T ratios of 11.4 on characteristic parameters. Dehydration caused a slight decrease of the unit cell volume of [Ga]-L. A random partitioning of gallium atoms between the two tetrahedral sites, T_4 and T_6, was found. Takaishi[316] concluded that defects have to be taken into account to reach consistency between Al distribution and recorded ^{29}Si MAS NMR spectra. Owing to the required long-range ordering, these details are detectable by neutron diffraction to a limited extent only. Recently, Yu et al.[317,318] studied the exchange of K^+ ions in K[Ga]-L (Si/Ga = 2.6) by Cu^{2+} ions through EPR and electron spin−echo modulation (ESEM) spectroscopy. Results were compared with those of Cu^{2+}-exchanged K[Al]-L. The state and coordination of the Cu^{2+} species were found to be quite similar with both types of zeolites. The interaction of various probe molecules (ammonia, pyridine, aniline, acetonitrile, hydrazine, carbon monoxide, benzene, propanol, and dimethyl sulfoxide) with Cu^{2+}-exchanged [Ga]-L revealed no differences with the exception of dimethyl sulfoxide. There ESEM data revealed a modified interaction.

7. [Ga]-Analcime

Its framework topology occurs in nature in several minerals but is also known for synthetic materials.[34] The irregular channels are formed by highly distorted oxygen-8-rings (Figure 48). Gallosilicates with the zeolite ANA framework are available by hydrothermal synthesis from $Na_2O-Cs_2O-SiO_2-Ga_2O_3-H_2O$ gels. Yelon et al.[319] found the best product yields with molar compositions of $2.95Na_2O{:}0.53Cs_2O{:}1Ga_2O_3{:}10.1SiO_2{:}110H_2O$ when the gel was aged at room temperature for 7 d prior to the crystallization process performed at 80 °C for 12 d. The gallosilicate had a Si/Ga ratio of 2.45. Substitution of aluminum by gallium in the ANA framework causes minor changes in framework geometry only. Dehydration is accompanied by a small lattice contraction (0.2%) and an approach of sodium cations to the oxygen-rings due to the loss of coordinating water molecules. Framework bond lengths and angles were found to be similar to those described for the analogous aluminosilicate zeolite. The T−O−T bond angles of 145.1(3)° are 0.5° larger than those observed in the mineral pollucite. In other frameworks, a slight reduction of the mean T−O−T angles is generally characteristic of gallium incorporation.[97,246]

Detailed ESCA and MAS NMR studies of [Al]-analcime (Si/Al = 1.82) and its gallosilicate analogue [Ga]-analcime (Si/Ga = 2.68) have been carried out by He et al.[320] The core level binding energies in [Al]-analcime are consistent with those for framework materials of similar chemical composition. The shift of binding energies in [Ga]-analcime suggests an increased ionicity of the Ga−O as compared to the Al−O bond.

8. [Ga]-X

X-type zeolites belong to the faujasite group and are very rich in Al (usually Si/Al = 1−1.2) and Ga (Si/Ga < 2). The faujasite structure consists of sodalite units which are linked via double-6-ring units. The large cavities have a diameter of 12.6 Å and are three-dimensional interconnected via 12-membered rings with a pore size of 7.4 Å (Figure 49). Timken et al.[321] synthesized gallium analogues of

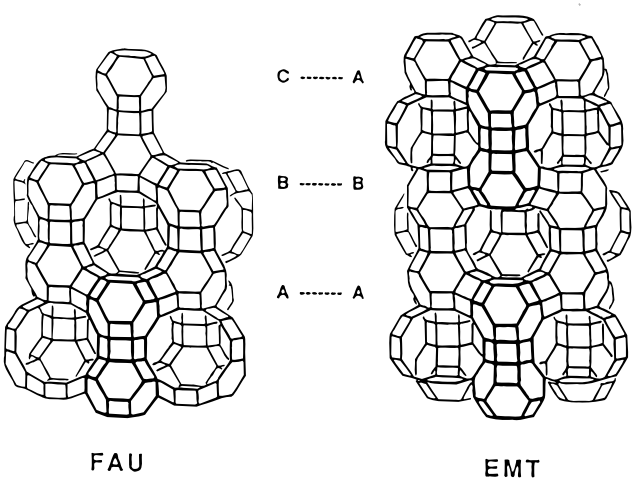

Figure 49. Comparison of the FAU (natural faujasites, zeolite X, Y, and dealuminated Y) and EMT framework topology evidencing the different stacking of sodalite building units.[352] The ABC and ABA stackings of the sodalite cage layers for the topologies are indicated. For clarity, oxygen bridges have been omitted and the smaller rings have been made opaque. (Reprinted with permission from ref 352. Copyright 1997 Butterworth-Heinemann.)

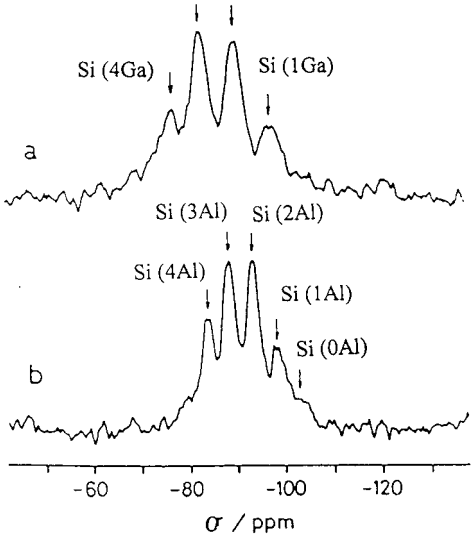

Figure 50. High-resolution ^{29}Si MAS NMR spectra of (a) Na[Ga]-X (Si/Ga = 1.47) and (b) Na[Al]-X (Si/Al = 1.63). (Reprinted with permission from ref 175. Copyright 1985 The Chemical Society of Japan.)

Na−X from a gel composition $2.1Na_2O$:$1.0Ga_2O_3$:$4SiO_2$:$60\ H_2O$ seeded with aluminosilicate 13X material (1% Al relative to Ga). The synthesis, performed after aging the gel for 24 h and autoclaving it at 100 °C for 8 h, yielded a product with a Si/Ga ratio of 1.63. In comparison to Na[Al]-X, a small expansion of the unit cell was observed for Na[Ga]-X.

Nuclear quadrupole coupling constants, electric field gradient tensor asymmetry parameters, and isotropic chemical shifts for the chemically distinct oxygens in the Si−O−Ga, Si−O−Si, and Al−O−P fragments were estimated from the solid-state ^{17}O NMR spectra of ^{17}O-enriched gallosilicates and porous aluminophosphates.[321] A comparison of the parameters with those derived from theoretical calculations indicates that nonframework Na^+ cations are preferentially coordinated to the Si−O−Ga linkages. The ^{29}Si MAS NMR spectrum of zeolite [Ga]-X consists of four well-resolved lines at −76.7, −83.3, −90.8, and −98.8 ppm (Figure 50), which are assigned to Si(4Ga), Si(3Ga), Si(2Ga), and Si(1Ga) units, respectively.

With gallosilicates, the line shift amounts to 6−8 ppm and thus is slightly larger than that for aluminosilicates (5−6 ppm). This is viewed to be due to a stronger deshielding of the silicon nucleus by gallium. The relative percentages of Si(*n*Ga) configurations were estimated to 19%, 41%, 31%, and 9% for $n = 4$, 3, 2, and 1, respectively. Vaughan et al.[322] reported the additional presence of Si(OGa) units in Na−X gallosilicates indicated by the line at $\delta = -104.2$ ppm (Si/Ga = 1.39).

9. [Ga,Al]-Y

Dwyer and Karim[138,139] described the successful substitution of a portion of framework aluminum by gallium following a postsynthesis treatment of zeolite Y (Si/Al ca. 2.4) with aqueous fluoride complexes as described in section III.

10. [Al,Ga]-ZSM-20

ZSM-20 is a large pore zeolite consisting of sodalite cages which are interconnected through hexagonal prisms. The cubic faujasite (FAU) structure is intergrown with the hexagonal Breck structure six (EMT).[323] Sheets of FAU and EMT alternate within the crystals. The EMT to FAU ratio is rather narrow (2:1).[324] Both structure types differ in the stacking of sodalite units leading to different large pores. In FAU, large cavities are tetrahedrally arranged (compare X- and Y-zeolites). EMT contains two different large cavities. The larger one has five oxygen-12-ring windows and forms straight channels (Figure 49). The smaller cavity has three oxygen-12-ring windows and is the lateral connection between the straight channels.[323,325] In comparison to normal FAU, the Si/Me ratio is increased. Hence, thermal stability and acidity are improved giving these materials attractiveness in catalysis.[326,328]

Partial substitution of ca. 1/3 of aluminum by gallium in zeolite ZSM-20 is achievable via the sol−gel route of gel preparation using tetraethylammoniumhydroxide (TEAOH) as template and tetraethylorthosilicate (TEOS) as silicon source.[329,330] [Ga,Al]-ZSM-20 was crystallized from a gel of composition $1.2\ Na_2O$:$0.33Ga_2O_3$:$0.67Al_2O_3$:$30.2SiO_2$:26.4TEAOH:$267H_2O$. The gel was hydrothermally treated at ca. 100 °C for 14 days without stirring. Template was removed by calcining the sample in air at 550 °C. Highly crystalline ZSM-20 crystals were obtained without any byproducts. Isomorphous substitution of Si by Al and Ga is indicated by an increase of the unit cell parameters. Signals of tetrahedrally coordinated Al and Ga appear at 59 and 163 ppm in the ^{27}Al and ^{71}Ga MAS NMR spectra, respectively. The total Me^{3+} content is in line with a Si/Me ratio of 3.6 estimated from ^{29}Si MAS NMR spectra. Ga substitution causes a shift of framework vibrations in the IR spectra to lower wavenumbers. Calcination results in a release of Al and most of the Ga from framework positions as shown by quantitative NMR data (Table 14).

Table 14. Summary of NMR Results of [Ga,Al]-ZSM-20[329]

	from ^{29}Si NMR spectra		relative intensities[a] ^{27}Al-signal		^{71}Ga-signal
[Ga,Al]-ZSM-20	Si/(Al + Ga)	number of (Al + Ga) per sodalite unit	FAL[b]	FAL + EFAL[c]	tetrahedral
as-synthesized	3.6	5.25 → 3.5 Al[d] 1.75 Ga[d]	100	100	100
calcined	4.2	4.6	74	83	67
H-form	5.2	3.9 → 3.0 Al[e] 0.9 Ga	59	74	29

[a] NMR measurements were done in the absolute intensity mode (AI-mode) in order to get the relative intensities by comparison of their integrated NMR signals. [b] Framework aluminum. [c] Sum of framework and extraframework aluminum. [d] Determined by chemical analysis. [e] Under the assumption that 0.5 Al is released from the framework as observed on [Al]-ZSM-20.

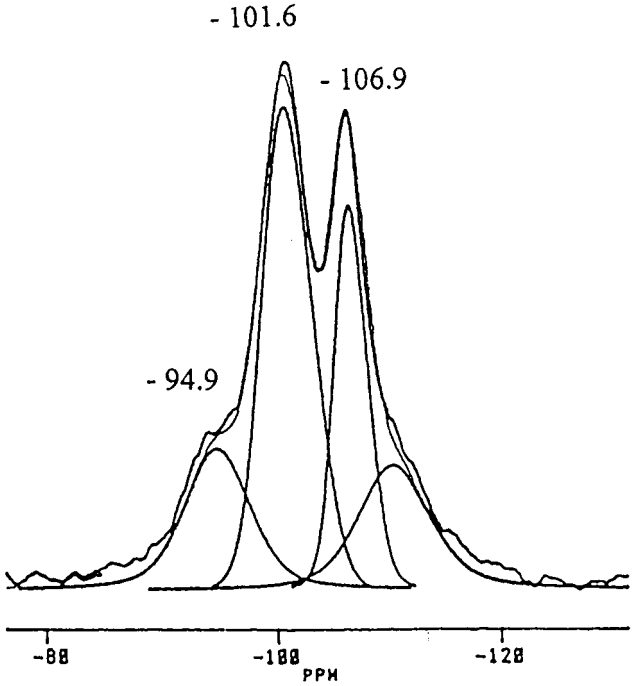

Figure 51. Deconvoluted ^{29}Si MAS NMR spectrum of H[Ga,Al]-ZSM-20, Si/(Al + Ga) = 5.2. (Reprinted with permission from ref 329. Copyright 1997 Marcel Dekker Inc.)

Tetrahedrally coordinated framework gallium is less stable than the aluminum species. In contrast to the low-silica zeolites [Ga]-X and [Ga]-Y, the [Ga,-Al]-ZSM-20 structure is stable even after calcination at 550 °C (Figure 51). The strength of acid sites is lower than that of [Al]-ZSM-20 as probed by interaction with NH_3. The desorption maximum of ammonia from Brønsted sites is shifted from 300 to 280 °C. The initial heat of ammonia chemisorption determined by microcalorimetry is by 10 kJ/mol lower than that of [Al]-ZSM-20 and amounts to 130 kJ/mol.[326]

Partial substitution (25%) of Al by Ga in the frameworks of FAU and EMT was confirmed recently.[331] Crystallization was carried out using crown ethers as templates and phosphate anions as complexing agents. Addition of small amounts of Ga leads to the formation of FAU/EMT intergrowths.

11. [Ga]-Rho

Zeolite rho was synthesized by Robson with Si/Al ratios from 2.5 to 3.5.[332] The mineral counterpart is the isotopological beryllophosphate phasapaite. Zeolite rho was found to be an active and selective catalyst for the synthesis of dimethylamine from ammonia and methanol.[333]

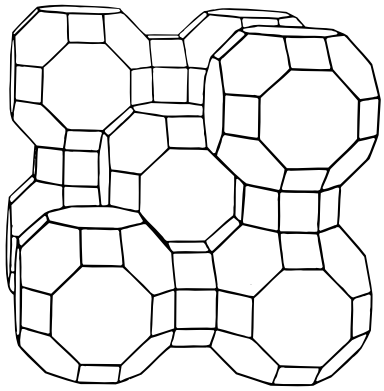

Figure 52. Framework structure of zeolite rho (RHO).

The gallosilicate zeolite [Ga]-ECR-10 was originally thought to possess a novel framework topology (with respect to the framework composition and to the unit cell volume). By a combination of distance least squares modeling and Rietveld analyses of powder neutron diffraction data, Newsam et al.,[334] however, could show that [Ga]-ECR-10 adopts the same framework topology as aluminosilicate zeolite rho (Figure 52). [Ga]-ECR-10 was prepared from gel compositions of aCs$_2$O:bNa$_2$O:Ga$_2$O$_3$:cSiO$_2$:dH$_2$O with $0.5 < a < 0.8$, $1.0 < b < 2.0$, $2 < c < 2.5$, and $50 < d < 100$. It has the typical composition of $Na_{2.7}Cs_{2.1}Si_{6.9}Ga_{4.8}O_{24}\cdot nH_2O$ (Si:Ga = 1.4) and a cubic unit cell with $a_0 \approx 14.9$ Å. Typical Si/Ga ratios of [Ga]-ECR-10 are substantially smaller than the Si/Al ratios of [Al]-rho (typically 2.9). Attempts to synthesize either ECR-10 or rho in overlapping composition domains have not been successful so far. On the basis of the structural analysis, it was concluded that framework gallium substitution leads to a substantial distortion of the 8-ring windows and hence to reduced effective pore dimensions. These findings point to a possible control of pore dimensions by isomorphous substitution.

C. Zeolites with Medium Si/Ga Ratios

1. [Ga]-Mordenite

Mordenite exists with two effective pore sizes differing in their adsorption behavior: small-port and large-port mordenites, with effective pore apertures of ca. 0.4 and ca. 0.7 nm, respectively.[6,335] Enlargement of the ports can be achieved by a simple thermal treatment, where dealumination of the zeolite frame-

work occurs. The transition from the small-port to the large-port form is complete when about 20% of the tetrahedral framework aluminum is converted into octahedrally coordinated nonframework aluminum. Van Geem et al.[335] suggested that the pore blocking of the small-port mordenite is caused by structural defects originating from differently oriented mordenite chains. The transition involves the removal of framework Al from the four-membered rings forming the wall of the eight-membered ring side channels. Thereby, connections between segments of the main channel system are formed. As Raatz et al.[336] could show that small-port mordenite does exist even in its pure H form, the hypothesis that pore blocking is caused by the interstitial alkali cations can be ruled out. Additionally, the authors stated that the transition to large-port mordenite can also be accomplished by a strong acid attack of the sodium small-port form. Calcination at inappropriate conditions can cause a blocking of the pore mouths of the emerging large-port form by octahedrally coordinated Al species from excessive framework dealumination, which—as described by Stach et al.[337]—may be generated (degree of dealumination of about 70%) by thermal treatment at 500 °C after ammonium exchange. The results demonstrate that the mordenite structure is sensitive to any heat treatment which causes the loss of a high percentage of framework aluminum even at relatively mild calcination conditions. According to Bodart et al.,[339] the dealumination mechanism consists of the removal of aluminum atoms two by two from the four-membered rings. Some structural reorganization must occur after a substantial degree of dealumination has been achieved. A pure silica polymorph with mordenite structure has not yet been obtained by direct hydrothermal crystallization.[160]

The gallosilicate analogue of large-port mordenite was synthesized with a Si/Ga ratio of 21 using tetraethylammonium bromide (TEABr) as template and gallium sulfate and silica sol as further components. In comparison with the [Al]-analogue, XRD data reveal an increase of the unit cell volume of the [Ga]-mordenite ([Al]-mordenite, Si/Al = 17.5, 2699.7 Å^3; [Ga]-mordenite, Si/Ga = 21, 2721.55 Å^3). Sorption capacities of benzene (12 wt %) indicate that the sample is of the large-port type. The IR framework vibration bands of [Ga]-mordenite are shifted to lower frequencies as compared with the [Al]-mordenite. TG/DTA results show that the thermal stability of the [Ga]-mordenite is somewhat lower than that of the [Al]-mordenite.

Chandwadkar et al.[161] reported a unit cell volume of 2745.56 Å^3 for [Al]-mordenite (Si/Al = 6.65) and of 2771.47 Å^3 for [Ga]-mordenite (Si/Ga = 9.5). In the FTIR spectra of dehydrated mordenites, OH vibration bands are observed at 3740 and 3603 cm^{-1} for [Al]-mordenite and at 3740 and 3616 cm^{-1} for [Ga]-mordenite. A band occasionally observed at 3660 cm^{-1} for [Al]-mordenite is assigned to the adsorption of water on acidic OH groups.[339] The vibration band of terminal SiOH groups at 3740 cm^{-1} is invariant to the substitution. The shift of the band of acidic bridging OH groups to lower wavenumbers reflects the higher covalency of the hydroxy groups with Ga−OH−Si as compared with Al−OH−Si. Adsorption studies ascertained that the mordenites are of the large-port type. Thermoanalytical investigations of the template decomposition showed a shift of the exothermic peaks in the DTA profile toward lower temperature after Ga substitution. This reflects a weaker fixation of the tetraethylammonium bromide cation to Ga-related surface sites. The occurrence of FTIR bands after pyridine adsorption at around 1445, 1600, and 1630 cm^{-1} is commonly taken as evidence for the existence of Lewis acid sites originating from nonframework Ga species.

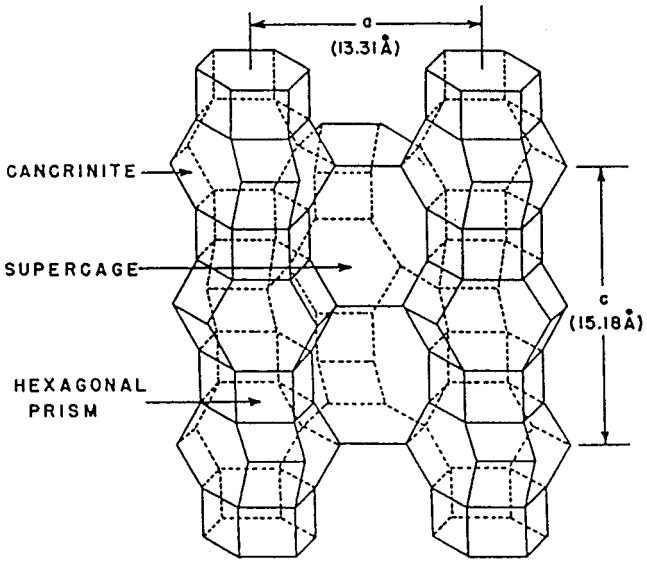

Figure 53. Framework structure of erionite (ERI). (Reprinted with permission from ref 343. Copyright 1970 Academic Press.)

2. [Ga]-Erionite

The aluminosilicate erionite (known in natural and synthetic varieties) belongs to the group of small-pore zeolites. In general, its elementary cell has the composition $(K,Na)_9(AlO_2)_9(SiO_2)_{27}\cdot 27\ H_2O$, comprising three types of structural units, viz. (i) hexagonal prisms, (ii) cancrinite cells, and (iii) erionite cavities (Figure 53). Erionite cavities are quite large (6.3 × 13.0 Å), but pore openings (windows) of the cavities are small (3.6 × 5.1 Å). The alkali form of the zeolite erionite was shown to exert molecular sieving effects for normal butenes differentiating between *cis*-but-2-ene and *trans*-but-2-ene due to their different sizes and polarities.[340]

Klyueva[341,342] reported the formation of [Ga]-erionite with 100% crystallinity from an initial synthesis gel comprising solutions of NaOH, KOH, gallium sulfate, and sodium silicate after 1−30 days of crystallization at 120 °C. The product had a Si/Ga ratio of 19.75, but only 50% of the gallium was tetrahedrally coordinated as proved by ^{71}Ga NMR spectroscopy. The erionites were applied as catalysts in the conversion of methanol.

3. [Ga]-Offretite

The structure of offretite is closely related to erionite (Figure 54). Both zeolites are constructed of the same secondary building units, hexagonal prisms

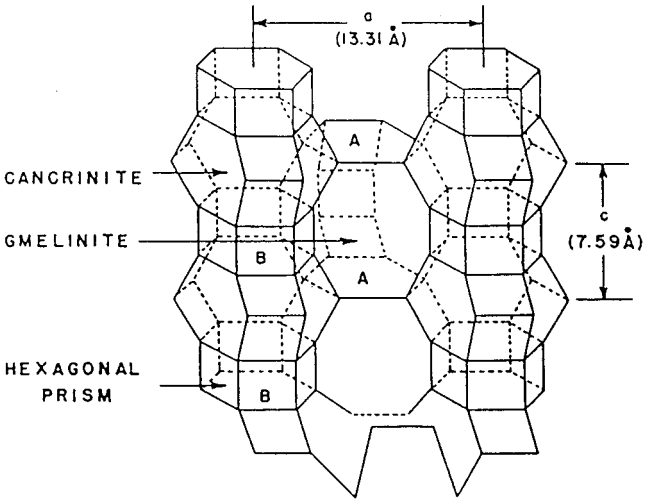

Figure 54. Framework structure of offretite (OFF). (Reprinted with permission from ref 343. Copyright 1970 Academic Press.)

(A) and cancrinite cages (B). They form columns of the stacking sequence ABAB... which are interconnected by oxygen bridges between the cancrinite units. Thereby supercages (gmelinite units) of 6.3−6.6 Å diameter and 7.39 Å length with oxygen-8-ring openings of 4−5 Å diameter are formed.[242]

Although offretite crystallizes from template-free aqueous hydrogels,[344] the use of organic additives such as trimethylammonium salts (TMA^+)[345] choline chloride, benzyltrimethylammonium chloride, and 1,4-diazobicyclo (2,2,2) octane[346] might be useful to prepare offretite of desired properties to prevent the formation of stacking disorders and to minimize erionite domain formation in offretite crystals.[347]

Occelli et al.[98,99] synthesized mixed aluminogallo- and pure gallosilicates of offretite structure type. Synthesis was performed reacting gels of the composition $(1 - x)Al_2O_3{:}xGa_2O_3{:}12SiO_2{:}yK_2O{:}(1 - y)$-$Na_2O{:}1TMA_2O{:}200H_2O$, with $0 \leq x \leq 1$ and $0 < y <$ 1, at 95 °C under stirring. The Si/Ga ratio was ≥3. Isomorphous substitution of silicon by gallium in tetrahedrally coordinated framework sites was evidenced by ^{71}Ga MAS NMR and by the unit cell expansion from 1118.1 ([Al]-offretite, Si/Al = 4.08) to 1160.7 Å^3 ([Ga]-offretite, Si/Ga = 4.08), which was in line with the Ga content. The detailed analysis of ^{29}Si NMR spectra (Figure 55) points to a nonrandom distribution of Ga atoms over different available framework T sites, suggesting preferred occupancy of T_2 position.[348] This framework position provides the most space for the substituting gallium atoms (long T−O distances). Nonframework gallium could not be detected. Data refer to dry, TMA^+-containing samples.

4. [Ga]-Beta

The aluminosilicate structure beta was first synthesized at the Mobil R&D Laboratories.[349] Framework topology and mechanism of faulting were reported by Higgins[350] in 1988 and by Stevens et al.[351] in 1995. Zeolite beta is the only structure with a medium Si/Al ratio exhibiting a three-dimensional pore system and chiral intersections (polytype A structure). The straight 12-membered ring channels run in the *a* and *b* directions. A more tortuous 12-membered ring channel system runs parallel to the *c* direction (Figure 56). Faulting arises from random dislocations of layers or sheets of the framework.

Synthesis of the gallosilicate analogue of zeolite beta is performed with TEOS or fused silica,[352] free of Al traces, gallium nitrate, and sodium hydroxide as well as TEAOH as templating agent. XRD data indicate an expansion of the [Ga]-beta framework (Si/Ga = 13)[353] as compared to [Al]-beta. Due to the incorporation of the larger and heavier Ga atoms, the IR lattice vibration bands shift to lower frequencies. The relative Brønsted acidity is found to be between the aluminum- and the boron-substituted beta zeolite.

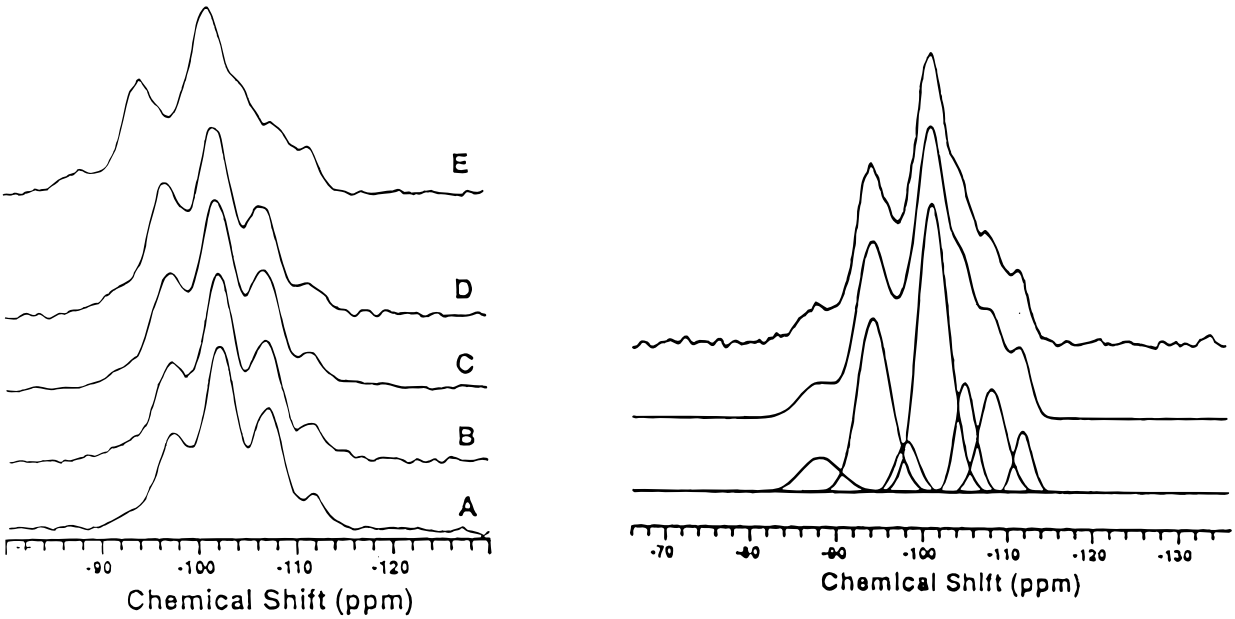

Figure 55. ^{29}Si MAS NMR spectra of several [Al,Ga]-offretites with Ga/(Ga + Al) mole fractions of (A) 0.0, (B) 0.04, (C) 0.08, (D) 0.13, and (E) 1.0 (left); deconvoluted spectrum E (right). (Reprinted with permission from ref 98. Copyright 1996 Marcel Dekker Inc.)

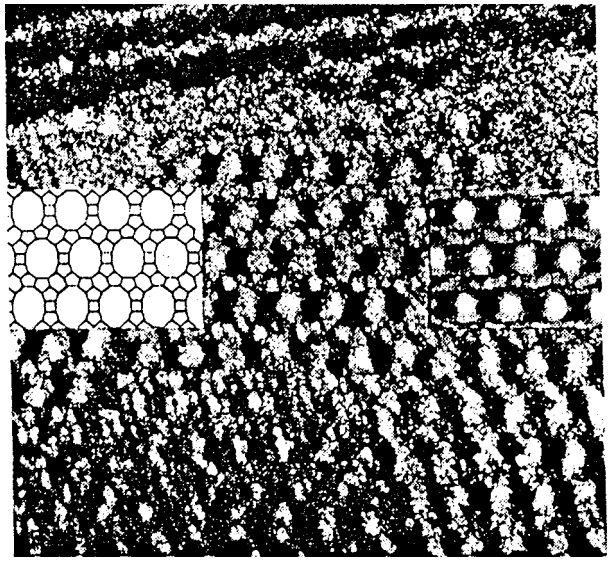

Figure 56. HRTEM bright view micrographs of a zeolite beta (b, BEA) crystallite viewed perpendicular to the "square" *c*-axis and its framework topology shown in the inset.[348] (Reprinted with permission from ref 348. Copyright 1988 Nature Publishing Group.)

Besides the stretching vibrations of terminal SiOH groups at 3747 cm^{-1}, the stretching vibration band of Ga-induced acidic bridging OH groups[166] is found at 3625 cm^{-1}. Most of the lattice vibration bands are shifted to lower frequencies compared to the Al analogue. A Si/Ga ratio of 15.4 was reached, corresponding to a Ga^{3+} ion concentration of 3.9 per unit cell. The Si/Ga ratio in the starting gel amounted to 25. At this ratio a crystallization time of 2 days was necessary to give highly crystalline [Ga]-beta. Lower concentrations of Ga require longer crystallization times and lead to lower zeolite yields. A ratio of 250 or more does not yield zeolite structures at all, even after crystallization times of 10 days or longer.[166] These difficulties are encountered for not only with the gallosilicate beta but are observed also with the aluminosilicate beta structure.[354]

D. Zeolites with High Si/Ga Ratios

1. [Ga]-ZSM-5

The gallium analogue of ZSM-5 was described in the 1970s[355] already and has become the most thoroughly studied system hitherto (Figure 57).[356] The continuous interest was promoted by the successful exploitation of the parent ZSM-5 in acid catalysis and petroleum chemistry. The interest was shifted to the gallium analogue after it was realized that gallium-modified ZSM-5 zeolites can effectively perform the conversion of low alkanes into aromatics (Cyclar process). Template-free synthesis routes for both the aluminosilicate and the gallosilicate ZSM-5 have been devised and patented.[91,357] Kinetics of the crystallization of [Ga]-ZSM-5[114] and a comparative study of the crystallization rates of [Al]- and [Ga]-ZSM-5 have been published.[358] The dependence of the crystallinity and of the degree of gallium incorporation on the crystallization time and gel compositions have been investigated.[359,360] A correlation between

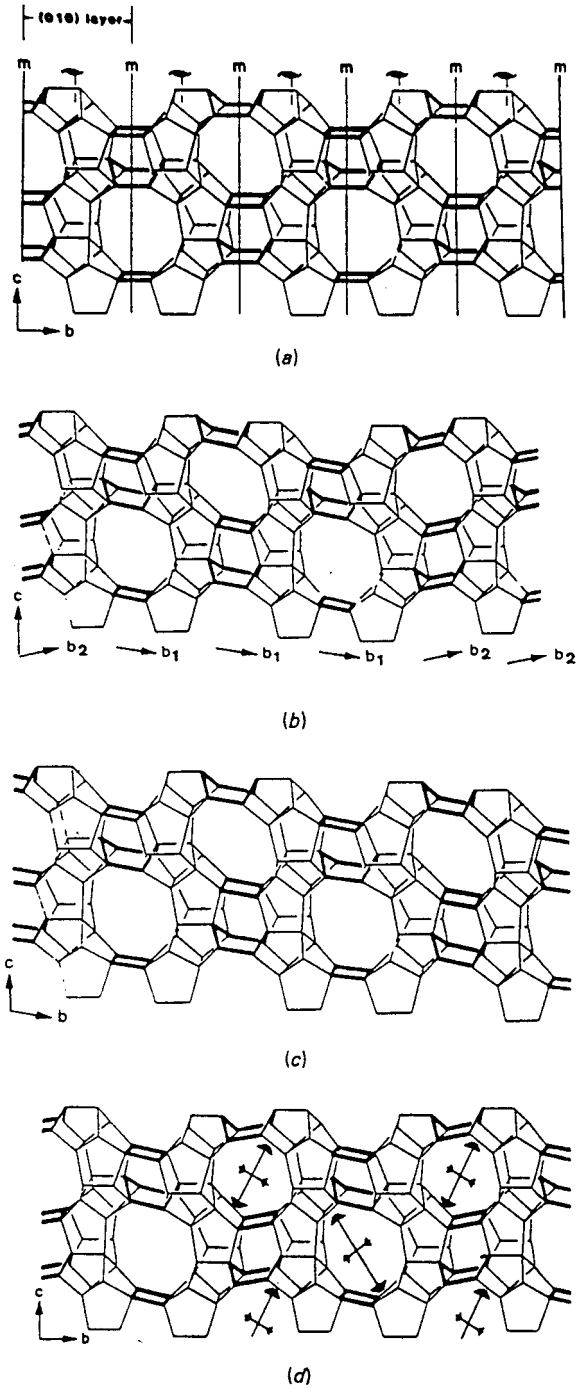

Figure 57. Framework and framework flexibility of zeolite ZSM-5 (MFI): (a) (100) pentasil layer in orthorhombic (ORTHO) as-synthesized isomorphously substituted ZSM-5; (b) (100) pentasil layer in monoclinic H-ZSM-5 at room temperature. Random (exaggerated) shift of (010) layers along $+c$ and $-c$. [Note: the size of the twin domains in the crystal is at least 50 unit cells or $\gg$1000 Å]. (c) As in part b but *after* application of mechanical stress, showing a perfect monoclinic (MONO) single crystal; (d) (100) pentasil layer in PARA, showing the strictly alternating shift of successive (010) layers along *c*. The arrows indicate the direction of the deformation of the framework upon adsorption of *p*-xylene. (Reprinted with permission from ref 356. Copyright 1989 Muuksgaard International Booksellers and Publishers, Copenhagen.)

the unit cell volumes and the Si/Ga ratio (extent of gallium incorporation) has been established (Table 15).

Table 15. Unit Cell Volumes of Silicalite-1 and [Ga]-ZSM-5 Samples with Various Si/Ga Framework Ratios

sample	Si/Ga ratio	U.c. volume (Å^3)	ref
[Ga]-ZSM-5	18.5	5402	114
[Ga]-ZSM-5	34.5	5432	345
[Ga]-ZSM-5	38.5	5389	119
[Ga]-ZSM-5	170.5	5351	119
[Ga]-ZSM-5	592.5	5280	119
silicalite-1	∞	5386	119

It is also acknowledged that a prolonged crystallization time leads to a reconstruction of the framework accompanied by further incorporation of nonframework gallium into tetrahedral framework positions. The maximum borderline value of gallium in framework T positions reported in the literature differs widely. Kosslick et al.[141] found a value of ca. 2 Ga atoms per unit cell (consisting of 96 tetrahedra), whereas 2.41 Ga atoms per unit cell is reported by Bayense et al.[129] and even 5.2 Ga atoms per unit cell by Liu and Klinowski.[165] Owing to a different crystal morphology, trace amounts of silicalite-1 were detected by SEM in [Ga]-ZSM-5 batches at gallium framework concentrations < 1.8 Ga/unit cell. There is additional evidence that the gallium insertion causes a partial disruption of the MFI framework. This is mainly concluded from IR spectra with framework vibrations at 990 and 950 cm^{-1} assigned to structural defects. Kosslick et al.[37] considered a vibration in the hydroxyl region at 3546 cm^{-1} to be caused by internal silanol groups, indicating structural defects. Below 3.1 Ga atoms per unit cell, the [Ga]-ZSM-5 crystallites contain defect sites (internal silanol groups). At higher Ga content, defect sites are not detectable.

XPS investigations showed that the surface Si/Ga ratio corresponds to the bulk ratio.[119] In contrast, EDX spectra of another [Ga]-ZSM-5 sample revealed an enrichment of gallium toward the core of gallosilicate crystals (Si/Ga = 184) whereas the outer shell showed only a negligibly small amount of gallium.[361,362] With [Al]-ZSM-5, Dessau et al.[87] confirmed aluminum zoning with high aluminum concentrations in the outer shell. This was concluded from SEM images, recorded after a selective removal of silica by treatment with bases, which showed a highly selective dissolution of the interior of the crystals. As outlined by Wallau et al.,[91] a homogeneous T-atom distribution throughout the crystal volumes is observed when samples are synthesized in a purely inorganic synthesis gel. Zoning effects, however, are detectable in the case of template-assisted synthesis routes. Gallium is enriched in the crystal core when synthesized in the presence of tetrapropylammonium bromide. In contrast, aluminum in [Al]-ZSM-5 is enriched in the outer shell. This is independent of the Si/T(III) ratios. The 50−70% maximum yield of crystalline material for template-free-synthesized [Ga]-ZSM-5 samples, however, is rather low. The distribution of aluminum and gallium over the crystal volume reasonably depends on the synthesis conditions and hence on the morphology, above all on the crystallite size.

Table 16. Ranges of the Chemical Shifts (ppm) of ^{29}Si Nuclei in Gallosilicates as Well as In Aluminosilicates[175]

n in Si(nM)	gallosilicates (M = Ga)	aluminosilicates (M = Al)
4	−74.9 to −78.3	−84
3	−82.4 to −94.6	−88
2	−89.0 to −101.4	−93.8 to −101.7
1	−94.9 to −104.5	−99.0 to −107.0
0	−101.3 to −116.9	−102.0 to −116.2

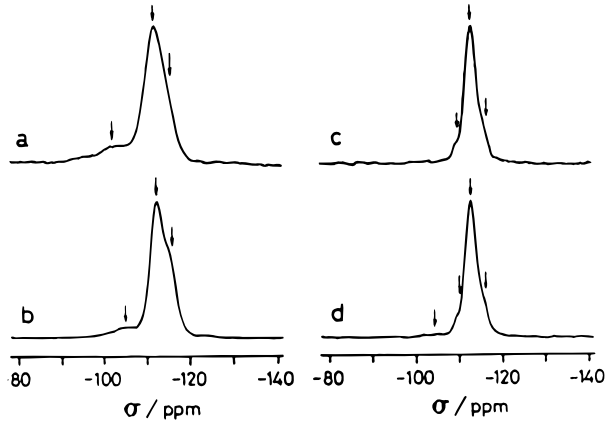

Figure 58. High-resolution ^{29}Si MAS NMR spectra of gallium and aluminum substituted H-ZSM-5: (a) Si/Ga = 31, (b) Si/Ga = 194, (c) Si/Al = 44, (d) Si/Al = 400. (Reprinted with permission from ref 175. Copyright 1985 The Chemical Society of Japan.)

Applying high-resolution electron microscopy, Acosta et al.[363] found that the dimensions of elliptical channels are larger in [Ga]-ZSM-5 than in [Al]-ZSM-5.

Hayashi et al.[175] summarized the ranges of the chemical shifts of ^{29}Si nuclei in gallosilicate as well as in aluminosilicate zeolites (Table 16).

^{29}Si MAS NMR spectra (Figure 58) reveal the uncertainties of the identification of detailed configurations of silicon-rich materials because no clearly separated peaks appear. The spectra of [Al]-ZSM-5 (Si/Al = 44) are deconvoluted into three signals corresponding to chemical shifts at −105.6, −112.3, and −115.6 ppm. With a higher Si/Al ratio (Si/Al = 400), four lines are found at −104.5, −110.3, −113.2, and −116.2 ppm. The line at ca. −105 ppm is assigned to Si(1Al) units, whereas all other lines are assigned to Si(0Al) units whose chemical shifts are dispersed because of the crystallographic inequivalence of sites.

2. [Ga]-ZSM-11

ZSM-11 is a pentasil-type zeolite. Like ZSM-5, this zeolite contains oxygen-10-ring openings and is built up by double-5-ring units. The chains, however, are mirror plane-like arranged to each other (Figure 59).[364] Liu and Thomas[134] described a route of preparation of [Ga]-ZSM-11 by hydrothermal treatment of silicalite-2, the pure siliceous form of zeolite ZSM-11, with an aqueous solution of sodium gallate, $NaGaO_2$, at 100 °C for 24 h. Results of extended characterization proved the insertion of gallium into the silicalite-2 framework without formation of byphases. [Ga]-ZSM-11 was rather rich in gallium (Si/Ga ratio of 9.83). The template had been removed

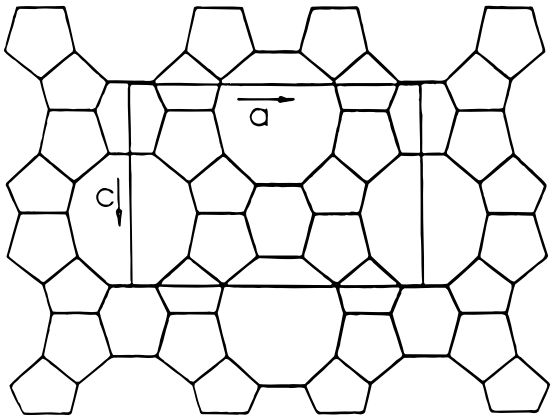

Figure 59. Framework structure of zeolite ZSM-11 (MEL) viewed along the 10-membered ring channel. (Reprinted with permission from ref 364. Copyright 1996 R. Oldenbourg Verlag München.)

through calcination at 550 °C. After transforming the galliated silicalite-2 into the H form, the resulting IR spectrum of [Ga]-ZSM-11 shows two peaks at 3742 and 3622 cm^{-1}, the latter being related to inserted gallium.[159] The vibration frequency of the Ga−OH−Si unit is not really different from that of the [Ga]-ZSM-5, found at 3620 cm^{-1}. This underlines the similarity of the [Ga]-MEL and [Ga]-MFI structures. The precise mechanism of the substitution of Si^{4+} by Ga^{3+} in tetrahedral framework positions has remained, up to now, enigmatic. The authors tried to extend this galliation procedure to silicalite-1 in order to gain a [Ga]-ZSM-5 zeolite. Silicalite-1, however, tends to lose its crystallinity when subjected to similar galliation procedures. According to the authors, highly siliceous forms of zeolite structures are more or less amenable to this galliation procedure and may serve for a preparation of active catalysts from virtually inactive materials.

3. [Ga]-ZSM-12

Besides TEA silicate, CZH-5, NU-13, and TPZ-2, this kind of zeolite belongs to the MTW structure type.[34] Ga analogues are reported for the ZSM-12 structure; accessible information, however, is rare.[174,358,365] ZSM-12 possesses a unidimensional linear channel system with apertures of 5.6 × 7.7 Å built by 12-membered rings. The synthesis of the aluminosilicate type was disclosed in 1974.[366] Commonly, tetraethyl- and methyltriethylammonium cations are suitable as efficient templates, although other organic molecules can be used.[367,368] Kosslick et al.[174] utilized sodium silicate, hydrated gallium nitrate, and methyltriethylammonim bromide for the synthesis of [Ga]-ZSM-12 at 170 °C. DTA analysis of the [Al]-ZSM-12 revealed three exothermic peaks attributed to the decomposition of the template (at ca. 375 and 450 °C) and to the oxidation of coke (at 540 °C). With [Ga]-ZSM-12, the two peaks of template decomposition were found at somewhat lower temperatures.

The thermal stability of the gallium-substituted MTW framework seems to be lower than that of [Ga]-ZSM-5. A crystallinity loss of 10% was observed after 10 h of calcination at 500 °C. The loss was accompanied by the release of gallium from tetrahedral framework positions. The original Si/Ga ratio of [Ga]-ZSM-12 was 14.[358] Fe-,[369] Ti-,[370,371] V-,[372] and Pb-substituted[373] ZSM-12 were synthesized as well.

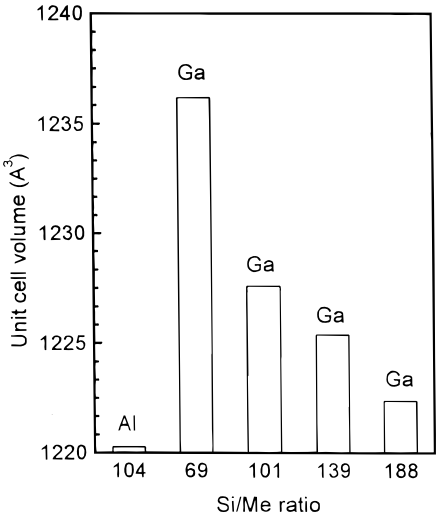

Figure 60. Influence of Al or Ga content on the unit cell volumes of [Al]-ZSM-22 and [Ga]-ZSM-22. (data from ref 164).

4. [Ga]-ZSM-22

The ZSM-22 (TON) framework is orthorhombic and consists of 5-, 6-, and 10-membered rings. The unidirectional channel system has free diameters of 0.55 and 0.45 nm, respectively. The framework topology is described in detail by Kokotailo et al.[374] Zeolites of TON-type structure can be synthesized with a great variety of organic templates.[375]

Singh and Reddy[164] synthesized [Ga]-ZSM-22 from a silica sol (containing 0.5% Na_2O, 0.05% Al_2O_3, 28.9% SiO_2, and 70.55% H_2O), potassium hydroxide, gallium sulfate, and 1-ethylpyridinium bromide as template. Owing to traces of Al present in the applied silica sol, the synthesized Ga analogue is not free of Al (Si/Al = 208). A synthesis time of 4 days was necessary for crystallization. Si/Ga ratios varied between 138 and 376. As observed with other zeolites, the incorporation of gallium into the framework is accompanied by an enlargement of the unit cell. At low gallium contents, the unit cell volume approaches 1220.3 $Å^3$ (Figure 60).

The morphology of the ZSM-22 structure is retained for the gallosilicate. Both crystallite structures are needle-shaped (0.8−1.0 μm long and 0.2−0.3 μm thick). Compared to other gallosilicate structures (see above), the oxidative decomposition of the organic template in the as-synthesized product of [Ga]-ZSM-22 occurs at somewhat lower temperatures. (DTA curves published by Singh et al.[164] seem to indicate the opposite, but the text shows that the DTA curves are obviously mixed up.) Results of characterization give no indication for the presence of framework Al. Unfortunately, OH vibration spectra are not reported. The catalytic properties of [Al]-ZSM-22 and [Ga]-ZSM-22 in the conversion of ethylbenzene at 455 °C were not significantly different. Physicochemical characterization and catalytic properties confirm the incorporation of Ga into framework positions of ZSM-22. Catalytic characterization of the aluminosilicate

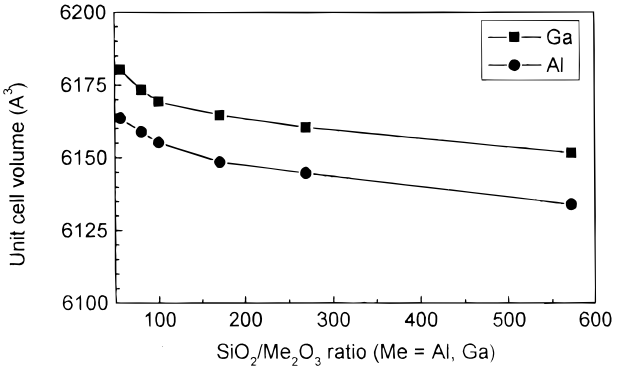

Figure 61. Unit cell volume of zeolite EU-1 vs Si/Al or Si/Ga modulus (SiO_2/Me_2O_3); data from ref 377.

structure [Al]-ZSM-22 is reported by Ernst et al.[375] It was claimed that [Al]-ZSM-22 is a very selective catalyst for the formation of 2-methyl-branched alkanes from *n*-alkanes.

5. [Ga]-EU-1

The synthesis and characterization of zeolite EU-1 were reported by Casci et al.[376] in 1984 as well as by Rao et al.[377] in 1989. A gallium-containing derivative of the EUO framework zeolite EU-1 has been synthesized from Al-free hydrogel systems in the presence of dibenzyldimethylammonium or hexamethonium cations by Rao et al. in 1992.[378] The EUO framework structure is characterized by 10-membered-ring main channels connected by 12-membered-ring apertures. Side pockets of 6.8 × 5.8 Å in cross section and 8.1 Å in depth are formed. XRD data confirmed the expansion of the unit cell volume due to incorporation of gallium (Figure 61).

The successful incorporation of gallium into framework positions was verified by XRD, IR spectroscopy of framework vibrations, and ^{71}Ga MAS NMR spectroscopy.

E. Gallium-Modified Mesoporous Silicates

The discovery of a new family of mesoporous materials known as M41S and FSM-16 has stimulated immediate research efforts of the catalytic community.[379−385] These silicate materials are characterized by an ordered arrangement of relatively uniform mesopores (Figure 62). Pore sizes may vary between 20 and 100 Å, but most of obtained materials have mean pore diameters of 20−45 Å. The thick walls[386−388] with widths of 6−10 Å stabilize these open structures up to temperatures of 800−900 °C. Some unique properties of these mesoporous silicates are especially interesting with respect to their application: large surface areas of 300−1300 m^2/g, wide pore volumes of 0.5−2.1 cm^3/g, long and uniform pores of 20−100 Å. Additionally, substitution of Si atoms in the walls by atoms of 3- and 4-valent elements is possible. By this, Brønsted acidity and redox centers can be introduced, making these materials attractive as potential catalyst components. The SiO_4 tetrahedra of the walls are disordered or at least display no long-range order. Therefore, these materials show no X-ray reflections of high order. Only low-angle reflections between $2\Theta = 1-10°$ appear, with the lowest angle reflection at ca. 2° often being observed only. The XRD pattern is due to the scattering of X-rays at the walls of the regularly arranged pores of uniform size leading to some "lattice" periodicity.

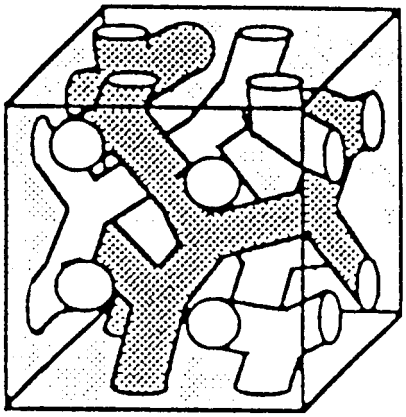

Figure 62. Pore system of the structured mesoporous molecular sieve MCM-48.

The synthesis of these new materials is achieved by combining an appropriate surfactant molecule, usually hexadecyltrimethylammonium bromide or hydroxide (CTABr or CTAOH) with a silicon source like SiO_2, silica sol, water glass, or tetraethylorthosilicate (TEOS) in aqueous solution.[379−382] Different pH values are applied: acidic, alkaline, or nearly neutral synthesis gels. The concentration of the surfactant must be high enough to ensure micelle formation. Different types of micelles can be formed at different concentrations of the surfactant. Therefore, the surfactant/silica ratio has an important impact on the actual structure type formed. Crystallization of mesoporous silicates is obtained by aging the gel at room temperature or by hydrothermal treatment between 40 and 50 °C, usually at 80−120 °C.

The mechanism of the formation of mesostructured M41S-type silicates (Figure 63) is still under discussion, and probably different routes are possible depending on the synthesis conditions.[389−391]

A liquid-crystal templating mechanism is favored as the most probable way to M41S materials. According to this, surfactant molecules with hydrophilic headgroups (amines) and a hydrophobic tail (hydrocarbon chain) undergo self-assembling in the gel. They form a rodlike structure with the hydrocarbon tails directed to the inner part and the hydrophilic amine headgroups "covering" the surface of the rods. The hydrophilic headgroups interact with silicate species in the gel.

After burning off the organic at 813−873 K for several hours, a mesostructured silicate is obtained. The hexadecyltrimethylammonium ions fit the geometrical requirements for mesostructure formation best. Using this surfactant, most of the M41S and related materials are obtained in high quality.

1. Synthesis and Structure

a. [Ga]-MCM-41 and Related Mesoporous Materials. The first reported structures were purely siliceous hexagonal MCM-41, lamellar MCM-50, and

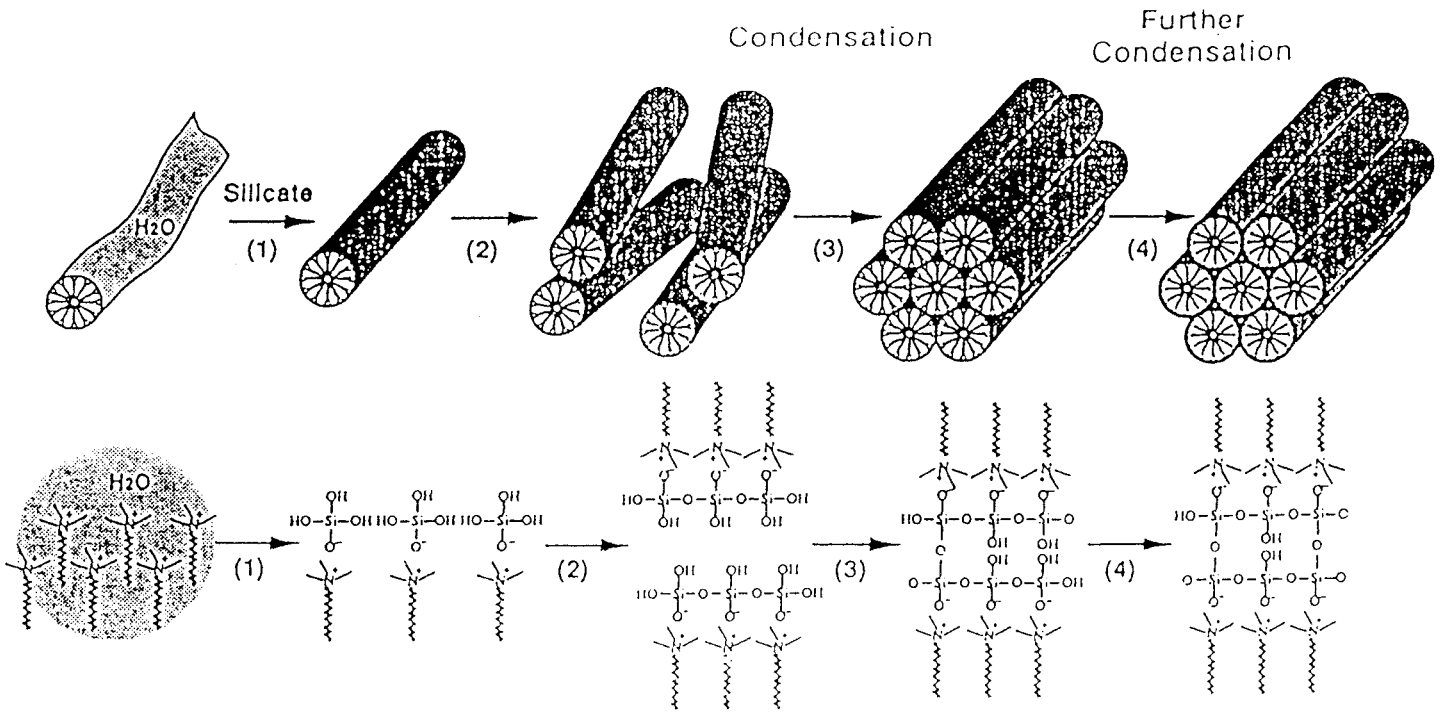

Figure 63. Proposed (liquid crystalline) mechanism for the formation of mesoporous MCM-41. (Reprinted with permission from ref 390. Copyright 1993 Elsevier Science.)

cubic MCM-48 phases.[379,380] More or less ordered mesoporous structures have been synthesized too, especially isomorphously substituted materials. Most of the published literature deals with less ordered structures characterized by one low-angle X-ray reflection only.[379,392,393]

As with zeolites, silicon atoms can be substituted by other elements such as B, Al, Fe, Ti, and Zr.[394−397] Also, gallium could be incorporated successfully into the walls of MCM-41[398,399] and of related mesoporous silicates such as of MCM-48.[400,401]

The synthesis of [Ga]-MCM-41 and [Ga,Al]-MCM-41 has been reported[398,402,403] starting from gels of the composition $0.0042-0.05Ga_2O_3:1SiO_2:0.2NaOH:0.27TMAOH:0.27CTACl:60H_2O$.

Cabosil M5, sodium silicate, and gallium nitrate were used as metal sources. The gel was adjusted to pH = 11 by adding sulfuric acid (25 wt % in water). At higher and lower pH values, less crystalline samples are obtained. The gel was aged for 16 h and then hydrothermally treated at 50 °C for 3 days. Si/Ga ratios in the samples varied between 12 and 97. BET surface areas of ca. 690 m^2/g and pore diameters of 30 Å were reported. This is confirmed by transmission electron micrographs. Samples contain both linear and curved tubular pores. A decrease of the *d* spacing (d^{10}_0 reflection) from 45.5 (a_0 = 52.5 Å) to 37.5 Å (a_o = 43.5 Å) was observed with increasing Ga contents. Possibly, gallium causes a higher degree of condensation of the silicate network. This assumption is supported by the increasing contents of Q^4 units $Si(OSi)_4$ as revealed by ^{29}Si MAS NMR spectrometry. Gallium incorporation is indicated by the appearance of broad signals at 139 (as-synthesized material) and 146 ppm (calcined material) in the ^{71}-Ga MAS NMR spectra. The intensity of the Ga signal depends on the Ga content. From the distinct decrease of the intensity of the ^{71}Ga NMR signal, the authors concluded that 25−75% of gallium was removed from tetrahedral framework positions after calcination.

Our results show that well-crystallized samples can be obtained up to a gallium content of 1.65 mmol/g (Si/Ga = 10) using a gel with the composition $0.625NaOH:0.03Ga_2O_3:1SiO_2:0.245CTABr:89H_2O$.

The synthesis was obtained by adding the template to the sodium hydroxide solution under stirring, followed by the addition of TEOS and sodium gallate solution (containing 0.287 mol/L Ga and 0.313 mol/L Na). The gel was hydrothermally treated at 100 °C for 4 days. Disordered gallium-substituted mesoporous silicates related to MCM-41[332] were obtained from modified synthesis batches containing 2-propanol. The XRD patterns of these materials show one main reflection only at $2\Theta = 0.89°$ ($d^{10}_0 = 99.2$ Å) for [Ga]-MCM-41, at $2\Theta = 0.87°$ ($d^{10}_0 = 102.0$ Å) for [Al]-MCM-41, and at $2\Theta = 0.8$ ($d^{10}_0 = 109.9$ Å) for [Fe]-MCM-41. Reflections at larger angles are absent or present in low intensities only. The absence of higher order reflections suggests a more randomly ordered arrangement of channels in these samples.[391,405] The reflections of substituted samples are relatively broad and asymmetric, probably indicating a wide-spread distribution of pore sizes.

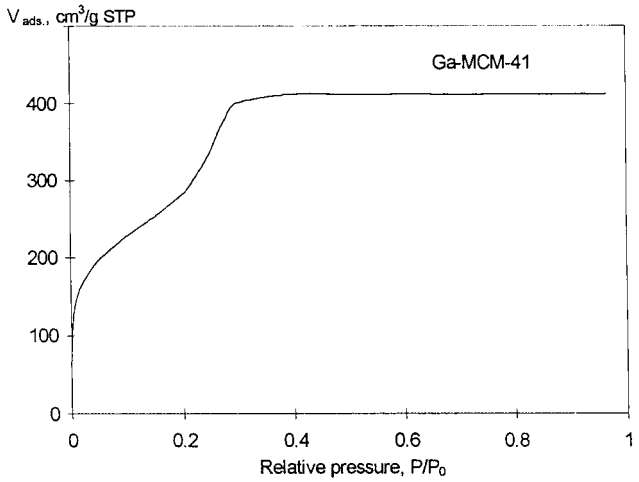

Figure 64. N_2 adsorption isotherm of Ga-modified MCM-41 (Si/Ga = 10). (Reprinted with permission from ref 37. Copyright 1993 The Royal Society of Chemistry.)

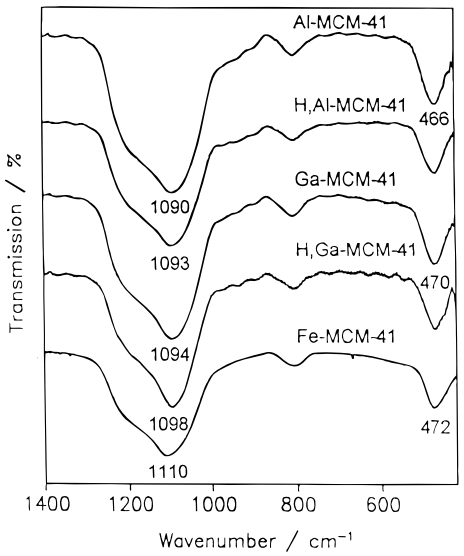

Figure 65. IR lattice vibration spectra of Me^{III}-substituted MCM-41 either calcined or in its H form (H,Me^{III}-MCM-41) with bulk ratios of Si/Al = 14.8, Si/Ga = 13.8, and Si/Fe = 15.2. (Reprinted with permission from ref 404. Copyright 1996 Elsevier Science.)

The BET surface areas of these materials vary between 300 and 1200 m^2/g and the total pore volume V_P between 0.5 and 1.5 cm^3/g (Figure 64).

Substitution of silicon by gallium is revealed by the IR lattice vibration spectra which show three main absorption bands at ca. 1095, 805, and 470 cm^{-1} (Figure 65). The bands are assigned to antisymmetric stretching vibrations of T−O−T-framework units, to symmetric stretching vibrations of T−O−T-framework units (T = Si, Al, Ga, Fe), and to deformation modes of the TO_4 tetrahedra, respectively. The spectra are very similar to those of amorphous silica. In contrast to zeolites, no structurally sensitive absorption band was observed. These findings and the absence of any X-ray reflections at higher 2Θ values gave rise to the conclusion that pore walls of substituted MCM-like materials show no long-range order of the TO_4 tetrahedra. Substitution of silicon by aluminum, gallium, or iron causes shifts of the lattice

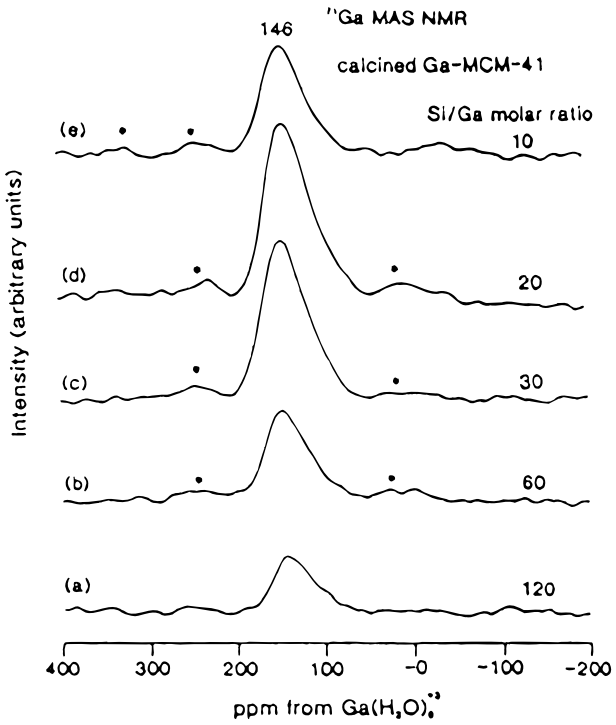

Figure 66. ^{71}Ga MAS NMR spectra of calcined Ga-modified MCM-41 with bulk Si/Ga ratios of (a) 120, (b) 60, (c) 30, (d) 20, and (e) 10. Dots indicate spinning sidebands. All samples were equilibrated with saturated water vapor at room temperature. (Reprinted with permission from ref 398. Copyright 1996 American Chemical Society.)

vibration bands to lower wavenumbers. Compared to the parent Si-MCM-41, the wavenumber of the antisymmetric T−O−T vibration band of Al-, Ga-, and Fe-substituted samples decreases to 1090, 1094, and 1110 cm^{-1}, respectively. The shifts are caused by the increase of the mean T−O distances in the walls after substitution of the small silicon (r_{Si}^{4+} = 0.26 Å) by the larger aluminum (r_{Al}^{3+} = 0.39 Å), gallium (r_{Ga}^{3+} = 0.47 Å), or iron ions (r_{Fe}^{3+} = 0.47 Å) (compare Table 2 in section I). The observed shifts, which depend as well on the change in the ionic radii as on the degree of substitution, are comparatively small. Therefore, only a low degree of substitution is suggested. Interestingly, shifts of the wavenumber decrease in the sequence Al > Ga > Fe, although the ionic radius of aluminum is smaller than that of gallium or iron. It is concluded that the degree of substitution decreases in the same order.

After transformation into the H-form, a shift of the antisymmetric T−O−T vibration band to higher wavenumbers is observed, indicating a partial removal of Al and Ga from tetrahedral framework positions during this procedure. It seems, that MCM-41 is more sensitive to thermal treatment than high-silica zeolites such as ZSM-5. Despite the high Me/Si ratios in the synthesis gel, IR spectra do not point to the incorporation of large amounts of Al, Ga, and Fe. Thermal treatment during calcination and transformation to the H-form leads to a considerable release of substituted atoms from the framework. The IR lattice vibration spectra of Al-, Ga-, and Fe-substituted MCM-41 support the assumption that ordered TO_4 tetrahedral structural units in the walls, usually known for zeolites, do not exist.

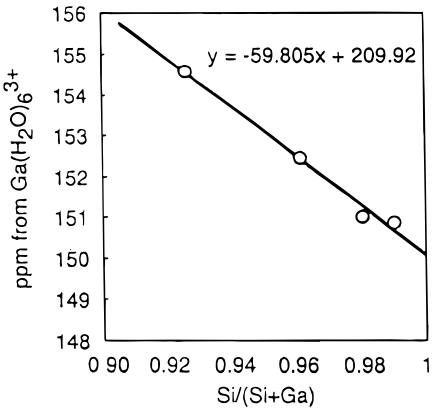

Figure 67. ^{71}Ga chemical shift of as-synthesized Ga−MCM-41 depending on the Si/(Si + Ga) mole fractions. (Reprinted with permission from ref 421. Copyright 1998 Academic Press.)

Ga incorporation into tetrahedral positions of the walls is indicated by the appearance of a signal at ca. 140−160 ppm in the ^{71}Ga MAS NMR spectra of as-synthesized and calcined [Ga]-MCM-41 which is assigned to tetrahedral $Ga(OSi)_4$ units. With the exception of the sample with the highest Ga content (Figure 66), the intensity of this ^{71}Ga signal increases and is shifted to a lower field (Figure 67) with growing Ga content.

The increased line widths of the ^{29}Si MAS NMR signals of the substituted samples reveal a certain structural disorder, i.e., a wide distribution of Si−O−Si angles and Si−O bond distances in the walls. Substitution of framework Si by Al, Ga, or Fe causes nearly identic chemical shifts of the ^{29}Si MAS NMR signal at −112 ppm to lower field.[404] Due to the low degree of substitution, the signal intensity of the Si(1Me) groups (Me = Al, Ga, or Fe) is weak and these signals can be overlapped by that of the silanol groups. Consequently, no separate line is observed for Si(1Me) groups. Due to framework distortion, a broadening of the ^{29}Si NMR signal at −112 ppm is sometimes observed. The signal width increases with growing incorporation in the order Fe < Ga < Al.

b. [Ga]-MCM-48. [Ga]-MCM-48 can be synthesized[400] by hydrothermal treatment of reaction mixtures of the composition $67Na,K_2O{:}1.025Ga_2O_3{:}100SiO_2{:}67.7CTABr{:}6771H_2O$.

Synthesis gels were kept at 110 °C for 2−3 days. The Si/Ga ratio could be varied between 100 and 24. XRD patterns are close to those of the siliceous MCM-48 (Figure 68). The pore diameter is ca. 30 Å, and the BET surface area amounts to about 1000 m^2/g.

For many MCM-like materials, a type IV adsorption isotherm according to the IUPAC classification is observed. The first plateau is due to the formation of an adsorption monolayer. The second plateau is due to capillary condensation of nitrogen in the mesopores. ^{29}Si and ^{71}Ga NMR spectra are similar to those of MCM-41. The amorphous walls of all mesoporous silicates show a low connectivity of the SiO_4 tetrahedra. This holds also for gallium-substituted materials. ^{29}Si MAS NMR spectra of mesoporous silicates show three signals at ca. −91, −101, and −110 ppm (Figure 69). The similarity of these spectra to those of silica gels implies an assignment

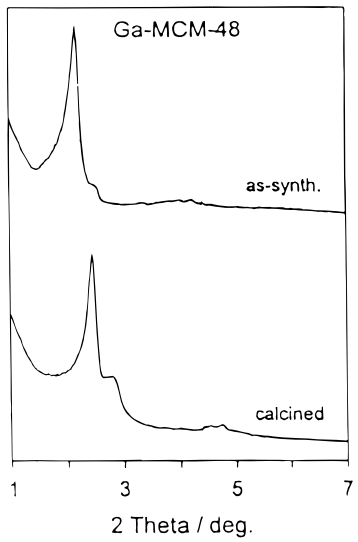

Figure 68. XRD pattern of as-synthesized Ga−MCM-48 with bulk ratio Si/Ga = 32. (Reprinted with permission from ref 421. Copyright 1998 Academic Press.)

of the recorded peaks to Q,[4] Q^3, and Q^2 units, i.e., to $Si(OSi)_4$, $(SiO)_3SiOH$, and $(SiO)_2Si(OH)_2$ groups, respectively. This means that the networks of mesoporous silicates are of a distinctly lower connectivity than those of zeolites which are usually 4-fold connected. Line deconvolutions show that 40−60% of Si network atoms in MCM-48 show no 4-fold connection. After calcination, the three resolved signals disappear. A broad signal located at −108 to −110 ppm with an extended high-field shoulder remains. The intensity decrease in the spectral range between −90 and −105 ppm is due to the condensation of silanol groups in the walls. The extended shoulder reflects broadening of the Q^4 signal caused by a wide-spread distribution of Si−O bond lengths and Si−O−Si angles. Unreacted Q^3 and Q^2 units also contribute to the broad signal as is evidenced by CP/MAS Si NMR spectra. After CP application, the "original" spectrum with resolved lines at −91 and −101 ppm reappears, indicating that these lines indeed belong to silanol groups rather than to silicate $(SiO)_3SiO^-$ anions. The remaining silanols should have the same near-range order (environment) as in the as-synthesized sample.

TG−DTA studies of the water loss between 200 and 900 °C show that the silanol concentration present in the different types of mesoporous silicates is comparably high (4−5 mmol/g).[406] On the basis of an internal surface area of 600 m^2/g, the OH density is estimated to 4−6 $SiOH/nm^2$. The interior surface has a hydrophilic rather than a hydrophobic character. An uptake of 10−15% of water from air humidity is observed for the dried samples. Under similar conditions, the hydrophobic silicalite-1 adsorbs only 1% of water.

The presence of large amounts of silanol groups is confirmed by IR OH vibration spectra. Three types of silanol groups are found: terminal (vibrating at 3740 cm^{-1}), internal H-bound (3710 cm^{-1}), and associated silanol groups giving rise to a broad absorption band between 3400 and 3600 cm^{-1}. Template interaction causes a broadening and the shift of the band at 3740−3690 cm^{-1} indicating strong host/guest interaction by hydrogen bonding. Silanols have no acidity and are inactive in acid-catalyzed reactions.

The acidic and catalytic properties of these materials will be discussed subsequently, because catalytic applications are not as numerous as in the case of microporous gallium zeolites.

2. Acidity of Mesoporous Materials

Very little information is available on the thermal stability and the strength of acid sites. Compared to the usual aluminosilicate zeolites, the acidity of Al-modified MCM-41 has to be classified as weak. The thermal stability of the acid sites has not been

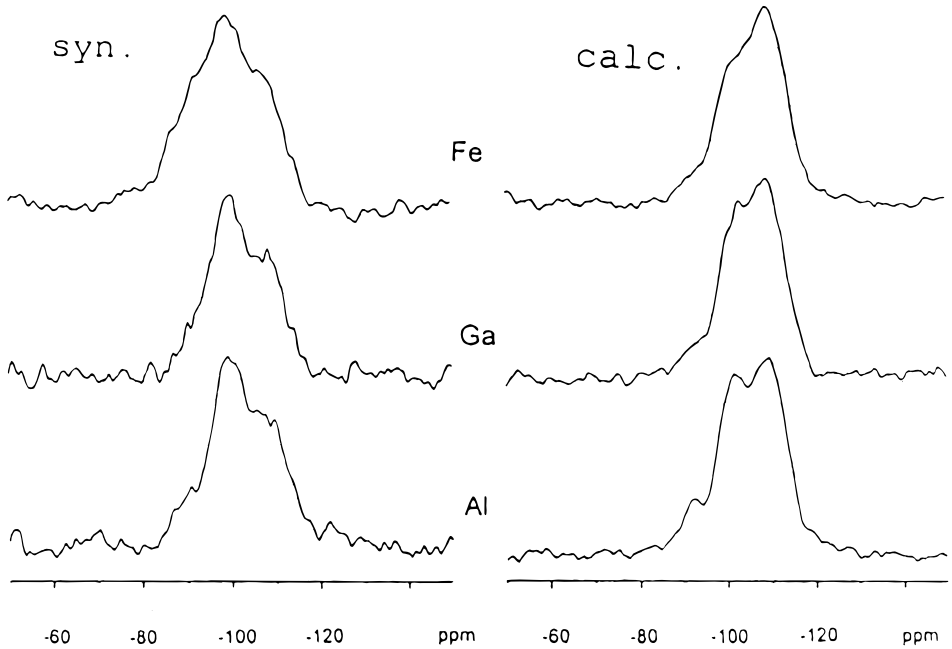

Figure 69. High-resolution ^{29}Si MAS NMR spectra of as-synthesized and calcined Al-MCM-48, Ga-MCM-48, and Fe−MCM-48. (Reprinted with permission from ref 400. Copyright 1998 Academic Press.)

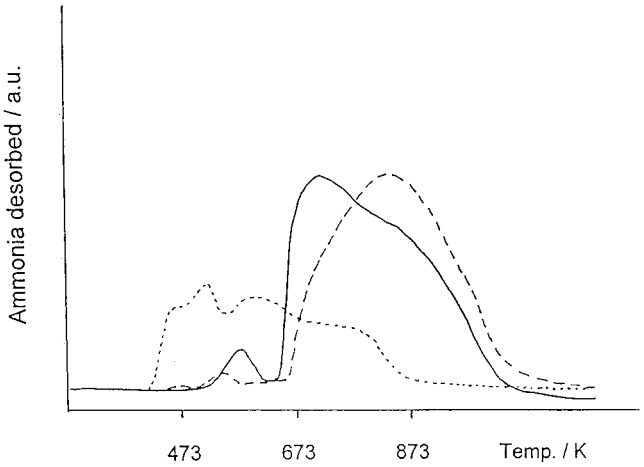

Figure 70. Temperature-programmed decomposition of NH_4-exchanged Al-substituted (—), Ga-substituted (- - -) and Fe-substituted (···) MCM-41. (Reprinted with permission from ref 411. Copyright 1999 Elsevier Science.)

profoundly investigated. The number of acid sites is small, and their acid strength[407−410] is relatively weak.

Both Brønsted and Lewis sites of different strength are present in any substituted sample. The occurrence of Brønsted acidity conclusively confirms the successful isomorphous substitution of Si by Al, Ga, and Fe in the MCM-41 framework. This type of acidity can be characterized by conventional temperature-programmed desorption of ammonia (TPDA), FTIR-TPDA, IR spectra of adsorbed pyridine, and microcalorimetry using NH_3 as a probe molecule.[399−401,404]

Typical TPDA profiles for [Ga]-MCM-41[411] and [Ga]-MCM-48[399] are shown in Figures 70 and 71.

Ammonia desorption from NH_4[Ga]-MCM-41 and MCM-41-related materials occurs over a wide temperature range between 350 and 700 °C. The desorption maximum is located at 450 °C and a shoulder near 600 °C. The maximum concentration of Brønsted acid sites was found to be ca. 0.6 mmol/g (Si/Ga = 27). By calcination, the concentration is decreased to ca. 0.25 mmol/g (Si/Ga = 65). The main ammonia desorption from the calcined sample proceeds between 150 and 400 °C. The profile exhibits a desorption maximum at 220 °C and a high-temperature shoulder at 350 °C. A small amount of strongly bound ammonia is desorbed between 400 and 500 °C.

The desorption profile of NH_4[Ga]-MCM-48 is different from that of MCM-41 and related mesoporous silicates. It exhibits three maxima located at 220, 430, and 590 °C (distinct shoulder). After calcination, the TPD profile shows similar changes to those observed with MCM-41. In any case, the high-temperature shoulder is attributed to the existence of Lewis acid sites, whereas desorption peaks between 300 and 500 °C are assigned to Brønsted sites.

TPDA profiles of the calcined [Ga]-MCM samples are similar to profiles observed for dealuminated large-pore zeolites of the faujasite family. The strength and distribution of acid sites of both structure types are comparable. Karge et al.[412] found four different acid sites in dealuminated zeolite Y: weak Brønsted and/or Lewis sites desorbing ammonia at 180 °C,

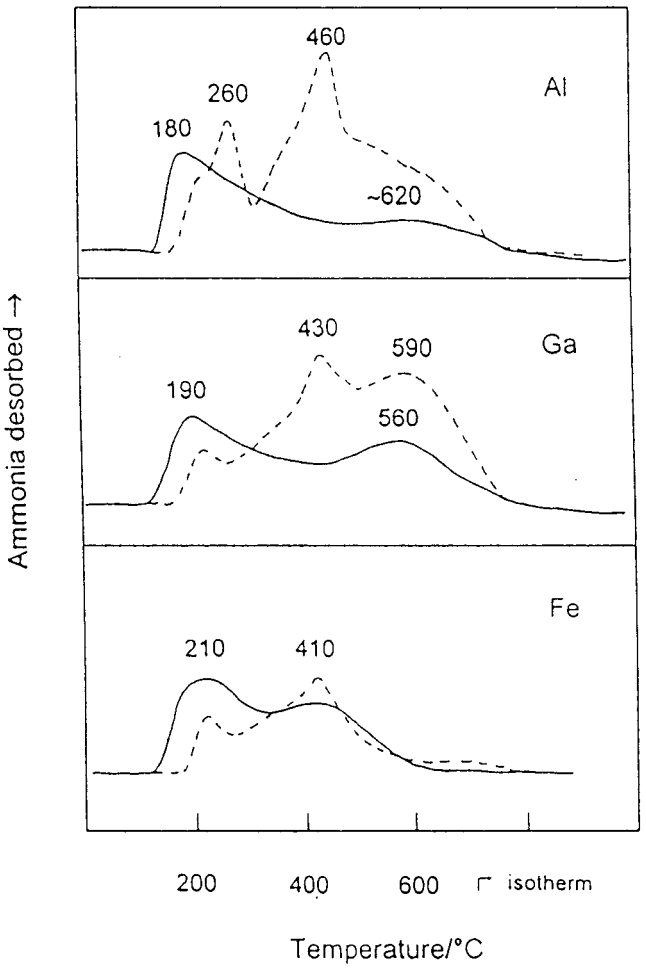

Figure 71. TPD of ammonia from Al-MCM-48, Ga-MCM-48, and Fe-MCM-48. Decomposition of the NH_4-exchanged MCM-48 (- - -), and conventional desorption from ammonia-loaded H,MCM-48 (—). (Reprinted with permission from ref 400. Copyright 1998 Academic Press.)

medium−strong Brønsted sites desorbing at 310 °C, strong Brønsted sites desorbing at 380 °C, and a small number of very strong Lewis sites desorbing ammonia above 400 °C. Apparently all these types of sites are present in [Ga]-MCM-41 and [Ga]-MCM-48. The formation of acidic structural Si−(OH)−Al,-Ga groups is confirmed by IR spectroscopy. Stretching vibration bands of the acidic bridging hydroxyls appear at 3591 (Ga) and 3605 cm^{-1} (Al). The low-frequency shift after transition from Al to Ga gives additional evidence for the isomorphous substitution because it is in line with corresponding shifts observed with other types of molecular sieves (zeolites).

Microcalorimetry yields ca. 140 ([Ga]-MCM-48) and ca. 160 kJ/mol ([Ga]-MCM-41) for the initial heats of chemisorption of ammonia. These values confirm the presence of a small number of very strong sites in the substituted mesoporous molecular sieves.

3. Catalytic Properties

Experimental investigations of acid-catalyzed reactions using MCM-based catalysts are rare. Some reluctance is reasonable because above all the acid site characterization showed properties less favorable for catalytic exploitation: concentrations of acid sites

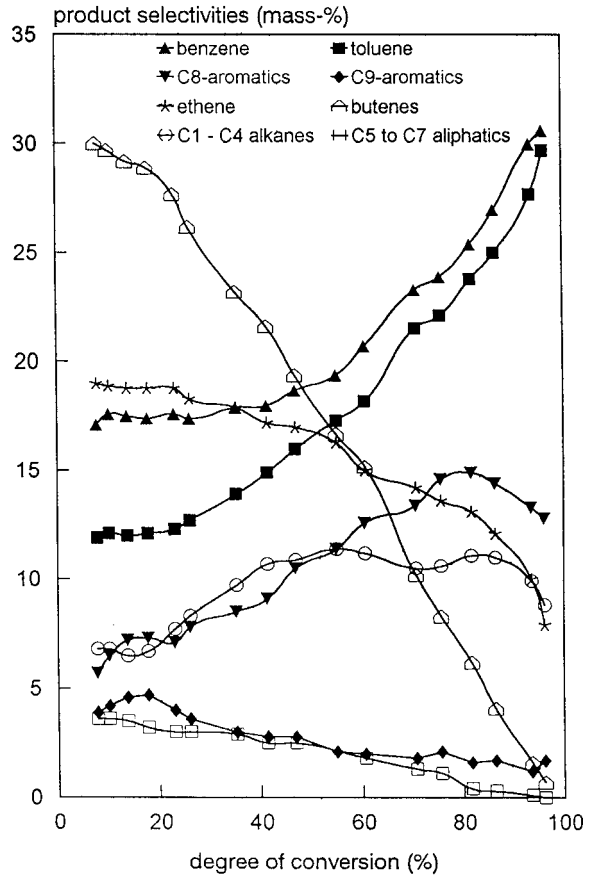

Figure 72. Aromatization of propene over Ga-MCM-41. Product selectivities vs propene conversion. Reaction conditions: temperature: 773 K, concentration of propene 5.0 vol %, catalyst weight: 1 g of Ga-MCM-41 bound with 2 g of Aerosil-200.[420]

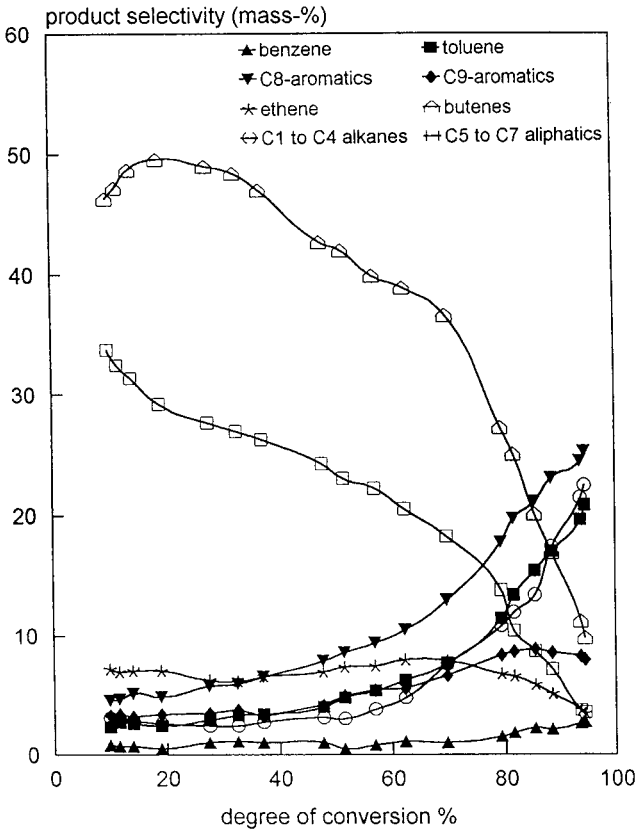

Figure 73. Aromatization of propene over Ga-MCM-41. Product selectivities vs propene conversion. Reaction conditions: temperature: 643 K, concentration of propene 5.04 vol %, catalyst weight 1 g of Ga-MCM-41 bound with 2 g of Aerosil-200.[420]

generated through substitution are low, acid strength are not really high, and the thermal stability of Brønsted acid sites is insufficient. Hence, little is known about catalytic properties of [Al]-MCM-41, and almost nothing is reported about Ga-substituted MCM materials. Some studies used MCM-41 as a catalyst support.[413−415] [Al]-MCM-41 was found to be active in the Friedel−Crafts alkylation of bulky aromatics with cinnamyl alcohol.[416] Alkali-containing MCM-41 was used in a base-catalyzed reaction.[417]

In the gas-phase conversion of acetone, however, Al-, Ga-, and Fe-substituted MCM materials showed a remarkable catalytic activity.[399,404] The activity decreases in the order [Al]-MCM > [Ga]-MCM > [Fe]-MCM, which parallels the decrease of strength and concentration of Brønsted acid sites. After an initial period, acetone is converted into isobutene with a high selectivity. Formation of isobutene is favored by an increasing acidity of the catalyst. Conversion of acetone proceeds via a two-path reaction mechanism.[418] In the temperature range from 643 to 773 K, [Ga]-MCM molecular sieves catalyze the formation of isobutene. A close similarity to [Al]-MCM-41 and -48, which have a higher isobutene selectivity, is observed. [Fe]-MCM-41 and -48 in turn clearly favor the second path of reaction, i.e., the formation of trimethylbenzenes and mesityl oxide. Catalysts exhibit a relatively high catalytic stability in nearly any case. Spent catalysts could be easily regenerated by thermal treatment in air at 500 °C. In any case, the coke could be rapidly burned off without residues. Resulting samples are white and catalytically active.

Like H-Ga-silicalite,[419] [Ga]-MCM-41 catalyzes the aromatization of propene.[420] As compared with [Al]-MCM-41, [Ga]-MCM-41 has a substantially higher stability during reaction. Less than 2% of the feed component is converted to higher boiling compounds and coke precursor products. Deactivation proceeds extremely slow. At 773 K, the total selectivity of aromatic compounds amounts to ca. 40% in the initial period of reaction (Figure 72). Simultaneously, butene and ethene are formed in considerable portions, perhaps via metathesis of propene. At later stages of the reaction (e.g., at a degree of conversion of 92.2%), aromatics achieve a total selectivity of ca. 75%. Formation of aromatic compounds is obviously enhanced by an increase of the temperature. At 643 K, the selectivity of aromatics is definitely lower. Then the formation of aliphatic intermediates (C_5−C_7) is favored (Figure 73).[420] Moreover, Brønsted acidity of Ga-substituted MCM-41 and -48 is sufficient to achieve cumene cracking[401] (Figure 74) and *n*-hexane conversion[421] (Figure 75).

In summary, it can be stated that the incorporation of metal components into the SiO_2 structure of MCM-41 gives rise to the formation of acid materials which are principally suitable for catalytic exploitation, although much still has to be done for a further improvement of their properties.

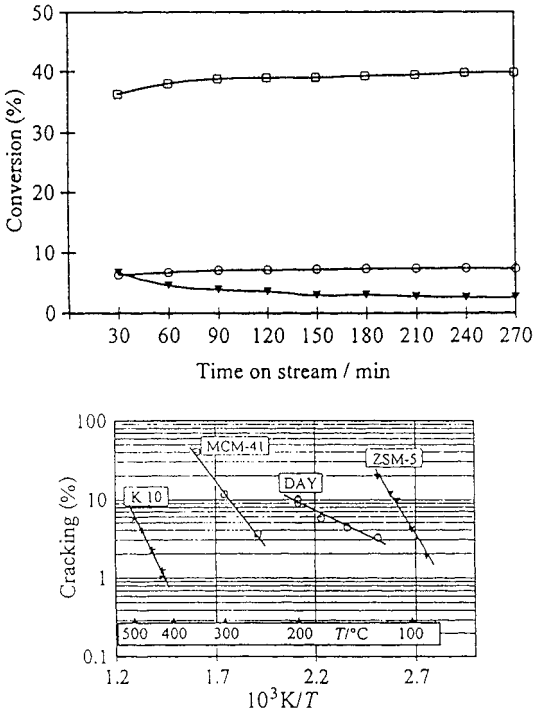

Figure 74. Catalytic activity in the cumene cracking/dehydrogenation at 375 °C over time-on-stream: (top) (□) Al-substituted, (○) Ga-substituted, and (▼) Fe-substituted H,MCM-48; (bottom) H,Al-MCM-41 as compared with two acidic zeolites ZSM-5 (Si/Al = 18) and DAY (Si/Al = 95), and a commercial cracking catalyst K10 (acidified montmorillonite Si/Al = 14, Südchemie). (Reprinted with permission from ref 401. Copyright 1998 The Royal Society of Chemistry.)

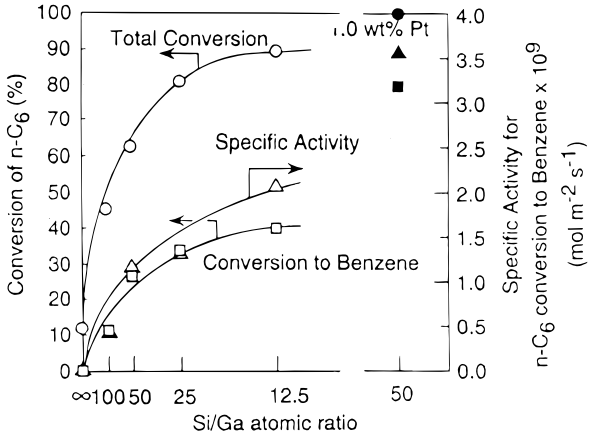

Figure 75. Conversion of *n*-hexane (left) and specific activity to benzene formation (right) for Ga-MCM-41 (open symbols) and Pt-loaded Ga-MCM-41 (Si/Ga = 50) (filled symbols) depending on the Si/Ga atomic ratio: Catalyst weight 300 mg, 15% *n*-hexane in He, flow rate 10 mL/min, reaction temperature 550 °C, time on stream 60 min. (Reprinted with permission from ref 421. Copyright 1998 Academic Press.)

F. Gallophosphates

Gallophosphates containing a porous framework structure were first prepared by Parise.[422] Since then, further structures have been synthesized, some of them structurally similar or identical with aluminosilicates or aluminophosphates; others are completely new. A survey has been given by Schott−Darie et al.[423] emphasizing the structure-directing effect of the template molecules. The following types are mentioned: $GaPO_4$-21, $GaPO_4$-34, ULM-1, ULM-2, ULM-5, LTA, cloverite, and several new gallophosphate phases.[424]

Two examples will be described briefly, i.e., $GaPO_4$-LTA which is structurally identical with the zeolite A (LTA) and $GaPO_4$-cloverite having a unique structure without any zeolitic analogue. The synthesis of both types is typically based on the following gel composition[423] $zR{:}1Ga_2O_3{:}1P_2O_5{:}xHF{:}yH_2O$ with $x = 0.2-2.0$, $y = 40-300$, $z = 1-6$, and R denoting the template molecule.

Another synthesis method starts from a nonaqueous gel with an alcohol (usually ethylene glycol) substituting water.[425]

As with other molecular sieves, the kinetics of crystallization and the kind of product depend on the gel composition and the chemicals used. The presence of a fluoride-containing compound is of primary importance (in nearly all cases HF is used). F^- obviously has a mineralizing function. The temperature and time of crystallization in the range of 80−220 °C may strongly vary between minutes or weeks (microwave crystallization).

1. $GaPO_4$-LTA

The gallophosphate LTA is isostructural with the well-known aluminosilicate. Except for the use of di-*n*-propylamine as organic template, conditions were comparable to the cloverite synthesis. Conditions of synthesis and physicochemical characterization are described in detail by Reinert et al.[426] The crystal structure was determined by Rietveld refinement.[427] No application is known up to now.

2. $GaPO_4$-Cloverite

Cloverite crystallizes in the presence of quinuclidine as template.[428] It seems to be one of the most interesting structures as it contains large cavities with a diameter of 30 Å at the crossing points of a three-dimensional system of super-wide pores with diameters of approximately 13 Å. (Figure 76). It is, therefore, one of the most open structures already acting as a link to the mesoporous materials.[18]

Cloverite has a complex interrupted framework built of double four-rings (D4R) with alternating Ga and P atoms. The D4Rs form α- and rpa-cages and contain a F^- ion in its center (counterion quinuclidine-H^+ in the "as-synthesized" form). In "as-synthesized" cloverite, Ga is pentahedrally coordinated whereas P is tetrahedrally coordinated. Two nonintersecting three-dimensional pore systems exist. The large pore system consists of supercages with a diagonal diameter of 2.9 nm forming four of the largest cavities known so far for molecular sieves. The large windows consist of 20-membered rings (free diameter = 1.32 nm) showing the shape of a cloverleaf. This unusual shape of the window is caused by terminal OH groups (attached to one type of D4Rs) reaching into the window. The small pore system (eight-membered rings, free diameter ~ 0.4 nm) runs through the α- and rpa-type cages.

The acidic properties of the cloverite material are controversially discussed.[429] Bedard et al.[430] assigned

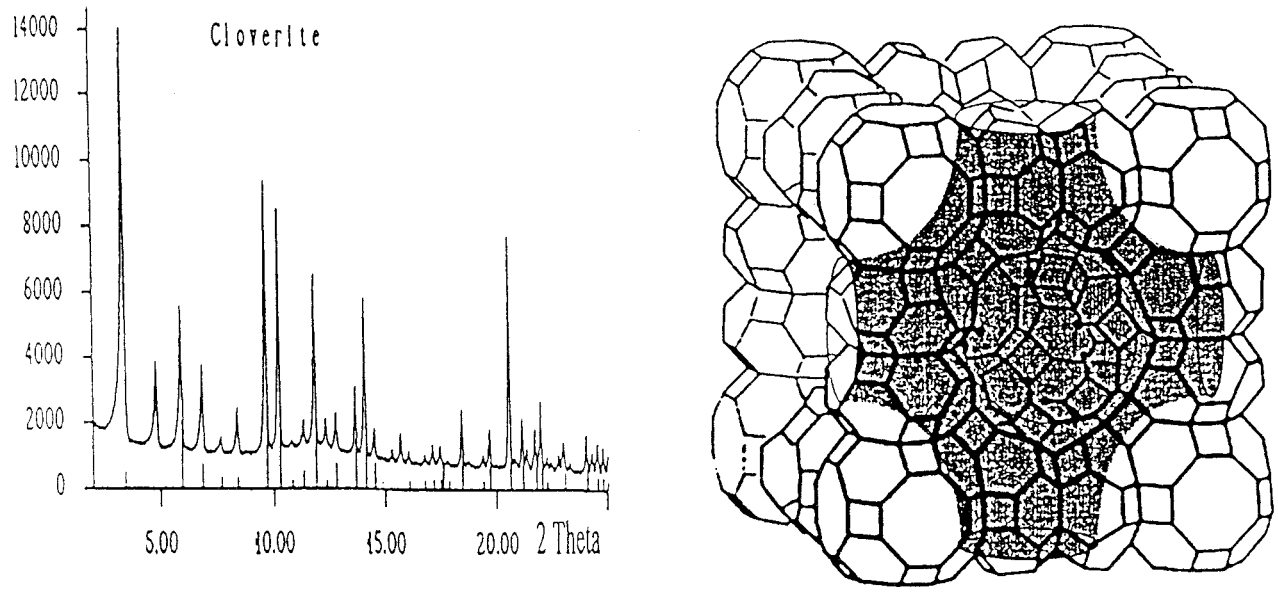

Figure 76. XRD pattern (left) and framework structure of cloverite (right). Open volume is shadowed. (Reprinted with permission from ref 428. Copyright 1997 American Ceramic Society.)

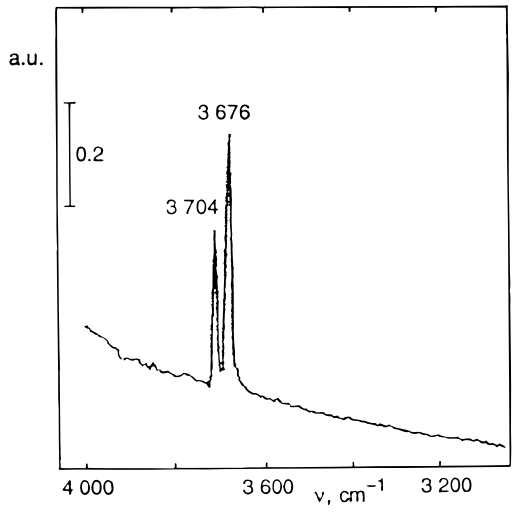

Figure 77. IR spectrum (OH vibration region) of Ti-cloverite showing the presence of acidic POH groups vibrating at 3676 cm^{-1}. (Reprinted with permission from ref 429. Copyright 1995 Academy of Sciences of the Czech Republic.)

a sharp OH vibration at 3676 cm^{-1} to P−OH and a broad absorption band at 3163 cm^{-1} to Ga−OH hydroxyl groups. This band was insensitive to acid−base titration by NH_3 and HCl. It was, therefore, assigned to nonpolar hydroxy groups located at interrupted Ga−O−P framework bridges.[431] By contrast, Barr et al.[167] reported that the molecular sieve cloverite revealed strong acidity after activation at 530 °C. Sharp OH vibration bands are found in the IR spectrum at ca. 3700 and 3670 cm^{-1} (Figure 77). They are assigned to two kinds of P−OH groups; benzene adsorption evidenced that those characterized by the 3670 cm^{-1} band corresponded to Brønsted acidic sites. With cloverite activated at 450 °C, Janin et al.[432] observed three OH bands at 3700, 3673, and 944 cm^{-1}. The bands at 3673 and 944 cm^{-1} are assigned to the stretching and bending modes of terminal P−OH groups, respectively. Barr et al. attributed the band at 3700 cm^{-1} to terminal Ga−OH groups.

The use of CO and C_2H_4 as probe molecules allowed a classification of the terminal hydroxyl groups with regard to their acid character. Accordingly, P−OH groups should be of medium Brønsted acidity ($H_0 = -6$) and Ga−OH groups exhibit weak acidity ($H_0 = -3$). According to Müller et al.,[433] structural Ga−(OH)−Si groups are strong Brønsted acid sites. One reason for the ambiguity in the classification of cloverite hydroxyls might be caused by a partial opening of the Ga−O bond next to the structural hydroxyl groups by adsorbed polar molecules. This way, the acidity characteristics of the material are modified. A concerted interaction of Brønsted (Ga−OH) and Lewis (Ga ion) adsorption sites with probe molecules is reported.[433] Changes induced by the interaction with polar molecules influence the catalytic properties. The interaction of methanol with cloverite as studied by FTIR spectroscopy revealed different surface species. While weakly hydrogen-bound molecules interacting with the P−OH groups are desorbed unreacted at 25 °C, the molecules sorbed at the Ga−OH groups react either to dimethyl ether (characteristic of Brønsted acid sites) or to formaldehyde (characteristic of Lewis acid sites). Another aspect is stressed by Richter et al.,[434,435] who first studied the catalytic properties of the gallophosphate cloverite under flow conditions. They observed that the cloverite material after in situ template decomposition shows a good performance for the etherification of alcohols by isobutene to asymmetric ethers. This ability points to the existence of strong acid sites, similar to other zeolites exhibiting strong protonic acidity. Analysis of the cloverite after template removal and after catalysis proved the presence of residual fluoride in any case (hydrogen fluoride is an imperative ingredient of the synthesis recipe). Residual fluoride apparently intensifies the acidic properties, thus promoting etherification at low reac-

tion temperatures. According to the proposed structure of cloverite after synthesis, F^- ions should be located in the four-ring subunits where they act as counterions for the quinuclidine cations. After detemplation, the residual fluoride ions could modify the acidity of adjacent hydroxyl groups. No direct evidence for this assumption, however, could be provided.

The stability of the cloverite structure was found to be strongly dependent on the coordination of the Ga ions. While the microporous structure is stable if the structural rearrangement of the Ga ions is confined to a 5-fold (as it occurs in the as-synthesized form or after sorption of larger polar molecules) or a 4-fold (activated form, in inert atmosphere) coordination, it collapses upon sorption of small polar molecules which force the Ga ion in an octahedral (6-fold) coordination. This happens, for example, with sufficiently high concentrations of water at 25 °C or with ammonia at elevated temperatures.

It could be shown[434,435] that cloverite, following the appropriate decomposition of the quinuclidine template in situ, catalyzes the gas-phase etherification of isobutene by methanol or ethanol to the corresponding methyl *tert*-butyl ether (MTBE) or ethyl *tert*-butyl ether (ETBE), respectively (atmospheric flow conditions in the temperature range from 70 to 130 °C). An additional etherification of primarily formed diisobutene by ethanol occurs yielding the C_{10} asymmetric ether, 2,4,4-trimethyl-2-ethoxy pentane. This reaction is not relevant for medium pore zeolites but can obviously proceed on cloverite owing to its large cavity size.

3. Other Gallophosphates

Recently, the synthesis of gallophosphates in the system $Ga_2O_3 \cdot {}_2O_5 \cdot HF \cdot H_2O \cdot (Cp_2Co)^+$ has been studied by Kallus et al.,[436] who obtained a novel type of gallophosphate (Mu-1) consisting of bis(cyclopentadienyl)cobalt(III) cations $(Cp_2Co)^+$ and $Ga_4P_4O_{12}(OH)_8$ double-4-ring units hosting F^- anions.

The gallophosphate structure Mu-1 was obtained by hydrothermal synthesis at 110−170 °C applying a modified version of the procedure developed by the authors themselves[437] in which fluoride anions are used as mineralizing agents.

A representative synthesis is described as follows. The starting mixture is prepared by addition of the gallium source to H_3PO_4. After mixing, cobaltocenium hexafluorophosphate and hydrofluoric acid are added successively. Finally, the pH is adjusted with tripropylamine. With 40% HF and an initial pH value of 6.5, pure Mu-1 is synthesized after 4 days at 403 K in an autoclave. The cobaltocenium cations (two per unit cell) balance the negative charge of the fluoride anions. The material is thus viewed as a salt. The thermal stability of the product was found to be poor because the structure collapsed after heating to 473 K.

The preparation and crystal structure of TREN−$GaPO_4$ by combined use of two amines, tris(2-aminoethylamine (TREN) and pyridine, has been reported recently.[424] This microporous molecular sieve contains 12-ring and 8-ring channels. The gallium framework atoms are tetrahedrally, pentahedrally, and octahedrally coordinated with fluorine completing Ga coordination.

Gallophosphates of laumontite structure,[438] $GaPO_4$-ZON,[439] Ga-containing $AlPO_4$-11 (AEL structure type),[440] $CoGaPO_4$-5,[441] and mesoporous galloaluminophosphates[442] have been synthesized too.

VI. Catalytic Properties of Gallium-Substituted Zeolites

Although a vast variety of Ga-modified zeolites is known, catalytic application is confined predominantly to the medium pore ZSM-5-type zeolites. Catalysis over Ga-based zeolites focuses on alkylation, isomerization, and disproportionation of aromatics. These reactions have been investigated in detail to optimize product selectivities by utilizing the shape-selective properties of zeolites. Aromatization of low alkanes (Cyclar process) has gained a commercial breakthrough. Detailed studies have proved that aromatization properties, however, are not necessarily confined to gallium in framework positions but are influenced by nonframework Ga species as well. Generally, active catalysts can be obtained by impregnating or refluxing (ion exchange) of the zeolite with an aqueous solution of a gallium salt. Even mere mechanical mixtures of a zeolite and a gallium compound—after a suitable activation—yield active catalysts. Attempts to apply Ga-based zeolites in the methanol-to-gasoline and methanol-to-olefin processes for commercial purposes have been performed already in the 1980s. Results, however, could not compete with the ZSM-5 or SAPO-34 catalysts. A novel field of application of gallium-containing zeolites is seen in the removal of NO_x from engine exhaust gas streams in the presence of excess air, which cannot be accomplished by traditional three-way metal catalysts.

The one-step synthesis of phenol by catalytic hydroxylation of benzene with nitrous oxide was reported to proceed over Ga-ZSM-5.[443]

Catalytic applications of Ga-modified and gallium silicate analogues of known zeolite structures are summarized under various aspects.

A. Aromatization of Alkanes/Alkenes

The aromatization of liquefied petroleum gas (LPG) alkanes into aromatic components (mainly benzene, toluene, and xylenes, BTX) on Ga-modified ZSM-5 catalysts is commercialized in the Cyclar process jointly developed by UOP and BP.[444−446] The process uses a catalyst formulation described as "a gallium-doped zeolite catalyst the hole shape of which is an ideal former for the aromatic ring".[447,448] The preparation route virtually consists of impregnating the zeolite component (ZSM-5) with a gallium salt solution by refluxing. This technique does not allow the large hydrated Ga^{3+} cations to pass the pore system of medium size zeolites such as ZSM-5 and to enter framework positions (except a minority healing lattice defects by incorporation). Thus, it can be assumed that the degree of ion exchange occurring during refluxing is low. After calcination, the gallium

Table 17. Aromatization of Hydrocarbons over Ga-Containing Catalysts

Reactants and conditions	Catalyst formulation: Ga-source	Applied Zeolite	Preparation	Pretreatment	Main results	Ref.
Natural gas 773-873 K, 73.6 wt.-% CH_4, remainder C_{2+}, flow reactor SV: 3000 cm^3/g h	Ga nitrate	(i) synthesized (ii) NH_4-ZSM-5 (iii) synthesized in the presence of Al	(i) MFI gallosilicate, Si/Ga = 30.1 (ii) Impregnation (iii) MFI galloaluminosilicate (Si/Al = 37.5, Si/Ga = 24.3)	Calcination in air at 873 K for 1 h	Performance decreases in the order: MFI galloaluminosilicate > MFI gallosilicate > Ga impregnated ZSM-5 Selectivity to aromatics ca. 90% at 873 K	488, 489, 490
Ethane 823 - 973 K, 80 kPa, flow reactor	(i) Ga nitrate (ii) Ga_2O_3	H-ZSM-5 Si/Al = 15, 25, 34, 50, 75, 95	(i) a) Ion exchange, 1.5 wt.-% Ga b) Incipient wetness, 1.5, 2.9, 3.1, 5.8 wt.-% Ga (ii) Mechanical mixing, 3.1 wt.-% Ga	Calcination in air at 858 K, 13-15 h	Preparation method has no influence on activity and selectivity	486
Ethane 803 - 843 K, 12 kPa in He, WHSV = 1 h^{-1}	(i) Ga nitrate (ii) β-Ga_2O_3	H-ZSM-5 Si/Al = 80	(i) Ion exchange, 2.22 wt.-% Ga (ii) Ball milling 3h, 5.17 wt.-% Ga	Reductive heating in flowing He to 773 K, in situ pretreatment at max. 848 K	No substantial influence of preparation mode on the catalytic properties. Optimum catalysts by reduction with hydrogen and reoxidation of reduced Ga to Ga^{3+}	196
Propane 750 - 840 K, pure feed 1 bar	Ga nitrate	H-ZSM-5 Si/Al = 18; 128	Ion exchange 1.6 wt.-% Ga	Stepwise calcination at 673, 723, 773, 823 K	Surface enrichment of Ga, migration of Ga during regeneration, maximum activity and selectivity to aromatics at the highest content of nonframework Ga species.	487
Propane 623 - 873 K WHSV = 2 h^{-1}	(i) Ga_2O_3	(i) synthesized (ii) H-ZSM-5	(i) Synthesis of MFI gallosilicate Si/Ga = 30, 45, 60 (ii) Mechanical mixing	Calcination in air at 823 K (3 h)	Dispersed Ga (framework or nonframework) possesses dehydrogenation activity	462
Propane, 773 K, 8 - 110 kPa	Ga nitrate	(i) synthesized (ii) MFI Ga-silicate Si/Ga = 45 (iii) H-ZSM-5	(i) Synthesis of MFI gallosilicate, Si/Ga = 45 (ii) Wet impregnation (1 wt.-% Ga) (iii) Wet impregnation	(i) Template decomposition at 823 K in air. (ii) Steaming at 823 K for 2.5 h under a flow of	Reaction order for propane: 1 (H-ZSM-5, gallosilicate), 0.7 (steamed gallosilicate), 0.65 (Ga-impregnated H-ZSM-5), 0.55 (Ga impregnated gallosilicate). Activity sequence:	471

		Si/Al = 15	(0.6 wt.-% Ga)	N_2 and H_2 (10 kPa). (iii) Redox cycles at 773 K	Ga-impregnated H-ZSM-5 > steamed gallosilicate > pure H-ZSM-5 > Ga-impregnated gallosilicate > gallosilicate.	
Propane, 800 K, WHSV = 3 - 8600 h^{-1}	Ga chloride	H-ZSM-5, Pt/H-ZSM-5	CVD (0.7, 1.88 and 1.36 % Ga)	Calcination at 773 K after sublimation (2 h)	Dehydrogenation activity after metal addition (Ga<Pt/Ga<Pt), no synergetic effects.	458
Propane, 823 K, 101 kPa	Ga nitrate	(i) synthesized	(a) Synthesis of galloaluminosilicate in the presence of Al and TBABr.	not specified	(a) Galloaluminosilicate with 1.5 wt.-% Al_2O_3 and 2.5 wt.-% Ga_2O_3 had the highest activity and aromatic yield.	552
			(b) Synthesis of MFI gallosilicate		(b) Activity increases with increasing Ga content	
		(ii) H-ZSM-5 Si/Al = 50, 140	Impregnation	not specified	Performance better than that of the gallosilicate (at comparable Ga contents).	
Propane, 873 K, WHSV = 4.7 h^{-1}	Ga nitrate	USY	Ion exchange (5.6 wt.-% Ga)	Calcination at 823 K	Propane activation is modified from cracking to dehydrogenation in the presence of Ga^{3+}	451, 553
Propane, 873 K	β-Ga_2O_3	H-ZSM-5 Si/Al = 70.	Mechanical mixing 10 wt.-% Ga_2O_3		Active sites are present immediately after preparation, sites are formed reversibly.	451, 464
Propane, 750 - 850 K, 14 kPa, WHSV = 1 h^{-1}	β-Ga_2O_3		Ball milling, 3 h (2,5,10 wt.-% Ga), RSSIE	T-programmed calcination in He or He/H_2, final temp. 848 K	Acidity of the zeolite and reduction by hydrogen are necessary to generate high activity.	454
Propane, 573 - 923 K, 20.2 kPa WHSV = 2000 h^{-1}	Ga sulfate	(i) synthesized	MFI gallosilicates (Si/Ga = 40, 25, 21, 15).	Calcination in air at 623 K, reduction by H_2 (20%) at 673 K	At Si/Ga = 15 ca. 85 % C_3H_8 conversion and ca. 70 % aromatics Performance declined at lower Ga contents. Pt promotes conversion of propane to ethane. Pt retards deactivation.	449
			Impregnation with $Pt(NH_3)_4Cl_2$, 0.5 wt.-% Pt			
		(ii) H-ZSM-5 Si/Al = 40	Ion exchange	Calcination in air at 623 K, reduction by H_2 (20%) at 673 K	At Si/Ga = 40, performance with the ion-exchanged sample better than with Ga-silicate.	449
Propane,	Ga nitrate	synthesized	Gallosilicates	Calcination	Comparison with [Al]-ZSM-5 (Si/Al = 30).	480

Table 17 (Continued)

Reactants and conditions	Catalyst formulation: Ga-source	Applied Zeolite	Preparation	Pretreatment	Main results	Ref.
803 K, 1 bar, WHSV = 2 - 80 h^{-1}			(Si/Ga = 30, 50, 180)	at 803 K (12 h)	Treatment of Ga-silicates at 997-1073 K in dry air enhances activity (formation of nonframework Ga species), Ga-silicate is less active than [Al]-ZSM-5	
Propane, 803 K, 50.5 kPa, WHSV = 456 h^{-1}	Ga chloride	H-ZSM-5 Si/Al = 20.5	Chemical vapor deposition, (0.77, 1.36, 2.95, 2.97, 3.70, 3.76 wt.-% Ga)	T-progr. Heating up to 773 K, *in situ* reduction with H_2 at 853 K (2 h)	Activity and selectivity to aromatics pass through a maximum in dependence on the degree of H^+ replacement by GaO^+, bifunctional mechanism.	152
Propane, 773 K, 101 kPa, WHSV = 5 - 628 h^{-1}	Ga nitrate	H-ZSM-5 and Na-H-ZSM-5 Si/Al = 15	Incipient wetness, 5 wt.-% Ga	Calcination in situ at 773 K under flowing oxygen	Gallium alkoxide intermediates (Ga_2O_3/H-ZSM-5), C_3H_7 carbenium ions over ZSM-5, dissociative adsorption of propane over Ga_2O_3, Na form less active.	459
Propane, 803 K, 101 kPa	not specified	synthesized	Alkali-free synthesized MFI gallosilicate (Si/Ga = 72.8)	(i) Calcination at 803 and 1023 K, (ii) Impregnation with 1 wt.-% Ga	Degalliation leads to a bifunctional x Ga_2O_3/ H-[Ga_y]-ZSM-5 catalyst (2x + y = 1.3) after high-temperature calcination wi h high activity.	554, 557
Propane in situ vacuum MAS NMR, 573 - 793 K	Ga nitrate	NH_4-ZSM-5, (Si/Al = 18, 128)	Impregnation, 1.6 wt.-% Ga	Calcination in air at 823 K overnight	Protonated cyclopropane intermediates, bifunctional configuration with $Ga^{3+}O^{2-}$ pairs and Brønsted acid sites	465
Propane, 823 K	Ga nitrate	NH_4-ZSM-5, (Si/Al = 88)	Impregnation, 1.5 wt.-% Ga	(i) Calcination in air at 573 K and 798 K (ii) Reduction with H^2 at 798 K (3 h)	Dispersion, mobility and valence state of Ga species determine activity.	555
Propane, 803 K, 101 kPa,	Ga nitrate	H-ZSM-5, (Si/Al = 23, 40, 140)	Ion exchange at 373 K (2.7, 3.1, 2.8 wt.-% Ga)	at 823 K (i) air (12 h), N_2 (0.5 h),	Brønsted acid centers serve as docking sites for migrating Ga_2O species.	200

flow reactor, WHSV = 2.3 h^{-1}				(ii) H_2 (12 h), N_2 (0.5 h),		
Propane, 773 - 823 K	Ga nitrate	H-ZSM-5, Si/Al = 15 and 30	Incipient wetness, 0.5 and 5.0 wt.-% Ga	Reductive and oxidative *in situ* treatment at 773 K	Effect of pretreatment depends on the Ga content. Pre-reduction improves performance at low Ga conc. but deteriorates activity at 5 wt.-% Ga.	556
Propane, flow reactor, 773 K WHSV = 12.2 h^{-1}	Ga nitrate	NH_4-ZSM-5, Si/Al = 124	Ion exchange under refluxing conditions	Calcination at 853 K (1.5 h), 4.1 wt.-% Ga_2O_3	No direct role of Ga species in propane activation, but transformation of intermediate products into aromatics.	
Propane 753 - 823 K, (i) normal pressure, WHSV = 1.8 h^{-1} (ii) 180 - 800 kPa (pilot plant) WHSV = 6.6 h^{-1}	not specified	ZSM-5, Si/Al not specified	ion exchange	not specified	E_a = 81.4 kJ/mole (microreactor) and 86.9 kJ/mole (pilot plant). Increased pressure leads to lower selectivity of BTX aromatics. Kinetic data fitted by an irreversible first order reaction	559
Propane, propene 803 K, 101 kPa, flow reactor	Ga nitrate	H-ZSM-5	Ion exchange under refluxing conditions, 2, 4, 6 wt.-% Ga	Calcination under a flow of dry nitrogen (10 h) at 803 K	Ga species have dehydrogenating activity, bifunctional mechanism, propene conversion >> propane conversion, product distribution different.	479, 560
Propane, 623 - 873 K, flow reactor, feed rate $1.2x10^{-5}$ mole/g s	Ga sulfate	synthesized	(i) MFI gallosilicate, Si/Ga = 30 (ii) Impregnation with Ga nitrate (1.5 wt.-% Ga)	Calcination in air at 720 K	Activity: 1.5 wt.-% Ga/H-ZSM-5 > H-ZSM-5 » 1.5 wt.-% Ga/Ga-silicate > Ga-silicate, Aromatic yield: 1.5 wt.-% Ga/H-ZSM-5 > 1.5 wt.-% Ga/Ga-silicate » H-ZSM-5 > Ga-silicate, Catalyst activity is attributed to Lewis acidity.	132
	Ga nitrate	H-ZSM-5 Si/Al = 23	Impregnation (1.5 wt.-% Ga)	Calcination in air at 720 K		
Propane, 50.5 kPa in Ar, 803 K, flow reactor, WHSV = 20 h^{-1}	Ga chloride (solid)	NaH-ZSM5, Si/Al = 16, 0.6 wt.-% Na	Sublimation of physical mixtures, 1.47 wt.-% Ga	not specified	Conversion: Ga/H-ZSM-5 (sublimated) > Ga/H-ZSM-5 (impregnated) > H-ZSM-5, Selectivity to aromatics: same sequence as for propane conversion.	153
Propane,	(i) Ga nitrate,	H-ZSM-5,	(i) Ion exchange,	not specified	NO poisons acid sites reversibly, O_2 increases	491

Table 17 (Continued)

Reactants and conditions	Catalyst formulation: Ga-source	Applied Zeolite	Preparation	Pretreatment	Main results	Ref.
Propane, 873 K, WHSV = 4.7 h^{-1} co-feed: NO, O_2, H_2	(i) Ga nitrate, (ii) ß-Ga_2O_3	H-ZSM-5, Si/Al = 70 and 560	(i) Ion exchange, (ii) Mechanical mixing, various ratios (10-90%)	not specified	NO poisons acid sites reversibly, O_2 increases propane conversion, propene yield and deactivation rate, excess H_2 has little effect.	491
Propane, 873 K, WHSV = 2 h^{-1}	$(CH_3)_3Ga$	H-ZSM-5, Si/Al = 20, H-Y, Si/Al = 2.15	Galliation at 0°C, 3.5 wt.-% Ga	Prior to use dealumination by acid leaching	A typical Ga/ZSM-5 product pattern is obtained. Ga/H-Y not tested	140
Propane 823 K, flow reactor, SV = 3100 cm^3/gh	Ga nitrate	synthesized	MFI gallosilicates (Si/Ga=53)	binder admixture, alumina or kaolin, 10 or 50 wt.-%	Binder addition modifies selectivities and coking but not the aromatization activity.	492, 493
Propene, 803 K, 1 bar, WHSV = 2 - 80 h^{-1}	Ga nitrate	synthesized	MFI gallosilicates (Si/Ga=30)	Calcination at 803 K (12 h)	Comparison with [Al]-ZSM-5 (Si/Al = 30). Rate ca. 50 times (ZSM-5) and 350 times (Ga-MFI) greater than for propane, product distribution nearly identical for both samples.	494
Propene, pure, 673 - 823 K, GHSV = 1000 h^{-1}	not specified	synthesized	MFI Gallosilicates (Rapid Crystallization Method), Ga-content (as Ga_2O_3) 13.4 wt.-% at maximum. Pt modification	not specified	Selectivity to hydrocarbons increases up to 7 wt.-% Ga_2O_3. Product distribution on Pt-loaded sample (Si/Ga = 20) is different. Strong dehydrogenation properties of Ga.	419
Propene, 50.5 kPa, 803 K, WHSV = 456 h^{-1}	Ga chloride	ZSM-5, Si/Al = 20.5	CVD, (0.77, 1.36, 2.95, 2.97, 3.70, 3.76 wt.-% Ga)	T- programmed heating up to 773 K, in situ reduction with H_2 at 853 K (2 h)	Conversion of propene decreases in dependence on the degree of H^+ replacement by GaO^+, selectivity to aromatics passes through a maximum.	161
Propene, 773 K, Pulse microreactor	δ-Ga_2O_3	H-ZSM-5 and Na-H-ZSM-5	Mechanical mixing, (0.75-10 wt.-% Ga)	Calcination in H_2, N_2, air at 773 K, 2 h	Best results after pretreatment in H_2 at 773 K and at ca. 1 wt.-% Ga. H_2 reduction results in migration of Ga species.	141

Propene, 20 kPa, 773 K, W/F = 7.0 g h/mole	Ga nitrate	NH_4-ZSM-5, Si/Al = 78	Ion exchange under refluxing conditions	Calcination at 853 K for 90 min in situ, 4.1 wt.-% Ga_2O_3	Aromatization is enhanced in comp. With H-ZSM-5. Ga is effective for converting olefins into aromatics.	504, 506
Propene, 773 K, pulse reactor	δ-Ga_2O_3	H-ZSM-5 or Na-ZSM-5	Mechanical mixing, Ga content ca. 1 wt.-%	Calcination for 6 h in N_2 or H_2 at 773 K	Activity of H-ZSM-5 is enhanced by Ga_2O_3 admixture. Improvement of H_2 transfer abilities.	198
n-Butane 813 K, flow reactor, WHSV = 0.5 h^{-1}	Ga oxide supported on silica or alumina (impregnation with Ga nitrate)	H-ZSM-5 Si/Al = 19 - 71	Mechanical mixture, (80% zeolite) extruded with bentonite clay (7%), 3 wt.-% Ga oxide	Calcination "Hybrid catalysts"	Supported Ga co-catalyst considerably enhances the aromatization activity of ZSM-5 No solid state ion exchange of Ga into the zeolite under reaction conditions	561
n-Butane, 813 K, flow reactor, WHSV = 0.5 h^{-1}	Co-catalyst, Ga oxide supported on silica	ZSM-5 Si/Al = 36	Mechanical mixture, (80% zeolite) 16 wt.-% co-catalyst, extruded with 4 wt.-% bentonite clay	Reduction with hydrogen at 813 K for 3 h.	Contact transfer, Ga species are transferred from the co-catalyst to the external surface of the zeolite during reduction. Highly dispersed Ga improves performance.	562
n-Butane, 723 K, flow reactor, WHSV = 5.8 h^{-1}	Ga nitrate solution	H-ZSM-5 Si/Al = 99.6	Ion exchange, 1.5 wt.-% Ga	not specified	Presence of 5 mole-% O_2 enhances selectivity to aromatics (oxidative dehydroaromatization).	563
n-Butane, 0.5 - 100 kPa, 573 - 773 K, flow reactor, GHSV = 300 - 10.000 h^{-1}	(i) Ga nitrate (ii) Ga_2O_3, dissolved in NaOH (iii) Ga nitrate	(i) H-ZSM-5 Si/Al = 70-84 (ii) H-ZSM-5 Si/Al = 460 (iii) synthesized	(i) Ion exchange, impregnation (ii) galliation (iii) MFI gallosilicates, Si/Ga = 120 (iv) Pt modification of (i)-(iii), 0.5 wt.-%	Calcination (not specified)	Active sites involve Pt, Ga^+ and protonic centers, Pt and Ga synergy promotes aromatization selectivity.	504, 484, 564
n-Butane 12 kPa in He, 803 - 843 K, WHSV = 1 h^{-1}	Ga nitrate	H-ZSM-5, Si/Al = 30	(i) Refluxing for 24 h, washing, drying, 2.9 wt.-% Ga oxide (ii) evaporation of Ga nitrate solution, 4, 3, 2 wt.-% Ga oxide	(i), (ii) Calcination in air at 823 K (10 h)	No substantial influence of preparation mode.	226

Table 17 (Continued)

Reactants and conditions	Catalyst formulation: Ga-source	Applied Zeolite	Preparation	Pretreatment	Main results	Ref.
n-Butane, 753 K, WHSV = 2.5 - 17.2 h^{-1}	Ga oxide on silica (580 m^2/g), prepared by impregnation and calcination, 3.0 wt.-% Ga oxide	H-ZSM-5, Si/Al = 36	Mechanical mixing of zeolite (75 parts) and Ga co-catalyst (5 parts), extrusion with bentonite (20 parts), hybrid catalyst	not specified	Aromatization performance H-ZSM-5 < Ga/ZSM-5 (Cyclar-type) < hybrid catalyst, Activation energy equal to 100 kJ/mole on all catalysts, Pre-exponential factors: H-ZSM-5 < Ga/ZSM-5 (Cyclar-type) < hybrid catalyst.	457
n-Butane, 573 - 773 K, WHSV = 300 - 10 000 h^{-1}		Ga-silicate with ZSM-5 structure, Si/Ga = 120	Impregnation with $[Pt(NH_3)_4]Cl_2$	Calcination in air or hydrogen at 723 K	Increase of activity and selectivity by Pt impregnation.	482
iso-Butane, *iso*-Butene, 823 K, feed rate 6 - 12 mmole/g s	Ga nitrate	H-ZSM-5	Impregnation, 1.5 wt.-% Ga	Calcination (3 h) at 873 - 1273 K	Cracking: H-MFI > Ga-MFI > Zn-MFI. Dehydrogenation: Zn-MFI > Ga-MFI > H-MFI.	226
n-Pentane, 673 - 1073 K, flow reactor,	Ga nitrate	NH_4-ZSM-5, Si/Al = 58, 78, 210	Ion exchange under refluxing conditions, 24 h	Calcination at 853 K for 1.5 h in situ, 2.2, 4.1, 2.3 wt.-% Ga_2O_3	Aromatization is enhanced in comparison with H-ZSM-5. Cracking prevails at short contact times.	558
n-Pentane, 3.9 kPa, 693 - 763 K, flow reactor, WHSV = 1.8 h^{-1}	β-Ga_2O_3	H-ZSM-5, Si/Al = 50.8	Ball-milling, 2 wt.-% Ga	Calcination at 773 K in situ in air (4 h) or in H_2 (1.5 h)	Hydrogen reduction yields active catalyst. Cracking products predominate over H-ZSM-5.	565
n-Hexane, 773 K, flow reactor, WHSV = 2 or 4 h^{-1}	Ga nitrate	(i) NH_4-ZSM-5, Si/Al = 148	Impregnation, 0.8, 1.5, or 3.0 wt.-% Ga_2O_3 (a) NH_4 form heated at 813 K in dry air for 2h (b) H form by ion exchange with HCl, 3% Ga as Ga_2O_3	Calcination in dry air for 2 h at 873 K	Activity and Aromatics (i) > (ii) < (iii), Active Ga species are nonframework species. HCl removed nonframework species.	450

		(ii) synthesized	(c) as (b) but further ion exchange with Ga^{3+} (0.7 wt.-% as Ga_2O_3) MFI gallosilicates (0.2 or 0.1 wt.-% respect. Al_2O_3 present in the catalyst)			450
n-Hexane, 773 K, flow reactor, WHSV = 2 or 4 h^{-1}	Ga nitrate	NH_4-ZSM-5, Si/Al = 148	Ion exchange, 0.9 wt.-% Ga_2O_3	Calcination in dry air (2 h) at 813, 873, 933, 1053 K	Influence of pretreatment temperatures on *n*-hexane conversion is low. Selectivity to products increase for Ga-ZSM-5 (not for H-ZSM-5)	172
n-Hexane, 773 K, flow reactor, WHSV = 8.6 h^{-1}	not specified	synthesized	MFI gallosilicates, Si/Ga = 25, 50, 100	Calcination of the NH_4-form at 823 K (6 h)	Activity is related to crystallinity, i. e. framework Ga content. Synergy between Brønsted and Lewis acid sites (nonframework Ga)	156
n-Hexane, 500 kPa, 723 K, flow reactor	Ga nitrate	synthesized	MFI gallosilicates, Si/Ga = 0.4, 0.2, 0.1	Calcination at 773 K (1 h)	Activity Al > Ga > Fe, linear increase of activity with Me^{3+} content in framework positions.	566

species present in the catalysts prepared by impregnation or ion exchange are most likely Ga_2O_3 particles deposited at the external crystal surface or even forming a separate phase.

A compilation of alkane aromatization studies over Ga-containing catalysts is given in Table 17. It is evident that the application of true gallosilicates is not really numerous.

1. Catalyst Formulations

The overwhelming majority of catalyst preparations are similar to the Cyclar-type route introducing the gallium by impregnating/refluxing or by admixing Ga_2O_3 mechanically, with subsequent thermal activation/reduction. The introduction of gallium into zeolites enhances the dehydrogenation activity and increases the selectivity of aromatics. Location of gallium species at/near cation positions in the windows, channels, and cavities of the zeolite lattice gives a high degree of dispersion and an enhanced stability of dispersed species. Results published by Inui et al.[449] on the gas-phase aromatization of light alkanes give evidence that MFI-gallosilicates are more effective than Ga ion-exchanged H-ZSM-5. Due to degalliation occurring during reaction, [Ga]-ZSM-5, however, deactivates faster than Ga-modified [Al]-ZSM-5. Kanai and Kawata[450] reported that a [Ga]-ZSM-5 catalyst showed much higher activity for the aromatization of *n*-hexane than a Ga ion-exchanged ZSM-5 or a mechanical mixture of Ga_2O_3/H-ZSM-5. Further investigations including Al-free microporous gallosilicates are reported (Table 17) mainly for the aromatization of propane. Due to the great variety of gallium species present, the unequivocal assignment of catalytic properties to a single type of gallium site is not justified. Additionally, redistribution and redispersion of gallium species occur during catalyst pretreatment and even under reaction conditions. Thus, the state of Ga has to be characterized after the standard activation procedures or even after catalytic use. Appropriate physicochemical methods for differentiation between framework and nonframework Ga are available. Information on the stability of framework gallium is accessible from separate studies of the influence of thermal or hydrothermal treatments on the distribution of gallium in gallosilicate zeolite structures.

Wet impregnation techniques of H-MFI structures with gallium salt solutions guarantee a high gallium dispersion, but nevertheless, most of the gallium is found to be located outside the zeolite crystals as a separate phase.[143,144] It is known that the treatment of Ga-modified zeolites (ion-exchanged or impregnated) in a hydrogen-containing gas flow at elevated temperatures reduces the valence state of the gallium and increases its dispersion. Gallium species of lower valence are supposed to migrate much easier into the zeolite pores to exchange protons of Brønsted acid sites than the large hydrated Ga^{3+} ions.[451−452]

Joly et al.[143] found that a hydrogen activation treatment at 550 °C of Ga/H-ZSM-5 prepared by wet impregnation induces gallium migration from the gallium platelets located outside the zeolite into the zeolite micropores resulting in a highly dispersed gallium phase located close to the acid sites.

The migration of low-valent Ga species across phase boundaries is favored with aluminum-rich zeolites. Joly et al.[200] assumed that the acidic Brønsted sites act as docking sites for Ga_2O. The process of Ga dispersion would deactivate strong acidic zeolite sites and thereby modify the mechanism of alkane activation (see below). From reduction studies on Ga-exchanged ZSM-5 catalysts, Dooley et al.[196] concluded that the ion exchange in aqueous solutions is performed by $Ga(OH)_2^+$ ions. These ions are reducible to Ga^+ by hydrogen. As to the catalytic properties in the aromatization, reduced catalysts of this type are similar to reduced catalysts prepared from mechanical mixtures of ZSM-5 and Ga_2O_3.

With the aromatization of propane, Price and Kanazirev[454] observed very long induction periods (up to 24 h) for ball-milled β-Ga_2O_3/H-ZSM-5 catalysts. The authors ascribed this effect to the slow reduction process creating redispersed active Ga^+ species that migrate into the zeolite interior where a solid-state ion exchange occurs. Pretreatment of the freshly prepared catalyst with hydrogen at elevated temperatures was found to shorten the induction period and to increase activity. This kind of thermal pretreatment obviously anticipates reduction/redispersion of Ga species otherwise proceeding in the early stages of the catalytic reaction. Le van Mao and Yao[455] could not confirm the transfer of gallium species into the interior of the zeolite. They found that extruding a wet mixture of a Ga-loaded silica cocatalyst, [Al]-ZSM-5, with a bentonite binder yields a hybrid catalyst for the aromatization of *n*-butane which is superior to the Cyclar catalyst. In this catalyst, gallium is considered to be very far away from the zeolitic acid sites. But due to the high Ga dispersion of the cocatalyst, a more rapid on-stream reduction is observed and the induction period of the catalytic reaction is shortened. The hybrid catalyst with separated zeolite and gallium component exhibits a long-term stability.[147] Considering the magnitude of distances (several micrometers) to be bridged by migration of gallium between the cocatalyst and the zeolite, it seems reasonable to modify the concept of bifunctional configuration of active sites based on adjacent gallium species and acidic protons. With zeolite matrix embedded α-quartz samples, an increase of the amount of quartz causes higher conversions of *n*-butane and a higher production of aromatics and molecular hydrogen. It is assumed that the contact areas between the quartz particles and the zeolite crystals are the actual places of activity.[456,457]

Kwak and Sachtler[152,458] found that the chemical vapor deposition technique (CVD) to introduce Ga into H-ZSM-5 acts as a true ion exchange replacing protons by GaO^+ ions. Conversion of propane and selectivity to aromatics run through a maximum with changing degrees of replacement of H^+ by Ga^+. Optimum yields were achieved with catalysts having $Ga/(Ga + H^+)$ ratios between 0.4 and 0.5. This points to a bifunctional mechanism catalyzing oligomerization and ring closure by acid sites. Nonframework Ga, in concert with H^+, acts as dehydrogenating site. This is essentially identical to the conclusion drawn earlier by Meriaudeau and Naccache[459] from their

studies on the role of Ga_2O_3 and of Brønsted acidity on Ga_2O_3/H-ZSM-5 catalysts in the conversion of propane.

Bayense et al.[140] introduced gallium into H-ZSM-5 and H-Y zeolites by a postsynthesis treatment with trimethylgallium. A problem for the selective introduction of framework gallium into the zeolite structures is the undesired reaction of trimethylgallium with the silanol groups on the outer surface of the zeolite particles. Besides, reactions between trimethylgallium and Brønsted sites are observed. Both reactions give rise to nonframework gallium species. Aromatization of propane over Ga-modified ZSM-5 yielded the typical product pattern observed for Ga-containing ZSM-5 catalysts prepared by other preparation routes.

After close inspection of the available catalytic data, it is evident that the method of catalyst preparation is not decisive because the active catalyst is 'prepared' by the rather drastic activation procedures and eventually during reaction itself. Specifically, redispersion of Ga species is occurring, and upon reductive treatments at elevated temperatures, reduction of Ga species is observed. This kind of pretreatment is of importance for the catalytic performance of Ga-containing catalysts.

2. Alkane Activation

Suggestions and possibilities are sketched in detail for propane, the most widely applied alkane in aromatization studies in Figure 78.

Both a monofunctional and a bifunctional activation have been proposed. The monofunctional activation of alkanes by a direct protonation of C−C or C−H bonds requires superacidic sites and gives rise to carbonium ions which rearrange to carbenium ions. Theoretical analyses on the basis of aluminosilicate model clusters[460] indicate that the carbonium ion is a transition state stabilized by nearly covalent interactions of two of its hydrogen atoms with two negatively charged oxygens in the vicinity of the aluminum atom. The reaction coordinate can be identified from a vibrational frequency analysis.

Ab initio quantum-chemical calculations of protolytic cracking of ethane at Brønsted acid sites of high-silica zeolites have shown that adsorbed carbonium ions are the active intermediates in catalytic transformations of paraffins.[461] The occurrence of H_2 during reaction is one argument in favor of the carbonium ion formation, even over Ga-modified zeolites with lower acid strength.

In the case of propane aromatization, the attack of zeolitic protons produces intermediate $C_3H_9^+$ carbonium ions which rearrange into $C_3H_7^+$ and H_2 or $C_2H_5^+$ and CH_4. The carbenium ion intermediates $C_3H_7^+$ and $C_2H_5^+$ themselves can decompose into propylene and ethylene, respectively, releasing a proton.

Analyzing initial product selectivities, Kwak et al.[458] found that the addition of Ga to H-ZSM-5 has no essential effect on the rate of propane cracking (equimolar formation of methane and ethylene) but increases the dehydrogenation rate 7.7-fold ($T = 803$ K).

An initial and direct carbenium ion formation is considered by several authors.[460,462] Hydride-ion abstraction from the alkane requires Lewis acid sites and leads immediately to carbenium ions. Lewis acid sites are assumed to originate from broken Si−O−Ga bonds in the zeolite framework or from amorphous Ga_2O_3.

The possibility of a dissociative adsorption of H_2 over Ga_2O_3 is confirmed by IR results.[463] In the following steps of the reaction, H^- ions fixed at the Lewis acid recombine with the H^+ of the bridged hydroxyl to form molecular hydrogen. Fixation of the carbenium ion occurs at the O^- of the Brønsted site. The intermediate decomposes into the alkene and provides a H^+ to reestablish of Brønsted site.

The bifunctional activation pathway comprises the concerted action of acid sites of the framework and those located at nonframework gallium. In a bifunctional action, a Brønsted site may be assisted by a gallium site to dehydrogenate an incoming alkane. The interference of different types of sites can take place at various stages of the activation process, e.g., during the initial C−H bond scission (concerted action of acid sites and Ga-related sites), during the combination of protons with hydride ions to form molecular hydrogen, during the decomposition of alkyl intermediates bound to Ga-related sites, or during the promotion of reduction and redispersion of Ga species (cf. Figure 78).

Buckles et al.[464] suggested that nonframework gallium acts as an hydride-ion (H^-) acceptor in the initial activation of propane forming carbenium ions $C_3H_7^+$ which subsequently react with the Brønsted sites. It is assumed that a C−H bond of one of the methyl groups is polarized by Ga_2O_3 and that the C−H bond cleavage itself occurs at the Brønsted acid sites. Active sites for propene formation are located at the interface between the gallium phase and the zeolite. Meriaudeau and Naccache[442] accepted that Ga_2O_3 can initiate H^- abstraction from propane but claimed a 'spill over' of $C_3H_7^+$ carbenium ions to Brønsted acid sites as a necessary intermediate step.

Derouane et al.[465] proposed another method of low-temperature propane activation (at 573 K) by heterolytic dissociation at nonframework or ion-exchanged Ga species (Figure 79). In situ ^{13}C MAS NMR investigation of the early stages of propane activation over Ga-modified ZSM-5 point to the existence of a protonated pseudo-cyclopropane intermediate. Thus, the activation of propane is assumed to occur via a bifunctional action between $Ga^{3+}O_2^-$ pairs and Brønsted acid sites. Intermediates decompose into methane, ethene, ethane, and propene releasing H_2 simultaneously.[466]

Independent of the way of initial alkane activation, carbenium ions are the common intermediate involved at certain stages on any reaction routes.

With olefinic reactants, the formation of carbenium ions by an attack of a proton at the double bond is commonly accepted. Viruela−Martin et al.[244] published results of ab initio MO calculations for the protonation of propylene and isobutene by acidic OH groups of isomorphously substituted zeolites with B and Ga in T positions. Results show that the adsorp-

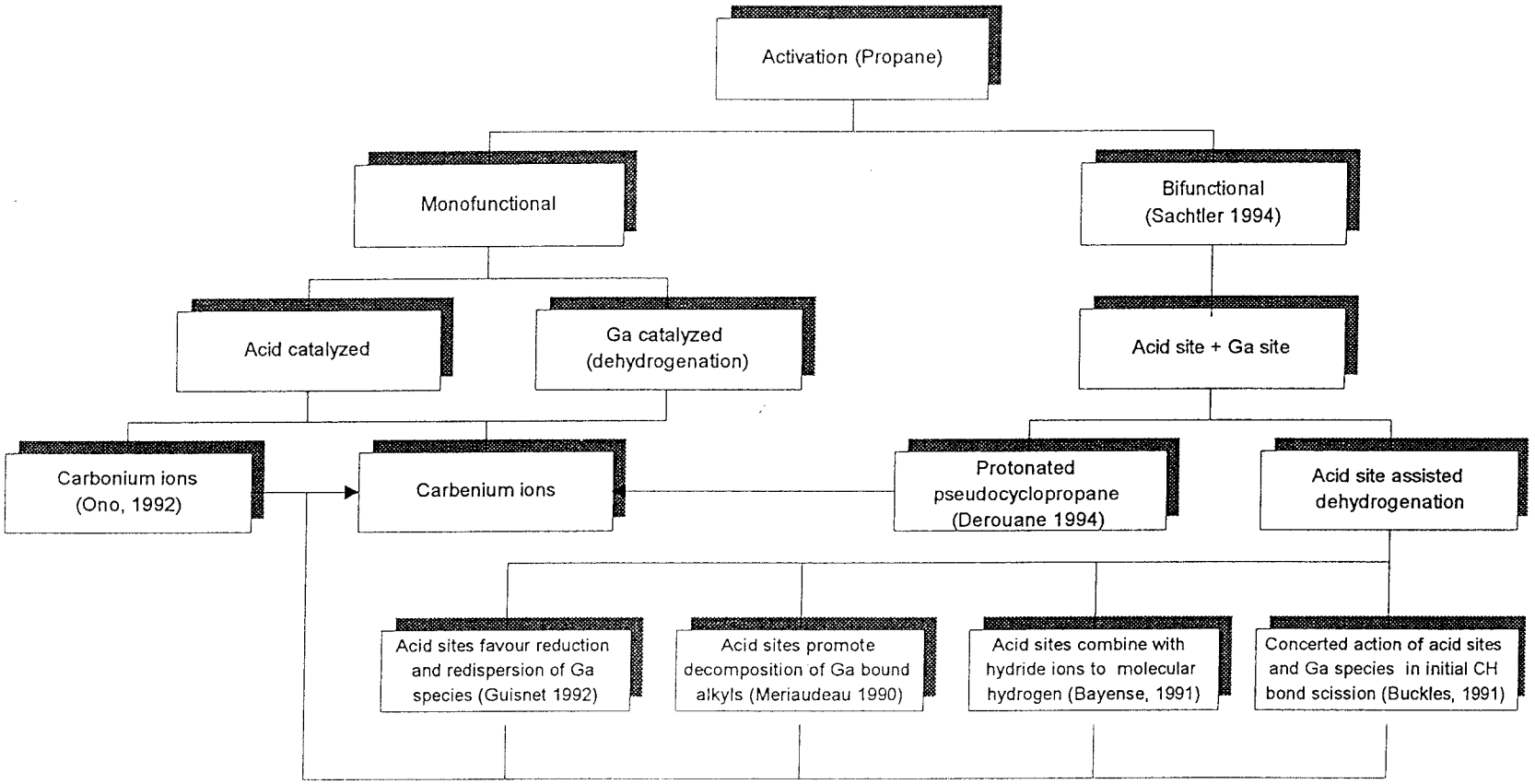

Figure 78. Possible reaction paths of the Ga-catalyzed transformation of alkanes (propane) to aromatics.

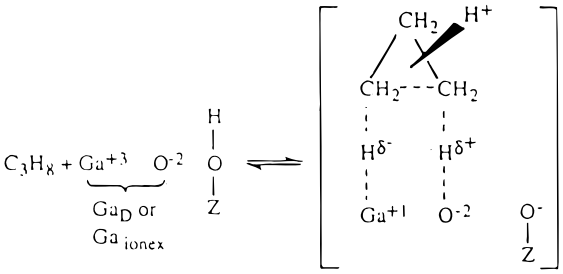

Figure 79. Scheme of the bifunctional activation of propane at Ga-containing H-MFI catalysts. Ga^{3+},O^{2-} ion pairs involve ion-exchanged gallium (Ga_{ionex}) and/or dispersed nonframework Ga species (Ga_D). Chemisorbed propane reduces Ga^{3+} to Ga^{+}. (Reprinted with permission from ref 465. Copyright 1994 Elsevier Science.)

tion of olefins takes place at acidic OH groups generating fairly stable zeolite−alkoxide structures with a covalent nature (via a π-complex). The further mechanism and the properties of the transition states are generally identical, irrespective of the framework T atoms. The authors concluded that the structure of the transition state can be more decisive for the mechanism than the chemical composition of the zeolite.

3. Reaction Course

Inui et al.[467,468] argued that gallium or zinc species have no dehydrogenation activity. Instead, the promoting effect of gallium is attributed to the 'reverse spill-over effect'. Hydrogen atoms at the zeolite surface migrate to reach gallium sites where they combine to hydrogen molecules which desorb subsequently into the gas phase. This effect is called 'back hydrogen spill-over', BHS. The existence of the BHS is supported by the positive influence of oxygen on the selectivity in the conversion of *n*-butane to aromatics over Ga-ZSM-5. Oxygen is assumed to remove surface hydrogen by oxidation, thus avoiding an inhibition of the reaction.

The presence of gaseous hydrogen has no effect on the conversion of *n*-butane and on product selectivities over H-ZSM-5, whereas in the case of Ga-ZSM-5, the selectivity to paraffins was enhanced at the expense of aromatics and C_2-C_4 olefins. Obviously, intermediate C_2-C_4 olefins are hydrogenated to a higher extent in the presence of gaseous H_2 than in the presence of N_2. H_2 adsorption at Ga-ZSM-5 was found to be faster and stronger as compared with the parent ZSM-5. This is explained by a spill-over of hydrogen after dissociative adsorption on Ga-related sites.

The reverse hydrogen spill-over is suggested to occur across particle boundaries. Basic support for this conclusion is provided from conversion−selectivity data of *n*-butane over a variety of Ga-containing catalysts (Table 18).[469] Catalysts prepared by intimate grinding of H-ZSM-5 with either Ga-impregnated Al_2O_3 (column 5) or Ga_2O_3 (column 6) are comparably as active and selective as Ga-impregnated ZSM-5. Ga-impregnated Al_2O_3 (column 4), however, has a minor activity in the aromatization of *n*-butane.

In summary, the slow hydrogen desorption rate is supposed to limit the progress of reaction to aromatics over H-ZSM-5 while the reverse hydrogen spill-

Table 18. Conversion and Product Distribution for the Aromatization of *n*-Butane over Various H-ZSM-5 Catalysts[469]

catalyst[a]	H−ZSM-5 (Si/Al = 50)	Ga−ZSM-5	Ga/Al_2O_3	H-ZSM-5 + Ga/Al_2O_3[b]	H-ZSM-5 + Ga_2O_3[c]
conversion (%)	41.6	47.9	0.7	47.7	52.4
H_2/converted *n*-butane (molar ratio)	0.3	1.4		1.3	1.2
		product distribution (C %)			
$C_1 + C_2$ paraffins	9.6	9.5	3.0	11.0	8.5
C_3H_8	58.6	52.5	3.5	51.7	55.1
iso-C_4H_{10}	3.7	3.5	0.0	3.2	7.1
C_2-C_4 olefins	16.3	10.0	88.1	13.0	9.5
C_5^+ aliphatics	3.0	2.5	0.5	1.7	2.3
aromatics	8.8	22.0	4.9	19.4	17.5

[a] Calcined in air at 500 °C for 3 h, reaction temperature 450 °C, feed 20 kPa of *n*-butane, 80 kPa of N_2, W/F = 10 g h/mol. [b] Content of Ga/Al_2O_3 = 20 wt %. [c] Content of Ga_2O_3 = 5 wt %.

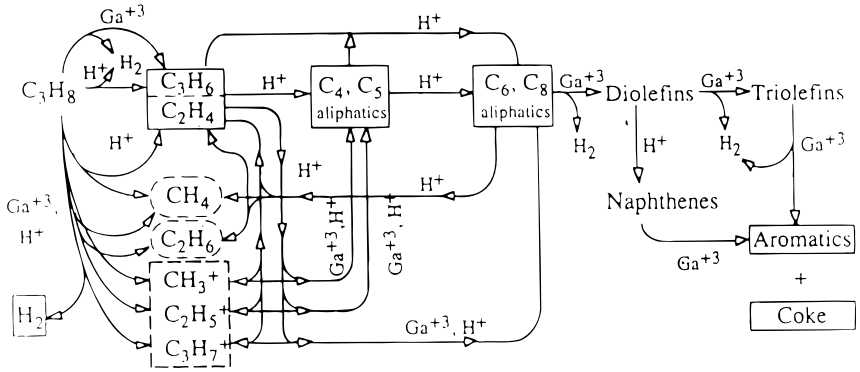

Figure 80. Overall mechanism for the aromatization of propane over Ga-containing H-ZSM-5 catalysts. (Reprinted with permission from ref 465. Copyright 1994 Elsevier Science.)

Table 19. Propane Transformation over Acid Solids (H-ZSM-5, Gallosilicates) and Ga-Loaded Zeolites[463] [a]

catalyst	H-ZSM-5	Ga/H-ZSM-5 (0.6 wt % Ga)	gallosilicate	Ga (1.0 wt %) impregnated gallosilicate	steamed gallosilicate
activity	10	100	0.4	5	27
S (propene)	25	78	29	75	79
S_{C_1} (methane)	25	7	24	8	7
S_{C_2} (ethylene)	50	14	47	16	13

[a] Reaction conditions: T = 500 °C. Feed: 8 kPa of C_3H_8, 0 kPa of H_2, diluted by N_2. Experimental conditions for steaming: T = 550 °C, $p(H_2O)$ = 25 kPa, duration = 2.5 h. Activities in relative units; the activity of 0.6 wt % Ga-H-ZSM-5 is set to 100%.

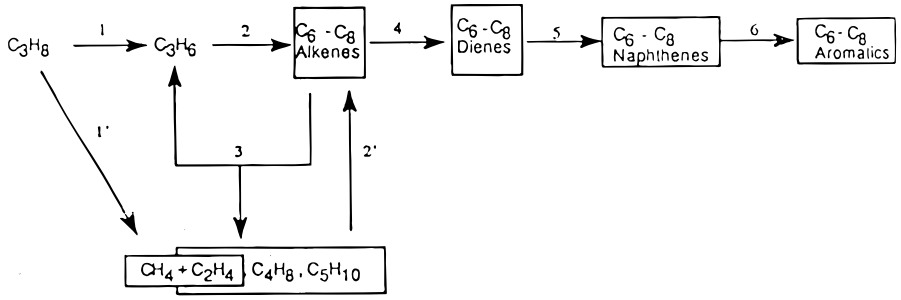

Figure 81. Reaction scheme of propane aromatization over H[Al]-ZSM-5 and H[Ga]-ZSM-5 catalysts. (Reprinted with permission from ref 472. Copyright 1994 Elsevier Science.)

over on Ga-ZSM-5 accelerates desorption of hydrogen, thus removing the kinetic bottleneck of aromatization. The adequacy of this BHS effect does not require a migration of Ga species, which, however, is shown to take place during reaction/regeneration or during reductive pretreatment procedures, especially in the presence of hydrogen.

A rather subtle overall mechanism of the propane aromatization over Ga-containing MFI zeolite catalysts (Figure 80) presented by Derouane et al.[465] gives different possible routes for the activation of alkane. (i) Dehydrogenation of propane to propene and transformation into $C_3H_7^+$ carbenium ions. This route implies the existence of various intermediate C_2-C_8 olefins. (ii) Direct activation with intermediate pseudoprotonated cyclopropane (cf. Figure 79) whose decomposition yields carbenium ions. C_6-C_8 aliphatics can be dehydrogenated at nonframework gallium sites forming diolefins and/or naphthenes by cyclization at protonic sites. Eventually, further dehydrogenation at gallium-related sites yields aromatics.

4. Kinetic Studies

Meriaudeau et al.[470] compared the performance of various Ga-containing catalysts in the conversion of propane at 773 K under atmospheric pressure in a microreactor. A H-[Al]-ZSM-5 (Si/Al = 15) and a H-[Ga]-ZSM-5 zeolite (Si/Ga = 45) were prepared according to literature recipes.[360] Both zeolites were modified by wet impregnation with 0.6 and 1.0 wt % of gallium (nitrate), respectively. A part of the pure gallosilicate was steamed at 873 K for 2.5 h under a flow of nitrogen and steam (p = 10 kPa) in order to remove gallium from framework positions. Gallium-impregnated samples were subjected to reduction/reoxidation cycles at 500 °C to promote the dispersion of the loaded gallium. Conversion rates of propane were kept smaller than 1% in order to avoid secondary reactions. Reaction kinetics over H[Al]-ZSM-5 and the gallosilicate in the presence of H_2 could be described by the same kinetic equation

$$r = k p_{C_3H_8}^{\ 1} p_{H_2}^{\ 0} \tag{29}$$

Product distributions were found to be identical.

The presence of nonframework gallium species introduced by impregnation or by extraction of Ga during steaming considerably enhances the propane conversion. Reaction orders are modified, and the reaction rate is given by

$$r = k p_{C_3H_8}^{\ 0.6} p_{H_2}^{\ -x} \tag{30}$$

The value of x has not been determined precisely. The negative reaction order with respect to hydrogen is explained in terms of a change of the rate-determining step. Dissociative adsorption of propane over gallium species is proposed to limit the overall rate. The competitive adsorption of C_3H_8 and H_2 molecules at nonframework gallium species causes an inhibition by hydrogen. This is in line with the mechanism proposed by Inui et al.[468] and Iglesia et al.[471] where recombination and removal of hydrogen from the active sites is considered the critical step within the reaction network (Table 19).

A kinetic modeling of the propane aromatization was performed by Guisnet and Lukyanov[472] according to the reaction scheme shown in Figure 81.

Forty-two compounds were considered representing all reaction components involved in the reaction, viz. 6 alkenes ($C_2^=-C_{10}^=$), 10 alkanes (C_1-C_{10}), hydrogen, 7 dienes (C_4-C_{10}), 5 alkylcyclohexenes (C_6-C_{10}), 5 alkylcyclohexadienes (C_6-C_{10}), and 5 alkylbenzenes (C_6-C_{10}). Adsorption equilibrium was assumed to be established. Reactions over zeolite and gallium sites were treated independently. The resulting differential equations from the set of 275 reaction steps have been solved numerically.[473]

By applying the model to experimental data obtained from flow reactor experiments over H-ZSM-5

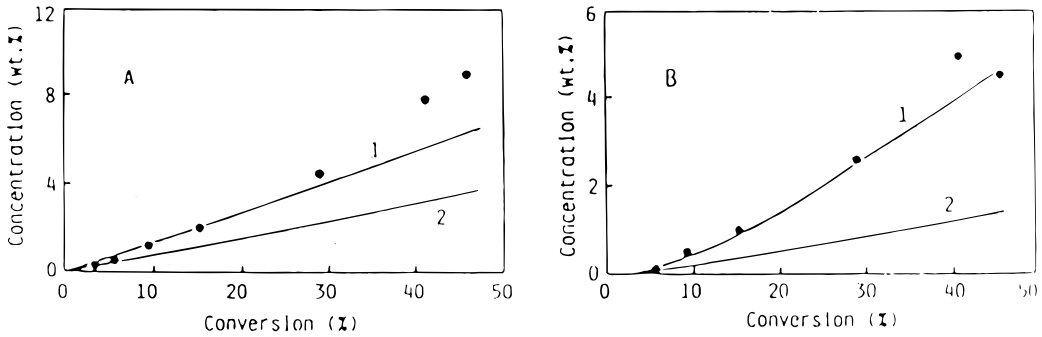

Figure 82. Conversion of propane over H[Ga]-ZSM-5. Experimental data and calculated curves for the concentration of methane (A) and ethane (B) as functions of the degree of conversion. Product formation is considered to occur either on both zeolite and gallium catalytic sites (curves 1) or only on zeolite acid sites (curves 2). (Reprinted with permission from ref 472. Copyright 1994 Elsevier Science.)

and Ga/ZSM-5 (the latter prepared by impregnation with gallium nitrate solution), a considerable improvement of model adequacy could be achieved by allowing propane cracking to undesired products (methane and ethane) and dehydrogenation of propane to propene (Figure 82).

5. Oxidation State of Ga

It was observed that treatment of gallium-containing catalysts with hydrogen at elevated temperatures led to an improved catalytic performance. The question is whether the reduction is accompanied by a chemical transformation resulting in new active sites or whether it merely creates Ga centers of low valence, e.g., Ga^+.

Price and Kanazirev[454,474] performed reduction experiments for a set of eight ball-milled Ga-modified ZSM-5 samples with various amounts of loading and milling times in a microbalance. The experimentally observed weight loss is reconcilable with the following stoichiometry of reduction

$$Ga_2O_3 + 2H^+Z^- + 2H_2 \rightarrow 2Ga^+Z^- + 3H_2O \quad (31)$$

which was proposed earlier by the authors.[454] Ga^+Z^- stands for a Ga^+ ion fixed to the anionic zeolite (Z^-). Catalysts can also be reduced by exposure to a propane feedstock.[454,474,475] The more intimately Ga_2O_3 and H-ZSM-5 are mixed, the faster proceeds reduction. The ultimate degree of reduction is limited by the zeolite. However, prereduction does not guarantee a better catalytic performance. Substantially reduced catalysts (Ga^+/Z^- ca. 1) are less active and less selective in the aromatization of ethane as well.[196]

6. Gallium Dispersion

Effects of hydrothermal treatments on the distribution of gallium within gallosilicates have been discussed earlier in this review. Mainly tetrahedrally coordinated Ga is removed from framework positions and forms agglomerated nonframework species. Consequences of thermal treatment for activity, selectivity, and deactivation in aromatization reactions are separately addressed by several authors. In the aromatization of propane, Choudhary et al.[127] attributed higher deactivation rates and modified product selectivities to the combined effect of decreased acidity and increased concentrations of nonframework (oxidic) gallium species in the zeolite pore system, caused by degalliation depending on the severity of hydrothermal conditions. The rate of propane conversion over a [Ga]-ZSM-5 gallosilicate (bulk Si/Ga = 33) declines dramatically if the sample has been hydrothermally pretreated[476] (Figure 83).

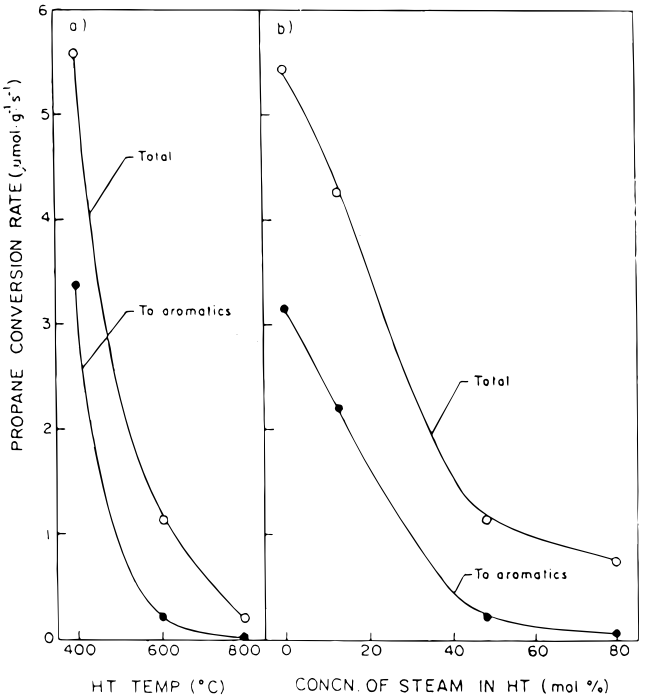

Figure 83. Propane aromatization over hydrothermally treated H[Ga]-ZSM-5. Influence of the temperature (part a, concentrated of steam: 48 mol %) and the concentration of steam (part b, temperature 873 K) on propane conversion rates (total and to aromatics). (Reprinted with permission from ref 476. Copyright 1996 Academic Press.)

Nonframework gallium species are extractable by acid leaching. Kanai and Kawata[450] observed a decrease of activity for aromatization of *n*-hexane if the gallosilicate catalyst was treated with 1 M HCl prior to use. Activity could be enhanced afterward by addition of minor concentrations of Ga^{3+}. These findings underline the supposition that nonframework gallium is the actual active species.

Simmons et al.[360] tried to elucidate the influence of nonframework gallium on activity in the catalytic cracking of *n*-butane at 773 K. A [Ga]-ZSM-5 zeolite (Si/Ga = 160) was prepared and handled carefully

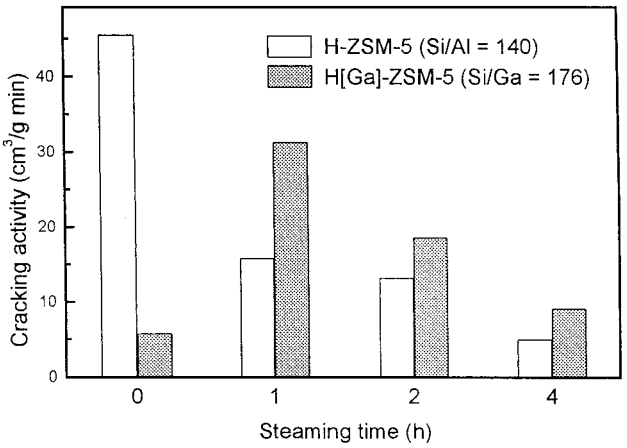

Figure 84. Influence of the steaming time at 873 K (in 100% steam) of H[Al]-ZSM-5 (Si/Al = 140) and H[Ga]-ZSM-5 (Si/Ga = 176) on the catalytic activity in *n*-butane cracking (values derived from ref 360).

after synthesis to avoid losses of framework gallium. Results of K^+ ion-exchange capacity confirmed the complete incorporation of gallium into framework positions. After 4 h of steaming at 823 K in 100% steam, a decreased ion-exchange capacity indicated a loss of framework gallium. If all of the gallium is in framework positions, [Ga]-ZSM-5 shows a product distribution very similar to that observed for H-ZSM-5. This underlines that the Brønsted acidity of pure [Ga]-ZSM-5 is very similar to that of the Al analogue. Only the presence of an amorphous gallium oxide phase in steamed sample causes a significant alteration of the product distribution in favor of C_2-C_4-olefins. The activity for *n*-butane cracking proceeds through a maximum depending on the steaming time (Figure 84). This behavior is ascribed to the dispersion of the gallium oxide which is assumed to be higher at short steaming times but deteriorates after prolonged treatment. Steaming of H-ZSM-5 causes a constant decrease of activity.

Bayense et al.[140] studied the removal of gallium from the framework of MFI-gallosilicates by ^{71}Ga MAS NMR spectroscopy. Steaming was carried out with an ammonium-exchanged gallosilicate (Si/Ga = 45) at 923 K for 3, 6, 12, and 24 h. Peak identification followed the assignment given by Timken and Oldfield.[181]

The spectra evidenced the removal of tetrahedrally coordinated gallium from the zeolite framework and the concomitant deposition of octahedrally coordinated gallium in the pores. The thermostability of framework gallium in gallosilicate MFI structures is lower than that of framework Al in ZSM-5.

Lanh et al.[172] performed the conversion of *n*-hexane over a series of gallosilicates with ZSM-5 structure and various Si/Ga ratios (12.5−100.0, gel composition). For all catalysts, the amount of framework gallium was determined by temperature-programmed desorption of ammonia (TPDA). The percentage of nonframework gallium resulted from the difference between total gallium content, determined by chemical analysis, and the content of framework gallium. The maximum of framework gallium content is reached at about 2 atoms per unit cell. Further enhancement of gallium contents leads merely to a higher percentage of nonframework gallium species. It could be shown that the *n*-hexane conversion taken after 90 min time on stream at 773 K correlates with the total amount of gallium (Figure 85), which points to a joint participation of both framework and nonframework gallium in the reaction.

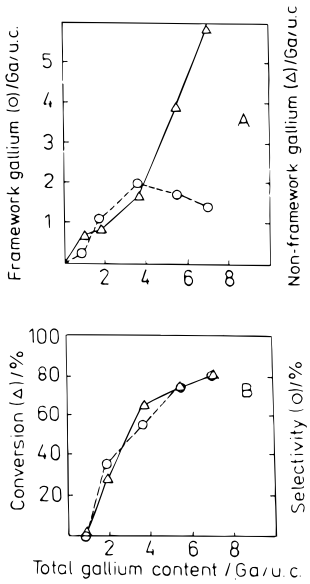

Figure 85. Conversion of *n*-hexane over H[Ga]-ZSM-5. (A) Distribution of framework gallium (○) and nonframework gallium (△); (B) conversion (△) and selectivity of aromatics (○) after 90 min time on stream at 773 K depending on the total content of gallium (per unit cell). (Reprinted with permission from ref 172. Copyright 1993 Elsevier Science.)

7. Participation of Nonframework Gallium Species in the Activation of Alkanes

There are two opposite views. One assumes that nonframework gallium of Ga-ZSM-5 does not directly participate in the activation of propane,[477,478] whereas the other one[479] claims that nonframework gallium does play a role in the direct activation of propane. The divergent views possibly originate from the fact that the fast secondary reactions mask the primary chemistry, thus rendering the elucidation of the participation of the different gallium species definitely more difficult. One attempt to clarify their role was performed by Buckles et al.[451] who studied the aromatization of propane on an ultra-stabilized Ga−Y zeolite prepared by ion exchange achieving a Ga loading of 5.6 wt %. This type of zeolite is far less active and is expected to minimize the effect of the secondary reactions. Results gave rise to the conclusion that the presence of Ga^{3+} replaces cracking by dehydrogenation in the activation of propane.

Gianetto et al.[480] investigated propane aromatization over MFI gallosilicates and compared the reaction characteristics of [Ga]-ZSM-5 (Si/Ga = 30) with those of [Al]-ZSM-5 (Si/Al = 30). H-[Al]-ZSM-5 was found to be 7 times more active than the gallosilicate. The activity difference was ascribed to the higher acid strength of Brønsted sites in the H[Al]-ZSM-5. Large differences were found in the product distribution. Treatment of gallosilicates at 973−1073 K under a flow of dry air caused a significant increase in catalyst activity and selectivity. The increase is

related to the formation of a small amount of nonframework gallium species well dispersed in the crystallites and highly active for dehydrogenation of propane and of naphthene intermediates. Framework gallium is much less active or even inactive for dehydrogenation. Degalliation occurs rapidly during calcination in dry air at temperatures above 873 K and is accompanied by a decrease of acidity, a partial collapse of the zeolitic structure, and a blocking of the pores owing to the deposition of nonframework species. Nonframework species are unavoidably present already in the as-synthesized samples if gallium incorporation into the zeolite framework is incomplete.[132] The Si/Ga ratio has a pronounced effect on product distribution; the lower the Si/Ga ratio, the higher the yield of aromatics. Higher gallium concentrations enhance the probability that nonframework gallium species are present a priori. The better overall performance observed at higher gallium contents is probably a consequence of an enhanced dehydrogenation activity due to nonframework gallium species.

Bayense et al.[140] found that highly dispersed gallium in the zeolite (framework or nonframework) possesses dehydrogenation activity.

Kwak et al.[458] showed that after addition of metals to H-ZSM-5 (either Ga by chemical vapor deposition or Pt by impregnation or both metals), catalysts developed dehydrogenation activity in the conversion of propane producing propylene whereas over metal-free H-ZSM-5 propane was converted to methane and ethylene in equimolar amounts. The effect is additive rather than synergistic. At higher conversions and longer times on stream, the formation of aromatics is highest on the Ga-modified ZSM-5. One further advantage of the Ga-modified ZSM-5 is the improved resistance against coking.

8. Role of Promotors

Inui et al.[449] compared the catalytic performance of (i) pure gallosilicates of various Si/Ga ratios, synthesized by the rapid crystallization technique, with the corresponding (ii) Pt-modified H-forms gained by treatment with $Pt(NH_3)_4Cl_2$ to reach Pt contents of 0.5 wt % each. The two catalyst series were compared with modified H-ZSM-5 samples (Si/Al = 40), one obtained by ion exchange with Ga and the other by impregnation with the platinum amine complex. Data given for the conversion of propane at 873 K and a WHSV of 2000 showed that Pt/Ga-silicate is more active than the nonmodified gallosilicates (specifically at the higher Si/Ga ratios). The selectivity of aromatics is comparable (excepting the sample with Si/Ga = 40). The authors suggested that Pt promotes the dehydrogenating step of propane to propene. The performance of the Ga ion-exchanged H-ZSM-5 gives poorer results in any respect. The Pt/H-ZSM-5 already reaches a 92% propane conversion at a temperature 100 K lower (773 K) but then with a selectivity to aromatics of only 25%.

Thermodynamic calculations[481] for the dehydrogenation of propane to propene at 773 K and 101 kPa predicted an equilibrium conversion of ca. 16%. Nearly complete conversion, however, is observed experimentally. This is possible due to a drain-off effect. The removal of the propene by further reactions prevents the establishment of equilibrium conditions. Dmitriev et al.[482] studied the promoting effect of Pt using a synthesized gallosilicate with MFI structure as a carrier in the aromatization of *n*-butane. Again, addition of platinum enhanced the activity (allowing lower reaction temperatures) and accelerated the dehydrogenation of initial paraffinic and alicyclic intermediates, thus suppressing cracking processes.

Sphiro et al.[483−485] studied the effects of additional Pt modification for Ga zeolite catalysts prepared through ion exchange, impregnation, galliation, or hydrothermal synthesis. Pt present on an ion-exchanged Ga-ZSM-5 shortened the induction period of activity stabilization during *n*-butane aromatization, even without preliminary treatment in hydrogen. Prereduced Pt-Ga-ZSM-5 samples showed no activation period at all. Formation periods of Ga-silicates with atomically dispersed gallium is attributed to the in situ establishment of an optimum ratio between framework and nonframework gallium sites. Observed degrees of reduction of 35−40% of the gallium obviously represent the percentage of gallium in nonframework positions. Further effects are a retardation of catalyst deactivation through spill-over of activated hydrogen species to coke precursors to hydrogenate them. According to the authors, hydrogen is activated on intra-zeolitic Pt clusters and is spilt over to Ga oxide on the external surface forming Ga^+H^- species. These are mobile at the elevated temperature and become accommodated at Pt particles to form "bimetallic clusters". The enhancement of Lewis acidity (reduced gallium ions) is one of the sources of increasing dehydrogenation and aromatization activity of the Pt−Ga samples. A synergism is assumed in the catalytic action between platinum and gallium through long-distance effects and intimate interaction.

In summary, the effect of platinum on Ga-containing zeolite catalysts in aromatization reactions is manifold. Platinum accelerates the reduction of gallium oxide, promotes the migration of dispersed gallium species into the zeolite pore system, activates hydrogen with subsequent spill-over to the gallium phase, and retards catalyst deactivation by hydrogenation and hydrogenolysis of coke precursors.[483,484]

B. Alkylation, Disproportionation, and Isomerization of Aromatics

Alkylation, isomerization, and disproportionation of aromatics are basic reaction types in petrochemistry. Owing to an improved selectivity and process economy (better energy balance, reduced corrosion, and wastewater problems), gas-phase ethylation of benzene with ethylene over P-modified ZSM-5 zeolites was commercialized in the 1970s (Mobil−Badger process)[498] replacing aluminum chloride in the liquid-phase alkylation. Analogously, alkylation of toluene to *p*-ethyltoluene results in high selectivity, opening the way to methylstyrene monomers.

Isomerization of C_8 aromatics (xylenes, ethylbenzene) aims at *p*-xylene, which is a basic material for

Table 20. Alkylation, Disproportionation, and Isomerization Reactions over Ga-Modified Zeolites and Molecular Sieves Published in the Open Literature

Reaction at T (K)	Zeolite structure type	Ga introduced by Ga source Ga content Al present (yes/no)	Performance compared with	Conclusions	Ref.
Disproportionation of ethylbenzene, 423 K	MFI (ZSM-5)	Synthesis Nitrate Si/Ga = 30.7 No	[B]-ZSM-5 [Al]-ZSM-5	Activity: Al > Ga > B	271
Disproportionation of ethylbenzene, 688 K	TON (ZSM-22)	Synthesis Sulfate Si/Ga = 138 - 376 Yes (0.05% of Al_2O_3)	[Al]-ZSM-22, (Si/Al = 208)	Ga analog shows lower activity but less activation	567
Methylation of xylenes, 513 - 573 K	MEL (ZSM-11)	Synthesis Nitrate Si/Ga = 39.0 No	[Fe]-ZSM-11 [Al]-ZSM-11	Activity: Al > Ga > B Selectivity to 1,2,4 TMB: Fe > Ga > Al	503
Methylation of aniline, 573 - 723 K	MFI (ZSM-5)	Synthesis Nitrate Si/Ga = 43.5 No	[Ge]-, [B]-, [Al]-, [Ti]-, [V]-, [Fe]-, [Ni]-, [Zr]-ZSM-5	Activity: Al > Zr > Ni ≈ Fe > Ge > B > Ti > V ≈ Ga	505
Toluene alkylation with ethanol, 573 - 648 K	MFI (ZSM-5)	Synthesis not specified Si/Ga = 100 (gel composition) No	[Al]-ZSM-5	Activity: Al > Ga	510
Ethylbenzene alkylation with ethanol	MFI (ZSM-5)	Synthesis Sulfate Si/Ga = 64 Yes (Si/Al = 1000)	[Al]-, [Sb]-, [Fe]-, [B]-ZSM-5	*para*-Selectivity: Sb > B > Fe ≈ Ga > Al Trace amounts of Al in B- and Ga-ZSM-5 contribute to activity	507
Toluene alkylation with ethanol, 623 K	MFI (ZSM-5)	Synthesis Si/Ga = 108, small crystals ca. 2.5 μm Si/Ga = 132, large crystals ca. 20 μm No	[Al]-, [B]-, [Fe]-ZSM-5	Acidity: Al > Ga > Fe > B, Activity: Al > Ga > Fe > B	517

Methylation of toluene, Isomerization of *ortho*-xylene, 673 K	MFI (ZSM-5)	Synthesis not specified Si/Ga = 64 No	[Al]-, [B]-, [Cr]-, [Sb]-, [As]-ZSM-5	*para*-Selectivity: Al > Sb > Cr = B > Ga > As *ortho*-Xylene isomerization activity: Al > Ga > B = Cr > Sb > As	511
Isomerization of C_8 aromatics, 1.4 wt.-% toluene 19.7 wt.-% ethylbenzene, 78.8 wt.-% xylenes	MFI (ZSM-5)	Ball-milling of HZSM-5, Si/Al = 51, β-Ga_2O_3, 2 wt.-% of Ga Yes	[Al]-ZSM-5 [Ga]-ZSM-5 (reduced/unreduced)	Ethylbenzene conversion: Ga (reduced) > Al > Ga (unreduced)	565
Isomerization of *meta*-xylene	MFI (ZSM-5)	Synthesis Na-gallate Si/Ga = 25, 50, 100 No	Fe-, [Al]-ZSM-5	Activity: Al > Ga > Fe *para*-Selectivity: Al > Ga > Fe	242
Toluene alkylation with ethylene	MFI (ZSM-5)	Synthesis	[Al]-, [Fe]-, [In]-, [B]- ZSM-5	Acidity: Al > Ga > In > B, Activity: same order	161
(i) Ethylbenzene conversion, (ii) Isomerization of *meta*-xylene, 623, 653, 723 K	MFI (ZSM-5)	Synthesis Ga_2O_3 Si/Ga = 50, No	Gallosilicates with various crystallization times	Crystallization times ≥ 24 h are necessary.	209
(i) Ethylbenzene alkylation with ethanol, 673 K (ii) Toluene disproportionation, 823 K (iii) Toluene methylation, 673 K	MFI (ZSM-5)	Synthesis Si/Ga = 64	[Al]-, [B]-, [Cr]-, [Sb]-, [As]-ZSM-5 additional impregnation with P or B	*para*-Selectivity: (i) *p*-DEB: As ≈ Sb > B > Fe ≈ Ga > Al (ii) *p*-Xylene: equilibrium (24 - 26%) (iii) *p*-Xylene: As > Sb ≈ Cr > B ≈ Ga > Al	141
Ethylbenzene alkylation with ethanol	MFI (ZSM-5)	Synthesis, Sulfate, Si/Ga = 170, No	[Al]-, [Fe]-ZSM-5	Conversion: Al > Ga > Fe *para*-Selectivity: Fe > Ga > Al	512
Dealkylation of cumene	MFI (ZSM-5)	Synthesis Sulfate Si/Ga = 30.3 No	[Al]-, [B]-ZSM-5	Acidity: Al > Ga » B Selectivities of cracking (benzene/propene), transalkylation (benzene/*n*-propylbenzene), Al = Ga (vacuum pretreated at 773 K)	506
(i) Disproportionation of toluene (ii) Ethylbenzene alkylation with ethanol	MFI (ZSM-5)	Synthesis ? Si/Ga = 64 Si/Al » 1000	[Al]-, [B]-, [Cr]-, [Sb]-, [As]-ZSM-5	*(i) para*-Selectivity: equilibrium established	218

Table 20 (Continued)

Reaction at T (K)	Zeolite structure type	Ga introduced by Ga source Ga content Al present (yes/no)	Performance compared with	Conclusions	Ref.
Isomerization of *meta*-xylene	MOR (Mordenite)	Synthesis, TEABr Ga nitrate Si/Ga = 9.5 No, (Si/Al > 500)	Al-mordenite Si/Al = 6.65	Ga mordenite less active, but higher percentage of disproportionation (Lewis acid properties of non-framework Ga).	515
Isomerization of *meta*-xylene 503 - 583 K	MOR, (Mordenite)	Synthesis, Ga sulfate Si/Ga = 21 No	Al mordenite Si/Al = 17.5	as in Ref. (218)	161
Alkylation of toluene with *iso*-propanol	MFI (ZSM-5)		[Al]-, [Fe]- ZSM-5	*para*-Cymene selectivity increases with decreasing acidity (Al > Ga > Fe)	160
Methylation of toluene	BEA (Beta)		[Al]-, [B]-Beta [Al]-, [Ga]-Beta	p-/o-Xylene ratio decreases SiAl > SiAlGa > SiGa > SiB	568
Isomerization of *meta*-xylene 453 - 603 K	MFI (ZSM-5)	Post-synthesis impregnation of ZSM-5 Ga nitrate solution 5 wt.-% of Ga Yes (Si/Al = 13.6)	Oxidized/reduced form	Change in H^+ concentration correlates with *m*-xylene isomerization rate	504
Isomerization of *meta*-xylene 623 K	MFI (ZSM-5)	Synthesis, Nitrate, Si/Ga = 30, 50, 180, No	[Al]-ZSM-5, Si/Al = 30	Activity: Al > Ga-silicates (> 30 > 50 > 180), *p*/*o*-Xylene ratio 1.7-2.2 (at 10% *m*-xylene conversion) independent of the catalyst	569
Disproportionation of toluene, 673 K	MFI (ZSM-5)	CVD, Ga chloride, 0.77, 1.36, 2.95, 2.97, 3.70, 3.76 wt.-% of Ga), Yes (Si/Al = 20.5)	with one another	Conversion of toluene decreases in dependence on the degree of H^+ replacement by GaO^+	480
Alkylation of toluene with *iso*-propanol, 498 K, Toluene/*iso*-propanol = 4	MFI (ZSM-5)	Synthesis, Si/Ga = 50 No	[Al]-ZSM-5 (Si/Al = 48), [Fe]-ZSM-5 (Si/Fe = 54)	*para*-cymene selectivity increases with decrease in acidity (Al > Ga > Fe)	152

Isomerization of C_8 aromatics, 553 K 19.7 % Ethylbenzene, 1.41 % Toluene 78.8 % Xylenes	MFI (ZSM-5)	Ball-milling of β-Ga_2O_3 with H-ZSM-5 (Si/Al = 50.8), 2 wt.-% of Ga Yes	H-ZSM-5 (Si/Al = 50.8)	Products on H-ZSM-5 and β-Ga_2O_3/H-ZSM-5 (unreduced) not different, higher ethylbenzene conversion and loss of xylenes on β-Ga_2O_3/H-ZSM-5 (pre-reduced)	568
(i) Alkylation of toluene by ethylene, 663 - 683 K, T/E = 2.5 (molar) (ii) Transalkylation of ethylbenzene, 658 - 668 K	MFI (ZSM-5), Si/Al = 190	Ion exchange	[Al]-ZSM-5 and other ion exchanged samples, (Ca^{2+}, Mg^{2+}, Y^{3+}, In^{3+}, Dy^{3+}, Sc^{3+}, Be^{2+})	Selectivity determined by aprotic (Lewis) acid sites	565
Alkylation of 2-methylnaphthalene with methanol, 723 K, 6.2 kPa 2-MN, 14.1 kPa MeOH	MFI (ZSM-5)	Synthesis Si/Ga = 42, No	[Fe]-ZSM-5 (Si/Fe = 37), [B]-ZSM-5, (Si/B = 70), [Sb]-ZSM-5 (by atom planting into silicalite) (Si/Sb = 120)	Conversion: H-ZSM-5 >[Ga]-ZSM-5 > [Fe]-ZSM-5 > [B]-ZSM-5 = [Sb]-ZSM-5, Fraction of 2,6 dimethylnaphthalene: Sb » Fe » B > Ga > Al	220

the production of phthalic acid derivatives. The process should guarantee minimum losses of the xylenes and a desired conversion of ethylbenzene, either by disproportionation (vapor-phase isomerization) or dealkylation (high-temperature isomerization).

The selective toluene disproportionation converts toluene to benzene and xylenes. The advantage of this process is that the xylenes from disproportionation of toluene do not contain ethylbenzene, which is always present in the C_8 aromatic fraction of the reformate.[499]

Characteristics of the reaction over gallosilicate catalysts are often compared to those over other metallosilicates or the aluminosilicate structure analogues (Table 20). Generally, the activity for alkylation, isomerization, and disproportionation depending on the substituting framework element decreases in the order Al > Ga > Fe > B at constant Si/Me framework ratios of the zeolites, i.e., at nearly equal Brønsted site concentrations. Besides, activity is related to the acid strength of the Brønsted sites which decreases in the same order.

1. Shape-Selective Effects

Shape selectivity in the conversion of aromatics is often understood as the percentage of the para-isomers among the products. Owing to its slim shape, the para-isomer has a high diffusivity and therefore responds more sensitively to geometric constraints of the zeolite pore system than the meta- and ortho-isomers. This product shape selectivity is based on the mass transport resistance inside the zeolite pores, the extent of which depends on the ratio between the activity and the diffusivity of the given components. The comparatively high flux of a slim component through the pore system protects it from being involved in further reactions. Thus, establishment of equilibrium and consumption by secondary steps are vastly suppressed.

Rapid reactions are more severely restricted by diffusive mass transport, especially in the case of large crystal sizes. For a rapid reaction in large crystals, only a small percentage of the internal sites of the zeolite is accessible to catalytic interaction. The reaction tends to be highly diffusion-controlled, and the reaction zone can be thought to be limited to a small shell near the outer surface of the zeolite crystal only. The extent of diffusion control is expressed by the Thiele modulus

$$\Phi = R\sqrt{k/D} \tag{32}$$

R denoting the radius or an equivalent geometric parameter, k the rate constant of the reaction assumed to be of first order, and D the effective diffusivity.

High values of the Thiele modulus correspond to low effectiveness and to strong diffusion limitations and vice versa. A shift of the reaction to either kinetic or diffusion control is possible at constant values for R and for diffusivity if the intrinsic rate constant k is varied. The reported different para-selectivities of MFI structures depending on the nature of the framework elements might actually have their origin

in different k values, depending on the nature and the concentration of active sites. For example, the activity of the alkylation of toluene with ethylene declines in the sequence [Al]-ZSM-5 > [Ga]-ZSM-5 > [Fe]-ZSM-5 > [In]-ZSM-5,[500] indicating a decrease of the rate constant k. The Thiele modulus decreases in the same order and diffusion control loses influence. Consequently, the observed para-selectivity is highest with [Al]-ZSM-5 and lowest with [In]-ZSM-5. Due to the slow reaction rate, the concentration gradients on [In]-ZSM-5 are not that steep and the flux of the component with higher mobility is less favored. This causes a low para-selectivity. No further assumptions (unit cell expansion, variation of diffusion coefficients by nonframework species, etc.) are needed.

The relationship between product shape selectivity, diffusivity, and rate constant was simulated by Emig et al.[501] for the microkinetic reaction scheme (eqs 33 and 34)

$$2A \rightarrow C + (I_1 + I_2 + I_3)_{pr}, \text{ rate constant } k_f \quad (33)$$

$$(I_1 + I_2 + I_3)_{pr} \rightarrow (I_1 + I_2 + I_3)_{sec}, \text{ rate constant } k_I \quad (34)$$

This scheme represents, e.g., the disproportionation of toluene to benzene and xylene isomers where I_1, I_2, and I_3 correspond to *o*-, *m*- and *p*-xylene, respectively. The primary isomer distribution $(I_1 + I_2 + I_3)_{pr}$ is changed into the experimentally observed distribution $(I_1 + I_2 + I_3)_{sec}$ by secondary isomerization. Without mass transfer restrictions the isomer distribution would assume thermodynamic equilibrium values (7% *o*-xylene, 63% *m*-xylene, and 30% *p*-xylene). Within microporous zeolite crystals, the geometrically slim para-isomer has a higher diffusion rate than the other isomers. Already an effective diffusivity of the para-isomer twice as high as that of the ortho-isomer (set equal to the diffusivity of the meta-isomer) leads to enhanced concentrations of the para-isomer in the exit stream (Figure 86). This para-selective effect is more pronounced at higher differences of the diffusivity. However, the para-selectivity depends on the value of the rate constant. At low values, the secondary isomerization step, eq 34, does not take place practically. Rate constants k_I from 10^{-5} to 1 s^{-1} lead to the isomer distribution $(I_1 + I_2 + I_3)_{sec}$ whose reestablishment of equilibrium is prevented due to the fast diffusion of the para-isomer out of the reaction zone. This "drain-off effect" favors additional formation of *p*-xylene and enhances the product yield. At higher rate constants, the isomers achieve equilibrium distribution despite the diverging diffusivity and the para-selective effects are lost.

Monte Carlo simulations of isomerization processes yielded similar results.[502] For a hypothetical isomerization of a component B

$$A \leftrightarrow B \leftrightarrow C \quad (35)$$

the calculated dependence of the selectivity ratio N_C/N_A on the Thiele modulus Φ and on the diffusivity ratio of components C and A is shown in Figure 87. N_C and N_A denote the number of molecules C and A,

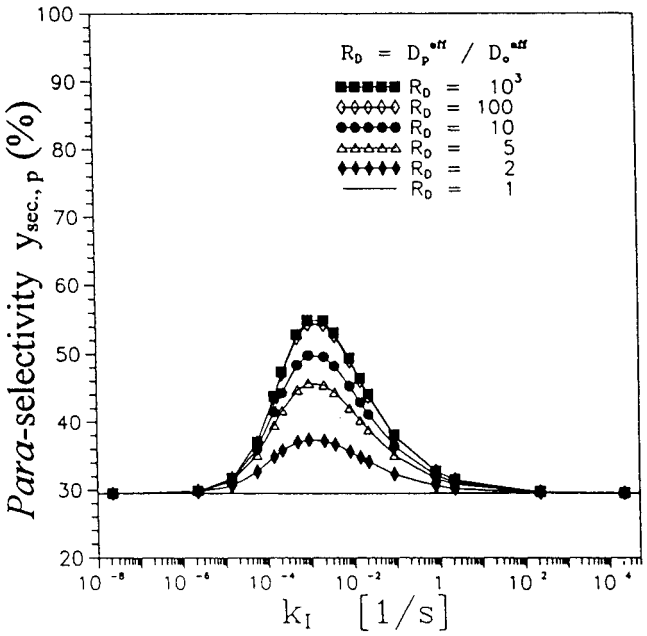

Figure 86. Extent of product shape selectivity (yield of para-isomer) depending on the rate constant k_I of the reaction step $(I_1 + I_2 + I_3)_{prim} \leftrightarrow (I_1 + I_2 + I_3)_{sec}$ and the diffusivity ratio $R_D = D_p^{eff}/D_o^{eff}$, ($D_p$ is assigned to I_3 and D_o to I_1). (Reprinted with permission from ref 501. Copyright 1994 VCH.)

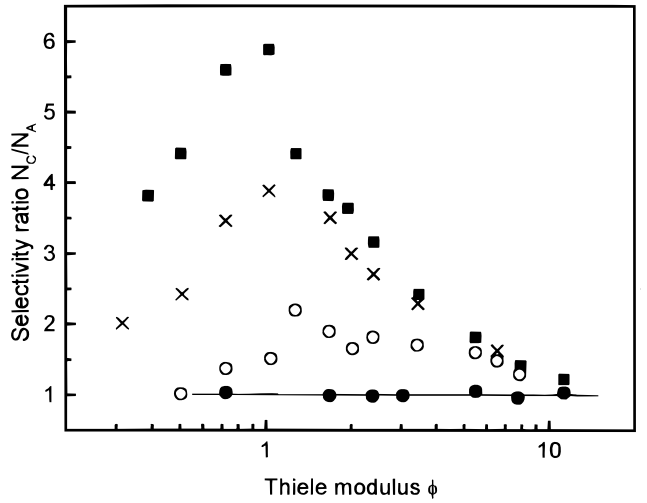

Figure 87. Results of a Monte Carlo simulation for the reaction A ↔ B ↔ C starting with compound B. Dependence of product selectivity of C on the Thiele modulus Φ for various D_C/D_A ratios: (■) 1000:1, (×) 100:1, (○) 10:1, (●) 1:1 (D_C = diffusivity of component C, D_A = diffusivity of component A). (Reprinted with permission from ref 502. Copyright 1994 Baltzer Science.)

respectively. The selectivity ratio N_C/N_A over the Thiele modulus Φ shows a volcano-shaped curve. For any diffusivity ratio $D_C/D_A > 1$, the selectivity ratio N_C/N_A runs through a maximum with growing Φ. For identical Φ-values, the selectivity ratio N_C/N_A increases with the diffusivity ratio. Results of the simulations confirm the experimental experience that product selectivity can be largely improved by increasing differences in diffusivity for parallelly formed product molecules. To achieve high para-selectivities, the reaction has to be performed at a suitable Thiele modulus.

Table 21. Comparison of the Catalytic Performance of [Ga]-ZSM-5 and [Al]-ZSM-5 in the Ethylation of Toluene[510] [a]

	[Ga]-ZSM-5	[Al]-ZSM-5
Product Composition, wt %		
lighters	0.15	0.65
toluene	85.31	82.53
C_8 aromatics	0.07	0.92
p-ethyltoluene	10.43	5.77
m-ethyltoluene	3.67	9.65
o-ethyltoluene	0.01	0.43
diethyltoluene	0.46	0.05
Performance		
toluene conversion (wt %)	14.69	17.47
total ethyltoluene selectivity (%)	96.00	91.00
ethyltoluene composition (%)		
p-ethyltoluene	73.90	36.40
m-ethyltoluene	26.00	60.88
o-ethyltoluene	0.10	2.72

[a] Reaction conditions: $T = 623$ K, WHSV $= 7$ h^{-1}, toluene/ethanol $= 6$ (mol/mol).

2. Alkylation

Gallium-based catalysts were applied in the gas-phase alkylation of toluene with methanol, ethanol, ethylene, and 2-propanol for the alkylation of ethylbenzene with ethanol, for the methylation of xylenes, for the transalkylation of alkylaromatics (cumene−benzene as well as cumene−toluene), and for the methylation of aniline (see Table 21). With few exceptions, [Ga]-ZSM-5 zeolites were used. Methylation of xylenes over [Ga]-ZSM-11 and methylation of toluene over [Ga]-beta have been studied by Raj et al.[503] and Corma et al.,[504] respectively.

The methylation of aniline reported by Park et al.[505] is the only exception showing the lowest activity of gallosilicates; the activity sequence related to the isomorphously substituted element is Al > Fe > B > Ga. Most likely, the low activity of the gallosilicate MFI structure is caused by the negligible insertion of gallium into the silicalite framework as indicated by the presented characterization data (TGA/TG of template decomposition, profiles of ammonia thermodesorption).

In the alkylation of monoalkylbenzenes, the alkyl group which is already present activates the ortho and para ring positions for alkylation. Variation of the residence time and determination of initial selectivities showed that the para-isomer is the only primary product. This is caused by the strong geometric restrictions imposed on the formation of the transition state by the medium size pore system of the MFI structures. Ortho- and meta-isomers are formed exclusively by secondary isomerization on acid sites preferentially located on the external zeolite surface. As is expected, para-selectivity can be enhanced by passivation of the external surface sites. A measurable effect of external surface passivation on the shape selectivity of para-isomers is known from aluminosilicates with small crystal sizes (1 μm), where, due to the comparatively large outer surface area, the concentration of external active sites is high compared with that of the sites inside the pores. The external surface of zeolites can be passivated e.g., by chemical vapor deposition of bulky organosilanes, which cannot penetrate the pore system, and subsequent thermal decomposition. Thus, a silica shell covers the external surface and reduces the pore entrance size of Ga-free ZSM-5. Halgeri and Bhat[506] have shown that chemical vapor deposition of silica blocks the nonselective external surface sites and the sites near the pore mouths, without altering the internal zeolite structure.

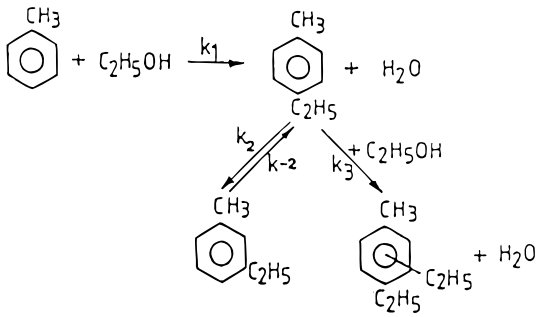

Figure 88. Proposed kinetic reaction scheme of toluene ethylation over [Ga]-ZSM-5. (Reprinted with permission from ref 508. Copyright 1989 Elsevier Science.)

Kim et al.[507] performed the alkylation of ethylbenzene with ethanol over H-ZSM-5 in the presence of 2,4-dimethylquinoline, whose molecular dimension excludes any access to internal active sites. The complete poisoning of the acid sites on the external surface was confirmed by the deactivation of the catalysts in the cracking of 1,3,5-triisopropylbenzene, a molecule which cannot enter the interior of the MFI structure. The effect of poisoning was found to be minute on both activity and selectivity. This may possibly be attributed to the crystal size that was, however, not reported. Experimental results considering the influence of the crystal size on para-selectivity are inconsistent. Jahn and Cardoso[508] found no relationship between ZSM-5 crystallite sizes and *p*-xylene selectivity for the methylation of toluene. The range of crystallite sizes investigated was rather small, 0.5−1.5 μm. In other cases, the distribution of crystal sizes is rather broad and crystal size effects are averaged.

Norval and Phillips[509] reported equilibrium data for the alkylation of toluene with ethylene initial C_7H_8:C_2H_4:H_2 ratios of 5:1:5 and 5:2:4 in the range 600−800 K under atmospheric pressure. By kinetic analysis, Parikh et al.[510] found that the alkylation of toluene with ethanol over [Ga]-ZSM-5 in a fixed bed flow reactor at atmospheric pressure could be described with good accuracy by the reaction network shown in Figure 88.

The network is characterized by primary alkylation forming *p*-ethyltoluene, its further alkylation to isomeric diethyltoluenes, and reversible isomerization of *p*-ethyltoluene to *m*-ethyltoluene. Formation of *o*-ethyltoluene was found to be negligible.

Apparent activation energies are derived from the temperature dependence of the rate constants for the primary ($E_a = 82.6$ kJ/ mole) and the further alkylation of toluene ($E_a = 43.5$ kJ/mol) and for the isomerization of *p*-ethyltoluene ($E_a = 26.6$ kJ/mol). The values are rather low pointing at an influence of internal diffusion. Intrinsic activation energies twice as high as the apparent activation energies are cited by the authors.

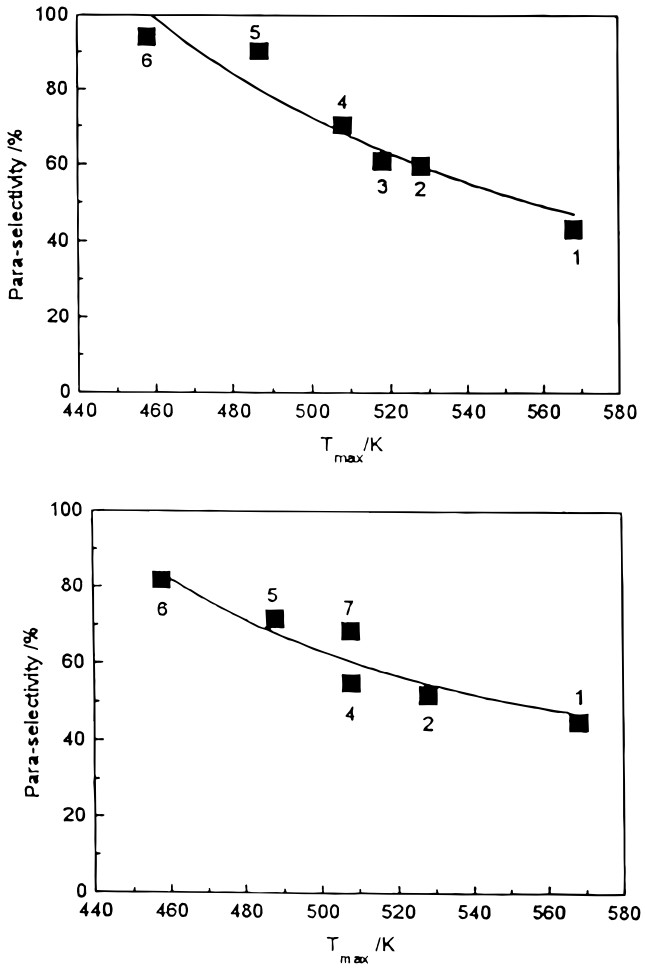

Figure 89. Ethylation of ethylbenzene (top) and methylation of toluene (bottom) over metallosilicate ZSM-5 type zeolites. Relationship between para-selectivity (percentage of *p*-diethylbenzene and *p*-xylene, respectively) and the peak maximum temperature of NH_3 desorption from Brønsted acid sites. (1) [Al]-ZSM-5 (Si/Al = 96), (2) [Ga]-ZSM-5 (Si/Ga = 64), (3) [Fe]-ZSM-5 (Si/Fe = 56), (4) [B]-ZSM-5 (Si/B = 70), (5) [Cr]-ZSM-5 (Si/Cr = 260), (6) [Sb]-ZSM-5 (Si/Sb = 120), (7) [As]-ZSM-5 (Si/As = 92). (Adapted from ref 512.)

A comparison between the performances at the [Ga]-MFI catalyst and a ZSM-5 zeolite (Si/M ratio, M = Ga, Al, adjusted to 100 in the synthesis gel) showed that the activity expressed in terms of toluene conversion is 3% lower over [Ga]-MFI (Table 21). The difference is ascribed to the lower acid strength of Brønsted sites in the gallosilicate. The observed higher *p*-ethyltoluene selectivity over [Ga]-MFI is attributed to the larger crystal size (10−12 μm instead of 1−3 μm for ZSM-5). A correlation between the formation the para-isomer and the peak maximum temperature of ammonia desorption from Brønsted acid sites (synonymous for the acid strength of Brønsted sites) is reported for the alkylation of toluene with ethanol[507] and methanol[511,512] and for the alkylation of ethylbenzene with ethanol[512−515] as well. Two examples are given in Figure 89.

For both the reactions a higher percentage of the para-isomers (*p*-diethylbenzene and *p*-xylene) among alkylation products is observed at sites of lower acid strength. The same relationship between para-selectivity and Brønsted acidity was reported by

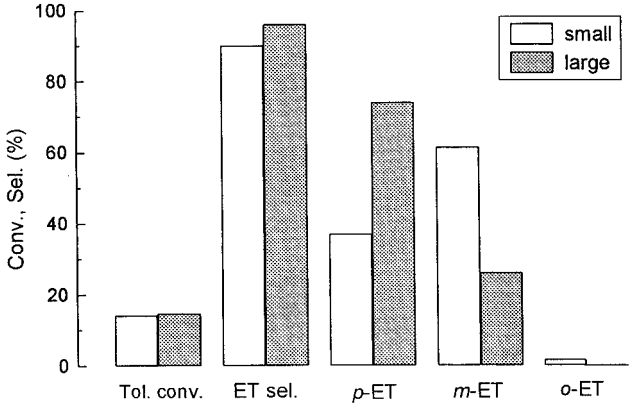

Figure 90. Influence of the crystal size on the alkylation of toluene with ethanol (toluene/ethanol ratio = 6) over [Ga]-ZSM-5. Small (spheroidal) crystals: ca. 2.5 μm, Si/Ga = 108. Large (oblong) crystals: ca. 20 μm, Si/Ga = 124. Reaction conditions: T = 623 K, WHSV = 9.6 h^{-1} (small crystals) and 6.83 h^{-1} (large crystals). Tol. conv. = toluene conversion, ET sel. = overall selectivity of ethyltoluenes, *p*-ET, *m*-ET, *o*-ET = percentage of *p*-, *m*- and *o*-ethyltoluenes, respectively. (adapted from ref 517.)

Cejka et al.[500,516] for the alkylation of toluene with ethylene over Al-, Fe-, and In-substituted ZSM-5 catalysts. No correlation was found between acidity parameters of microporous metallosilicates and conversion/selectivity values for the alkylation of toluene with 2-propanol.[516] The desorption/transport of the bulky propyltoluenes out of the pore system is responsible for the leveling of the primary para-selectivity. Parikh et al.[517] studied the influence of the crystal size on the para-selectivity of toluene alkylation for a series of [Al]-ZSM-5, [Ga]-ZSM-5, and [Fe]-ZSM-5 catalysts. Figure 90 shows results for two [Ga]-ZSM-5 samples with significantly different crystal sizes, viz. 2.5 and 20 μm. With the larger crystal size, the distribution of the three ethyl toluene isomers is shifted in favor of the para-product. This is in line with the expected effect of internal diffusion on the product shape selectivity. Crystal size had a larger impact on the selectivity than the kind of isomorphously substituted element.

A high percentage of the 1,2,4-isomer (98.5%) among trimethylbenzenes (TMB) gained by gas-phase methylation of xylenes over Al-, Ga-, and Fe-silicates with MEL (ZSM-11) structure was observed by Raj et al.[503] As 1,2,4-TMB has the smallest kinetic diameter (0.68 nm) within the isomers, the very high selectivity of this isomer can be attributed to the shape-selective effect of the MEL metallosilicates. However, it could not be decided unambiguously whether product shape selectivity or transition state shape selectivity is responsible. The yield of TMBs is enhanced over the metallosilicates in the order Al < Ga < Fe. The conclusion has been drawn that alkylation of xylenes at weaker acid sites is able to compete more efficiently with other reactions such as isomerization of *m*-xylene and conversion of methanol to hydrocarbons.

3. Disproportionation

Substrates such as toluene and ethylbenzene are of primary interest for disproportionation reactions. Disproportionation of toluene produces benzene and

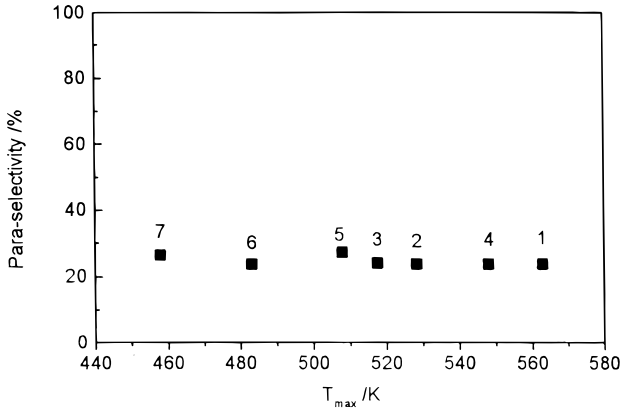

Figure 91. Disproportionation of toluene over metallosilicate ZSM-5-type zeolites. Relationship between para-selectivity (percentage of *p*-xylene in the sum of xylenes produced at 4−5% yield) and the peak maximum of the NH_3-TPD profile: (1) [Al]-ZSM-5 (Si/Al = 96), (2) [Ga]-ZSM-5 (Si/Ga = 64), (3) [Fe]-ZSM-5 (Si/Fe = 56), (4) [B]-ZSM-5 (Si/B= 70), (5) [Cr]-ZSM-5 (Si/Cr = 260), (6) [Sb]-ZSM-5 (Si/Sb = 120), (7) [As]-ZSM-5 (Si/As = 92). (Adapted from ref 512.)

xylenes. The reaction requiring acid sites of high strength[518] is accompanied by a competitive dealkylation of toluene resulting in C_1-C_4 hydrocarbons. At a reaction temperature of 770 K and a WHSV of 2.7 h^{-1}, Cejka et al.[516] found a maximum toluene conversion of 5% over [Fe]-ZSM-5 (containing 2.48 Fe^{3+} per unit cell) and of 22.2% over [Al]-ZSM-5 (containing 4.02 Al^{3+} per unit cell) after 15 min of time on stream. [Ga]-ZSM-5 was not included in the investigation. Kim et al.[515] and Namba et al.[511] tried to clarify which of the xylene isomers is the primary product of toluene disproportionation. They analyzed the isomer distribution in the produced xylenes with decreasing residence times (W/F ratios, where W denotes the catalyst mass and F the feed rate), giving infinitesimally low conversions to primary products only. It was found that all three xylene isomers had initial selectivities different from zero deviating only slightly from thermodynamic equilibrium values. It is suggested that the near-equilibrium distribution of xylenes is due mainly to the high reaction temperatures allowing a fast adjustment of the isomerization equilibrium. The slightly enhanced para-selectivity at short residence times is attributed to mass transport effects, i.e., to product shape selectivity. A distinct correlation between para-selectivity of toluene disproportionation and the acid strength of Brønsted sites of the various ZSM-5-type metallosilicate (B, Al, Ga, Fe, Cr, Sb, As) catalysts has not been found (Figure 91).

For a series of gallosilicates, Choudhary et al.[476] reported a linear relationship (Figure 92b) between acid-catalyzed disproportionation of toluene and the concentration of strong acid sites (measured in terms of pyridine chemisorbed at 673 K). Furthermore, a linear dependence between the concentration of strong acid sites and the number of framework gallium atoms per unit cell was established. Altogether, the results show that toluene disproportionation proceeds on single sites without structural sensitivity. The turnover frequency per active site is constant, irrespective of the density of sites.

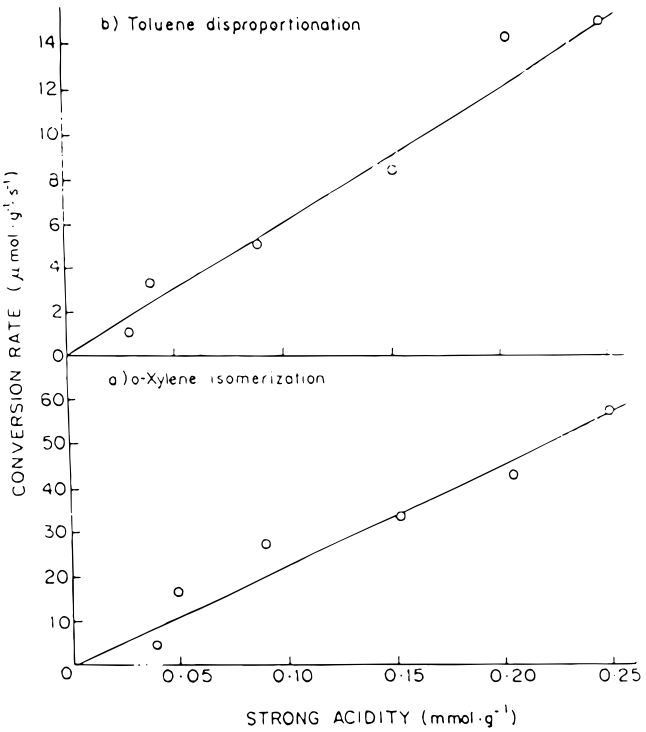

Figure 92. Relationship between the catalytic activity of hydrothermally treated H[Ga]-ZSM-5 samples and the concentration of Brønsted acid sites: (a) *o*-xylene isomerization, (b) toluene disproportionation. Pulse microreactor studies at (a) 400 and (b) 500 °C. (Reprinted with permission from ref 476. Copyright 1996 Academic Press.)

Two possible reaction pathways[519] over acid catalysts are discussed (Figure 93). The first pathway (Figure 93a) starts with protonation of a toluene molecule followed by transfer of the methyl group through a bimolecular transition complex. The subsequent step is the transfer of a proton of the dimethylbenzene carbocation to another toluene molecule. This mechanism does not account for the formation of fused-ring aromatics which represent coke components. The second mechanism (Figure 93b) starts with hydride-ion abstraction from the methyl group of the toluene (most likely preceded by protonation of a C−H bond of the methyl group) followed by the scission of molecular hydrogen. The benzyl cation forms a diarylmethane intermediate with a second toluene molecule. Rearrangement or deprotonation−protonation steps produce benzene and the dimethylbenzene carbocation. This scheme includes a route for coke formation starting from the diarylmethane intermediate.

Kinetics of toluene disproportionation over ZSM-5 catalysts are of pseudo-first order with an activation energy of 118.8 kJ/mol. The reaction rate depends linearly on the Si/Al ratio of the zeolite. *p*-Xylene in excess is observed for crystal sizes larger than 1 μm.[520]

Under mild conditions (reaction temperature 523 K), the conversion of ethylbenzene over acidic catalysts is predominantly restricted to the disproportionation to diethylbenzene (DEB) isomers and benzene. Whereas this reaction route is the only one occurring on Al- and Ga-silicate, styrene is dehydrogenated over [B]-ZSM-5[271,521] and [Fe]-ZSM-5. It is

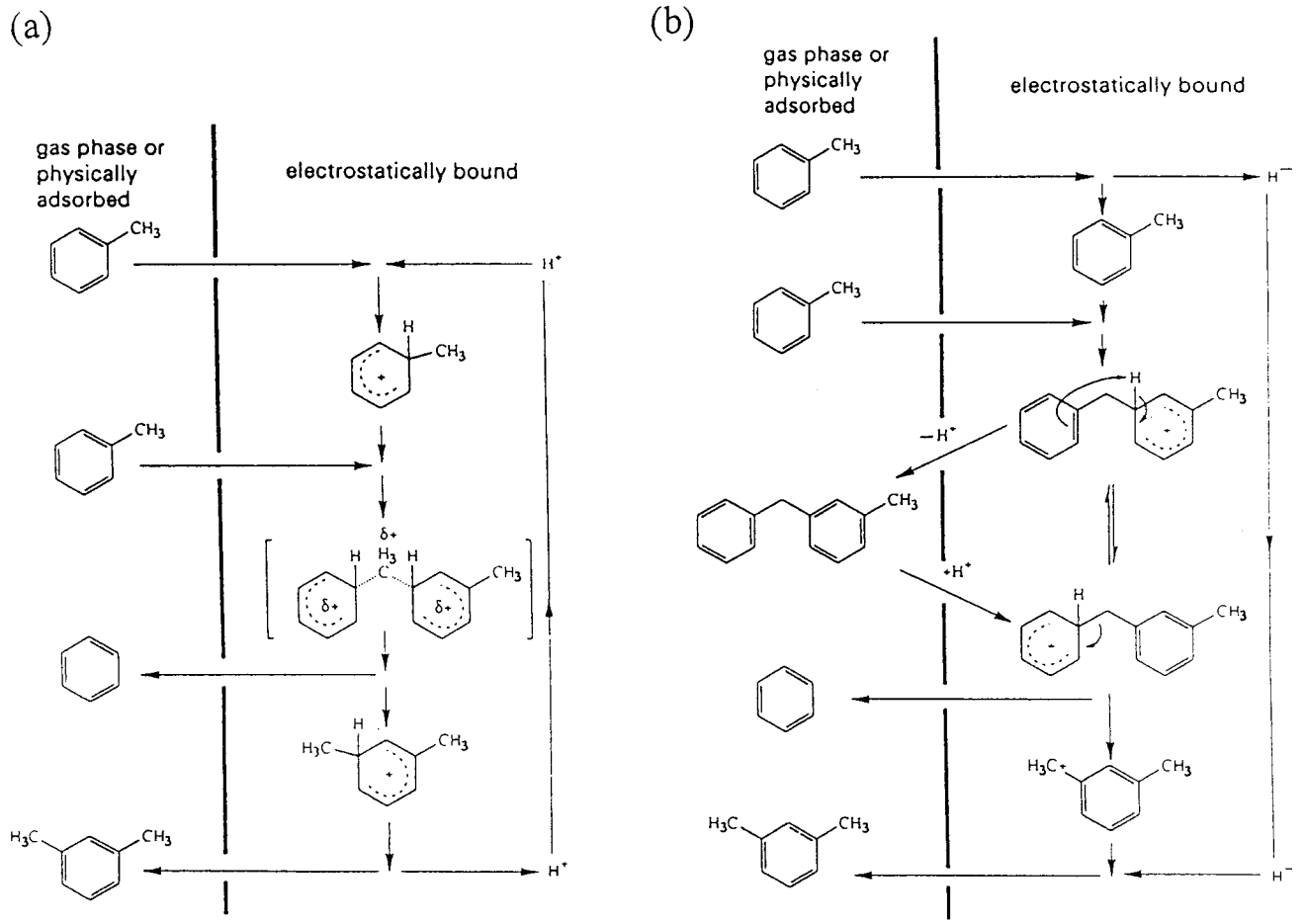

Figure 93. Scheme for disproportionation of toluene by (a) protonation forming carbocations and (b) hydride ion abstraction forming benzyl cations. (Reprinted with permission from ref 519. Copyright 1994 The Royal Society of Chemistry.)

suggested that dehydrogenation of ethylbenzene over [Fe]-ZSM-5 is performed by nonframework oxidic iron species.[141,522] Characteristically, the formation of *o*-DEB is suppressed over ZSM-5-type catalysts. The ratio of *m*- to *p*-DEB achieves nearly the thermodynamic value. With longer times on stream, the portion of *p*-DEB increases owing to coke deposition which narrows the effective pore diameter. At 688 K, disproportionation of ethylbenzene proceeds with lower activity over [Ga]-ZSM-22 (Si/Ga = 278, WHSV = 5 h^{-1}) than over [Al]-ZSM-22 (Si/Al = 208, WHSV = 7 h^{-1}). The degree of conversion is in the range between 3% and 8%.[160] Deactivation is found to be less severe with [Ga]-ZSM-22.

The disproportionation of xylenes is one of the secondary reactions accompanying isomerization of xylenes. The disproportionation/isomerization ratio D/I, defined as the ratio of toluene to the sum of xylene isomers, is tunable through a modification of the strength of the acid sites. Generally, gallosilicates exhibit a lower D/I ratio than aluminosilicates[523] (Figure 94).

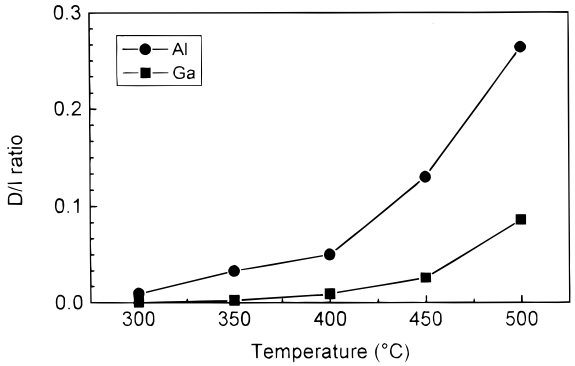

Figure 94. Ratio between disproportionation and isomerization of xylenes (*D*/I) over H[Al]-ZSM-5 (Si/Al = 20) and H[Ga]-ZSM-5 (Si/Ga = 26). Reaction conditions: catalyst mass 1 g, gas feed 1 vol % of *m*-xylene in N_2, flow rate 10 L/h. Steady values after 5 h time on stream. (Reprinted with permission from ref 242. Copyright 1992 Wiley-VCH.)

4. Isomerization

Besides the technological interest in the conversion of *m*-xylene of the C_8 fractions into the valuable *p*-xylene, the isomerization of xylenes is considered a model reaction for probing shape-selective zeolite properties. Owing to its small kinetic diameter (para 0.67 nm, meta 0.71 nm, ortho 0.74 nm), *p*-xylene has the highest diffusivity among the isomers in medium pore MFI structures. Additional influences on the mass transport resistance occurring by zeolite modification causes an alteration of para-selectivity.

The previously estimated high diffusivity of *p*-xylene as compared with the other isomers could not be confirmed experimentally. The difference in favor of *p*-xylene diffusity is only 1 rather than 3 orders of magnitude.

Xylene isomerization is accomplished by Brønsted acidic sites. An additional hydrogenating/dehydrogenating activity of the catalyst is not required. The first step is the interaction between aromatics and protons of the Brønsted sites giving carbocations (carbenium ions). The attack takes place at a ring C atom bearing a CH_3 group followed by a subsequent 1,2 rearrangement of the methyl group. In analogy to liquid-phase isomerization, a bicyclic intermediate is assumed to occur.

The stability of the carbenium ions virtually determines the isomer distribution. Owing to its high ability to compensate for the positive charge of the ion, *m*-xylene is the abundant isomer under equilibrium conditions. This mechanism is the only one reconcilable with the proposed stepwise reaction

$$o\text{-xylene} \leftrightarrow m\text{-xylene} \leftrightarrow p\text{-xylene} \qquad (36)$$

because a direct transformation of *o*-xylene into *p*-xylene and vice versa would require a bridge to the next but one C atom temporarily canceling the aromatic state. The absence of a direct ortho−para transformation is confirmed by kinetic measurements. *m*-Xylene is the only product formed at low conversions of either *o*- or *p*-xylene.

Due to their electron-donating properties (+I effect), alkyl substituents at the aromatic ring enhance the electron density in ortho and para ring positions directing alkylating carbenium ions to these positions. With xylenes, the meta-isomer is favored thermodynamically, whereas from a geometrical point of view, the para-isomer has the most favorable shape allowing easy movement in small channels of the zeolite.

Recently, Corma et al.[504] proposed that the isomerization of xylenes over faujasites with Si/Al ratios between 4.3 and 99 can proceed following a bimolecular reaction. Arguments were provided by results of kinetic measurements. (i) Turnover frequencies (i.e., the number of molecules reacting per active site and time unit) should tend to be constant at a complete site isolation (which is claimed to be achieved at a Si/Al ratio of 99). Experimentally, however, a volcano-type curve was observed over the whole Si/Al range of tested faujasites. (ii) The isomerization of a mixture of *p*-xylene with its perdeuterated analogue $CD_3C_6H_4CD_3$ yielded "mixed" *m*- and *o*-xylene with one $-CH_3$ and one $-CD_3$ group. This implies a bimolecular reaction pathway with an intermediate formation of trimethylbenzenes which are transalkylated by further *p*-xylene. The reaction over MFI structures, however, gave no indication of a substantial participation of bimolecular isomerization.

As found with the disproportionation of toluene, a linear relationship between the concentration of strong acid sites and catalytic activity is observed for the isomerization of *o*-xylene (Figure 92a).[476]

The deterioration of the catalytic performance of H[Ga]-ZSM-5 by degalliation after calcination or steaming is shown in Figure 95.

A typical product distribution of the conversion of C_8 alklyaromatics over [Ga]-ZSM-5 and [Al]-ZSM-5, received under technical conditions, is shown in Figure 96.[523] It is found that the reaction proceeds with lower extents of side reactions, e.g., with disproportionation is suppressed. Results found in lab-scale investigations over [Ga]-ZSM-5 for the isomerization of *m*-xylene discussed before are confirmed.

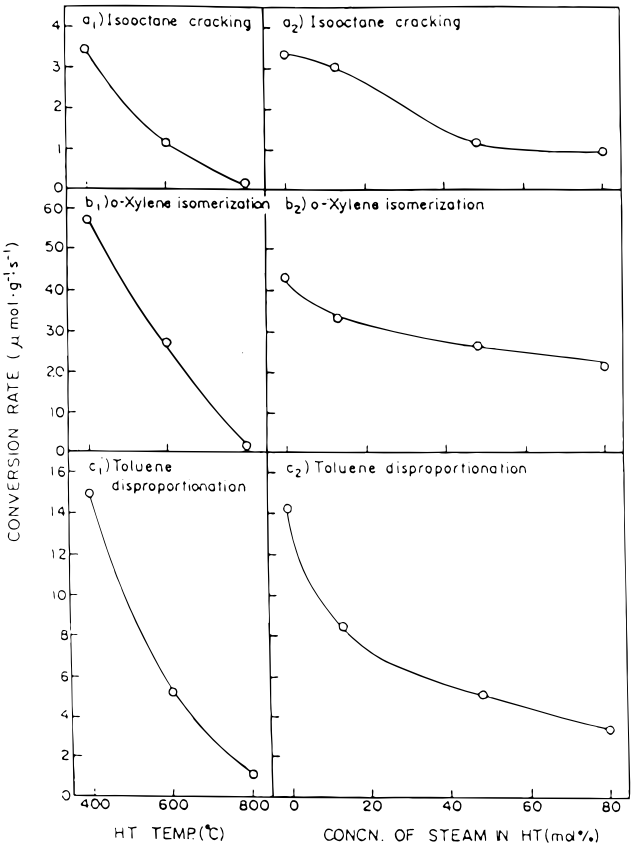

Figure 95. (a) Isooctane cracking at 673 K, (b) *o*-xylene isomerization at 673 K, and (c) toluene disproportionation at 773 K over hydrothermally treated H[Ga]-ZSM-5. Influence of steaming temperature (concentration of steam: 48 mol %) and steam concentration (temperature 873 K) on the conversion rates. (Reprinted with permission from ref 476. Copyright 1996 Academic Press.)

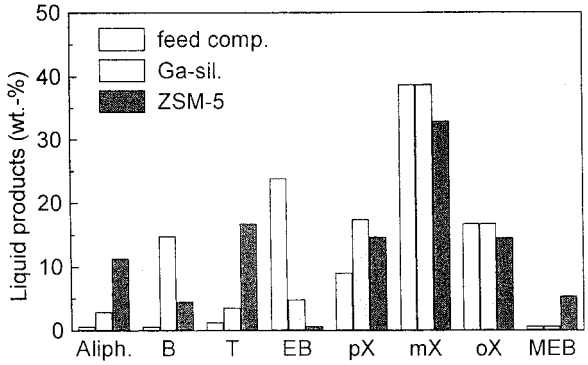

Figure 96. Conversion of C_8 alkylaromatics over Pt-modified [Ga]-ZSM-5 (40 wt % boehmite binder) and Pt-modified [Al]-ZSM-5 (50 wt % boehmite binder). Pilot plant results, reaction conditions: $T = 693$ K, $p = 1.25$ MPa, feed = 9% C_8 aromatics in hydrogen, charge = 2 LHSV, time on stream 180 h. (Reprinted with permission from ref 539. Copyright 1994 Baltzer Science.)

The acid-catalyzed isomerization of 1,3,5-trimethylbenzene (1,3,5-TMB, mesitylene) is of technical interest because the 1,2,4-isomer (pseudocumene) can be further converted to trimellitic acid/anhydride, the

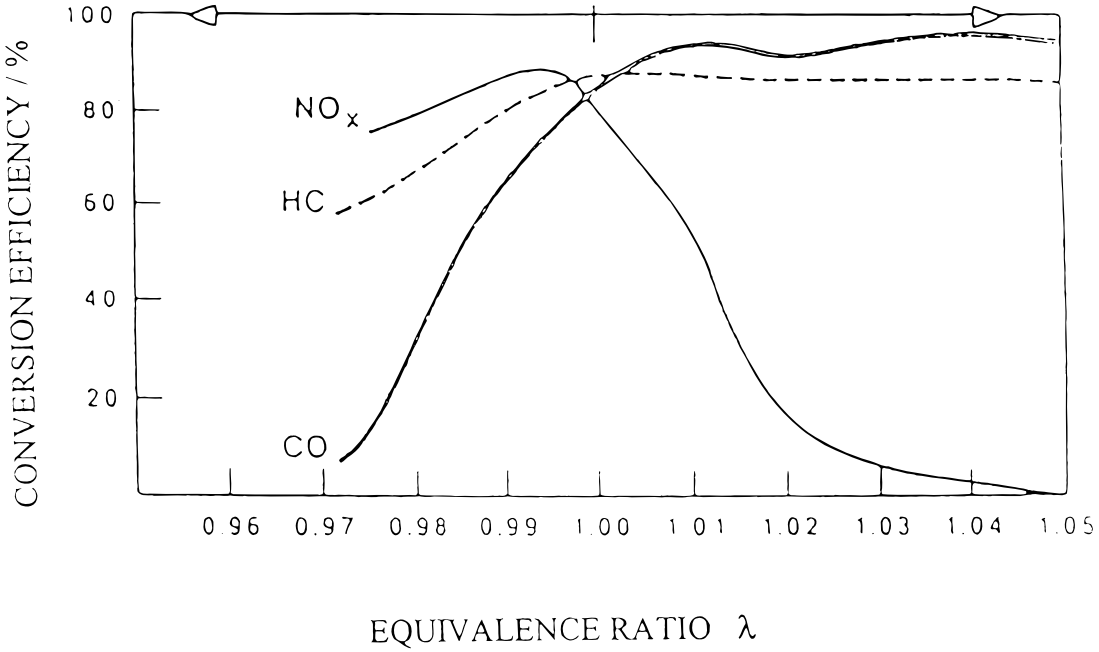

Figure 97. Effect of exhaust gas stoichiometry on the conversion efficiency over a noble metal three-way catalyst. (Reprinted with permission from ref 527. Copyright 1992 Baltzer Science.)

starting material for the manufacturing of plasticizers, polyesters, and temperature-resistant polyimides.

Sasidharan and Kumar[524] studied the isomerization of 1,3,5-TMB over the large pore substituted NCL-1 zeolite with a void space comparable to mordenite.[525] Conversion was found to decrease in the order Al > Ga > Fe-NCL-1 under comparable conditions, whereas the selectivity of the isomerization (competing with disproportionation) obeyed the reverse order. This is in accordance with the view that isomerization selectivity increases with decreasing acid strength for a given zeolite structure. The reaction is thought to proceed via the classical 1,2-methyl shift.

C. NO_x Reduction

Over conventional three-way catalysts (TWC), the three main pollutants of internal combustion engine exhaust gases, i.e., carbon monoxide, hydrocarbons, and nitrogen oxides, are converted to an extent of more than 90%. The TWC systems have to be operated around the so-called stoichiometric point (corresponding to a λ equivalence ratio of 1), where neither air nor fuel is in excess at the intake to the engine (Figure 97)

To guarantee a λ value of 1, a ratio of 14.7 parts of air to 1 part of gasoline is required for a typical gasoline composition. Lean operation of the engine involves the burning of fuel with an excess of air. Under lean conditions, however, the TWC cannot accomplish an efficient NO_x ($x = 1, 2$) reduction. To meet legal requirements for lower NO_x emissions[526] under lean burn conditions, new catalyst systems are under development. A vast majority of scientific work has been devoted to Cu-modified zeolites. Currently Ga- and In-modified zeolites are considered to be promising alternatives when methane is applied as reductant. Typical conditions for catalytic testing are adjusted to an average exhaust gas composition of Otto engines at a medium performance level: 1000−2000 ppm NO, 500−1500 ppm hydrocarbons (HC), and 1−3 vol % of oxygen. The desired main reaction is the reduction of NO to molecular nitrogen (for the sake of clarity, the reaction is formulated assuming methane as hydrocarbon substitute)

$$2NO + CH_4 + O_2 \rightarrow N_2 + CO_2 + 2H_2O \quad (37)$$

Simultaneously, methane is oxidized by molecular oxygen

$$CH_4 + 2O_2 \rightarrow CO_2 + 2H_2O \quad (38)$$

A good catalyst should promote reaction 37 but should suppress direct oxidation of hydrocarbons by oxygen according to reaction 38. Thus, a selectivity factor $\alpha = 0.5X_{red}/X_{total}$ can be defined where X_{red} represents the CH_4 conversion according to reaction 37 and X_{total} the overall conversion of methane according to reactions 37 and 38. The constant 0.5 accounts for the stoichiometry of the reaction steps.

Further secondary reactions are

$$2CO + 2NO \rightarrow 2CO_2 + N_2 \quad (39)$$

where CO is either present in the exhaust gas or formed during the incomplete oxidation of the hydrocarbons. Separate studies of reaction step 39 revealed that CO is not an efficient reductant for NO.

In the presence of steam, the water gas shift reaction proceeds

$$CO + H_2O \rightarrow CO_2 + H_2 \quad (40)$$

and NO is hydrogenated to ammonia

$$^5/_2H_2 + NO \rightarrow NH_3 + H_2O \quad (41)$$

which is an undesired side reaction leading to a secondary emission of ammonia.

The direct decomposition of NO according to eq 42

$$NO_{(g)} \rightarrow {}^1/_2N_2 + {}^1/_2O_2 \qquad (42)$$

is thermodynamically possible ($\Delta G° = -86.6$ kJ/mol at 298 K), but activities of all catalyst systems tested so far are not sufficiently appealing for industrial exploitation.

The main applications of Ga-based catalyst systems are summarized in Table 22, including reaction conditions and achieved maximum performances.

Predominantly formulated catalysts are MFI-type structures modified by gallium ion exchange. Other zeolite structures involved are ferrierite, mordenite, and Y. Gallium silicates (besides further metallosilicates) with MFI structure were investigated by Inui et al.[527] Methane, ethane, propane, propene, *n*-octane, and cetane served as reductants. Results of the decomposition of NO in the presence of 10 vol % O_2 found by Witzel et al.[528,529] over MFI and MEL ion-exchanged with Co^{2+}, Ni^{2+}, and Cu^{2+} point to a correlation between rates of formation of N_2 (from NO) and of CO_2 (from methane, propane, isobutane, isoheptanes, or isooctanes) which is independent of the applied hydrocarbon (provided that the flux of carbon to the system was maintained constant, Figure 98).

Inui et al.[33] studied the effect of the kind of hydrocarbon for the NO reduction in the presence of 10 vol % O_2 for Ga-, Fe-, and Co-silicate MFI structures. Figure 99 presents the results obtained over the Ga-silicate catalyst with various hydrocarbon reductants (propane, propene, *n*-octane, and *n*-cetane) at constant molar concentrations of carbon. The effect is not very pronounced but nevertheless visible. The largest conversion is observed with propane at a maximum reaction temperature of 873 K.

Yogo et al.[530,531] compared the ability of H-ZSM-5 (Si/Al ratio 46.6), Ga-ZSM-5, and Cu-ZSM-5 (the latter two prepared by ion exchange from the parent H-ZSM-5) to convert NO in the presence of 200−1000 ppm propane and 10 vol % O_2. Ga-modified ZSM-5 is far better than the Cu-modified version, which is even less active than unmodified ZSM-5. This indicates that the reaction can be accomplished to a considerable extent in the absence of any metal-related redox centers. Besides Cu-ZSM-5, samples modified by Zn or Sn yielded poorer results than H-ZSM-5. At temperatures between 573 and 673 K, In-ZSM-5 alone was found to develop an activity comparable to that of Ga-ZSM-5 but it suffered a decline of activity at further increased temperatures. The investigation of other parent zeolites modified by Ga ion exchange, e.g., mordenite (Si/Al ratio = 38.6), ferrierite (Si/Al ratio = 35.6), and zeolite Y (Si/Al ratio = 29.0), showed that at 773 K mordenite and ferrierite are nearly as active as ZSM-5.

Over H forms of zeolites, the selectivity for NO reduction by methane in the presence of O_2 was found to decrease in the order H-ferrierite > H-mordenite > H-ZSM-5 ≫ H−USY while the conversion of NO and methane was highest on H-ZSM-5, maximum NO conversion not exceeding 50%.[531]

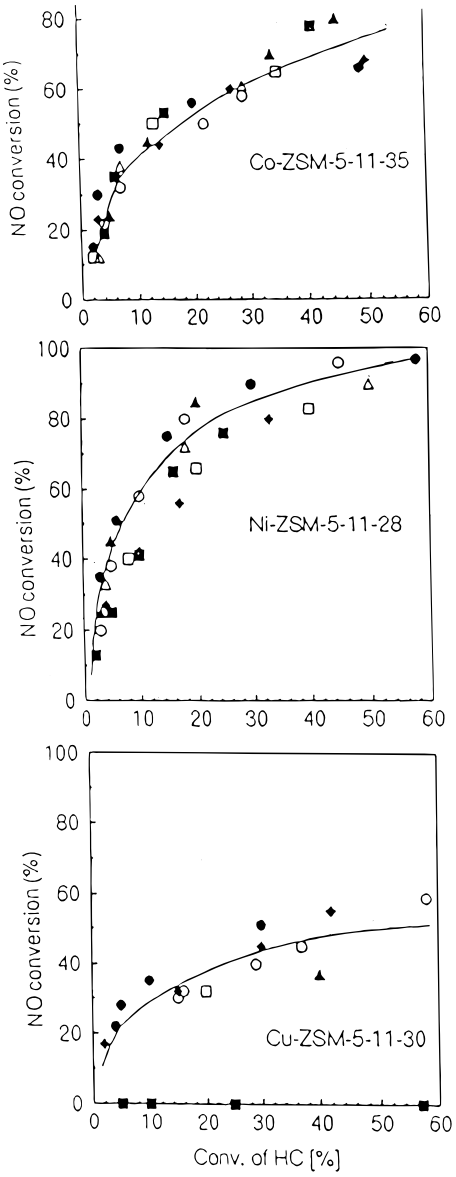

Figure 98. NO conversion to N_2 vs hydrocarbon (HC) conversion to CO_2 over Me-modified ZSM-5 catalysts, hydrocarbon conversion being adjusted by variation of the reaction temperature. Si/Al atomic ratio 11; exchange degrees 35% (Co), 28% (Ni), and 30% (Cu). Catalyst mass 0.25 g; feed gas 0.2 vol % of NO, 10 vol % of O_2. (■) methane (0.8%), (□) propane (0.27%), (▲) isobutane (0.2%), (△) pentane (0.16%), (◆) neopentane (0.16%), (○) 3,3-dimethylpentane (0.11%), (●) 2,2,4-trimethylpentane (0.1%). (Reprinted with permission from ref 529. Copyright 1994 Elsevier Science.)

Li and Armor[32] confirmed that zeolite protonic acidity is necessary for NO reduction: In contrast to H,Ga-ZSM-5, Na,Ga-ZSM-5 was inactive. The authors concluded that a synergism does exist between Ga species and H^+ enabling the catalyst to activate the reductant (methane) for NO decomposition in the presence of O_2. In the NO reduction, Ga-H-ZSM-5 was more selective than Co-ZSM-5 but the former is more sensitive to water. Kikuchi and Yogo[532] had the same experience. NO reduction over Ga-H-ZSM-5 is strongly inhibited by steam. Indium-based zeolite

Table 22. Selective Catalytic Reduction of NO_x in Excess Oxygen over Ga-Containing Catalysts

Catalyst formulation	Reductant	Reaction conditions	Maximum conversion at T	Comparison	Ref.
Ga-ZSM-5, (Si/Al = 46.6), ion exchanged (92%), Ga-ferrierite, Ga-mordenite, Ga-USY	Methane	Flow reactor, feed: 1000 ppm NO, 150-2000 ppm CH_4, 10% O_2, balance He, 0.05-0.5 g catalyst, flow rate: 100 cm^3/min, 573 - 873 K	90% at 773 K over Ga-ZSM-5, 1000 ppm methane, 0.5 g catalyst	Ga-free zeolites, Indium ion exchanged zeolites, unsupported Ga_2O_3, Ga/Al_2O_3, Al_2O_3,	532
as in Ref. (532)	Methane	as in Ref. (532), additionally transient response catalytic measurements	90 % at 773 - 873 K	In-ZSM-5	531
as in Ref. (532)	Methane, Ethane	as in Ref. (532)	100 % at 773 - 873 K over Ga-ZSM-5 and ethane as reductant	Al_2O_3	570 571
as in Ref. (532)	Propane	as in Ref. (532), 1000 ppm propane	91.1 % at 673 K over GaH-ZSM-5, exchange degree 79%	Al-, Zn-, In-, Sn-, Cu-ZSM-5, ion exchanged	530, 572
Ga-ZSM-5 (Si/Al = 12), ion exchanged, 4.2 wt.-% of Ga, Ga-mordenite, (Ga/Al = 0.40) ion exchanged, 5.3 wt.-% of Ga, Ga-Y, (Ga/Al = 0.37) ion exchanged, 8.9 wt.-% of Ga,	Methane	Flow reactor, feed: 1610 ppm NO, 1000 ppm CH_4, 2.5% O_2, He balance, flow rate 100 cm^3/min, GHSV = 30 000 h^{-1}, 623 - 823 K	34 % at 773 K over GaH-ZSM-5	Ga/ZSM-5 impregnated, Ga/Na-ZSM-5, impregnated Ga/γ-Al_2O_3, impregnated, 3.2 wt.% Ga each, Co-ZSM-5	32
Ga-ZSM-5 (Si/Al = 100), ion exchanged, 1.2 wt.-% Ga,	Methane	Ultra high vacuum system, TPD, heating rate 100 K/min, Isotopic exchange in a closed circulation system using CD_4	Ga-ZSM-5 did not adsorb oxygen, dissociative adsorption of methane	Cu-ZSM-5	535
[Ga]-ZSM-5, rapid crystallization method, Si/Ga = 20	*n*-Cetane	Flow reactor, feed: 1.0 vol.-% NO, 1320 ppm *n*-$C_{16}H_{34}$, 10 vol.-% O_2, balance He, GHSV = 2500 h^{-1}, 423 - 873 K	100 % at 623 K over [Fe]-ZSM-5, (Si/Fe = 25)	[Al]-, [Fe]-, [Mn]-, [Cr]-, [Cu]-ZSM-5	527
as in Ref. (527)	*n*-Cetane	Flow reactor, feed 1 000 ppm NO, 560 ppm *n*-$C_{16}H_{34}$, 10 vol.-% O_2, balance N_2, SV = 30 000 h^{-1}	55.5 % at 873 K	[Al]-, [Fe]-, [Co]-, [Ni]-, [Mn]-, [Cu]-ZSM-5	33
as in Ref. (527)	*n*-Octane, (propane, propene, *n*-cetane)	Flow reactor, feed: 1000 ppm NO, 1100 ppm *n*-C_8H_{18}, 10 % O_2, balance N_2, GHSV = 30 000 h^{-1} 473 - 873 K	70% at 873 K over [Ga]-ZSM-5 and with propane as reductant	[Co]-, [Fe]-ZSM-5	495

$Ga/S-ZrO_x$, S-GaZr/Zeolite (ZSM-5, Mordenite, Ferrierite, Y)	Propane, propene, methane, CO	Flow reactor, feed 250 ppm NO, 333 ppm C_3 (1000 ppm C_1 and CO), 10 % O_2, 50 ppm SO_2, GHSV ca. 75 000 h^{-1}	65 % at 848 - 863 K over $Ga/S-ZrO_x$ (4 wt.-% Ga). 75 % at 873 K over S-Ga/Zr/ZSM-5 (reductant propane)	Cu-ZSM-5 (Si/Al = 80), 3 wt.-% Cu by ion exchange	496
Ga-supported sol-gel alumina	Methane, ethene, propene, methanol, ethanol, 2-propanol	Quartz flow reactor, feed: 1000 ppm NO, 1000 ppm reductant (400 ppm 2-propanol), 10 vol.-% O_2, 0 or 8 vol.-% H_2O, GHSV ca. 10 000 h^{-1}	100 % at 773 K (reductant propene, dry feed) 60 % at 823 K (reductant propene, wet feed)	Co, Ag and Sn supported on sol-gel alumina	497

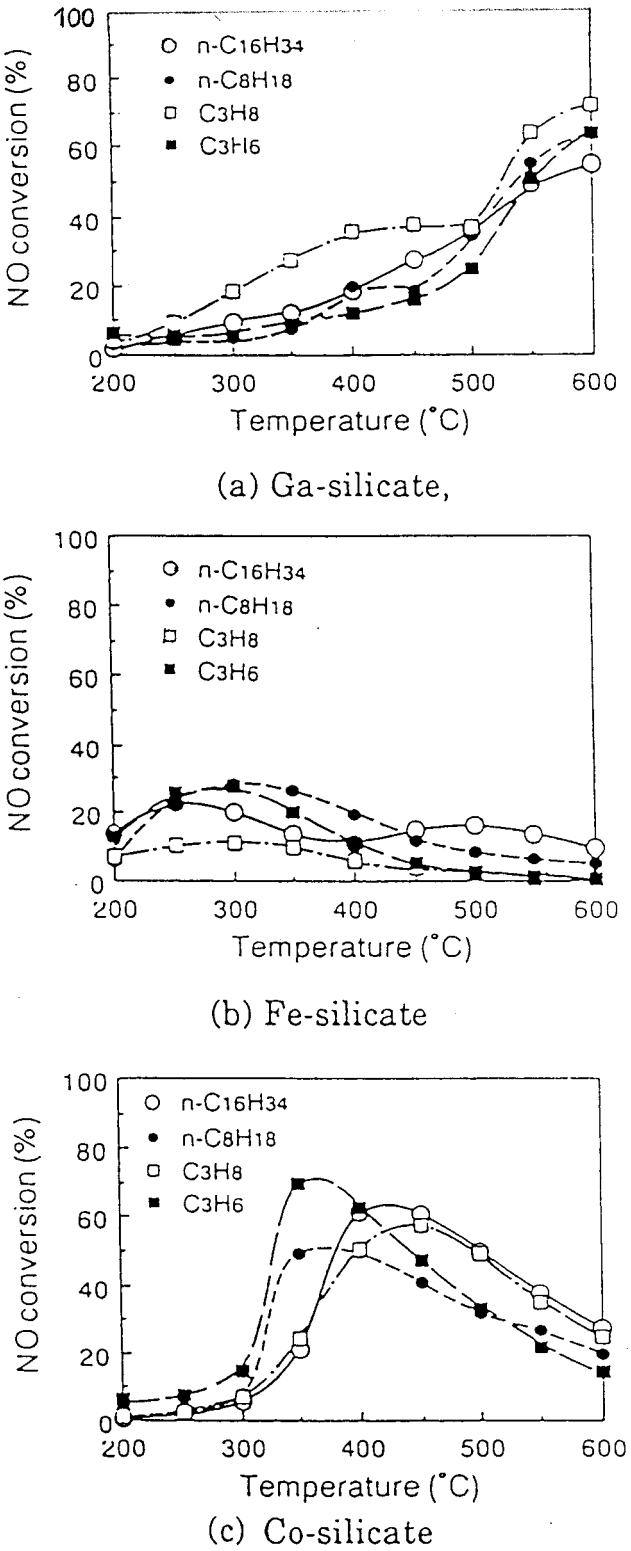

Figure 99. Conversion of NO over various metallosilicate catalysts. Effect of the temperature and the kind of the hydrocarbon: (a) Ga-silicate, (b) Fe-silicate, and (c) Co-silicate. Feed: 1000 ppm NO, 10.0 vol % of O_2 and hydrocarbons, balance nitrogen. Space velocity: 30 000 h^{-1}. (Reprinted with permission from ref 513. Copyright 1994 Baltzer Science.)

modifications are claimed to be more resistant against steam while preserving fairly high activities.

One question addressed separately by the authors is that on the intermediate state of NO_2 in the NO conversion process. The equilibrium of the reaction

$2NO + O_2 \rightleftarrows 2NO_2$ lies far to the right at room temperature but is shifted to $NO + O_2$ at the applied reaction temperature. Owing to the very short residence time of the gas which practically removes any NO_2 formed immediately from the reaction zone, equilibrium cannot be established. Separate studies of NO oxidation by O_2 were aimed at clarifying how far NO_2 formation takes place under the conditions of the overall process. Shelef et al.[533] studied this reaction step over H-ZSM-5 (Si/Al ratio = 60) and Cu-ZSM-5 (2.41 wt % Cu) with inlet concentrations of 500 ppm NO and 4.9 vol % O_2. They found that Cu-ZSM-5 was quite active in the NO_2 formation, reaching ca. 350 ppm NO_2 between 573 and 673 K. The parent H-ZSM-5, however, was only marginally active. Blank experiments with the empty reactor gave no NO conversion. In the absence of oxygen, NO_2 is decomposed into NO but not reduced to N_2. Experimental results neither support nor deny the role of NO_2 as an intermediate. Yogo and Kikuchi[531] found a considerable activity of H-ZSM-5 (Si/Al ratio = 11.7) for the oxidation of NO (1000 ppm NO, 10 vol % O_2, GHSV ca. 60 000 h^{-1}) to NO_2 reaching 40% NO conversion at 573 and 673 K and ca. 20% at 773 K. The negative temperature dependence indicates that at temperatures above 673 K, the conversion is limited by thermodynamics. NO is primarily oxidized to NO_2 at zeolitic acid sites. Subsequently, NO_2 interacts with methane adsorbed at Ga or In sites yielding an activated intermediate, which, as derived from transient kinetic studies, reacts either with NO to give CO and N_2 in equimolar ratios or with gaseous NO_2 yielding CO_2 and N_2. In further work, Kikuchi et al.[534] studied the conversion of both NO and NO_2 (1000 ppm each) in the presence of 1000 ppm methane and 10 vol % O_2 over Ga- and In-containing zeolite ZSM-5 (Ga loading 2.4 wt %). The modification was accomplished either by conventional ion exchange or by mechanical mixing of the oxides with the H or the Na form of the zeolite (Si/Al ratio = 11.7). Calcination of the physical mixtures at progressively increased temperatures was performed in dry oxygen. Ga-ZSM-5 gained by ion exchange yielded nearly the same levels of conversion to N_2 with both NO and NO_2 as reactants (GHSV = 7200 h^{-1}, T = 673, 773, and 873 K). The degree of conversion of NO_2 over the Ga_2O_3/H-ZSM-5 mechanical mixture is distinctly lower and corresponds nearly to the activity of the nonmodified H-ZSM-5. Nonsupported Ga_2O_3 exhibits only a marginal activity. The mechanical mixture of Ga_2O_3 and Na-ZSM-5 is nearly inactive, see Figure 100.

The nearly identical conversion levels for NO and NO_2 seem to indicate that an equilibrium between NO, NO_2, and O_2 is established. The fact that ion-exchanged Ga-ZSM-5 showed the best performance as compared with the other catalyst preparations underlines the necessity of the presence of both Brønsted acidity and redox capacity for NO and NO_2 reduction.

To explain the oxidative properties of H-ZSM-5, an adsorption of oxygen at Lewis acid sites with activation by an electrostatic polarization through the zeolite framework is suggested. Calcination of protonic zeolites partially converts Brønsted into Lewis acid sites by dehydroxylation. The conversion of NO to NO_2 increases after calcination of H-ZSM-5, confirming that Lewis acid sites are involved in the reaction. The origin of the selectivity of Ga-modified zeolites for the selective NO reduction is not fully understood. Tabata et al.[535] performed comparative studies characterizing adsorption properties of Ga-ZSM-5 (and Cu-ZSM-5) for oxygen and methane in an ultrahigh vacuum system by temperature-programmed desorption. Results show that Cu-ZSM-5 is able to adsorb O_2 dissociatively while Ga-ZSM-5 did not adsorb O_2 at all. It is, however, not clear whether differences between the types of adsorption are of significance for the steady-state reaction under normal pressure.

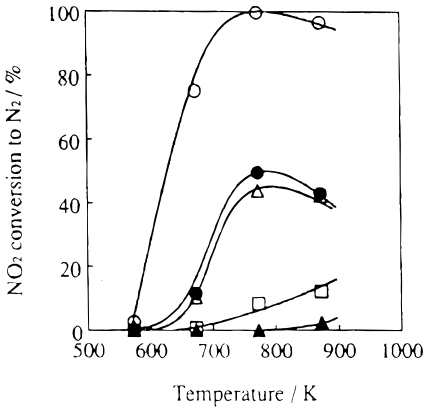

Figure 100. Ga-containing catalysts. Conversion of NO_2 to N_2 over the reaction temperature, gas feed: 1000 ppm NO_2, 1000 ppm methane, 10 vol % O_2; GHSV = 7,200 h^{-1}. (○) Ga-H-ZSM-5, ion exchanged, 2.4 wt % Ga, (△) Ga_2O_3/H-ZSM-5, mechanical mixture, 2.4 wt % of Ga, (▲) Ga_2O_3/Na-ZSM-5, (□) Ga_2O_3, treated at 813 K, (●) H-ZSM-5 (Si/Al ratio = 11.7). (Reprinted with permission from ref 534. Copyright 1996 Academic Press.)

Metal cations with a reduced oxidation state like Cu^+ or Ga^+, probably present after reductive activation, might regain higher oxidation states by interaction with oxygen under reaction conditions. Results obtained for Cu-modified zeolite systems imply that just the maintenance of a low steady valence state (+1) of copper is essential for catalytic activity. Thus, the observed inertness of Ga-ZSM-5 toward O_2, favoring the lower valence states of Ga despite the oxygen excess, might explain the better catalytic performance of Ga-ZSM-5 as compared with Cu-ZSM-5. IR studies of the latter showed that NO can be coordinatively bound to Cu^+ forming dinitrosyl complexes.[536] Bands for the mononitrosyls on both Cu^+ and Cu^{2+} are observable even at higher temperatures (473 K). This lends support to the idea that NO disproportionates to N_2O and NO_2, the latter decomposing to N_2 and O_2. The dinitrosyl complex formed on a Cu^+ site would facilitate the coupling of two nitrogen atoms. Analogous experiments for the Ga zeolite system have not been reported so far.

Miyamoto et al.[537] simulated the location of gallium species such as Ga^{3+}, GaO^+, $Ga(OH)^{2+}$, and $Ga(OH)_2^+$ inside the pore system of ZSM-5 by molecular modeling. It was found that the gallium behavior is similar to that of copper in that it tends to migrate toward

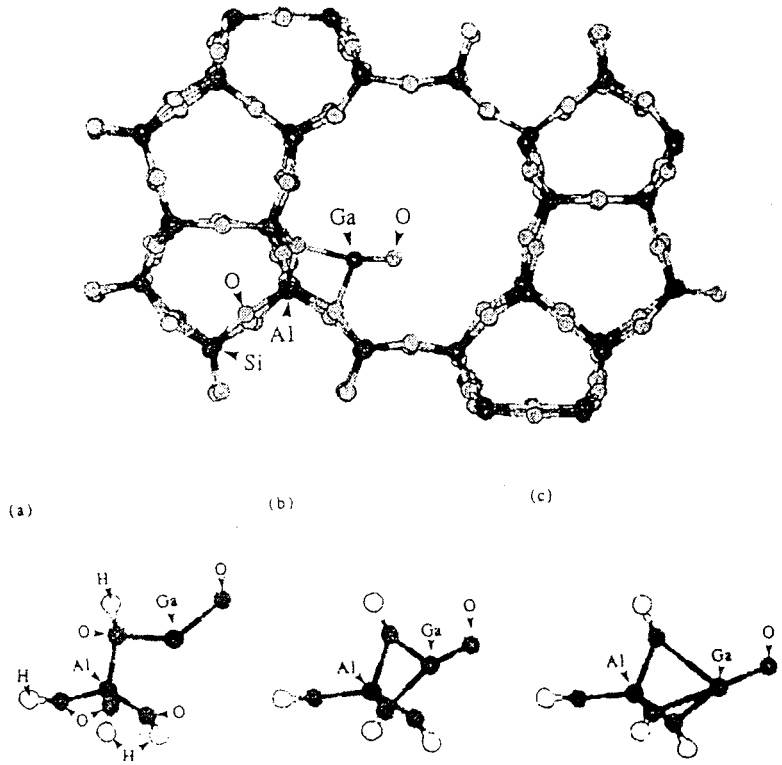

Figure 101. Cluster models with (a) single, (b) double, and (c) triple connection of the GaO unit in the ZSM-5 framework. (Reprinted with permission from ref 538. Copyright 1995 American Chemical Society.)

the T12 site. Coordination of a maximum of three $Ga(OH)_2^+$ ions is derived with Ga located near framework aluminum. Dehydration of $Ga(OH)_2^+$ is thought to yield GaO^+

$$Ga(OH)_2^+ \rightarrow GaO^+ + H_2O \qquad (43)$$

Furthermore, it was found that water is preferentially adsorbed at GaO^+ or $Ga(OH)^{2+}$ generating $Ga(OH)^{2+}$. Hydroxylation (reverse reaction of eq 43) increases the coordination of Ga ions rendering the adsorption of NO more difficult. Oxygen attached to Ga^{3+} should exhibit a high mobility, thus facilitating the approach of NO and/or hydrocarbons to the Ga^{3+}.

Himei et al.[538] applied quantum chemical methods, molecular dynamics, and computer graphics for modeling the adsorption and activation of methane at Ga^{3+}-exchanged ZSM-5 catalysts to a study the CH_4-based NO_x reduction under lean conditions. The authors considered GaO^+ cluster models fixed to basic oxygens of the zeolite lattice either through 1-, 2-, or 3-fold connection (Figure 101a−c).

Quantum chemical total energy minimization showed that the double-coordinated bridging site (Figure 101b) is the most stable. Activation of methane over this site with dissociation of a C−H bond yields CH_3 attached to Ga at a distance of 0.2 nm and H bound to nonframework oxygen. The estimated stabilization energy of −263 kJ/mol guarantees an energetically favorable complex. As methane activation is a crucial step for subsequent reduction of NO_x over Ga-ZSM-5 catalysts, the results might provide guidelines for the generation of appropriate catalysts.

According to results reported by Burch and Scire,[539] who performed NO reduction by hydrogen in the absence of oxygen, carbonaceous residues as active intermediates in the selective reduction of NO on zeolite-based catalysts should be of minor importance. Higher conversions than those observed by ethane or methane as reductants have been achieved. The reaction, however, could not be performed in the presence of O_2 because hydrogen preferentially reacts with O_2 rather than with NO. The authors considered the mechanism in the presence of oxygen to be of a simple redox-type. Adsorption and decomposition of NO_x proceeding at (reduced) metal sites are followed by removal of remaining adsorbed oxygen by the reducing hydrocarbon, thus restoring the (reduced) active site.

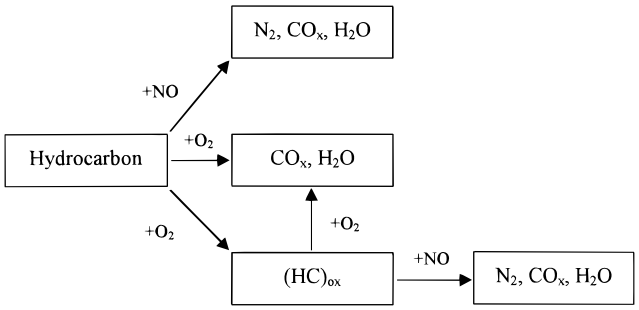

Figure 102. Reaction routes for NO conversion including the possible role of oxygenated hydrocarbon species at the catalyst surface.

Experimental results for the reduction of NO by hydrocarbons in excess oxygen point to the role of oxygenated hydrocarbon species as intermediates because NO conversion without gaseous oxygen is quite low compared with the conversion in the presence of oxygen. The reaction routes can thus be formulated schematically as shown in Figure 102.

Table 23. Main Properties of Various Metallosilicates with ZSM-5 Structure and Their Maximum NO Conversions[33]

metallosilicate catalysts					maximum data of NO conversion (%)				
							conversion of cetane (%)		
cat. no	kind of metal[a]	acidity[b]	redox[c] property	activity[d] for HC combustion	temp. (°C)	NO conv. (%)	to CO_2	to CO	to CO_2 + CO
cat. 1	none[e]	+	−	+	450	14.9	17	39	56
cat. 2	Al	+++++	−	+	600	27.1	53	47	100
cat. 3	Ga	++++	+	+	600	55.5	41	40	81
cat. 4	Fe	+++	+++	+++++	250	22.3	32	10	42
cat. 5	Co	++	++	+++	400	61.6	53	14	67
cat. 6	Ni	++	+++	+++	380	48.9	74	10	84
cat. 7	Mn	+	+++	+++	350	23.0	56	13	69
cat. 8	Cu[f]	+	+++++	++++	300	22.3	57	0	67

[a] Content of metal: Si/Me = 20, NO 1000 ppm, O_2 10.0%, N_2 diluted, SV = 30 000 h^{-1}. [b] Estimated by NH_3-TPD measurements, the unit is the amount of NH_3 adsorbed per unit catalyst weight. [c] Estimated by weight decrease by hydrogen reduction and oxygen uptake using a thermogravimetric analyzer, the unit is weight decrease or gain per unit catalyst weight. [d] Compared at oxygen excess using cetane as hydrocarbon, the unit is the amount of hydrocarbon converted by unit catalyst volume and unit time. [e] Si/Me = ca. 5000. [f] Si/Cu = 185.

Table 24. Methanol-to-Hydrocarbon and Related Processes over Ga-Containing Catalysts

reactant	products	conditions	catalyst formulation	ref
(i) methanol, (ii) C_2−C_4 olefins	gasoline	tubular flow reactor, 514−643 K, 20−100 mol % MeOH, GHSV = 400−4000 h^{-1}	Ga-silicate with MFI structure, prepared by the rapid crystallization method, Si/Me ca. 3200	469,221
(i) methanol, (ii) 2-propanol	(i) hydrocarbons, (ii) propene	tubular flow reactor, 633−653 K, LHSV = 1−5 h^{-1}	Ga-silicate analogues of zeolites X and ZSM-5: [Ga]-NaX, [Ga]-CaNaX, [Ga]-ZSM-5	575
methanol	olefins	fluidized bed microreactor, pulse mode, 623−723 K	Ga-erionite and Ga-mordenite (11.7 and 5.2 wt % Al_2O_3, respectively, in the gel)	341
methanol	olefins	flow recycling reactor, 643 K, 3−50 vol % MeOH	[Ga,Al]-ZSM-5 (Si/Al ratio = 37.5−200)	543
methanol	olefins	pulse microreactor, 723 K, 125 μmol MeOH pulses	MFI-gallosilicates, Si/Ga ratios 17.5, 24.6, 30.3, 51.6, 65.7	545
methanol	aromatics	pulse microreactor, 673 K, 0.4 μL pulses	MFI gallosilicates, Si/Ga ratios 33.0, 50.0, 68.0, 129	550
methanol	dimethyl ether gasoline	Pyrex capsule for in situ NMR measurements 423 K, 50 Torr MeOH	Aluminosilicate (Si/Al = 3.9), galloaluminosilicate (Si/Al = 4.5, Si/Ga = 25.7) and gallosilicate (Si/Ga = 3.8) offretites	573, 574
ethanol	hydrocarbons	high-pressure fixed bed flow reactor, 633 K, 10 bar, WHSV = 1 h^{-1}	H−ZSM-5 (Si/Al = 164), impregnated with Ga nitrate, 3 wt % of Ga	576

Recently, Inui[33] studied NO reduction properties of different Me-modified ZSM-5-based catalysts. He emphasized that appropriate acid strength and redox capacity are essential for an efficient NO_x reduction under lean conditions. This is shown for various metal components in Table 23.

MFI gallosilicates are reported to have a low redox capacity because the gallium-related sites are reducible only at higher temperatures. The acid strength of their Brønsted sites is fairly high. Therefore, good NO conversion levels are reached at relatively high temperatures only. High oxidation capacity for the hydrocarbon (as found for ferrisilicates) allows the reaction to proceed at low temperatures already. Increasing temperatures, however, shift the reaction to a mere oxidation of the hydrocarbon and the selectivity of NO conversion deteriorates.

Notwithstanding the knowledge and the mechanistic understanding of the removal of NO_x from O_2-rich exhausts by selective hydrocarbon reduction acquired so far, much has still to be done with respect to the design of an appropriate catalyst for practical application.[540] The progress reached in 1994 was recently summarized by Iwamoto.[541]

D. Methanol Conversion and Related Processes

Methanol is a versatile basic chemical. Its application as alkylating agent for the transformation of aromatics was described in section VI.B. The production of the gasoline additive methyl *tert*-butyl ether (MTBE) by the acid-catalyzed equilibrium reaction of methanol and isobutene over ion-exchange resin catalysts at low temperatures (330−350 K) consumed more than 20 million tons in 1994.[542] Methanol can be converted to gasoline, to aromatics, or to olefins over acidic catalysts at 670 K or higher temperatures. The chain length of olefins can be controlled by shape-selective zeolites to give maximum C_2 − C_4 olefin yields.

Applications of Ga-based zeolite catalysts are not very numerous, as can be seen from Table 24. Inui[469] tested a great variety of Al-free ZSM-5 catalysts containing Ga, Cr, V, Sc, Ge, Mn, La, Al, Ni, Zr, Ti, Fe, Co, and Pt at Si/Me ratios <3200. Characterization of catalysts is based upon methanol-to-hydrocarbon conversion at 573 K under flow conditions (GHSV = 2000 h^{-1}) using a gaseous mixture of 20% MeOH and 80% N_2. The zeolites would contain one Brønsted acid site per 33 unit cells provided that each

of the metal atoms has been incorporated into the framework. Fe-, Co-, and Pt-modified catalysts were found to be much more effective than [Al]-ZSM-5. Unfortunately, the authors gave no conversion data for methanol. Besides aliphatics, aromatics are detected among the products of reaction. Ga-modified ZSM-5 mostly produces C_5-C_{11} aliphatics.

Romannikov et al.[543] studied the methanol-to-olefin (C_2-C_4) conversion on Al,B-ZSM-5, Al-ZSM-5, Ga-ZSM-5, and Al,Ga-ZSM-5 containing the metals in framework and nonframework position, as well. At 643 K, GHSV = 3600 h^{-1} and methanol concentration = 3−50%. The selectivity of C_2-C_4 olefins is recorded to be dependent on the Me content. In any case, selectivity decreases with increasing Si/Me ratios. Compared with Al-ZSM-5, Ga-ZSM-5 catalysts exhibit higher selectivities of C_2-C_4 olefins, which is ascribed to their weaker acidity suppressing secondary reactions of the intermediate olefins. In further contributions, the Novosibirsk school studied hydrocarbon synthesis from methanol over B^{3+}-, Ga^{3+}-, and Fe^{3+}-modified zeolites of crystallographically pure erionite and mordenite structures at 623−723 K.[341,342] With erionite,[71]Ga MAS NMR spectroscopy revealed that ca. 50% of the Ga has remained outside the framework. The chemical (total) composition of the [Ga]-erionite was 0.21 mol of Ga_2O_3 per mol of Al_2O_3 corresponding to a Si/Ga ratio of 79. Catalytic studies were based on the pulse technique in a pseudofluidized catalyst bed with a feed gas containing 20 vol % of MeOH. Results are hardly comparable with those obtained under flow conditions. Olefin selectivity was found to be higher on [Ga]-erionite than on the corresponding [Ga]-mordenite. It should be noted that the Si/Al ratios of both catalysts were different (16.6 with erionite and 42.0 with mordenite), necessarily implying a higher concentration of acid sites for [Ga]-erionite. Despite a rather broad spectrum of the strength of acid sites, Brønsted sites at the mordenite can be assumed to be the stronger ones. According to given zeolite compositions, 0.03 mol of Na_2O was present in both structures and 0.28 mol of K_2O (per mol of Al_2O_3) additionally in the erionite. It is not reported whether residual Na^+ and K^+ ions were exchanged by H^+ ions. In particular, the exchange of K^+ ions within the erionite structure is not easy to accomplish.[544] Lalik et al.[545] used methanol conversion to dimethyl ether under mild conditions (T < 573 K) to check the Brønsted acidity of Al-free gallosilicates with various Si/Ga ratios (65.7, 51.6, 30.3, 24.6, 17.5) and a Ga-impregnated silicalite (Si/Ga = 19.8) as a reference. Scanning electron micrographs revealed a poor crystallinity and the presence of amorphous material with increasing amounts at higher Ga concentration.

Handreck and Smith[546] studied the morphology of gallosilicates (synthesized in the presence of 0.005 wt % Al_2O_3) by SEM images. At low Ga contents, samples consist of intergrown particles with a size of 1−3 μm. The morphology changes with increasing Ga contents. Polycrystalline aggregates with sizes of 0.3−1 μm are observed at higher Ga content. The highest achieved Ga content corresponded to a Si/Ga ratio of 34.4, i.e., 2.72 Ga atoms/unit cell. Detailed studies[242] revealed a dependence of the crystal morphology of [Ga]-ZSM-5 zeolites on synthesis time. Synthesized crystals generally had a well-defined shape, with spherical agglomerates dominating. On the basis of selectivity data for varying Ga contents, it is argued that Brønsted acidity associated with framework Ga is responsible for the formation of dimethyl ether (DME). At higher Ga concentrations (and higher temperatures), the nonframework Ga begins to operate favoring aromatization of olefins. Because of their capability to aromatize alkane/alkene intermediate products, Ga-containing zeolites are not well suited for an optimum production of light alkenes from methanol.

Ione et al.[275] investigated the properties of ZSM-11-type metallosilicates. [Al]-ZSM-11 proved to be the most active zeolite for the conversion of methanol to olefins. The selectivities of light olefins are 68.5% on [Al]-ZSM-11 (total conversion of methanol), 66.0% on [Ga]-ZSM-11, and 77.0% on [Fe]-ZSM-11 (degrees of conversion not specified).

The conversion of methanol to olefins over zeolites has currently been reviewed by Froment et al.[547] With microporous aluminophosphates[548] and their Si-substituted analogues, the chabazite structure SAPO-34 was found to be highly selective for the production of light olefins with molar selectivities up to 96% at 100% methanol conversion.[549] Thus, other catalyst systems seem less attractive.

The conversion of methanol to aromatics over [Ga]-ZSM-5 has been studied thoroughly by Choudhary and Kinage.[550] The authors used a batch of hydrothermally synthesized MFI gallosilicate in its Na^+ form and prepared samples with degrees of ion exchange (Na^+ with NH_4^+) for between 5% and 96%. A selected [Ga]-ZSM-5 sample (Si/Ga = 33, NH_4^+ exchange degree = 96%) was subjected to thermal (between 873 and 1373 K) or hydrothermal (between 676 and 1073 K) treatment. For each sample, the concentration of strong acidic Brønsted sites was determined by chemisorption of pyridine at 673 K using a GC pulse method. Prior to catalysis, the binder-free [Ga]-ZSM-5 (particle size 0.2−0.3 μm) was calcined. The catalytic reaction was performed at 673 in a K microflow reactor containing 0.1 g of catalyst by injecting pulses of 0.4 μL of methanol into a stream of pure nitrogen at a feed rate of 20 cm^3/min. Conversion and selectivities were calculated on the basis of the product analysis following the first methanol pulse. Thus, results do not reflect stationary values. Samples with an NH_4^+ exchange level of 96% and 4 h thermal pretreatment at 873 K were used (Figure 103a−c).he catalytically active sites were progressively poisoned by contacting the catalyst off-line with pyridine pulses, 3 μL each, at 673 K. The influence of the Si/Ga ratio on methanol conversion and product distribution was found to be moderate.

Nearly complete conversion of methanol was achieved over any of the [Ga]-ZSM-5 catalysts (Si/Ga ranging from 33 to 129) if the NH_4^+/Na^+ exchange degree was higher than 90%. At low NH_4^+ exchange degrees, the selectivity is shifted in favor of C_1-C_4 hydrocarbons reaching nearly 90% selectivity at 5%

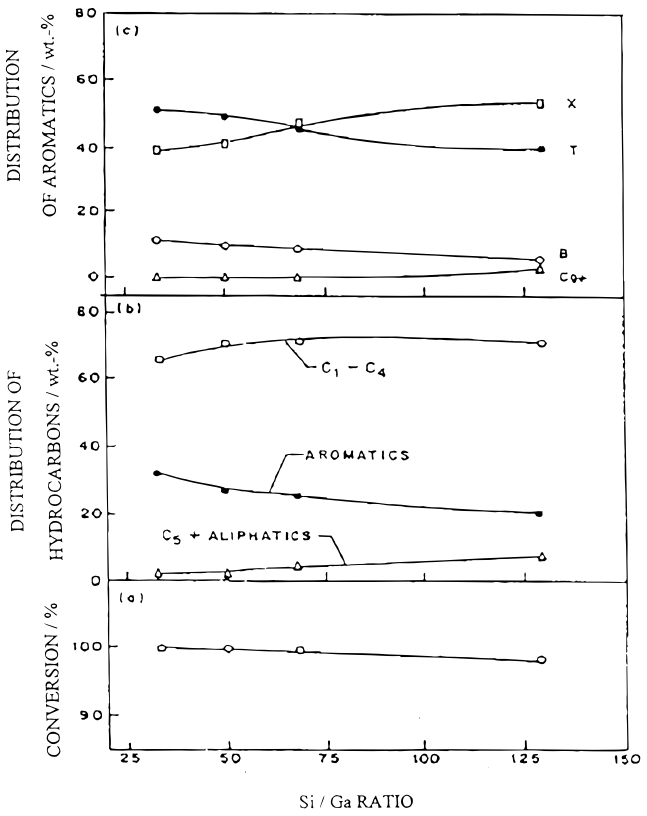

Figure 103. Methanol-to-aromatics conversion over Ga-MFI (exchange degree = 90%). Influence of the Si/Ga ratio (a) on the degree of methanol conversion and on the (b) distribution of aliphatics and (c) aromatics. Pulse reaction of 0.4 μL of MeOH over 0.1 g of catalyst at 400 °C. X = xylenes, T = toluene, B = benzene, C_{9+} = aromatics with ≥9 C atoms. (Reprinted with permission from ref 550. Copyright 1995 Elsevier Science.)

ion exchange. Calcination without or in the presence of steam leads to a decline of methanol conversion if the temperature exceeds 1023 (dry calcination) and 873 K (wet impregnation). In both cases, lower methanol conversion increases the selectivity of C_1–C_4 hydrocarbons at the expense of aromatics (benzene, toluene, xylenes, and ethylbenzene) and C_5^+ products. A few percent of strong acid sites among the total amount is sufficient to guarantee high methanol conversion levels. Higher concentrations of Brønsted sites, however, are necessary to allow formation of aliphatics and aromatics. This is in line with the common experience that methanol conversion to dimethyl ether can be accomplished by weak (Lewis) acid sites already. A further progress of the reaction to desired products requires strong Brønsted acid sites. In contrast to the methanol conversion on [Al]-ZSM-5, the conversion of methanol to hydrocarbons on [Ga]-ZSM-5 was found to be remarkable even in samples where only 5% of the Na^+ ions are replaced with H^+, i.e., at very low exchange degrees. This is ascribed to the more pronounced dehydrogenation activity of gallium. Due to the pulse technique, coke formation and its impact on the reaction characteristics could not be observed.

Handreck and Smith[551] presented one of the few thorough studies on the coking of MFI zeolites during methanol conversion. The coke content was determined thermogravimetrically as a function of the time on stream; the residual ion-exchange capacity at various stages of the reaction and the adsorption capacity of the external sites by adsorption of methylene blue (spectrophotometrical detection) were checked. Experiments were carried out in a flow reactor at 643 K under a WHSV of 1 h^{-1}. The point of deactivation was defined as the reaction time at which the hydrocarbon production ceased and methanol was converted into DME only. Deactivation decreases if [Ga]-ZSM-5 or [Fe]-ZSM-5 are used instead of [Al]-ZSM-5. Correspondingly, the amount of coke deposited after a passage of 300 g of MeOH/g of zeolite decreased in the order Al > Ga > Fe. Since no conversion levels of methanol are given, this fact might simply reflect differences in activity which are just in the same order as those observed for plenty of reactions. Consequently, high activity of the parent ZSM-5 leads to a more rapid coking and to an earlier point of deactivation, because active sites which catalyze further conversion of intermediate DME to hydrocarbons are blocked first. After all, different activities (at comparable concentration of acid sites) reflect the well-known modification of acidic strength associated with the isomorphous replacement of tetrahedrally coordinated Al by Ga or Fe in the ZSM-5 framework. The coke content does not increase monotonically with methanol supply (with the exception of the Fe silicate) but runs through at least two stages with distinctly slower coke increments. The decline of ion-exchange capacity proceeds in stages too. The modification of the adsorption of dyes at coke-containing zeolites, however, is almost completely irregular. These facts have not be interpreted convincingly so far.

VII. Conclusions and Outlook

Zeolitic materials are vastly applied as ion exchangers, selective adsorbents, catalysts, and catalyst supports. Further prospective fields of application have been discovered during the past few years. Zeolites, e.g., may act as hosts for encapsulation of various molecules, offering them an individual structural environment. This is a prerequisite for the manufacture of nanosized sensors, optical data storage devices, molecular switches, and enzyme mimicking (the function of the protein mantle in enzymes is replaced by the inorganic framework).[577]

Zeolite membranes are becoming important not only for separation processes on a molecular level but also for combining a catalytic conversion of reactants and separation of products.

Incorporation of gallium into zeolitic materials aims, in the first place, at isomorphous substitution of framework elements by gallium during the synthesis stage. In numerous cases, a stable crystalline framework can be synthesized from Si and Ga materials. Such "pure" gallosilicates have no natural analogues and are only accessible by a synthetic procedure. Table 13 included all gallosilicate analogues of zeolite structure types described so far, comprising 22 out of 126 listed in the *Atlas of Zeolite Structures*. This points to the difficulties in preparing gallosilicate analogues of most structure types and implies that development of appropriate syntheses

strategies will remain a challenge for inorganic chemists and mineralogists.

Ion exchange of gallium into zeolite structures has to consider that precipitation of $Ga(OH)_3$ in aqueous solutions under neutral or weakly basic conditions readily occurs on the external surface of the zeolite crystals. This is due to the fact that equilibria between single mononuclear and polynuclear species depend on the concentration and the pH value during the preparation procedure. Calcination transforms the hydroxide into the oxide, which retains high dispersion on the outer zone of the crystallites, but partly moves into the channel system by solid-state ion exchange. Exchange in aqueous solution can favorably be replaced by solid-state ion exchange. In this way, difficulties to keep gallium hydroxy cations in solution during the exchange process could be avoided.

Acidity is one of the fundamental inherent properties of the synthesized materials. Brønsted acidity within silicate-like materials is generated when tetravalent Si^{4+} is replaced with trivalent ions such as Al^{3+} or Ga^{3+}. Substitution of Al^{3+} by Ga^{3+} in aluminophosphates has no primary effect on Brønsted acidity. Brønsted acid sites found in the gallophosphate cloverite emerge due to structural peculiarities, intensifying the acid strength of terminal Ga−OH groups.

Nonframework gallium is the source of Lewis acidity. Oxo cations GaO^+ on exchange positions of the framework behave as Lewis acids. Owing to the presence of coordinatively unsaturated surface ions, agglomerated oxide-like species loosely fixed to the inner walls and to the external surface area are carriers of Lewis acid sites

A differentiation between Brønsted and Lewis acid functions of the solid materials is most favorably achieved by IR spectroscopic utilizing probe molecules, e.g., pyridine.

The nature of nonframework species and the way they contribute to catalytic reactions are not yet fully understood. To a great extent, the difficulties result from the in situ modification that catalysts suffer during the reaction. Obviously a concerted action of framework and nonframework gallium contributes to the catalytic activity. Lewis acid sites, for example, are able to activate alkanes by hydride-ion abstraction. This is probably one reason for the beneficial aromatization activity found in the Cyclar catalyst type. On the contrary, carbocation chemistry is associated with Brønsted acid sites. The advantage of using "pure" gallosilicates in acid-catalyzed reactions is the profitable shift of selectivities according to molecule sizes (product shape selectivity).

Application of gallium-modified zeolite-based catalysts in the exhaust gas cleaning suffers from structural changes occurring in the presence of moisture. Notwithstanding the efforts undertaken to improve the hydrothermal resistance of catalyst materials, a sufficient long-term stability during reaction is not yet achieved. The inherent hydrophilic character of aluminosilicate and gallosilicates zeolites as well as gallophosphates promotes dealumination or degalliation under reaction conditions accompanied by losses of activity. Improvement of the resistance against moisture is one aspect of further development. Approaches to be used are the postsynthesis silylation of hydrophilic sites on the external crystal surface and modification of the crystallization process. A slow crystal growth should result in lower concentrations of terminal OH groups, decreasing the hydrophilic character of the material.

Synthesis efforts will be extended to other solid materials. Utilization of sophisticated templating agents and sol−gel techniques allows the synthesis of mesoporous metal oxides, e.g., titanium oxide, manganese oxides, and alumina.

The state of the art is constituted by the manufacturing of mesoporous silicates. Introduction of Brønsted acidity by incorporation of aluminum into siliceous materials of the M41S family broadens catalytic applicability. Further functionalizing includes the anchoring of oxo species on the pore walls of the materials. Chromium oxo species and vanadium oxo species were successfully anchored and used for oxidation reactions in gas or liquid phases.

Owing to the large surface areas, the generation of relatively high concentrations of species is possible while maintaining site isolation. Due to the mesopores, the interior of the materials is accessible to large molecules in liquid-phase reaction. Solid-state ion exchanges and transport limitations are not as severe as they are in microporous materials. Modified mesoporous materials can be applied for the oxidation of bulky organic molecules or even for enantioselective reactions if combined with a chiral modifier. Introducing chirality into the solid material at the synthesis stage is a dream that has not become true. The first attempts to apply chiral templates in a synthesis recipe have been made for zeolite beta but without success so far. Last but not least, the contribution of theoretical methods and molecular modeling to the understanding of structural properties and to the prediction of material properties is expected to grow substantially.

VIII. List of Abbreviations

BTMAOH	benzyl trimethylammonium hydroxide
BTX aromatics	benzene, toluene, xylenes
CRAMPS (NMR)	combined rotation and multipulse sequence (NMR)
CTABr	hexadecyl trimethylammonium bromide
CTACl	hexadecyl trimethylammonium chloride
CTAO	hexadecyl trimethylammonium hydroxide
CVD	chemical vapor deposition
DAS (NMR)	dynamic angle spinning (NMR)
DEB	diethylbenzene
DME	dimethyl ether
DOR (NMR)	double-oriented rRotation
ESEM (spectroscopy)	electron spin−echo modulation (spectroscopy)
ETBE	ethyl *tert*-butyl ether
LHSV	liquid hourly space velocity (h^{-1})
MTBE	methyl *tert*-butyl ether
RSSIE	reductive solid-state ion exchange
SAXS	small-angle X-ray diffraction
TEABr	tetraethylammonium bromide

TEAOH	tetraethylammonium hydroxide
TEBABr	triethylbutylammonium bromide
TEMPO	2,2,6,6-tetramethylpiperidine-1-oxyl
TEOS	tetraethylorthosilicate
TMA	trimethylammonium
TMAOH	tetramethylammonium hydroxide
TPA	tetrapropylamine
TPA_2O	tetrapropylammonium oxide
TPAOH	tetrapropylammonium hydroxide
TPDA	temperature-programmed desorption of ammonia
TREN	tris(2-aminoethyl) amine
WAXS	wide-angle X-ray diffraction
WHSV	weight hourly space velocity (h^{-1})

IX. Acknowledgments

Authors express their thanks for the financial support of the work by the Federal Ministry of Education and Research and the Senate of Berlin. R.F. and M.R. are indebted to the VCI (Verband der Chemischen Industrie).

X. Addendum

A further thorough study on the synthesis and characteristics of zeolite structure [Ga]-beta is reported by Ocelli et al.[578] Results are in line with the evaluation given in section V.C.4.

A concise review on the application of solid-state MAS NMR to study zeolites ZSM-5, ZSM-11, and Ga-substituted variants has been published by Derouane et al.[579] Emphasis is placed on the use of ^{13}C-labeled organic substrates for studying mechanistic details of catalytic cumene formation on zeolite H-ZSM-12, the activation of propane on Ga-ZSM-5, as well as the alkylation of benzene with propane. In situ ^{13}C MAS NMR spectra were recorded after sealing the solid sample loaded with the desired reactant in the NMR cell. Catalytic conversion was achieved by rapid heating of the cell to a selected temperature for different times. Spectra were recorded after quenching at liquid nitrogen temperature. With respect to the CYCLAR process, Derouane et al. confirmed the mechanism described in section VI.A, including a bifunctional activation of propane on Ga-containing H-ZSM-5 catalysts with a protonated pseudo-cyclopropane intermediate as shown in Figure 80.

A novel catalytic application is claimed to be feasible with a commercial H[Ga] silicate (Si/Ga = 25, CHEMCAT), viz. polyethylene degradation with formation of BTX aromatics at 400−525 °C.[580]

A new pyridine-templated open framework gallophosphate was successfully synthesized at the University of St. Andrews, Scotland. The gallophosphate consists of zeolite like layers linked by $Ga_2F_2O_8$ dimers. The structure was resolved using microcrystal X-ray diffraction at a synchroton source.[581]

Silicoaluminophosphate SAPO-34 has been synthesized with partial substitution of Al^{3+} by Ga^{3+}.[582] However, the structure collapsed at Al/Ga ratios lower than 10 and changed into a dense phase at complete replacement of Al^{3+} by Ga^{3+}. The application as catalyst for the conversion of methanol to short olefins revealed no advantage in comparison to catalyst formulations listed in Table 24.

The application of zeolite-based materials, i.e., Ga-containing zeolites, for the selective catalytic reduction of NO_x with hydrocarbons has recently been reviewed by Y. Traa et al.[583]

XI. References

(1) Barrer, R. M. *Zeolites and Clay Minerals as Sorbents and Molecular Sieves*; Academic Press: London, 1978.
(2) (a) Smith, J. V. *Adv. Chem. Ser.* **1971**, *101*, 171. (b) Smith, J. V. *Chem. Rev.* **1988**, *88*, 149.
(3) Meier, W. M. In *Molecular Sieves*; Society of Chemical Industry: London, 1968.
(4) Rabo, J. A. *Zeolite Chemistry and Catalysis;*, ACS Monograph 171; American Chemical Society: Washington, D.C., 1976.
(5) Szostak, R. *Molecular Sieves: Principle of Synthesis and Identification;* Van Nostrand Reinhold: New York, 1989.
(6) Breck, D. W. *Zeolite Molecular Sieves: Structure, Chemistry, and Use*; Wiley & Sons: London, 1974.
(7) Kleber, W. *An Introduction to Crystallography*; Verlag Technik: Berlin, 1970.
(8) Chapus, T.; Tuel, A.; Ben Taarit, Y.; Naccache, C. *Zeolites* **1994,** *14*, 349.
(9) Ione, K. G.; Vostrikova, L. A.; Mastikin, M. *J. Mol. Catal.* **1985**, *31*, 355.
(10) Barrer, R. M. *Hydrothermal Chemistry of Zeolites*; Academic Press: London, 1982.
(11) Ione, K. G.; Vostrikova, L. A. *Uspechi Chimii* **1987,** *56*, 393.
(12) Allred, A. L.; Rochow, E. J. *J. Inorg. Nucl. Chem.* **1958**, *5*, 264. Little, E. J., Jr.; Jones, M. M. *J. Chem. Educ.* **1960**, *37*, 231.
(13) Pauling, L. *The Nature of the Chemical Bond*, 3rd ed.; Cornell University Press: Ithaka, NY, 1967.
(14) Shannon, R. D.; Prewitt, C. T. *Acta Crystallogr.* **1970**, *B26*, 1046. Shannon, R. D.; Prewitt, C. T. *Acta Crystallogr.* **1969**, *B25***,** 925. Shannon, R. D. *Acta Crystallogr.* **1976**, *A32*, 751.
(15) Axon, S. A.; Fox, K. K.; Carr, S. W.; Klinowski, J. In *Synthesis of Microporous Materials*; Occelli, M. L., Robson, H., Eds.;, van Nostrand Reinholds; New York, 1992; Vol. 1, p 537.
(16) Baes, Ch. F., Jr.; Mesmer, R. E. *The Hydrolysis of Cations*; Robert E. Krieger Publishing Co.: Malabar, FL, 1986.
(17) de Man, A. J. M.; van Santen, R. A.; Vogt, E. T. C. *J. Phys. Chem.* **1992**, *96*, 10460.
(18) Estermann, M.; McCusker, L. B.; Baerlocher, C.; Merrouche, A.; Kessler, H. **Nature 1991**, *352*, 320.
(19) Wilson, S. T.; Flanigen, E. M. Eur. Patent Appl. 0132708, 1985. Wilson, S. T.; Flanigen, E. M. U.S. Patent 4,567,029, 1986.
(20) Montes, C.; Davis, M. E.; Murray, B.; Narayana, M. *J. Phys. Chem.* **1990**, *94*, 6425.
(21) Akporiaye, D. E.; Andersen, A.; Dahl, I. M.; Mostad, H. B.; Wendelbo, R. *J. Phys. Chem.* **1995**, *99*, 14142.
(22) Liebau, F. *Structural Chemistry of Silicates*; Springer-Verlag: Berlin, 1985.
(23) Pujadó, P. E.; Rabo, J. A.; Antos, G. J.; Gembicki, S. A. *Catal. Today* **1992**, *13*, 113.
(24) Davis, M. E., Ed.; Special Issue Large Pore Molecular Sieves. *Catal. Today* **1994**, *19* (1).
(25) Corma, A. In *Zeolite Microporous Solids: Synthesis, Structure, and Reactivity*; Derouane, E. G., Lemos, F., Naccache, C., Ribeiro, F. R., Eds.; NATO ASI Series C; Kluwer Academic Publishers: Dortrecht, 1992; Vol. 352, p 373.
(26) Dartt, C. B.; Davis, M. E. *Catal. Today* **1994**, *19*, 151.
(27) Corbin, D. R.; Herron, N. *J. Mol. Catal.* **1994**, *86*, 343.
(28) Sheldon, R.; Dakka, J. *Catal. Today* **1994**, *19*, 215.
(29) Dai, P.-S. E. *Catal. Today* **1995**, *26*, 3.
(30) Shelef, M. *Chem. Rev.* **1995**, *95*, 209.
(31) Armor, J. N. *Catal. Today* **1995**, *26*, 147.
(32) Li, Y.; Armor, J. N. *J. Catal.* **1994**, *145*, 1.
(33) Inui, T.; Iwamoto, S.; Kojo, S.; Shimizu, S.; Hirabayashi, T. *Catal. Today* **1994**, *22*, 41.
(34) Meier, W. M.; Olson, D. H.; Baerlocher, Ch. *Atlas of Zeolite Structure Types*, 4th ed.; Elsevier: Amsterdam, 1996.
(35) Flanigen, E. M. In *Introduction to Zeolite Science and Pratice*; van Bekkum, H., Flanigen, E. M., Jansen, J. C., Eds.; Elsevier: Amsterdam, 1991; p 13.
(36) Gilson, J. P. In *Zeolite Microporous Solids: Synthesis, Structure, and Reactivity*; Derouane, E. G., Lemos, F., Naccache, C., Ribeiro, F. R., Eds.; NATO ASI Series C; Kluwer Academic Publishers: Dortrecht, 1992; Vol. 352, p 19.
(37) Kosslick, H.; Tuan, V. A.; Parlitz, B.; Fricke, R.; Peuker, Ch.; Storek, W. *J. Chem. Soc., Faraday Trans.* **1993**, *89*, 1131.
(38) Kosslick, H.; Tuan, V. A.; Fricke, R.; Jedamzik, J.; Lanh, H. D. *J. Thermal. Anal.* **1991** *37*, 2631.
(39) Nowotny, M.; Lercher, J.; Kessler, H. *Zeolites* **1991**, *11*, 454.
(40) Jansen, J. C. In *Introduction to Zeolite Science and Pratice*; van Bekkum, H., Flanigen, E. M., Jansen, J. C., Eds.; Elsevier: Amsterdam, 1991; p 77.

(41) Kocirek, M.; Struve, P.; Fiedler, K.; Bülow, M. *J. Chem. Soc., Faraday Trans. 1* **1988**, *89*, 3001.
(42) Kärger, J.; Ruthven, D. *Diffusion in Zeolites and other Microporous Solids*; Wiley: New York, 1992.
(43) Chen, N. Y.; Garwood, W. E.; Dwyer, F. G. *Shape Selective Catalysis in Industrial Applications*; Marcel Dekker: New York, 1992.
(44) Robson, H. *Chemtech* **1978**, *178*.
(45) Vaughan, D. E. W. In *Catalysis and Adsorption by Zeolites*; Öhlmann, G., Pfeifer, H., Fricke, R., Eds.; Elesevier: Amsterdam, 1991; p 275.
(46) Brinker, C. J.; Bunker, B. C.; Tallan, D. R.; Ward, K. J. *J. Chem. Phys.* **1986**, *83*, 851.
(47) Tang, A.; Xu, R.; Li, S.; An, Y. *J. Mater. Chem.* **1993**, *3*, 893.
(48) Gibbs, G. V. *Am. Miner.* **1982**, *67*, 421.
(49) Shluger, A. *J. Phys. Chem. Solids* **1986**, *47*, 659.
(50) Lobo, R. F.; Zones, S. I.; Davis, M. E. *J. Incl. Phenom. Mol. Recogn. Chem.* **1995**, *21*, 47.
(51) Chakoumakos, B. C.; Hill, R. J.; Gibbs, G. V. *Am. Miner.* **1981**, *66*, 1237.
(52) Jacobs, P. A.; Martens, J. A. *Synthesis of High-Silica Aluminosilcate Zeolites*; Elsevier: Amsterdam, 1987.
(53) Lok, B. M.; Cannan, T. R.; Messina, C. A. *Zeolites* **1983**, *3*, 282.
(54) Wilson, S. T. In *Introduction to Zeolite Science and Pratice*; van Bekkum, H., Flanigen, E. M., Jansen, J. C., Eds.; Elsevier: Amsterdam, 1991; p 137.
(55) Merrouche, A.; Patarin, J.; Kessler, H.; Soulard, M.; Delmotte, L.; Guth, J. L.; Joly, J. F. *Zeolites* **1992**, *12*, 226.
(56) Davis, M. E.; Lobo, R. F. *Chem. Mater.* **1992**, *4*, 756.
(57) Shimizu, A.; Taniguchi, Y. *Bull. Chem. Soc. Jpn.* **1990**, *63*, 3295.
(58) Wiebke, M. *J. Chem. Soc., Chem. Commun.* **1991**, 1509.
(59) Bissert, G.; Liebau, F. *Z. Kristallogr.* **1987**, *174*, 357.
(60) Parise, J. B.; Hriljac, J. A.; Cox, D. E.; Corbin, D. R.; Ramamurthy, V. *J. Chem. Soc., Chem. Commun.* **1993**, 226.
(61) Chatterjee, A.; Vetrivel, R. *J. Chem. Soc., Chem. Commun.* **1995**, 4313.
(62) Ginter, G. M.; Radke, C. J.; Bell, A. T. In *Zeolites: Facts, Figures, and Future*; Jacobs, P. A., van Santen, R. A., Eds.; Elsevier: Amsterdam, 1989; p 161. Barrer, R. M. *Zeolites* **1981**, *1*, 130.
(63) Knight, C. T. G.; Kirkpatrick, R. J.; Oldfield, E. *J. Magn. Reson.* **1988**, *79*, 31.
(64) Nazarenko, V. P.; Newekaja, E. M. *Gidrolys Ionow Metallow w Razbawlennych*; Rastworach: Atomisdat, 1979; p 84 (Russian)
(65) Doktor, W. H.; van Garderen, H. F.; Beelen, T. P. M.; van Santen, R. A.; Bras, W. *Angew. Chem.* **1995**, *107*, 122.
(66) Gabelica, Z.; Nagy, J. B.; Debras, G.; Derouane, E. G. In *Proceeding of the 6th International Zeolite Conference*, 1983, Olsen, D. H., Bisio, A. G., Eds.; Butterworth: Boston, 1984; p 914.
(67) Doktor, W. H.; Beelen, T. P. M.; van Garderen, H. F.; Rummens, C. P. J.; van Santen, R. A.; Ramsay, J. D. F. *Colloids Surf. A* **1994**, *85*, 89.
(68) Xu, W.; Li, J.; Li, W.; Zhang, H.; Liang, B. *Zeolites* **1989**, *9*, 468.
(69) Iton, L. E.; Trouw, F.; Brun, T. O.; Epperson, E.; White, J. W.; Henderson, S. J. *Langmuir* **1992**, *8*, 1045.
(70) McNicol, B. D.; Pott, G. T.; Loos, K. R.; Mulder, N. *Adv. Chem. Ser.* **1973**, *121*, 152.
(71) Flanigen, E. M. *Adv. Chem. Ser.* **1973**, *121*, 119.
(72) Zhdanov, S. P. *Adv. Chem. Ser.* **1973**, *121*, 20.
(73) Lechert, H. *Stud. Surf. Sci. Catal.* **1984**, *18*, 107.
(74) Twomey, T. A. M.; Mackay, M.; Kuipers, H. P. C. E.; Thompson, R. W. *Zeolites* **1994**, *14*, 162.
(75) Jacobs, P. A. In *Zeolite Microporous Solids: Synthesis, Structure, and Reactivity*; Derouane, E. G., Lemos, F., Naccache, C., Ribeiro, F. R., Eds.; NATO ASI Series; Kluwer Academic Publishers: Dortrecht, 1992; Vol. 352, p 3.
(76) Feijen, J. P.; Martens, J. A.; Jacobs, P. A. In *Zeolites and Related Microporous Materials: State of the Art 1994*; Weitkamp, J., Karge, H. G., Pfeifer, H., Hölderich, W., Eds.; Elsevier: Amsterdam, 1994; p 3.
(77) Zhadanov, S. P.; Samulevich, N. N. *Proceedings of the 5th International Zeolite Conference;* Rees, L. V., Ed.; Heyden: London, 1980; p 75.
(78) Iler, R. K. *The Chemistry of Silica*; John Wiley & Sons: New York, 1979.
(79) Tytko, K.-H. *Chem. Unserer Zeit* **1979**, *13*, 184.
(80) den Ouden, C. J. J.; Thompson, R. W. *Ind. Eng. Chem. Res.* **1992**, *31*, 369.
(81) Inui, T. *ACS Symp. Ser.* **1989**, *398*, 479. Inui, T.; Makino, U. A.; Miyamoto, A. *Ind. Eng. Chem. Res.* **1987**, *26*, 647.
(82) Takeguchi, T.; Kagawa, K.; Kim, J.-B.; Inui, T.; Wie, D.; Haller, G. L. *Catal. Lett.* **1997**, *46*, 5.
(83) Dwyer, J.; Zhao, J.; Rawlence, D. *Proceedings of the 9th International Zeolite Conference*, Montreal, 1992, von Ballmoos, R., Higgins, J. B., Treacy, M. M. J., Eds.; Butterworth-Heinemann, Boston, 1993; Vol. I, p 155.
(84) Guth, J. L.; Kessler, H.; Wey, R. *Pure Appl. Chem.* **1986,** *58*, 1389.
(85) Axon, S. A.; Klinowski, J. In *Recent Advances in Zeolite Science, Proceedings of the 1989 Meeting British Zeolite Association*, Cambridge; Klinowski, J., Barrie, P. J., Eds.; Elsevier: Amsterdam, 1989; p 113.
(86) Axon, S. A.; Klinowski, J. *Appl. Catal. A: General* **1992**, *81*, 27.
(87) Dessau, R. M.; Schmitt, K. D.; Kerr, G. T.; Woolery, G. L.; Alemany, L. B. *J. Catal.* **1987**, *104*, 484.
(88) Tissler, A. Ger. Patent 4 021 118, 1992.
(89) Tissler, A.; Polanek, P.; Girrbach, U.; Müller, U.; Unger K. In *Zeolites as Catalysts, Sorbents and Detergent Builders*; Elsevier: Amsterdam, 1988; *Stud. Surf. Sci. Catal.* **1989**, *46*, 399.
(90) Shiralkar, V. P.; Clearfield, A. *Zeolites* **1989**, *9*, 363.
(91) Wallau, M.; Schüth, F.; Brenner, A.; Melson, S.; Spichtinger, R.; Unger, K.; Tissler, A.; Zibrowius, B. In *Proceedings of the 9th International Zeolite Conference*, Montreal, 1992; von Ballmoos, R., Higgins, J. B., Treacy, M. M. J., Eds.; Butterworth-Heinemann: Boston, 1993; Vol. I, p 643.
(92) Lautenschläger, W.; Schweizer, T. *LaborPraxis* **1990**, 376.
(93) Ginter, D. M. Ph.D. Thesis, Berkeley, CA, 1991.
(94) McCormic, A. V.; Bell, A. T.; Radke, C. J. *J. Phys. Chem.* **1989**, *93*, 1733.
(95) Engelhardt, G.; Michel, D. *High-Resolution Solid State NMR of Silicates and Zeolites*; Wiley: Chichester, 1987.
(96) Lievens, J. L.; Mortier, W. J.; Verduijn, J. P. *J. Phys. Chem.* **1992**, *96*, 5473.
(97) Newsam, J. M.; Vaughan, D. E. W. In *Proceedings of the 7th International Zeolite Conference*; Murakami, Y., Iijima, A., Ward, J. W., Eds.; Elsevier: Amsterdam, 1987; p 457.
(98) Occelli, M. L.; Eckert, H.; Iyer, P. S.; Ritz, P. In *Synthesis of Porous Materials: Zeolites, Clays, and Nanostructures*; Occelli, M. L., Kessler, H., Eds.; Marcel Dekker: New York, 1996; p 283.
(99) Occelli, M. L. U.S. Patent 5 133 951, 1992.
(100) Loewenstein, W. *Am. Miner.* **1954**, *39*, 92.
(101) Ermoshin, V. A.; Smirnov, K. S.; Bougeard, D. *J. Mol. Struct. (Theochem.)* **1997**, *393*, 171.
(102) Petit, J.-C.; Della Mea, G.; Dran, J.-C.; Magonthier, M.-C.; Mando, P. A.; Paccagnella, A. *Geochim. Cosmochim. Acta* **1990**, *54*, 1941.
(103) Mikowski, R. J.; Marshal, J. F. *J. Catal.* **1976**, *44*, 170.
(104) Takaishi, T. *J. Chem. Soc., Faraday Trans. 1* **1987**, *83*, 2681.
(105) Klinowski, J. *Chem. Rev.* **1991**, *91*, 1459.
(106) Beagley, B.; Dwyer, J.; Fitch, F. R.; Mann, R.; Walters, J. *J. Phys. Chem.* **1984**, *88*, 1744.
(107) Mortlock, R. F.; Bell, A. T.; Radke, C. J. *J. Phys. Chem.* **1992**, *96*, 2968.
(108) Tuan, V. A.; Fricke, R.; Jänchen, J.; Kosslick, H. *Cryst. Res. Technol.* **1992**, *27*, 755.
(109) Swaddle, T. W.; Salerno, J.; Tregloan, P. A. *Chem. Soc. Rev.* **1994**, 319.
(110) Newsam, J. M.; Jörgensen, J. D. *Zeolites* **1987**, *7*, 569.
(111) Dooryhee, E.; Neville Greaves, G.; Steel, A. T.; Townsend, R. P.; Carr, S. W.; Thomas, J. M.; Catlow, C. R. A. *Faraday Discuss. Chem. Soc.* **1990**, *89*, 119.
(112) Okabe, K.; Matsubayashi, N.; Sayama, K.; Arakawa, H.; Nishijima, A. *Bull. Chem. Soc. Jpn.* **1991**, *64*, 2602.
(113) Lechert, H.; Kacirek, H. *Zeolites* **1993**, *13*, 192. Lechert, H.; Staelin, P.; Kuntz, C. *Zeolites* **1996**, *16*, 149 and references therein.
(114) Awate, S. V.; Joshi, P. N.; Shiralkar, V. P.; Kotasthane, A. N. *J. Incl. Phenom.* **1992**, *13*, 207.
(115) Kotasthane, A. N. Ph.D. Thesis, University of Pune, India, 1985.
(116) Ruen, X.; Wenqin, P. *Stud. Surf. Sci. Catal.* ***1985***, *24*, 27.
(117) Joshi, P. N.; Rao, G. N.; Kotasthane, A. N.; Shiralkar, V. P. *J. Incl. Phenom.* **1990**, *9*, 91.
(118) Derouane, E. G.; Detremmerie, S.; Gabelica, Z.; Blom, N. *Appl. Catal.* **1981**, *1*, 201.
(119) Gianetto, G.; Monque, R.; Perez, J.; Papa, J.; Garcia, L. *Zeolites* **1993**, *13*, 557.
(120) Ivanov-Emin, B. N.; Nisel'son, L. A.; Larionova, L. E. *Zh. Neorg. Chim. (Russ. J. Inorg. Chem.)* **1962**, *7*, 266.
(121) Greenwood, N. N.; Earnshaw, A. *Chemistry of the Elements*; Pergamon Press: Oxford, 1985.
(122) Gabelica, Z.; Gianetto, G.; Dos Santos, F.; Monque, R.; Galiasso, R. In *Proceedings of the 9th International. Zeolite Conference*, Montreal, 1992; von Ballmoos, R., Higgins, J. B., Treacy, M. M. J., Eds.; Butterworth-Heinemann: Boston, 1993; Vol. I, p 229.
(123) Gabelica, Z.; Mayanez, C.; Monque, R.; Galiasso, R.; Giannetto, G. In *Molecular Sieves*; Occelli, M. L., Robson, H. E., Eds.; Van Nostrand Reinhold: New York, 1992; Vol. 1, p 190.
(124) Bradley, S. M.; Kydd, R. A. *J. Chem. Soc., Dalton Trans.* **1993**, *15*, 2407.
(125) Kosslick, H.; Tuan, V. A.; Fricke, R. *Cryst. Res. Technol.* **1991**, *26*, K64.
(126) Chao, K.-J.; Chang Tasi, T.; Chen, M.-S. *J. Chem. Soc., Faraday Trans. 1* **1981**, *77*, 547.
(127) Choudhary, V. R.; Kinage, A. K.; Sivadinarayana, C.; Devadas, P.; Sansare, S. D.; Guisnet, M. *J. Catal.* **1996**, *158*, 34.

(128) Bayense, C. R.; van Hooff, J. H. C.; Kentgens, A. P. M.; de Haan, J. E.; van de Ven L. J. M. *J. Chem. Soc., Chem. Commun.* **1989**, 1292.
(129) Bayense, C. R.; Kentgens, A. P. M.; de Haan, J. E.; van de Ven, L. J.; van Hooff, J. H. C. *J. Phys. Chem.* **1992**, *96*, 775.
(130) Freude, D.; Fröhlich, T.; Pfeifer, H.; Scheler, G. *Zeolites* **1983**, *3*, 171.
(131) Minachev, Kh. M.; Kharson, M. S.; Dergachev, A. A.; Gorbatkina, I. E.;. Bondarenko, T. B.; Konovalchikov, L. D.; Nefedov, G. K. *Izv. Acad. Nauk USSR Ser. Khim.* **1990**, 2373.
(132) Khodakov, A. Yu.; Kustov, L. M.; Bondarenko, T. N.; Dergachev, A. A.; Kazansky, V. B.; Minachev, Kh. M.; Borbely, G.; Beyer, H. K. *Zeolites* **1990**, *10*, 603.
(133) Thomas, M.; Liu, X.-S. *J. Phys. Chem.* **1986**, *90*, 4843.
(134) Liu, X.-S.; Thomas, J. M. *J. Chem. Soc., Chem. Commun.* **1985**, 1544.
(135) Endoh, A.; Nishimiya, K.; Tsutsumi, K.; Takaishi, T. In *Zeolites as Catalysts, Sorbents and Detergent Builders*; Karge, H.-G., Weitkamp, J., Eds.; Elsevier: Amsterdam, 1989; *Stud. Surf. Sci. Catal.* **1989**, *46*, 799.
(136) Liu, X. S.; Lin, J.; Liu, X. X.; Thomas, J. M. *Zeolites* **1992**, *12*, 936.
(137) Karim, K.; Dwyer, J.; Rawlence, D. J.; Tarig, M.; Nabhan, A. *J. Mater. Chem.* **1992**, *2*, 1161.
(138) Dwyer, J.; Karim, K. *J. Chem. Soc., Chem. Commun.* **1991**, 905.
(139) Dwyer, J.; Dewing, J.; Karim, K.; Holmes, S.; Ojo, A. F.; Garforth, A. A.; Rawlence, D. J. In *Zeolite Chemistry and Catalysis, Proceedings of the International Symposium,* Prague, 1991; Jacobs, P. A., Jaeger, N. I., Kubelkova, L., Wichterlova, B., Eds.; Elsevier: Amsterdam, 1991; p 1.
(140) Bayense, C. R.; van Hooff, J. H. C.; de Haan, J. W.; van de Ven, L. J. M.; Kentgens, A. P. M. *Catal. Lett.* **1993**, *17*, 349.
(141) Kosslick, H.; Richter, M.; Tuan, V. A.; Parlitz, B.; Szulzewsky, K.; Fricke, R., In *Zeolite Chemistry and Catalysis*; Jacobs, P. A., Jaeger, N. I., Kubelkova, L., Wichterlova, B., Eds.; Elsevier: Amsterdam, 1991; p 109.
(142) Kampmann, L.; Kahlweit, M. *Ber. Bunsen-Ges. Phys. Chem.* **1967**, *71*, 78.
(143) Joly, J. F.; Ajopt, A. E.; Merlen, E.; Raatz, F.; Alario, F. *Appl. Catal. A: General* **1991**, *79*, 249.
(144) Yakerson, V. I.; Vasina, T. V.; Lafer, L.-I.; Sytnyk, V. P.; Dykh, Z. H. L.; Mokhov, A. V.; Bragin, O. V.; Minachev, Kh. M. *Catal. Lett.* **1989**, *3*, 339.
(145) Karge, H. G.; Beyer, H. K. In *Zeolite Chemistry and Catalysis, Proceedings of the International Symposium,* Prague, 1991; Jacobs, P. A., Jaeger, N. I., Kubelkova, L., Wichterlova, B., Eds.; Elsevier: Amsterdam, 1991; p 43.
(146) Karge, H. G. In *Zeolites and Microporous Crystals*; Hattori, T., Yashima, T., Eds.; *Proceedings of the International Symposium on Zeolites and Microporous Crystals;* Nagoya, Japan, 1993; Kodansha Ltd. and Elsevier: Tokyo and Amsterdam, 1994; p 135.; *Stud. Surf. Sci. Catal.* **1994**, *83*, 135.
(147) Carli, R.; Bianchi, C. L.; Giannantonio, R.; Ragaini, V. *J. Mol. Catal.* **1993**, *83*, 379.
(148) Kanazirev, V.; Price, G. L. In *Zeolites and Related Materials: State of the Art, Proceedings 10th International Zeolite Conference*; Weitkamp, J., Karge, H. G., Pfeifer, H., Hölderich, W., Eds.; Garmisch-Partenkirchen, 1994; *Stud. Surf. Sci. Catal.* **1994**, *98C*, 1935.
(149) Kanazirev, V.; Price, G. L.; Dooley, K. M. In *Zeolite Chemistry and Catalysis, Proceedings of the International Symposium,* Prague, 1991; Jacobs, P. A., Jaeger, N. I., Kubelkova, L., Wichterlova, B., Eds.; Elsevier: Amsterdam, 1991; p 277.
(150) Kanazirev, V.; Neinska, Y.; Tsoncheva, T.; Kosova, L. In *Proceedings of the 9th International Zeolite Conference,* Montreal, 1992, von Ballmoos, R., Higgins, J. B., Treacy, M. M. J., Eds.; Butterworth-Heinemann: Boston 1993; Vol. I, p 461.
(151) Neinska, Ya.; Minchev, Ch.; Dimitrova, R.; Micheva, N.; Minkov, V.; Kanazirev, V. In *Zeolites and Related Materials. State of the Art 1994, Proceedings of the 10th International Zeolite Conference,* Weitkamp, J., Karge, H. G., Pfeifer, H., Hölderich, W., Eds.; Garmisch-Partenkirchen: 1994; *Stud. Surf. Sci. Catal.* **1994**, *98C*, 989.
(152) Kwak, B. S.; Sachtler, W. M. H. *J. Catal.* **1994**, *145*, 456.
(153) Kwak, B. S.; Sachtler, W. M. H. *J. Catal.* **1993**, *141*, 729.
(154) Wu, P.; Kommatsu, T.; Yashima, T.; Nakata, S−i.; Shouji, H. *Microporous Mater.* **1997**, *12*, 25.
(155) Chu, C. T.-W.; Chang, C. D. *J. Phys. Chem.* **1985**, *89*, 1569.
(156) Post, M. F. M.; Huizinga, T.; Emeis, C. A. In *Zeolites as Catalysts, Sorbents and Detergent Builders*; Karge, H. G., Weitkamp, J., Eds.; Elsevier: Amsterdam, 1989; *Stud. Surf. Sci. Catal.* **1989,** *46*, 365.
(157) Dompas, D. H.; Mortier, W. J.; Kenter, O. C. H.; Janssen, M. J. G.; Verduijn, J. P. *J. Catal.* **1991**, 129, 19.
(158) Szostak, R.; Thomas, T. L. *J. Catal.* **1986**, *101*, 549.
(159) Thomas, J. M.; Liu, X.-Sh. *J. Phys. Chem.* **1986**, *90*, 4843.
(160) Eapen, M. J.; Reddy, K. S. N.; Joshi, P. N.; Shiralkar, V. P. *J. Incl. Phenom Mol. Recogn. Chem.* **1992**, *14*,119.
(161) Chandwadkar, A. J.; Abdulla, R. A.; Hegde, S. G.; Nagy, J. B. *Zeolites* **1993**, *13*, 470.
(162) Jacob, N. E.; Joshi, P. N.; Shaikh, A. A.; Shiralkar, V. P. *Zeolites* **1993**, *13*, 431.
(163) Mirajkar, S. P.; Eapen, M. J.; Tamhankar, S. S.; Rao, B. S.; Shiralkar, V. P. *J. Incl. Phenom. Mol. Recogn. Chem.* **1993**, *16*, 139.
(164) Singh, A. P.; Reddy, K. R. *Zeolites* **1994**, *14*, 290.
(165) Liu, X.; Klinowski, J. *J. Phys. Chem.* **1992**, *96*, 3403.
(166) Camblor, M. A.; Perez-Pariente, J.; Fornes, V. *Zeolites* **1992**, *12*, 280.
(167) Barr, T. L.; Klinowski, J.; He, H.; Alberti, K.; Müller, G.; Lercher, J. A. *Nature* **1993**, *365*, 429.
(168) Flanigen, E. M. In *Zeolite Chemistry and Catalysis*; Rabo, J. A., Ed.; ACS Monograph; American Chemical Society: Washington, D.C., 1976*;* p 80.
(169) Jacobs, P. A.; Beyer, H. K.; Valyon, J. *Zeolites* **1981**, *1*, 161.
(170) Flanigen, E. M.; Khatami, H.; Szymanski, H. *Adv. Chem. Ser.* **1971**, *101*, 201.
(171) Löffler, E.; Peuker, Ch.; Jerschkewitz, H. G. *Catal. Today* **1988**, *3*, 415.
(172) Lanh, H. D.; Tuan, V. A.; Kosslick, H.; Parlitz, B.; Fricke, R.; Völter, J. *Appl. Catal. A* **1993**, *103*, 205.
(173) Kosslick, H.; Tuan, V. A.; Fricke, R.; Peuker, Ch.; Pilz, W.; Storek, W. *J. Phys. Chem.* **1993**, *97*, 5678.
(174) Storek, W.; Kosslick, H. Unpublished results.
(175) Hyashi, S.; Suzuki, K.; Shin, S.; Hayamizu, K.; Yamamoto, O. *Bull. Chem. Soc. Jnp.* **1985**, *58*, 52.
(176) Fyfe, C. A.; Gobbi, G. C.; Klinowski, J.; Thomas J. M.; Ramdas, S. *Nature* **1982**, *298*, 530.
(177) Trewella, J. C.; Schlenker, J. L.; Woessner, D. E.; Higgins, J. B. *Zeolites* **1985**, *5*, 130.
(178) Bradley, M. S.; Howe, R. F.; Kydd, R. A. *Magn. Reson. Chem.* **1993**, *31*, 883.
(179) Bradley, M. S.; Howe, R. F. *Microporous Mater.* **1995**, *4*, 131.
(180) Ione, K. G.; Vostrikova, L. A.; Mastikhin, V. M. *J. Mol. Catal.* **1985**, *31*, 355.
(181) Timken, H. K. C.; Oldfield, E. *J. Am. Chem. Sc.* **1987**, *109*, 7669.
(182) Diaz, A.; Monque, R.; Bussolo, M. *Bull. Magn. Reson.* **1993**, *15*, 112.
(183) Dybowski, C.; Bansal, N.; Duncun, T. M. *Annu. Rev. Phys. Chem.* **1991**, *42*, 433.
(184) Barrie, P. J.; Klinowski, J. *Prog. NMR Spectrosc.* **1992**, *24*, 31.
(185) Fraissard, J.; Ito, T. *Zeolites* **1988**, *8*, 350.
(186) Ripmeester, J. A.; Ratcliffe, C. I. *J. Phys. Chem.* **1990**, *94*, 7652.
(187) Alexander, S. M.; Coddington, J. M.; Howe, R. F. *Zeolites* **1991**, *11*, 368.
(188) Axon, S. A.; Huddersman, K.; Klinowski, J. *Chem. Phys. Lett.* **1990**, *172*, 398.
(189) Behrens, P.; Felsche, J.; Niemann, W. *Catal. Today* **1991**, *8*, 479.
(190) Behrens, P.; Felsche, J.; Vetter, S.; Schulz-Ekloff, G.; Jaeger, N. I.; Niemann, W. *J. Chem. Soc., Chem. Commun.* **1991**, 678.
(191) Xu, Y.; Couves, J. W.; Jones, R. H.; Catlow, C. R. A.; Greaves, G. N. *J. Phys. Chem. Solids* **1991**, *52*, 1229.
(192) Behrens, P.; Kosslick, H.; Tuan, V. A.; Fröba, M.; Neissendorfer, F. *Microporous Mater.* **1995**, *3*, 433.
(193) Kofke, T. J. G.; Gorte, R. J.; and Kokotailo, G. T. *Appl. Catal.* **1989**, *54*, 177.
(194) Monque, R.; Parisi, A.; Gonzalez, S.; Giannetto, G. *Zeolites* **1992**, *12*, 806.
(195) Price, G. L.; Kanazirev, V. I.; Dooley, K. M. *Zeolites* **1995**, *15*, 725.
(196) Dooley, K. M.; Chang, C.; Price, G. L. *Appl. Catal. A* **1992**, *84*, 17.
(197) Meitzner, G. D.; Iglesia, E.; Baumgartner, J.; Huang, E. S. *J. Catal.* **1993**, *140*, 209.
(198) Jia, S.; Wu, S.; Meng, Z. *Appl. Catal. A: General* **1994**, *103*, 259.
(199) Petit, L.; Bournonville, J. P.; Roatz, F. In *Zeolites: Facts, Figures, Future*; Jacobs, P. A., Santen, R. A., Eds.; Elsevier: Amsterdam, 1989; *Stud. Surf. Sci. Catal.* **1989**, *49*, 1163.
(200) Joly, J. F.; Ajot, H.; Alario, F.; Taleb, D. A.; Gnep, N. A.; Guisnet, M. In *Proceedings of the 9th International Conference on Zeolites,* Montreal, 1992; von Balmoos, R., Higgins, J. B., Treacy, M. J. J., Eds.; Butterworth-Heinemann: Boston, MA, 1992; Vol. II, p 501.
(201) Carli, R.; Bianchi, C. L. *Appl. Surf. Sci.* **1994**, *74*, 99.
(202) Shpiro, E. S.; Shevchenko, D. P.; Kharson, M. S.; Dergachev, A. A.; Minachev, Kh. M. *Zeolites* **1992**, *12*, 670.
(203) Tielen, M.; Geelen, M.; Jacobs, P. A. In *Proceedings of the International Symposium on Zeolite Catalysis,* Siofok, Hungary, 1989; p 1.
(204) Strodel, P.; Neyman, K. M.; Knözinger, H.; Rösch, N. *Chem. Phys. Lett.* **1995**, *240*, 547.
(205) Stave, M. S.; Nicholas, J. B. *J. Phys. Chem.* **1995**, *99*, 15046.
(206) van Santen, R. A.; de Man, A. J. M.; Kramer, G. J. *Catal. Lett.* **1991**, *9*, 273.
(207) Limtrakul, J.; Yoinuan, J.; Tantanak, D. *J. Mol. Struct.* **1994**, *312*, 183.
(208) Dwyer, J.; O'Malley, P. J. *Chem. Phys. Lett.* **1988**, *143*, 97.

(209) Zahradnik, R.; Hobza, P.; Wichterlova, B.; Cejka, J. *Collect. Czech. Chem. Commun.* **1993**, *58*, 2474.
(210) O'Malley, P. J.; Dwyer, J. *Chem. Phys. Lett.* **1988**, *143*, 97.
(211) Langenaeker, W.; Coussement, N.; De Proft, F.; Geerlings, P. *J. Phys. Chem.* **1994**, *98*, 3010.
(212) Post, M. F. M.; Huizinga, T.; Emeis, C. A.; Nanne, J. M.; Stork, W. H. J. In *Zeolites as Catalysts, Sorbents and Detergent Builders*; Karge, H. G., Weitkamp, J., Eds.; Elsevier: Amsterdam, 1989; p 365.
(213) Kassab, E.; Seiti, K.; Allavena, M. *J. Phys. Chem.* **1988**, *92*, 6705.
(214) Vetrivel, R.; Catlow, C. R. A.; Colbourn, E. A.; Leslie, M. In *Zeolites as Catalysts, Sorbents and Detergent Builders*; Karge, H. G., Weitkamp, J., Eds.; Elsevier: Amsterdam, 1989;p 409.
(215) Sauer, J. In *Zeolites and Related Microporous Materials*: *State of the Art* 1994, *Proceedings of the 10th International* Zeolite *Conference*, Garmisch-Partenkirchen: 1994; Weitkamp, J., Karge, H.-G., Pfeifer, H., Hölderich, W., Eds.; Elsevier Science B. V.: Amsterdam, 1994; *Stud. Surf. Sci Catal.* **1994**, *84*, 2039.
(216) Inui, T.; Matsuba, K.; Tanaka, Y. *Catal. Today* **1995**, *23*, 317.
(217) Dasgupta, S.; Goddard, W. A. *J. Phys. Chem.* **1989**, *90*, 7207.
(218) Beyer, H. K.; Borbely, G., In *Proceedings of the 7th International Zeolite Conference*; Murakami, Y., Iijima, A., Ward, J. W., Eds.; Kodansha and Elsevier: Tokyo and Amsterdam, 1986; p 866.
(219) Shertukde, P. V.; Hall, W. K.; Marcelin, G. *Catal. Today* **1992**, *15*, 991.
(220) Challoner, R.; Harris, R. K.; Barri, S. A. I.; Taylor, M. J. U *Zeolites* **1991**, *11*, 827.
(221) Inui, T. In *Proceedings of the 8th International Congress of Catalysis*, Berlin, 1984; Vol 3, p 569.
(222) Berndt, H.; Martin, A.; Kosslick, H.; Lücke, B. *Microporous Mater.* **1994**, *2*, 197.
(223) Mirsojew, I.; Ernst, S.; Weitkamp, J.; Knözinger, H. *Catal. Lett.* **1994**, *14*, 235. Sigl, M.; Ernst, S.; Weitkamp, J.; Knözinger, H. *Catal. Lett.* **1997**, *45*, 27.
(224) Corma, A.; Fornes, V.; Rey, F. *Zeolites* **1993**, *13*, 57.
(225) Anunziata, O. A.; Pierella, L. B. *Catal. Lett.* **1993**, *19*, 143.
(226) Minachev, Kh. M.; Dergachev, A. A.; Bondarenko, T. N.; Kharson, M. J.; Tyurin, A. A. *Pet. Chem.* **1994**, *34*, 7.
(227) Li, C.; Yan, W.; Xin, Q. *Catal. Lett.* **1994**, *24*, 249.
(228) Romannikov, V. N.; Paukshtis, E. A.; Ione, K. G. *Stud. Surf. Sci. Catal.* **1991**, *60*, 311.
(229) Defosse, C.; Canesson, P. *J. Chem. Soc., Faraday Trans. I* **1976**, *11*, 2565.
(230) Borade, R. B.; Adnot, A.; Kaliaguine, S. *J. Catal.* **1990**, *126*, 26.
(231) Borade, R. B.; Sayari, A.; Adnot, A.; Kaliaguine, S. *J. Phys. Chem.* **1990**, *94*, 5989.
(232) Borade, R. B.; Clearfield, A. *J. Phys. Chem.* **1992**, *96*, 6729.
(233) Borade, R. B.; Adnot, A.; Kaliaguine, S. *J. Chem. Soc., Faraday Trans.* I **1990**, *86*, 3949.
(234) Guimon, C.; Zoniten, A.; Boreave, A.; Quet, C. *J. Chem. Soc., Faraday Trans. 1* **1994**, *90*, 3461.
(235) Kanazirev, V. I.; Price, G. L.; Dooley, K. M. *Catal. Lett.* **1994**, 24, 227.
(236) Kanazirev, V. I.; Price, G. L.; Dooley, K. M. *J. Catal.* **1994**, *148*, 164.
(237) Kofke, T. J. G.; Gorte, R. J.; Farneth, W. E. *J. Catal.* **1988**, *114*, 34.
(238) Kofke, T. J. G.; Kokotailo, G. T.; Gorte, R. J.; Farneth, W. E. *J. Catal.* **1989,** *115*, 265.
(239) Pereira, C.; Gorte, R. J. *Appl. Catal. A: General* **1992**, *90*, 145.
(240) Auroux, A.; Jiu, Y. S.; Vedrine, J. C.; Benoist, L. *Appl. Catal.* **1988**, *36*, 323.
(241) Giannetto, G.; Montes, A.; Gnep, N. S.; Florentino, A.; Cartraud, P.; Guisnet, M. *J. Catal.* **1994**, *145*, 86.
(242) Richter, M.; Kosslick, H.; Tuan, V. A.; Richter-Mendau, J.; Parlitz, B.; Ehrhardt, K.; Vorbeck, G.; Szulzewski, K. *Ber. Bunsen-Ges. Phys. Chem.* **1992**, *96*, 586.
(243) Martens, J. A.; Tielen, M.; Jacobs, P. A.; Weitkamp, J. *Zeolites* **1984**, *4*, 98.
(244) Viruela-Martin, P.; Zicovich-Wilson, C. M.; Corma, A. *J. Phys. Chem.* **1993**, *97*, 13713.
(245) Kühl, G. H. *J. Inorg. Nucl. Chem.* **1971**, *33*, 3261.
(246) Newsam, J. M. *Mater. Res. Bull.* **1986**, *21*, 661.
(247) Newsam, J. M. *J. Chem Soc., Chem. Commun.* **1986**, 1295.
(248) Yang, J.; Xie, D.; Yelon, W. B.; Newsam, J. M. *J. Phys. Chem.* **1988**, *92*, 3586.
(249) Jarman, R. H.; Jacobson, A. J.; Melchior, M. T. *J. Phys. Chem.* **1984**, *88*, 5748.
(250) Yelon, W. B.; Xie, D.; Newsam, M.; Dunn, J. *Zeolites* **1990**, *10*, 553.
(251) Hegde, S. G.; Abdullah, R. A.; Bhat, R. N.; Ratnasamy, P. *Zeolites* **1992**, *12*, 951.
(252) Borade, R. B.; Clearfield, A. *Prepr.−Am. Chem. Soc., Div. Pet. Chem.* **1993**, *38*, 498.
(253) Occelli, M. L. U.S. Patent 4 931 266, 1990.
(254) Mastikhin, V. M.; Kluera, N. V.; Ione, K. G.; Zamaraev, K. I. *React. Kinet. Catal. Lett.* **1987**, *33*, 465.
(255) Selbin, J.; Mason, R. B. *J. Inorg. Nucl. Chem.* **1961**, *20*, 222.
(256) Newsam, J. M.; Jacobson, A. J.; Vaughan, D. E. W. *J. Phys. Chem.* **1988**, *90*, 6858.
(257) Xiao, F.; Liu, X.; Xu, R.; Wei, Q. *Shiyou Xuebao, Shiyou Jiagong* **1992**, *8*, 67.
(258) Occelli, M. L. U.S. Patent 4 803 060, 1989.
(259) Delprato, F.; Guth, J. L.; Zivkov, C. Fr. Demande FR 2 650 582, 1991.
(260) Sulikowski, B.; Klinowski, J. *J. Chem. Soc., Chem. Commun.* **1989**, 1289.
(261) Wright, P. A.; Thomas, J. M.; Cheetham, A. K.; Nawak, A. *Nature* **1985**, *318*, 611.
(262) Vaughan, D. E. W. U.S. Patent 4 552 731, 1985.
(263) Xu, R.; Liu, X. *Chim. Sinica* **1984**, *42*, 227.
(264) Occelli, M. L. U.S. Patent 4 919 907, 1990.
(265) Newsam, J. M.; Jarman, R. H.; Jacobson, A. *J. Mater. Res. Bull.* **1985**, *20*, 125.
(266) Vaughan, D. E. W.; Strohmaier, K. G. *Molecular Sieves*; Van Nostrand Reinhold: New York, 1992; p 92.
(267) Ueda, S.; Fukuya, N.; Niihara, K. *Nendo Kagaku* **1993**, *32*, 264.
(268) Reddy, J. S.; Reddy, K. R.; Kumar, R. In *Recent Developments in Catalysis, Proceedings of the 10th National Symposium on Catalysis and 4th Indosoviet Seminar on Catalysis*; Narosa Publishing House: New Dehli, 1991; p 575.
(269) Liu, X.; Yu, J.; Kan, Q.; Ding, H. *Chem. Res. Chin. Univ.* **1991**, *7*, 135.
(270) Khadzhiev, S. N.; Agabalyan, L. G.; Mamaeva, I. M. *Catal. Today* **1992**, *13*, 635.
(271) Weitkamp, J.; Beyer, H. K.; Borbély, G.; Cortés-Corberán, V.; Ernst, S. *Chem-Ing. Tech.* **1986**, *58*, 969.
(272) Kentgens, A. P. M.; Bayense, C. R.; Van Hooff, J. H. C.; De Haan, J. W.; Van de Ven, L. J. M. *Chem. Phys. Lett.* **1991**, *176*, 399.
(273) Challoner, R.; Harris, R. K.; Barris, S. A. I.; Taylor, M. J. *Zeolites* **1991**, *11*, 827.
(274) Seive, A.; Guth, J. L.; Raatz, F.; Petit, L. Eur. Pat. Appl. 342 075, 1989.
(275) Ione, K. G.; Vostrikova, L. A.; Petrova, A. V.; Mastikin, V. M. In *Structure and Reactivity of Modified Zeolites*; Jacobs, P. A., Jaeger, N. I., Jiru, P., Kazansky, V. B., Schulz-Ekloff, G., Eds.; Elsevier: Amsterdam, 1984; p 151.
(276) Barri, S. A. I.; Young, D. EP 130 013, 1985.
(277) Barri, S. A. I. U.K. Patent 2 144 727 A, 1985.
(278) Moini, A. U.S. Patent 5 332 566 A, 1994.
(279) Fyfe, C. A.; Strobl, H.; Kokotailo, G. T.; Pasztor, C. T.; Barlow, G. E.; Bradley, S. *Zeolites* **1988**, *8*, 132.
(280) Occelli, M. L.; Goldish, E.; Eckert, H. In *Zeolites and Related Materials*: *State of the Art*; Weitkamp, J., Karge, H. G., Pfeifer, H., Hölderich, W., Eds.; Garmisch-Partenkirchen: 1994; Part A; *Stud. Surf. Sci. Catal.* **1994**, *84*, 597.
(281) McCusker, L. B. *Zeolites* **1984**, *4*, 51.
(282) Kyung, H.; Timken, C.; Oldfield, E. *J. Am. Chem. Soc.* **1987**, *109*, 7669.
(283) Barrer, R. M.; Baynham, J. W.; Bultitude, F. W.; Meier, W. M. *J. Chem. Soc. (London)* **1959**, 195.
(284) Goldsmith, J. R. *Miner. Mag.* **1952**, *29*, 952.
(285) Barri, S. A. I.; Young, D. EP 106 478, 1984.
(286) Marler, B. *Zeolites* **1987**, *7*, 393.
(287) Gonzalez, F.; Pesquera, C.; Blanco, C.; Benito, I.; Mendioroz, S. *Inorg. Chem.* **1992**, 727.
(288) Molina, R.; Moreno, S.; Vieira-Coelho, A.; Martens, J. A.; Jacobs, P. A.; Poncelet, G. *J. Catal.* **1994**, *148*, 304.
(289) Schott-Darie, C.; Kessler, H.; Benazzi, E. In *Zeolites and Microporous Crystals, Proceedings of the International Symposium*, Nagoya, 1993; Hattori, T., Yashima, T., Eds.; Kodansha and Elsevier: Tokyo and Amsterdam, 1994; p 3.
(290) Bradley, S. M.; Howe, R. F.; Hanna, J. V. *Solid State Nucl. Magn. Reson.* **1993**, *2*, 37.
(291) Meyerzualtenschildesche, H.; Muhr, H. J.; Nesper, R. *Microporous Mater* **1993**, *1*, 257.
(292) Loiseau, T.; Taulelle, F.; Ferey, G. *Microporous Mater.* **1996,** *5*, 365.
(293) Loiseau, T.; Ferey, G. *J. Mater. Chem.* **1996**, *6*, 1073.
(294) Zones, S. I.; Santilli, D. S.; Ziemer, J. N.; Holtermann, D. L.; Pecoraro, T. A.; Innes, R. A. WO 8 909 185 A1, 1989.
(295) Casci, J. L. EP 463768 A2, 1992.
(296) Zones, S. I.; Harris, T. V.; Rainis, A.; Santilli, D. S. WO 9 111 258 A1, 1991.
(297) Keijsper, J. J.; MacKay, M. EP 508540 A2, 1992.
(298) Vaughan, D. E. W.; Strohmaier, K. G.; Treacy, M. M. J.; Newsam, J. M. U.S. Patent 5 116 590 A, 1992.
(299) Valyocsik, E. W. U.S. Patent 5 068 096 A, 1991.
(300) Nakagawa, Y. U.S. Patent 5254514 A, 1993.
(301) Bennett, J. M.; Chang, C. D.; Lawton, S. L.; Leonowicz, M. E.; Lissy, D. N.; Rubin, M. K. U.S. Patent 5 236 575 A, 1993.
(302) Smith, W. J. EP 526252 A1, 1993.
(303) Nakagawa, Y. WO 9 4088 999 A1, 1994.
(304) Leonowicz, M. E.; Lawton, J. A.; Lawton, S. L.; Rubin, M. K. *Science* **1994**, *264*, 1910.
(305) Wu, J.; Gatte, R. R.; Roberie, G. G. EP 638 517 A, 1995.
(306) Newsam, J. M. *J. Phys. Chem.* **1988**, *92*, 445.

(307) Kerr, I. S. *Z. Kristallogr.* **1974**, *139*, 186.
(308) Suzuki, K.; Kiyozumi, Y.; Shin, S.; Ueda, S. *Zeolites* **1985**, *5*, 11.
(309) Beagley, B.; Titeloye, J. O. *Struct. Chem.* **1992**, *3*, 429.
(310) McCusker, L. B.; Meier, W. M.; Shin, S. *Zeolites* **1986**, *6*, 388.
(311) Barrer, R. M.; Villigier, H. *J. Chem. Soc. D* **1969**, 659.
(312) Galli, E. *Cryst. Struct. Commun.* **1974**, *3*, 339.
(313) Rinaldi, R.; Pluth, J. J.; Smith, J. V. *Acta Crygtallogr.* **1975**, *B 31*, 1603.
(314) Yu, J.-S.; Kim, J. Y.; Lee, C. W.; Kim, S. J.; Hong, S. B.; Kevan, L. *J. Chem. Soc., Faraday Trans.* **1997**, *93*, 4211.
(315) Occelli, M. L.; Goldish, E.; Eckert, H. *Stud. Surf. Sci. Catal.* **1994**, *84A*, 597.
(316) Takaishi, T. *J. Chem. Soc., Faraday Trans.* **1988,** *84*, 2967.
(317) Yu., J.-S.; Kim, S. J.; Hong, S. B.; Kevan, L. *J. Chem. Soc., Faraday Trans.* **1996**, *92*, 855.
(318) Yu., J.-S.; Hong, S. B.; Kevan, L. *Appl. Magn. Reson.* **1996**, *10*, 575.
(319) Yelon, W. B.; Xie, D.; Newsam, M.; Dunn, J. *Zeolites* **1990**, *10*, 553.
(320) He, H. Y.; Cheng, C. F.; Seal, S.; Barr, T. L.; Klinowski, J. *J. Phys. Chem.* **1995**, *99*, 3235.
(321) Timken, H. K. C.; Janes, N.; Turner, G. L.; Lambert, S. L.; Welsh, L. B.; Oldfield, E. *J. Am. Chem. Soc.* **1986**, *108*, 7236.
(322) Vaughan, D. E. W.; Melchior, M. T.; Jacobson, A. J. In *Intrazeolite Chemistry*; Stucky, G. D., Dwyer, F. G., Eds.; ACS Symposium Series; American Chemical Society: Washington, D.C.,-1984; Vol. 218, p 231.
(323) Fülöp, V.; Borbely, G.; Beyer, H. K.; Ernst, S.; Weitkamp, J. *J. Chem. Soc., Faraday Trans. 1* **1989**, *85*, 2127.
(324) Newsam, J. M.; Treacy, M. M. J.; Vaughan, D. E. W.; Strohmaier, K. G.; Mortier, W. J. *J. Chem. Soc., Chem. Commun.* **1989**, *85*, 493.
(325) Baerlocher, Ch.; McCusker, L. B.; Chiappetta, R. *Microporous Mater.* **1992**, *2*, 269.
(326) Kosslick, H.; Richter, M.; Tuan, V. A.; Fricke, R.; Storek, W. *J. Chem. Soc., Faraday Trans.* **1992**, *96*, 2421.
(327) Miessner, H.; Kosslick, H.; Lohse, U.; Parlitz, B.; Tuan, V. A. *J. Phys. Chem.* **1993**, *97*, 9741.
(328) Kosslick, H.; Berndt, H.; Lanh, H. D.; Martin, A.; Miessner, H.; Tuan, V. A. *J. Chem. Soc., Faraday Trans.* **1994**, *90*, 2837.
(329) Kosslick, H.; Tuan, V. A.; Walther, G.; Miessner, H.; Fricke, R.; Storek, W. In *Synthesis of Porous Materials: Zeolites, Clays, and Nanostructures*; Occelli, M. L., Kessler, H., Eds.; Marcel Dekker: New York, 1996; p 299.
(330) Tuan, V. A.; Fricke, R.; Szulzewsky, K.; Kosslick, H. *Cryst. Res. Technol.* **1989**, *26*, 161.
(331) De Witte, B.; Patarin, J.; Cholley, T. *Microporous Mater.* **1997**, *10*, 189.
(332) Robson, H. E. U.S. Patent 3,720,753, 1973.
(333) Shannon, R. D.; Keane, M. J.; Abrams, L.; Staley, R. H.; Geir, T. E.; Corbin, D. R.; Sonnichsen, G. C. *J. Catal.* **1988**, *133*, 367.
(334) Newsam, J. M.; Vaughan, D. E. W.; Strohmaier, K. G. *J. Phys. Chem.* **1995**, *99*, 9924.
(335) van Geem, P. C.; Scholle, K. F.; van der Velden, G. P. M.; Veeman, W. S. *J. Phys. Chem.* **1988**, *92*, 1585.
(336) Raatz, F.; Freund, E.; Marcilly, Chr. *J. Chem. Soc., Faraday Trans. 1* **1983**, *79*, 2299.
(337) Stach, H.; Jänchen, J.; Jerschkewitz, H.-G.; Lohse, U.; Parlitz, B.; Zibrowius, B.; Hunger, M. *J. Phys. Chem.* **1992**, *96*, 8473.
(338) Bodart, P.; Nagy, J. B.; Debras, G.; Gabelica, Z.; Jacobs, P. A. *J. Phys. Chem.* **1986**, *90*, 5183.
(339) Maache, M.; Janin, A.; Lavalley, J. C.; Benazzi, E. *Zeolites* **1995**, *15*, 507.
(340) Richter, M.; Ehrhardt, K.; Roost, U.; Kosslick, H.; Parlitz, B. *Stud. Surf. Sci. Catal.* **1994**, *84C*, 1285.
(341) Klyueva, N. V.; Tien, N. D.; Ione, K. G. *React. Kinet. Catal. Lett.* **1985**, *29*, 427.
(342) Klyueva, N. V.; Tien, N. D.; Ione, K. G. *Siofok* **1985**, 525.
(343) Whyte, T. E., Jr.; Wu, E. L.; Kerr, G. T.; Venuto, P. B. *J. Catal.* **1970**, *20*, 88.
(344) Occelli, M. L.; Perrotta, A. J. In *Intrazeolite Chemistry*; Stucky, G. D., Dwyer, F. G., Eds.; ACS Sympsium Series; American Chemical Society: Washington, D.C., 1983; Vol. 218, p 21.
(345) Aillo, R.; Barrer, R. M.; *J. Chem. Soc. (A)* **1970**, 1470.
(346) Anderson, M. W.; Occelli, M. L.; Klinowski, J. *J. Phys. Chem.* **1991**, *96* 388.
(347) Howden, M. G. *Zeolites* **1987**, *7*, 255.
(348) Treacy, M. M. J.; Newsam, J. M. *Nature* **1988**, *332*, 249.
(349) Wadlinger, R. L.; Kerr, G. T.; Rosinski, E. J. U.S. Pat. 3 308 069, 1967.
(350) Higgins, J. B., LaPierre, R. B.; Schlenker, J. L.; Rohrmann, A. C.; Wood, J. D.; Kerr, G. T.; Rohrbaugh, W. J. *Zeolites* **1988**, *8*, 446.
(351) Stevens, A. P.; Cox, P. A. *J. Chem. Soc., Chem. Commun.* **1995**, 343.
(352) Chao, K. J.; Sheu, S. P.; Lin, L.-H.; Genet, M. J.; Feng, M. H. *Zeolites* **1997**, *18*, 18.
(353) Reddy, K. S. N.; Eapen, M. J.; Joshi, P. N.; Mirajkar, S. P.; Shiralkar, V. P. *J. Incl. Phenom.* **1994**, *20*, 198.
(354) Lohse, U.; Altrichter, B.; Donath, R.; Fricke, R.; Jancke, K.; Parlitz, B.; Schreier, E. *J. Chem. Soc., Faraday Trans.* **1996**, *92*, 159.
(355) Kouwenhoven, H. W.; Stork, W. H. J.; Schaper, L. OS 2 755 770, 1978.
(356) van Koningsveld, H.; Tuinstra, F.; van Bekkum, H.; Jansen, J. C. *Acta Crystallogr.* **1989**, *B45*, 423.
(357) Wallau, M.; Tissler, A.; Thome, R.; Unger, K. EP 443 539, 1991.
(358) Lambert, S. L. In *Proceedings of the 9th International Conference,* Montreal 1992; van Ballmoos, R., Higgins, R. J. B., Treacy, M. M. J., Eds.; Butterworth-Heinemann: Boston, 1993; Vol. I, p 223.
(359) Ernst, S.; Kumar, R.; Weitkamp, J. In *Proceedings of the 9th International Zeolite Conference,* Montreal, 1992; van Ballmoos, R., Higgins, R. J. B., Treacy, M. M. J., Eds.; Butterworth-Heinemann: Boston, 1993; Vol. I, p 287.
(360) Simmons, D. K.; Szostak, R.; Agrawal, P. K.; Thomas, T. L. *J. Catal.* **1987**, *106*, 287.
(361) Struve, P.; Bergmann, A.; Brenner, A.; Bülow, M.; Unger, K. K., In *Fundamentals of Adsorption, Proceedings of the IVth International Conference on Fundamentals of Adsorption,* Kyoto, 1992; International Adsorption Society: 1993; p 615.
(362) Althoff, R.; Schulz-Dobrick, B.; Schüth, F.; Unger, K. *Microporous Mater.* **1993**, *1*, 207.
(363) Acosta, D. R.; Loske, A.; Schifter, I.; Guzman, M. L. *Microporous Mater.* **1993**, *1*, 309.
(364) Hochgräfe, M.; Marler, B.; Gies, H.; Fyfe, C. A.; Feng, Y.; Grondey, H.; Kokotailo, G. T. *Z. Kristallogr.* **1996**, *211*, 221.
(365) Zhi, Y. X.; Tuel, A.; Ben Taarit, Y.; Naccache, C. *Zeolites* **1992**, *12*, 138.
(366) Rosinski, E. J.; Rubin, M. K. U.S. Patent 3 832 449, 1974.
(367) Ernst, S.; Jacobs, P. A.; Martens, J. A.; Weitkamp, J. *Zeolites* **1987**, *7*, 458.
(368) Chiche, B. H.; Dutartre, R.; Di Renzo, F.; Fajula, F.; Katovic, A.; Regina, A.; Giordano, G. *Catal. Lett.* **1995**, *31*, 359.
(369) Zhao, Y.; Xiang, S.; Li, H. *Ranliao Huaxue Xuebao* **1992**, *20*, 32; *Chem. Abstr.* **1992**, *118*, 72340p.
(370) Yu, L.; Jiang, H.; Pang, W. Q. *Acta Chim. Sin.* **1993**, *51*, 780.
(371) Tuel, A. *Zeolites* **1995**, *15*, 236.
(372) Moudrakovski, I.; Sayari, A.; Ratcliffe, C. I.; Ripmeester, J. A.; Preston, K. F. *J. Phys. Chem.* **1994**, *98*, 10895.
(373) Zhao, X.; Wang, Q.; Li, H. *Cuihua Xuebao* **1994**, *15*, 148; *Chem. Abstr.* **1994**, *120*, 288379x.
(374) Kokotailo, G. T.; Schlenker, J. L.; Dwyer, F. G.; Valyocsik, E. W. *Zeolites* **1985**, *5*, 349.
(375) Ernst, S.; Weitkamp, J.; Martens, J. A.; Jacobs, P. A. *Appl. Catal.* **1989**, *48*, 137.
(376) Casci, J. L.; Whittam, T. V.; Lowe, B. M. In *Proceedings of the 6th International Conference on Zeolites*; Olson, D. H., Bisio, A. G., Eds.; Butterworth: Boston, 1984; p 894.
(377) Rao, G. N.; Joshi, P. N.; Kotasthane, A. N.; Ratnasamy, P. *Zeolites* **1989**, *9*, 483.
(378) Rao, G. N.; Shiralkar, V. P.; Kotasthane, A. N.; Ratnasamy, P. In *Molecular Sieves, Synthesis of Microporous Materials*; Occelli, M. L., Robson, H. E., Eds.; Van Nostrand Reinhold: New York, 1992; Vol. I p 153.
(379) Kresge, C. T.; Leonowicz, M. E.; Roth, W. J.; Vartuli, J. C.; Beck, J. S. *Nature* **1992**, *359*, 710.
(380) Behrens, P.; Glaue, A.; Haggenmüller, C.; Schehner, G. *Solid State Ionics* **1997**, *101−103*, 255.
(381) Beck, J. S.; Vartuli, J. C.; Roth, W. J.; Leonowicz, M. E.; Kresge, C. T.; Schmitt, K. D.; Chu, C. T.-W.; Olson, D. H.; Sheppard, E. W.; McCullen, S. B.; Higgins, J. B.; Schlenker, J. L. *J. Am. Chem. Soc.* **1992**, *114*, 10834.
(382) Monnier, A.; Schüth, F.; Huo, Q.; Kumar, D.; Margolese, D., Maxwell, R. S.; Stucky, G. D.; Krishnamurty, M.; Petroff, P.; Firouzi, A.; Janicke, M.; Chmelka, B. F. *Science* **1993**, *261* 1299.
(383) Yanagisawa, T.; Shimuzu, T.; Kuroda, K.; Kato, C. B*ull. Chem. Soc. Jpn.* **1990**, *63*, 988.
(384) Inagaki, S.; Fukushima, Y.; Okada, A.; Kurauchi, T.; Kuroda, K.; Kato, C., In *Proceedings of the of the 9th International Conference on Zeolites*; Montreal, 1992, van Ballmoos, R., Higgins, R. J. B., Treacy, M. M. J., Eds.; Butterworth-Heinemann: Boston, 1992; p 305.
(385) Inagaki, S.; Fukushima Y.; Kuroda, K. *J. Chem. Soc., Chem. Commun.* **1993**, 680.
(386) Feuston, B. P.; Higgins, J. B. *J. Phys. Chem.* **1994**, *98*, 4459.
(387) Coustel, N.; Di Renzo, F.; Fajula, F. *J. Chem. Soc., Chem. Commun.* **1994**, 967.
(388) Van den Bossche, G.; Sorby, R., Fontaine, F.; Clacens, J.-M.; Gabelica, Z. *J. Appl. Crystallogr.* **1997**, *30*, 1065.
(389) Chen, C.-Y.; Li, H.-X.; Davis, M. E. *Microporous Mater.* **1993**, *2*, 17.
(390) Chen, C.-Y.; Burkett, S. L.; Li H−X.; Davis, M. E. *Microporous Mater.* **1993**, *2*, 27.
(391) Tanev, P. T.; Pinnavaia, T. J. *Science* **1995**, *267*, 1324.
(392) Rathousky, J.; Zukal, A.; Franke, O.; Schulz-Ekloff, G. *J. Chem. Soc., Faraday Trans.* **1994**, *90*, 2827.

(393) Hitz, S.; Prins, R. *J. Catal.* **1997**, *168*, 194.
(394) Sayari, A.; Danumah C.; Moudrakovski,I. L. *Chem. Mater.* **1995**, *7*, 813.
(395) Zhao, D.; and Goldfarb, D. *J. Chem. Soc., Chem. Commun.* **1995**, 875.
(396) Reddy, K. M.; Moudrakovski, I.; Sayari, A. *J. Chem. Soc., Chem. Commun.* **1994**, 1059.
(397) Tanev, P. T.; Chibwe, M.; Pinnavaia, T. J. *Nature* **1994**, *368*, 321.
(398) Cheng, C. F.; He, H. Y.; Zhou, W. Z.; Klinowski, J.; Goncalves, J. A. S.; Gladden, L. F. *J. Phys. Chem.* **1996**, *100*, 390.
(399) Kosslick, H.; Landmesser, H.; Fricke, R. *J. Chem. Soc., Faraday Trans.* **1997**, *93*, 1849.
(400) Kosslick, H.; Lischke, G.; Landmesser, H.; Parlitz, B.; Storek, W., Fricke, R. *J. Catal.* **1998**, *176*, 102.
(401) Landmesser, H.; Kosslick, H.; Kürschner, U.; Fricke, R. *J. Chem. Soc., Faraday Trans.* **1998**, *94*, 971.
(402) Cheng, C. F.; Alba, M. D.; Klinowski, J. *Chem. Phys. Lett.* **1996**, *250*, 328.
(403) Cheng, C. F.; Klinowski, J. *J. Chem. Soc., Faraday Trans.* **1996**, *92*, 289.
(404) Kosslick, H.; Lischke, G.; Walther, G.; Storek, W.; Martin, A.; Fricke, R. *Microporous Mater.* **1996**, *9*, 13.
(405) Bagshaw, S. A.; Prouzet, E.; Pinnavaia, T. J. *Science* **1995**, *269*, 1242.
(406) Landmesser, H.; Kosslick, H.; Storek, W.; Fricke R. *Solid State Ionics* **1997**, *101*, 271.
(407) Chen, C.-Y.; Xiao , S.-Q.; Davis, M. E. *Microporous Mater.* **1995**, *4*, 1.
(408) Luan, Z.; Cheng, C.-F.; He. H.; Klinowski, J. *J. Phys. Chem.* **1995**, *99*, 10590.
(409) Corma, A.; Fornes, V.; Navarro, M. T.; Perez-Pariente, J. *J. Catal.* **1994**, *148*, 569.
(410) Schüth, F. *Ber. Bunsen-Ges. Phys. Chem.* **1995**, *99*, 1306.
(411) Kosslick, H.; Lischke, G.; Parlitz, B.; Storek, W.; Fricke, R. *Appl. Catal A* **1999**, *184*, 49.
(412) Karge, H. G.; Dondur, V.; Weitkamp, J. *J. Phys. Chem.* **1995**, *95*, 283.
(413) Corma, A. Martinez, A.; Martinez-Soria, V.; Monton, J. B. *J. Catal.* **1995**, *153*, 25.
(414) Inui, T.; Kim, J.-B.; Seno, M. *Catal. Lett.* **1994**, *29*, 271.
(415) Kozhevnikov, J. V.; Sennema, A.; Jansen, R. J. J.; Pamin, K.; van Bekkum, H. *Catal. Lett.* **1995**, *30*, 241.
(416) Armengol, E.; Cano, M. L.; Corma, A.; Garcia, H.; Navarro, M. T. *J. Chem. Soc., Chem. Commun.* **1995**, 519.
(417) Kloetstra, K. R.; van Bekkum, H. *J. Chem. Soc., Chem. Commun.* **1995**, 1005.
(418) Kubelkova, L.; Cejka, J.; Novakova, L.; Lercher, J. A.; Jahn, E. *Z. Phys. Chem. (NF)* **1990**, *168*, 231.
(419) Inui, T.; Nagata, H.; Matsuda, H.; Kim, J.-B.; Ishihara, Y. *Ind. Eng. Chem. Res.* **1992**, *31*, 995.
(420) Lischke, G. Unpublished data.
(421) Takeguchi, T.; Kim, J.-B.; Kang, M.; Inui, T.; Cheuh, W.-T.; Haller, G. L. *J. Catal.* **1998**, *175*, 1.
(422) Parise, J. B. *J. Chem. Soc., Chem. Commun.* **1985**, 606.
(423) Schott-Darie, C.; Kessler, H.; Soulard, M.; Gramlich, V.; Benazzi, E. In *Zeolites and Related Materials. State of the Art;* Weitkamp, J., Karge, H. G., Pfeifer, H., Hölderich, W., Eds.; Garmisch-Partenkirchen: 1994; *Stud. Surf. Sci. Catal.***1994**, *84A*, 101.
(424) Weigel, S. J.; Weston, S. C.; Cheetham, A. K.; Stucky, G. D. *Chem. Mater.* **1997**, *9*, 1293.
(425) Tieli, W.; Guangdi, Y.; Shouhua, F.; Changjiang, S.; Ruren, X. *J. Chem. Soc. Chem. Commun.* **1989**,*14*, 948.
(426) Reinert, P.; Schott-Darie, C.; Patarin, J. *Microporous Mater.* **1997**, *9*, 107.
(427) Simmen, A.; Patarin, J.; Baerlocher, C. In *Proceedings of the of the 9th International Conference on Zeolites*, Montreal, 1992, von Balmoos, R., Higgins, J. B., Treacy, M. J. J., Eds.; Butterworth-Heinemann: Stoneham, 1993; Vol. I, p 433.
(428) Kosslick, H.; Zubowa, H.-L.; Lohse, U.; Landmesser, H.; Fricke, R.; Caro, J. In *Proceedings of the on the 1st World Congress of Microwave Processing and Radio Frequency Heating,* Florida, 1997.
(429) Zubowa, H.-L.; Schreier, E.; Jancke, K.; Steinike, U.; Fricke, R. *Collect. Czech. Chem. Commun.* **1995**, *60*, 1 and 403.
(430) Bedard, R. L.; Bowes, C. L.; Coombs, N.; Holmes, A. J.; Jiang, T.; Kirkby, S. J.; McDonald, P. M.; Malek, A. M.; Ozin, G. A.; Petrov, S.; Plavac, N.; Ramik, R. A.; Steele, M. R.; Young, D. *J. Am. Chem. Soc.* **1993**, *115*, 2300.
(431) Barr, T. L.; Klinowski, J.; He, H. Y.; Alberti, K.; Muller, G.; Lercher, J. A. *Nature* **1993**, *365*, 429.
(432) Janin, A.; Lavalley, J. C.; Benazzi, E.; Schott-Darie C.; Kessler, H. In *Proceedings of the ZEOCAT '95*, Szombathely, Hungary, 1995; Beyer, H. K., Karge, H. G., Kiricsi, I., Nagy, J. B., Eds.; Elsevier: Amsterdam, 1995; p 124.
(433) Müller, G.; Eder-Mirth, G.; Kessler H.; Lercher, J. A. *J. Phys. Chem.* **1995**, *99*, 12327.
(434) Richter, M.; Zubowa, H.-L.; Eckelt, R.; Fricke, R. *Microporous Mater.* **1996**, *7*, 119.
(435) Richter, M.; Fischer, H.; Bartoszek, M.; Zubowa, H.-L.; Fricke, R. *Microporous Mater.* **1997**, *8*, 69.
(436) Kallus, S.; Patarin, J.; Marler, B. *Microporous Mater.* **1996**, *7*, 89.
(437) Guth, J. L.; Kessler, H.; Wey, R. *Stud. Surf. Sci. Catal.* **1986**, *28*, 21.
(438) Bond, A. D.; Chippindale, A. M.; Cowley, A. R.; Readman, J. E.; Powell, A. V. *Zeolites* **1997**, *19*, 326.
(439) Meden, A.; Grosse-Kunstleve, R. W.; Baerlocher, C.; McCusker, L. B. *Z. Kristallogr.* **1997**, *212*, 801.
(440) Machado, F. J.; Lopez, C. M.; Goldwasser, J.; Mendez, B.; Campos, Y.; Escalante, D.; Tovar, M., Ramirez-Agudelo, M. M. *Zeolites* **1997**, *19*, 387.
(441) Chippindale, A. M.; Cowley, A. R. *Zeolites* **1997**, *18*, 176.
(442) Holland, B. T.; Isbester, P. K.; Blanford, C. F.; Munson, E. J.; Stein, A. *J. Am. Chem. Soc.* **1997**, *119*, 6796.
(443) Häfele, M.; Reitzmann, A.; Roppelt, D.; Emig, G. *Appl. Catal. A: General* **1997**, *150*, 153.
(444) Davies, E. E.; Kolombos, A. J. Austr. Patent 509 285, 1979.
(445) Mowry, J. R.; Anderson, R. F.; Johnson, J. A. *Oil Gas J.* **1985**, *83*, 128.
(446) Mowry, J. R.; Martindale, D. C.; Hall, A. H. P. *Arabian J. Sci. Eng.* **1985**, *10*, 367.
(447) Editorial note in *Chemistry in Britain* **1984**, *20*, 684.
(448) Guisnet, M.; Gnep, N. S.; Alario, F. *Appl. Catal. A: General* **1992**, *89*, 1.
(449) Inui, T.; Makine, Y.; Okazumi, F.; Miyamoto, A. *J. Chem. Soc., Chem. Commun.* **1986**, 571.
(450) Kanai, J.; Kawata, N. *Appl. Catal.* **1989**, *55*, 115.
(451) Buckles, G.; Hutchings, G. J.; Williams, C. D. *Catal. Lett.* **1991**, *11*, 89.
(452) Kazansky, V. B.; Kustov, L. M.; Khodakov, A. Yu. In *Zeolites: Facts, Figures, Future*; Jacobs, P. A., van Santen, R. A., Eds.; Elsevier: Amsterdam, 1989; p 1173.
(453) Ono, Y. *Catal. Rev.-Sci. Eng.* **1992**, *34*, 179.
(454) Price, G. L. Kanazirev, V. *J. Catal.* **1990**, *126*, 267.
(455) Mao, R. le van; Yao, J. *Appl. Catal. A: General* **1991**, *79*, 77.
(456) Le van Mao, R.; Dufresne, L.; Yao, J. *Appl. Catal.* **1990**, *65*, 143.
(457) Yao, J.; Le van Mao, R.; Dufresne, L. *Appl. Catal.* **1990**, *65*, 175.
(458) Kwak, B. S.; Sachtler, W. M. H.; Haag, W. O. *J. Catal.* **1994**, *149*, 465.
(459) Meriaudeau, P.; Naccache, C. *J. Mol. Catal.* **1990**, *59*, L31.
(460) Lercher, J. A.; van Santen, R. A.; Vinek, H. *Catal. Lett.* **1994**, *27*, 91.
(461) Kazansky, V. B.; Senchenya, I. N.; Frash, M.; van Santen, R. A. *Catal. Lett.* **1994**, *27*, 345.
(462) Bayense, C. R.; van der Pol, A. J. H. P.; van Hooff, J. H. C. *Appl. Catal.* **1991**, *72*, 81.
(463) Meriaudeau, P.; Naccache, C. In *New Frontiers in Catalysis, Proceedings of the 10th International Congress of Catalysis*, Budapest, 1992; Elsevier: Amsterdam, 1993; *Stud. Surf. Sci. Catal.* **1993**, *75*, 2431.
(464) Buckles, G.; Hutchings, G. J. *Catal. Lett.* **1994**, *27*, 361.
(465) Derouane, E. G.; Hamid, S. B. A.; Ivanova, I. I.; Blom, N.; Højlund-Nielsen, P.-E. *J. Mol. Catal.* **1994**, *86*, 371.
(466) Hamid, S. B. A.; Derouane, E. G.; Meriaudeau, P.; Naccache, C.; Yarmo, M. A. *Stud. Surf. Sci. Catal.* **1994**, *84C*, 2335.
(467) Inui, T. *Stud. Surf. Sci. Catal.* **1989**, *44*, 189.
(468) Inui, T.; Miyamoto, A.; Matsuda, H.; Nagata, H.; Makimo, Y.; Fukuda, K.; Okazumi, F. *New Developments in Zeolite Science and Technology, Proceedings of the 7th International Zeolite Conference*, Tokyo, 1986; Murakami, Y., Iijima, A., Ward, J. W., Eds.; Kodansha and Elsevier: Tokyo and Amsterdam, 1986; p 859.
(469) Fujimoto, K.; Toyoshi, S. In *New Horizons in Catalysis, Proceedings of the 7th International Congress of Catalysis*, Tokyo, 1980; Seiyama, T., Tanabe, K., Eds.; Elsevier: Amsterdam, 1980; p 235.
(470) Meriaudeau, P.; Sapaly, G.; Naccache, C. *J. Mol. Catal.* **1993**, *81*, 293.
(471) Iglesia, E.; Baumgartner, J. E.; Price, J. L. *J. Catal.* **1992**, *134*, 549.
(472) Guisnet, M. R.; Lukyanov, D. *Stud. Surf. Sci. Catal.* **1994**, *90*, 367.
(473) Lukyanov, D.; Gnep, N. S.; Guisnet, M. R. *Ind. Eng. Chem. Res.* **1994**, *33*, 223.
(474) Price, G. L. Kanazirev, V. *J. Mol. Catal.* **1991**, *66*, 115.
(475) Kanazirev, V.; Price, G. L.; Dooley, K. M. *J. Chem. Soc., Chem. Commun.* **1990**, *9*, 712.
(476) Choudhary, V. R.; Devadas, P.; Kinage, A. K.; Sivadinarayana, C.; Guisnet, M. *J. Catal.* **1996**, *158*, 537.
(477) Kitagawa, H.; Sendoda, Y.; Ono, Y. *J. Catal.* **1986**, *101*, 12.
(478) Ono, Y.; Nakatami, H.; Kitagawa, H.; Suzuki, E. In *Successful Design of Catalysts, Proceedings of the Worldwide Catalysis Seminar*, Japan, 1988; Inui, T., Ed.; Elsevier: Amsterdam, 1988; p 279.
(479) Gnep, N. S.; Ribeiro, F. R.; Guisnet, M. *Appl. Catal.* **1988**, *43*, 155.

(480) Gianetto, G.; Montes, A.; Gnep, N. S.; Florentine, A.; Cartrand, P.; Guisnet, M. *J. Catal.* **1993**, *145*, 86.
(481) Mole, T.; Anderson, J. R.; Creer, G. *Appl. Catal.* **1985**, *17*, 141.
(482) Dmitriev, R. V.; Schevchenko, D. P.; Sphiro, E. S.; Dergachev, A. A.; Tkachenko, O. P.; Minachev, Kh. M. In *Zeolite Chemistry and Catalysis, Proceedings of the International Symposium*, Prague, 1991; Jacobs, P. A., Jaeger, N. I., Kubelkova, L., Wichterlova, B., Eds.; Elesevier, Amsterdam, 1991; p 381.
(483) Sphiro, E. S.; Shevchenko, O. P.; Dmitriev, R. V.; Tkachenko, O. P.; Minachev, Kh. M. *Appl. Catal. A: General* **1994**, *107*, 147.
(484) Sphiro, E. S.; Shevchenko, O. P.; Dmitriev, R. V.; Tkachenko, O. P.; Minachev, Kh. M. *Appl. Catal. A: General* **1994**, *107*, 165.
(485) Sphiro, E. S.; Shevchenko, O. P.; Dmitriev, R. V.; Tkachenko, O. P.; Minachev, Kh. M. *New Aspects of Spillover Effect in Catalysis, Proceedings of the 3rd International Conference on Spillover*, Kyoto, Japan 1993; Inui, T., Fujimoto, K., Uchijima, T., Masai, M., Eds.; Elsevier: Amsterdam, 1993; p 159.
(486) Schulz, P.; Baerns, M. *Appl. Catal. A: General* **1991**, *78*, 15.
(487) Hamid, S. B. A.; Derouane, E. G.; Demortier, G.; Riga, J. Yarmo, M. A. *Appl. Catal. A: General* **1994**, *108*, 85.
(488) Choudhary, V. R.; Kinage, A. K.; Choudhary, T. V. *Appl. Catal. B: Environmental* **1997**, *162*, 239.
(489) Choudhary, V. R.; Kinage, A. K.; Choudhary, T. V. *Science* **1997**, *275*, 1286.
(490) Choudhary, V. R.; Kinage, A. K.; Choudhary, T. V. *Angew. Chem.* **1997**, *109*, 1362.
(491) Buckles, G. J.; Hutchings, G. J. *J. Catal.* **1995**, *151*, 33.
(492) Choudhary, V. R.; Devadas, P.; Kinage, A. K.; Guisnet, M. *Appl. Catal. A: General* **1997**, *162*, 223.
(493) Choudhary, V. R.; Devadas, P. *J. Catal.* **1997**, *172*, 475.
(494) Stakheev, A. Y.; Khodakov, A. Y.; Kustov, L. M.; Kazansky, V. B.; Minachev, K. M. *Zeolites* **1992**, *12*, 866.
(495) Iwamoto, S.; Shimizu, S.; Inui, T. In *Zeolites and Related Materials. State of the Art, Proceedings of the 10th International Zeolite Conference*; Weitkamp, J., Karge, H. G., Pfeifer, H., Hölderich, W., Eds.; Garmisch-Partenkirchen: 1994; *Stud. Surf. Sci. Catal.* **1994**, *84C*, 1523.
(496) Feeley, J. S.; Deeba, M.; Farrauto, R. J.; Beri, G.; Haynes, A. *Appl. Catal. B: Environmental* **1995**, *6*, 79.
(497) Maunula, T.; Kintatitschi, Y.; Inaba, M.; Haneda, M.; Sato, K.; Hamada, H.; *Appl. Catal. B: Environmental* **1998**, *15*, 291.
(498) Young, L. B. U.S. Patent 3 962 364, 1976.
(499) Shanker, U.; Rawat, D. S.; Bawa, J. S.; Dabral, R. P.; Bhattacharya, K. K. *Erdöl und Kohle, Erdgas, Petrochemie* **1990**, *43*, 489.
(500) Cejka, J.; Vondrova, A.; Wichterlova, B.; Vorbeck, G.; Fricke, R. *Zeolites* **1994**, *14*, 147.
(501) Emig, G.; Klemm, E.; Seiler, H. *Chem. Ing. Techn.* **1994**, *66*, 956.
(502) Wang, J.; Li, Y.; Chen, S.; Peng, S. *Catal. Lett.* **1994**, *24*, 395.
(503) Raj, A.; Reddy, J. S.; Kumar, R. *J. Catal.* **1992**, *138*, 518.
(504) Corma, A.; Lopis, L. L.; Zicovich-Wilson, C. *J. Am. Chem. Soc.* **1994**, *116*, 134.
(505) Park, Y. K.; Park, K. Y.; Woo, S. J. *Catal. Lett.* **1994**, *26*, 169.
(506) Halgeri, A. B.; Bhat, Y. S. In *Zeolites and Microporous Crystals, Proceedings of the International Symposium on Zeolites and Microporous Materials*, Nagoya, Japan, 1993; Hattori, T., Yashima, T., Eds.; Kodansha and Elsevier: Tokyo and Amsterdam, 1994; *Stud. Surf. Sci. Catal.* **1994**, *83*, 163.
(507) Kim, J. H.; Namba, S.; Yashima, T. *Zeolites* **1991**, *11*, 59.
(508) Jahn, S. L.; Cardoso, D. *Catal. Today* **1989**, *5*, 515.
(509) Norval, G. W.; Phillips, M. J. *React. Kinet. Catal. Lett.* **1989**, *38*, 261.
(510) Parikh, P. A.; Subrahmanyam, N.; Bhat, Y. S.; Halgeri, A. B. *Ind. Eng. Chem. Res.* **1992**, *31*, 1012.
(511) Namba, S.; Ohta, H.; Kim, J.-H.; Yashima, T. In *New Frontiers in Catalysis, Proceedings of the 10th International Congress of Catalysis*, Budapest, Hungary, 1992, Guczi, L., et al., Eds.; Elsevier: Amsterdam, 1993; p 1685.
(512) Namba, S.; Ohta, H.; Kim, J.-H.; Yashima, T. In *Zeolites and Microporous Crystals, Proceedings of the International Symposium on Zeolites and Microporous Materials*, Nagoya, Japan, 1993; Hattori, T., Yashima, T., Eds.; Kodansha and Elsevier: Tokyo and Amsterdam, 1994;, *Stud. Surf. Sci. Catal.* **1994**, *83*, 279.
(513) Kim, J.-H.; Namba, S.; Yashima, T. *Bull. Chem. Soc. Jpn.* **1988**, *61*, 1051.
(514) Kim, J.-H.; Yamagishi, K.; Namba, S.; Yashima, T. J. *J. Chem. Soc., Chem. Commun.* **1990**, 1793.
(515) Kim, J.-H.; Namba, S.; Yashima, T. *Appl. Catal. A* **1992**, *83*, 51. Kim, J.-H.; Namba, S.; Yashima, T. *Appl. Catal. A: General* **1992**, *83*, 51.
(516) Cejka, J.; Kapustin, G. A.; Wichterlova, B. *Appl. Catal. A: General* **1994**, *108*, 187.
(517) Parikh, P. A.; Subrahmanyam, N.; Bhat, Y. S.; Halgeri, A. *Catal. Lett.* **1992**, *14*, 107.
(518) Halgeri, A. B.; Prasada Rao, T. S. R. In *Acid−Base Catalysis*; Hattori, H., Misono, M., Ono, Y., Eds.; VCH: New York, 1989; p 319.
(519) Rhodes, N. P.; Rudham, R. *J. Chem. Soc., Faraday Trans.* **1994**, *90*, 809.
(520) Bhaskar, G. V.; Do, D. D. *Ind. Eng. Chem. Res.* **1990**, *29*, 355.
(521) Weitkamp, J.; Ernst, S.; Jacobs, P. A.; Karge, H. G. *Erdöl, Erdgas, Kohle, Petrochem.* **1986**, *39*, 13.
(522) Vorbeck, G.; Richter, M.; Fricke, R.; Parlitz, B.; Schreier, E.; Szulzewsky, K.; Zibrowius, B. In *Catalysis and Adsorption by Zeolites, Proceedings of the ZEOCAT 90*, Leipzig, 1990; Öhlmann, G., Pfeifer, H., Fricke, R., Eds.; Elsevier: Amsterdam, 1991; *Stud. Surf. Sci. Catal.* **1991**, *65*, 631.
(523) Richter, M. Unpublished results.
(524) Sasidharan, M.; Kumar, R. *Catal. Lett.* **1996**, *38*, 245.
(525) Kumar, R.; Reddy, K. R. *Microporous Mater.* **1994**, *3*, 195.
(526) Truex, T. J.; Searles, R. A.; Sun, D. C. *Platinum Metals Rev.* **1992**, *36*, 2.
(527) Inui, T.; Iwamoto, S.; Kojo, S: Yoshida, T. *Catal. Lett.* **1992**, *16*, 223.
(528) Witzel, F.; Sill, G. A.; Hall, W. K. *J. Catal.* **1994**, *149*, 229.
(529) Witzel, F.; Sill, G. A.; Hall, W. K. In *Zeolites and Related Microporous Materials, State of the Art, Proceedings of the 10th International Zeolite Conference*; Garmisch-Partenkirchen, 1994, Weitkamp, J., Karge, H. G., Pfeifer, H., Hölderich, W., Eds.; Elsevier: Amsterdam, 1994; *Stud. Surf. Sci. Catal.* **1994**, *84C*, 1531.
(530) Yogo, K.; Tanaka, S.; Ihara, M.; Hishiki, T.; Kikuchi, E. *Chem. Lett.* **1992**, 1025.
(531) Yogo, K.; Kikuchi, E. In *Zeolites and Related Materials. State of the Art, Proceedings of the 10th International Zeolite Conference*, Garmisch-Partenkirchen, 1994, Weitkamp, J., Karge, H. G., Pfeifer, H., Hölderich, W., Eds.; Elsevier: Amsterdam, 1994; *Stud. Surf. Sci. Catal.* **1994**, *84B*, 1547.
(532) Kikuchi, E.; Yogo, K. *Catal. Today* **1994**, *22*, 73.
(533) Shelef, M.; Montreuil, C. N.; Jen, H. W. *Catal. Lett.* **1994**, *26*, 277.
(534) Kikuchi, E.; Ogura, M.; Terasaki, I.; Goto, Y. *J. Catal.* **1996**, *161*, 465.
(535) Tabata, T.; Kokitsu, M.; Okada, O. *Catal. Lett.* **1994**, *25*, 393.
(536) Hoost, T. E.; Laframboise, K. A.; Otto, K. *Catal. Lett.* **1995**, *33*, 105.
(537) Miyamoto, A.; Himei, H.; Oka, Y.; Maruya, E.; Katagiri, M.; Vetrivel, R.; Kubo, M. *Catal. Today* **1994**, *22*, 87.
(538) Himei, H.; Yamadaya, M.; Kubo, M.; Vetrivel, R.; Broclawik, E.; Miyamoto, A. *J. Phys. Chem.* **1995**, *99*, 12461.
(539) Burch, R.; Scire, S. *Catal. Lett.* **1994**, *27*, 177.
(540) Armor, J. N. In *Environmental Catalysis;* Armor, J. N., Ed.; ACS Symposium Series; American Chemical Society: Washington, D.C., 1994; Vol. 552, p 5.
(541) Iwamoto, M. *Catal. Today* **1996**, *29*, 29.
(542) Hutchings, G. J.; Nicolaides, C. P.; Scurrell, M. S. *Catal. Today* **1992**, *15*, 23.
(543) Romannikov, V. N.; Chumachenko, L. S.; Mastkhin, V. M.; Ione, K. G. *React. Kinet. Catal. Lett.* **1985**, *29*, 85.
(544) Kogelbauer, A.; Lercher, J. A.; Steinberg, K.-H.; Roesssner, F.; Soellner, A.; Dimitriev, R. V. *Zeolites* **1989**, *9*, 224.
(545) Lalik, E.; Liu, X.; Klinowski, J. *J. Phys. Chem.* **1992**, *96*, 805.
(546) Handreck; G. P.; Smith, T. D. *J. Chem. Soc., Faraday Trans. 1* **1989**, *85*, 3215.
(547) Froment, G. F.; Dehertog, W. J. H.; Marchi, A. J. In *Catalysis*; Spivey, J. J., Ed.; Royal Society of Chemistry: Cambridge, 1992; Vol. 9, p 1.
(548) Wilson, S. T.; Lok, B. M.; Messina, C. A.; Cannan, T. R.; Flanigen, E. M. *J. Am. Chem. Soc.* **1982**, *104*, 1146.
(549) Kaiser, S. W. *Arabian J. Sci. Eng.* **1985**, 361.
(550) Choudhary, V. R.; Kinage, A. K. *Zeolites* **1995**, *15*, 732.
(551) Handreck, G. P.; Smith, T. D. *J. Catal.* **1990**, *123*, 513.
(552) Minachev, Kh. M.; Chadziev, S. N.; Dergacev, A. A.; Bondarenko, T. N.; Charson, M. S.; Kosolapova, A. P. *DAN SSSR* **1994**, *337*, 215.
(553) Buckles, G.; Hutchings, G. J.; Williams, C. D. *Catal. Lett.* **1991**, 8, 115.
(554) Giannetto, G.; Leon, G.; Papa, J.; Monque, R.; Galiasso, R.; Gabelica, Z. *Catal. Lett.* **1993**, *22*, 381.
(555) Tkacenko, O. P.; Shpiro, E. S.; Vasina, T. V.; Preobrazenskij, A. V.; Bragin, O. V.; Minachev, Kh. M. *DAN SSSR* **1990**, *314*, 668.
(556) Meriaudeau, P.; Sappaly, G.; Dufaux, M.; Naccache, C., In *Proceedings of the 9th International Zeolite Conference*, Montreal, 1992, von Ballmoos, R., Higgins, J. B., Treacy, M. M. J., Eds.; Butterworth-Heinemann: Boston, 1993; Vol. II, p 335.
(557) Giannetto, G.; Monque, R.; Galiasso, R.; Papa, J.; Gabelica, Z., In *Zeolites and Related Materials, State of the Art 1994, Proceedings of the 10th International Zeolite Conference*, Garmisch-Partenkirchen, 1994; Weitkamp, J., Karge, H. G., Pfeifer, H., Hölderich, W., Eds.; *Stud. Surf. Sci. Catal.* **1994**, *84B*, 981.
(558) Sirokman, G.; Sendoda, Y.; Ono, Y. *Zeolites* **1986**, *6*, 299.
(559) Harris, J. L.; Krisko, N.; Wang, X. M. *Appl Catal. A* **1992**, *83*, 5.
(560) Gnep, N. S.; Doyemet, I. Y.; Seco, A. M.; Ribeiro, F. R.; Guisnet, M. *Appl. Catal.* **1987**, *35*, 93.
(561) Le van Mao, R.; Yao, J.; Sjiariel, B. *Catal. Lett.* **1990**, *6*, 23.

(562) Le van Mao, R.; Carli, R.; Yao, J.; Ragaini, V. *Catal. Lett.* **1992**, *16*, 43.
(563) Fujimoto, K.; Nakamura, I.; Yokota, K. *Zeolites* **1989**, *9*, 120.
(564) Minachev, Kh. M., In *New aspects of spillover effect in catalysis*, *Proceedings of the 3rd International Conference on Spillover*, Kyoto, Japan, 1993; Inui, T., Fujimoto, K., Uchijima, T., Masai, M., Eds.; Elsevier: Amsterdam, 1993; p 159.
(565) Kanazirev, V.; Mavrodinova, V.; Kosova, L.; Price, G. L. *Catal. Lett.* **1991**, *9*, 35.
(566) Ono, Y.; Kanae, K. *J. Chem. Soc., Faraday Trans.* **1991**, *87*, 669.
(567) Komatsu, T.; Araki, Y.; Namba, S.; Yashima, T. In *Zeolites and Related Materials. State of the Art, Proceedings of the 10th International Zeolite Conferenc*, Garmisch-Partenkirchen, 1994; Weitkamp, J., Karge, H. G., Pfeifer, H., Hölderich, W., Eds.; *Stud. Surf. Sci. Catal.* **1994**, *98C*, 1821.
(568) Parikh, P. A.; Subrahmanyam, N.; Bhat, Y. S.; Halgeri, A. B. *Appl. Catal. A: General* **1992**, *90*, 1.
(569) Meriaudeau, P.; Sapaly, G.; Wicker, G.; Naccache, C. *Catal. Lett.* **1994**, *27*, 143.
(570) Yogo, K.; Tanaka, S.; Ihara, M.; Hishiki, T.; Kikuchi, E. *Appl. Catal. B: Environmental* **1993**, 2, L1.
(571) Yogo, K.; Ihara, M.; Terasaki, I.; Kikuchi, E. *Chem. Lett.* **1993**, 229.
(572) Yogo, K.; Tanaka, S.; Ihara, M.; Hishiki, T.; Kikuchi, E. *Catal. Lett.* **1993**, *17*, 303.
(573) Alba, M. D.; Romero, A. A.; Ocelli, M. L.; Klinowski, J. *J. Chem. Soc., Faraday Trans.* **1997**, *93*, 1221.
(574) Alba, M. D.; Romero, A. A.; Ocelli, M. L.; Klinowski, J. *J. Phys. Chem. B* **1997**, *101*, 5166.
(575) Zulfugarov, Z. G.; Suleimanov, A. S.; Samedov, Ch. R. In *Structure and Reactivity of Modified Zeolites;* Jacobs, P. A., Jaeger, N. I., Jiru, P., Kazanski, V. B., Schulz-E Ekloff, G., Eds.; Elsevier: Amsterdam, 1984; p 167; *Stud. Surf. Sci. Catal.* **1984**, *18*, 167.
(576) Saha, S. K.; Sivasanker, S. *Catal. Lett.* **1992**, *15*, 413.
(577) Parton, R.; De Moos, D.; Jacobs, P. A., In *Zeolite Microporous Solids: Synthesis, Structure, and Reactivity*; Derouane, E. G., Lemos, F., Naccache, C., Ribeiro, F. R., Eds.; NATO ASI Series C; Kluwer Academic Publishers: Dortrecht, 1992; Vol. 532, p 555.
(578) Occelli, M. L.; Eckert, H.; Wölker, A.; Auroux, A. *Microporous Mesoporous Mater.* **1999**, *30*, 219.
(579) Derouane, E. G.; He, H.; Derouane-Abd Hamid, S. B.; Ivanova, I. I. *Catal. Lett.* **1999**, *58*, 1.
(580) Uemichi, Y.; Ktakuma; Ayame, A. *J. Chem. Soc., Chem. Commun.* **1998**, 1975.
(581) Wragg, D. S.; Bull, I.; Hix, G. B.; Morris, R. E. *J. Chem. Soc., Chem. Commun.* **1999**, 2037.
(582) Kang, M.; Lee, Ch.-T. *J. Mol. Catal. A: Chemical* **1999**, *150*, 213.
(583) Traa, Y.; Burger, B.; Weitkamp, J. *Microporous Mesoporous Mater.* **1999**, *30*, 3.

CR9411637